HILLSLOPE DYNAMICS IN THE PAONIA-MCCLURE PASS AREA, COLORADO, USA

A Dissertation

by

NETRA RAJ REGMI

Submitted to the Office of Graduate Studies of
Texas A&M University
in partial fulfillment of the requirements for the degree of

DOCTOR OF PHILOSOPHY

August 2010

Major Subject: Geology

Hillslope Dynamics in the Paonia-McClure Pass Area, Colorado, USA

HILLSLOPE DYNAMICS IN THE PAONIA-MCCLURE PASS AREA, COLORADO, USA

A Dissertation

by

NETRA RAJ REGMI

Submitted to the Office of Graduate Studies of
Texas A&M University
in partial fulfillment of the requirements for the degree of

DOCTOR OF PHILOSOPHY

Approved by:

Chair of Committee,	John R. Giardino
Committee Members,	John D. Vitek
	Christopher C. Mathewson
	Jean-Louis Briaud
	Douglas J. Sherman
Head of Department,	Andreas Kronenberg

August 2010

Major Subject: Geology

ABSTRACT

Hillslope Dynamics in the Paonia-McClure Pass Area, Colorado, USA.

(August 2010)

Netra Raj Regmi, B.S.; M.S., Tribhuvan University

Chair of Advisory Committee: Dr. John Rick Giardino

Mass movement can be activated by earthquakes, rapid snowmelt, or intense rainstorms in conjunction with gravity. Whereas mass movement plays a major role in the evolution of a hillslope by modifying slope morphology and transporting material from the slope to the valley, it is also a potential natural hazard. Determining the morphology of the mountain slopes and the relationships of frequency and magnitude of landslides are fundamental to understanding the role of landslides in the study of landscape evolution, and hazard assessment.

Characteristics of the geomorphic zones in a periglacial landscape were evaluated by plotting local slopes and the drainage areas in Paonia-McClure Pass area of western Colorado. The study suggested that the steepness and concavity of mountain slopes and stream channels in the study area are related by an exponential equation. Seven hundred and thirty five shallow landslides (<160,000 m^2) from the same study area were mapped to determine the frequency-magnitude relationships of shallow landslides and to develop an optimum model of mapping susceptibility to landslides. This study suggests that the frequency-magnitude of the landslides in Paonia-McClure

Pass area are related by a double pareto equation with values $\alpha = 1.1$, and $\beta = 1.9$ for the exponents. The total area of landslides is 4.8×10^6 m^2 and the total volume of the landslides is 1.4×10^7 m^3. The areas (A) and the volumes (V) of landslides are related by $V = 0.0254 \times A^{1.45}$. The frequency-magnitude analysis shows that landslides with areas ranging in size from 1,600 m^2 - 20,000 m^2 are the most hazardous landslides in the study area. These landslides are the most frequent and also do a significant amount of geomorphic work.

Three quantitative approaches: weight of evidence; fuzzy logic; and logistic regression; were employed to develop models of mapping landslides in western Colorado. The weight of evidence approach predicted 78% of the observed landslides, the fuzzy-logic approach also predicted 78% of the observed landslides, and the logistic regression approach predicted 86% of the observed landslides.

ACKNOWLEDGEMENTS

As an advisor on all the research presented herein, I would like to express my deepest gratitude to my advisor, Dr. John R. Giardino. Throughout the course of my dissertation, Dr. Giardino has encouraged me to be a better scientist. His kindness, continuous follow-up, useful advice and constructive criticism have been so inspiring to me.

I would like to thank my committee Dr. John D. Vitek, Dr. Christopher C. Mathewson, Dr. Jean-Louis Briaud, and Dr. Douglas J. Sherman for providing guidance, stimulating discussion, and inspiration throughout my study at the Texas A&M University, and revising the dissertation. I also would like to thank Dr. Jack Shroder, Mr. Jonathan White, Dr. Takashi Oguchi, and many anonymous reviewers for their advice and revision of some of the chapters of this dissertation.

I am grateful to the members of the High Alpine and Arctic Research Program (HAARP) for their insightful discussions. Special thanks go to Perry Hotz, Terry Hotz, Dr. John Degenhardt, William Jorgenson, Dr. Douglas Rodriquez, Joni Kincaid, Mark Barker, and Elky Sauter for their time and effort during the fieldwork. I am also grateful to Linda Bledsoe for providing necessary soil data, Rob Hunker for providing high resolution aerial photographs of a landslide in my study area, and Ben Sutherland for helping me in the immersive visualization laboratory.

I am deeply indebted and grateful to the unlimited support provided by my family who encouraged me a lot in order to reach my goal. I would like to take this

opportunity to thank my parents Krishna Kanta Regmi and Deepa Regmi, brother Dr. Murari Regmi, in law Bidhya Regmi, wife Kopila Regmi Paudel, nephew Adarsha Regmi, niece Akriti Regmi and daughter Aanchal Regmi for their love and support.

Finally, I appreciate the help of all the professors and administrative team of the Department of Geology & Geophysics at the Texas A&M University.

Thanks to all who are mentioned above and my apologies if I forgot anyone.

TABLE OF CONTENTS

CHAPTER Page

CHAPTER Page

LIST OF FIGURES

Page

Page

Page

Page

LIST OF TABLES

Page

CHAPTER I

INTRODUCTION

Introduction

Mass movement is a dynamic gravitational process that can be activated by earthquakes, rapid snowmelt, or intense rainstorms. Whereas mass movement plays a major role in the evolution of a hillslope by modifying slope morphology and transporting material from the slope to the valley, it also poses as a potential natural hazard. In recent years landslide studies primarily focused on: acquisition of landslide data, contribution of landslides in the evolution of hillslopes, frequency and magnitude of landslides, and risk and hazard/susceptibility of landslides to human. Identification, mapping, and prediction of the landslides and the volume of mass transported by landslides on potentially unstable slopes are considered as the most important steps in such studies.

Two common methods of acquisition of landslide and landslide dependent data are field survey and classification of remotely sensed imagery. Data acquisition by field survey is time consuming and may be almost impossible in highly rugged terrains and remote areas. Likewise, data acquisition from the remotely sensed imagery is limited by the resolution of the imagery. High resolution satellite data are expensive and only limited information can be obtained from the low resolution satellite imagery. Furthermore, some characteristics of landslides such as type, volume of mass transported,

---

This dissertation follows the style of *Geomorphology*.

and the depths of the slip surface are impossible to determine from even high resolution satellite imagery. Therefore, a method which integrates field survey and remote sensing techniques is necessary to map landslides.

Fluvial incision, glacial erosion, and mass movement modify the topography of a mountain by changing relief, slope, and slope length. Although many studies have been conducted to understand the morphology of incised channels in tectonically active areas, very few studies are focused on the study of channel and hillslope morphology in the areas severely impacted by the mass movements. Furthermore, very few studies are conducted to evaluate the relationship of landslides to other surface processes in regards to the role in hillslope modification.

In recent years mapping susceptibility to landslides and risk has become a topic of major interest among geoscientists, engineering professionals, and community and local administrators in many parts of the world. Remote sensing and GIS techniques have been vigorously used to map landslide hazard/susceptibility and to perform stability analysis of slopes. Combinations of GIS, remote sensing, statistics and computer programming have proven mapping susceptibility to landslides in multiple scales is possible. The current need in landslide studies is a method of mapping landslides in multiple scales and visualizing landslides in three-dimensions.

Problem statement

Similar to the glacial erosion and river incision, landslides modify the relief, slope and slope length of a mountain by transporting material from the slope to the

valley. Not enough observation-based studies have been completed to understand the morphology of the hillslopes developed by landslides. Furthermore, no studies have been carried out to compare the role of landslides and other surface geological process in the evolution of hillslopes.

Previous studies on the frequency and magnitude of landslides suggest that frequency-magnitude of landslides can be explained by an inverse power relationship with two different power values for large landslides and small landslides. The rollover in the value of power function is considered as: the result of undersampling of landslide data, physical condition of the landscape, and geotechnical properties of the materials involved. But we still need to understand what factor is the most responsible for such relationship between landslide frequency and magnitude, and what range of sizes of landslides are most frequent and perform the most geomorphic work.

Similarly, geomorphologists have developed various qualitative and quantitative techniques to map landslide hazards/susceptibility. The qualitative maps of landslide hazard/susceptibility are decision based, and not reproducible. Quantitative maps of landslide hazard/susceptibility, on the other hand, are reproducible, but they contain large uncertainties in dealing with multi-scale landslides. Thus, what is needed is a reproducible and cost effective scale-independent methodology to map susceptibility to landslides. I will develop quantitative methods of mapping landslides for one region of western Colorado, but the methods will be independent of geographic location. In other words, the method should have application to any region without significant error.

Western Colorado, particularly the area ranging from Grand Mesa to McClure Pass, is severely affected by mass-movement of various spatial dimensions. These mass movements damage real estate and destroy structures. From a scientific point of inquiry, one can ask what mass movement processes operate in this area of western Colorado? And, from a practical point of view, one can ask did no one know this place was unstable? Such destruction highlights the need for understanding the processes and for mapping of the landslides in these areas to ensure proper future planning and landslide hazard mitigation.

I will discuss above mentioned issues of landslides in this dissertation based on the landslide and landslide related data collected from western Colorado.

Goals and objectives

The goal of the dissertation research is to understand the dynamics of the hillslope in Paonia-McClure Pass area and use this information to develop valid methods that can be used to map at various scales, ranging from individual landslides to a complete region impacted by mass movement, as part of an overall landslide susceptibility mapping scheme. The focus of this dissertation will be on landslides specifically. I will map other types of mass movement phenomena, but the focus will be the landslides.

To fulfill the goal of the proposed research, the following objectives have been established:

- Create a GIS database of landslides and factors predisposing landslides;

- Plot slope and drainage areas for different landforms developed by the different surface geological processes, and compare the morphology of each types of landforms ;
- Determine the frequency-magnitude relationships of landslides; and
- Create a landslide susceptibility map of the area to understand and evaluate the distribution of the unstable zones in the region;

Description of the dissertation

This dissertation presents new perspectives to evaluate the geomorphology of a periglacial landscape, frequency and magnitude of landslides, mapping landslides and susceptibility to landslides, and visualizing pre-and post- failure three-dimensional morphology of a landslide in immersive technology. In addition to the introduction, the six chapters have been written to fulfill the objectives of the study.

The composition of this dissertation is different than a traditional dissertation. It consists of seven chapters in which five chapters are written in the form of articles for the journal *Geomorphology*. Chapter II presents a methodology to evaluate the morphology of valley heads, colluvial channels, bedrock channels and alluvial channels. The chapter describes how the landscape organizes in response to the different surficial geological processes. Chapter III presents frequency and magnitude of landslides in Paonia-McClure Pass area. The chapter explains major factors behind the rollover effect in inverse power relationship of landslide frequency and magnitude. The chapter also describes the spatial distribution of the landslides in the study area and determines sizes

of landslides which are frequent and perform more geomorphic work. Chapters IV, V, and VI present three methodologies of mapping susceptibility to landslides. These chapters determine major factors causing landslides in western Colorado; calibrate models of mapping susceptibility to landslides; and then validate these models. Chapter IV presents a weight of evidence approach of mapping landslides. Chapter V integrates weight of evidence and fuzzy-logic approaches to prepare maps of susceptibility to landslides. Chapter VI prepares maps of susceptibility to landslides based on the logistic regression approach. Chapter VII presents the conclusion of the study and future directions for the research on landslides. The conclusion involves main results addressing the objectives that were established to answer the problem stated in the Chapter I.

CHAPTER II

CONTRIBUTION OF MASS MOVEMENTS TO LANDSCAPE EVOLUTION

Synopsis

Fluvial incision, glacial erosion, and mass movement, modify topography of a mountain by changing relief, slope and slope length. Under steady state conditions (dz/dt = 0) the local gradient of a channel slope (S) decreases as a power law function of drainage area (A). The intercept of the equation provides information on steepness (k_s), and the power of the equation provides information on concavity (θ) of the channel. A slope-area plot exhibits the geomorphic zones or process domains in mountain topography and provides information about where channels begin.

I employed the slope-area approach to evaluate the morphology of a periglacial landscape in Paonia-McClure Pass area of western Colorado. Forty-six glacial cirques, fifty rock avalanches, nine slope units finely dissected by streams and less influenced by glacial and large deep-seated mass movements, eighty-one landslides including bedrock slides (45) and debris flows (36), and seventy-five channels (17 colluvial channels, 31 bedrock channels influenced by glacial processes, 15 bedrock channels influenced by landslides, and 12 bedrock channels) were mapped at 1:12,000 scale from NAIP 1m resolution orthorectified color aerial photograph and 10m horizontal resolution USGS DEM. The concavity and steepness of these landforms were evaluated and used to interpret the geomorphic changes of the channels as a result of the flux of large amounts of materials from the mountain slopes.

The slope-area plot showed that the study area has five geomorphic zones or process domains: hillslopes (A = 0-0.00085 km^2); valley head (A = 0.00085-0.008 km^2); colluvial channel (A = 0.008-1 km^2); bedrock channel (A = 1-25 km^2); and alluvial channel (A = 25-2500 km^2). The steepness-concavity relationship of these zones can be defined by an exponential relationship. The intercept of this equation defines the processes operating on the mountain slope and the geology, whereas the exponent defines the stability of the landform. The contributing area needed to initiate the channel is the lowest for rock avalanche and the highest for glacial cirques. Average index of steepness and the concavity of the bedrock and alluvial channel is the highest and the colluvial channel is the lowest. The concavities of the colluvial and bedrock channels are found either convex or slightly concave in the river basin where the densities of landslides, glacial cirques, and rock avalanches are high.

Introduction

Fluvial incision, glacial erosion, and mass movement, modify topography of a mountain by changing relief, slope, and slope length (Ahnert, 1970; Brocklehurst and Whipple, 2002; Burbank et al., 1996; Carson and Petley, 1970; Hooke, 2003; Kirkbride and Mathews, 1997; Kuhni and Pfiffner, 2001; Lague and Davy, 2003; Montgomery, 2002; Montgomery and Brandon, 2002; Roe et al., 2003; Roering et al., 2001; Schmidt and Montgomery, 1995; Small and Anderson, 1998; Stock and Dietrich, 2003; Whipple, 2004; Whipple and Tucker, 1999; Whipple and Tucker, 2002). Generally mountain slopes have five types of geomorphic zones or process domains: hillslopes, valley heads,

colluvial channel, bedrock channel and alluvial channel (Montgomery, 2001). The morphology of these zones is the function of the rate of upliftment, and the rate of bedrock incision by the surface processes such as, stream erosion, glacial erosion, and mass movements. Mass movement moves material from the hillslope and valley heads to the channels and modifies the morphology of hillslopes and channels. The modification depends on the flux of the sediments depleted from the hillslope and deposited in the channels. If the sediments from mass movement is debris dominated and the steepness and or energy of the channel is not enough to move the sediments downstream, the morphology of the channel changes.

In this study, I have tested two hypotheses which are very important in understanding the evolution of the periglacial landscape. The first hypothesis is: in a mountainous region impacted by periglacial processes the large amounts of slope material cascading downslope by mass movement can significantly change the morphology of the channels. The second hypothesis is that the valley heads in such terrain tend to remain in a hillslope threshold condition. This study evaluates the role of Earth surface processes in shaping the morphology of landscapes in the basin of North Fork of the Gunnison River in western Colorado.

The study area

The morphology of the North Fork Gunnison River basin and (Fig. 1) its surrounding areas in western Colorado can be described by: a) steep high elevation mountains in which glacial and periglacial processes shaped the Tertiary igneous rocks

including basalt and batholiths of granodiorite (e.g. Chair Mountain, West Elk Mountain, Elk Mountain); b) upland plateaus (e.g., Grand Mesa, Blue Mesa) capped by fluvial deposits and Tertiary basalts; c) mass movement dominated gentle to steep slopes of upland plateaus formed by Cretaceous sedimentary rocks, including shale, mudstone and

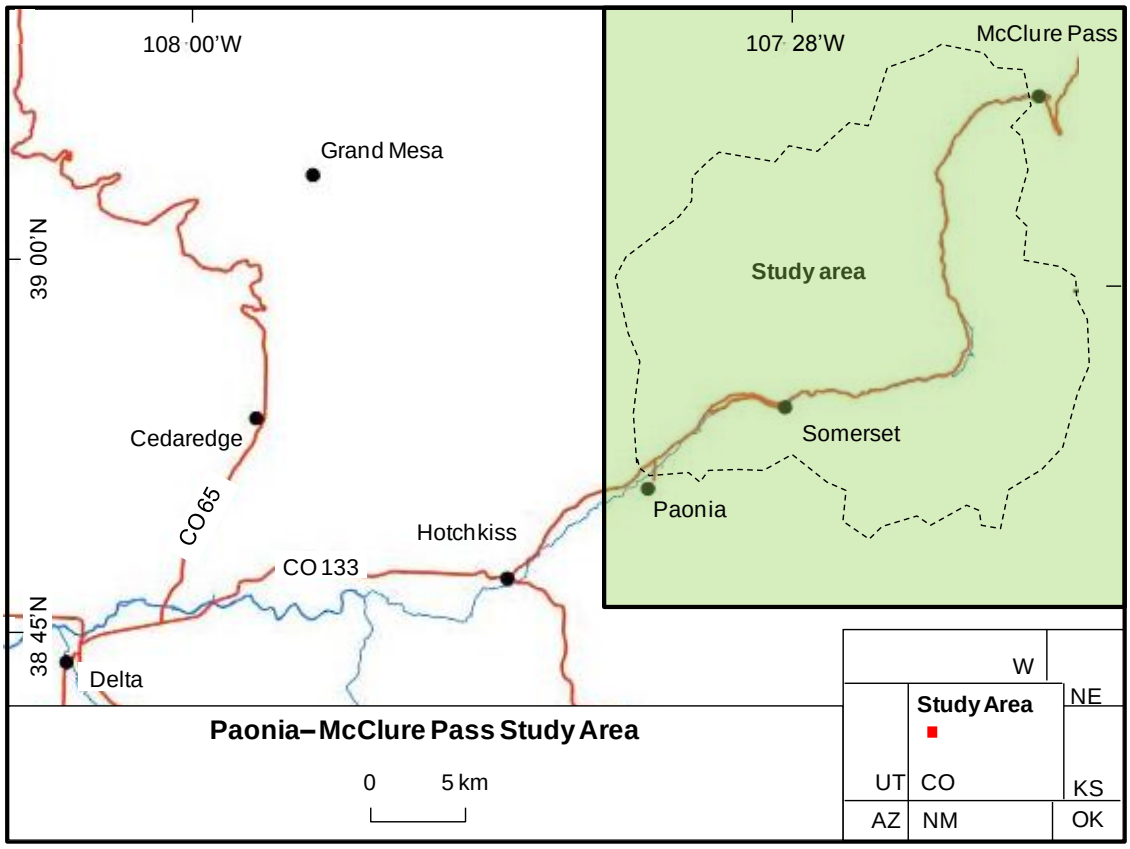

Fig. 1. Location map of Paonia-McClure Pass study area. The dashed line represents the North Fork Gunnison River basin.

sandstone and Quaternary deposits including alluvium, colluvium and mixed deposits; d) river terraces and flood plains; and e) canyons (e.g., Grand Canyon, Gunnision River Canyon) developed by the incision of the major rivers.

Although the geologic setting of western Colorado is a culmination of more than 1.8 billion years of geologic processes, the present topography of the area is dominated by a major period of uplift, erosion, and deposition that started in early Miocene, significantly disrupting and dissecting an Eocene regional erosion surface and continued into the Quaternary time following Canyon cutting and pedimentation until a stable base was achieved (Epis et al., 1980). A major climatic cooling event initiated glaciation, which continued from about 500,000 years ago into the late Pleistocene, ending approximately 15,000 years ago (Epis et al., 1980). The high elevation alpine topography with deep U-shaped valleys, prominent glacial cirques, and sharp peaks and ridges in the study area are largely a product of glacial erosion. Glacial advances deposited numerous sheets of till and outwash gravel in stream valleys. Fluvial geomorphology in the study area is largely characterized by climatically controlled cycles of aggradation and incision (Darling et al., 2009) and result in a series of terraces. The study area includes many upland plateaus, which are relict topography of the Quaternary Period. Some of the plateaus exhibit Quaternary fluvial deposits. The total relief of one of the plateaus near Somerset, with respect to the nearest point at the North Fork of Gunnison River, is ~ 800 m which indicates that the river incised at least 800 m during the Quaternary period. The rate of incision of the Gunnison River, based on the study at and around the Black Canyon of Gunnison and Unaweep Canyon in western Colorado, varies from 61 to 142 m/Ma (Aslan et al., 2008). Similarly, I assessed the total incision of the Gunnison River as ~1,550 m over 10 Ma based on the elevation of the 10 Ma old basalt capped Grand Mesa (3,050 m) and Delta (1,500 m) which indicates that

the rate of incision of the Gunnison River is at least 155 m/Ma. The present landforms in the study area developed by the Quaternary climate change, river incision and associated mass movement are glacial cirques, highly dissected regions, and large and deep seated landslides and rock avalanches.

Many glacial cirques, developed on Chair Mountain and West Elk Mountain, are occupied by rock glaciers, and talus deposits. Some cirques have been impacted by river incision. Talus deposits have accumulated at the base of the cirques and steep slopes. Steep slopes on Chair Mountain and West Elk Mountain exhibit zones of many active rock avalanches. These processes developed small linear gullies on the slopes and deposited huge amounts of debris at the base of the slope.

The study area has a finely dissected landscape around the Somerset (Figs. 1 and 2). The area has a higher value of drainage density and standard deviation of elevation (100 m diameter window) in comparison to its surrounding regions. The area is comprised of inter-layered sandstone and mudstone of the Mesaverde Formation. I believe the landscape is mainly the result of the stream erosion. Although very shallow landsliding and surface erosional features are present, the area has no signatures of glacial erosion and large deep-seated mass movements. High shear resistance to erosion is the main reason the area preserved the dissected landscape.

Whereas the study area has steep and stream dissected slopes on the lowland, the upland slopes have bench-like, low-gradient topography with poorly developed drainage networks. Landslides are common on slopes of Quaternary deposits. On the middle and the lowland slopes, the valley network facilitates the delivery of sediment from

hillslopes and topographic hollows to higher-order channels via active small debris flows, debris slides, rock slides and soil slides. The edges of the upland with a gentle to flat landscape are degraded by the large bedrock landslides and debris flows. Large landslides are mostly stable and dormant and occurred at the heads of the streams incising uplands. The headscarps of some landslides are still active and producing shallow landslides. In this study only large landslides (>160,000 m^2) were included in the analysis. Among the landslides studied, most of the large landslides are very old. The surfaces of these landslides are covered by dense vegetation, whereas small landslides, including debris flows and shallow bedrock slides, occurring at the headscarps of large deep-seated landslides are active and devoid of vegetation. Most of the large landslides originated from the ridge of the basin and extended to the major channels. Landslides are clustered and found at the head of the upland incising streams and show typical characteristics of upland steepening. Other examples of large landslides are at the edges of a plateau at the central area of the map (Fig. 2). These large landslides show an example of how an upland plateau degrades because of the retrogression of the large landslides as well as how landslides modify the topography by upslope steepening and the downslope becoming a gentle.

Methods

The morphology of a landscape can be described by its: a) concavity, and b) steepness. Under steady state conditions ($dz/dt = 0$) the local gradient of a channel slope (S) decreases as a power law function of drainage area (A). The intercept of the equation

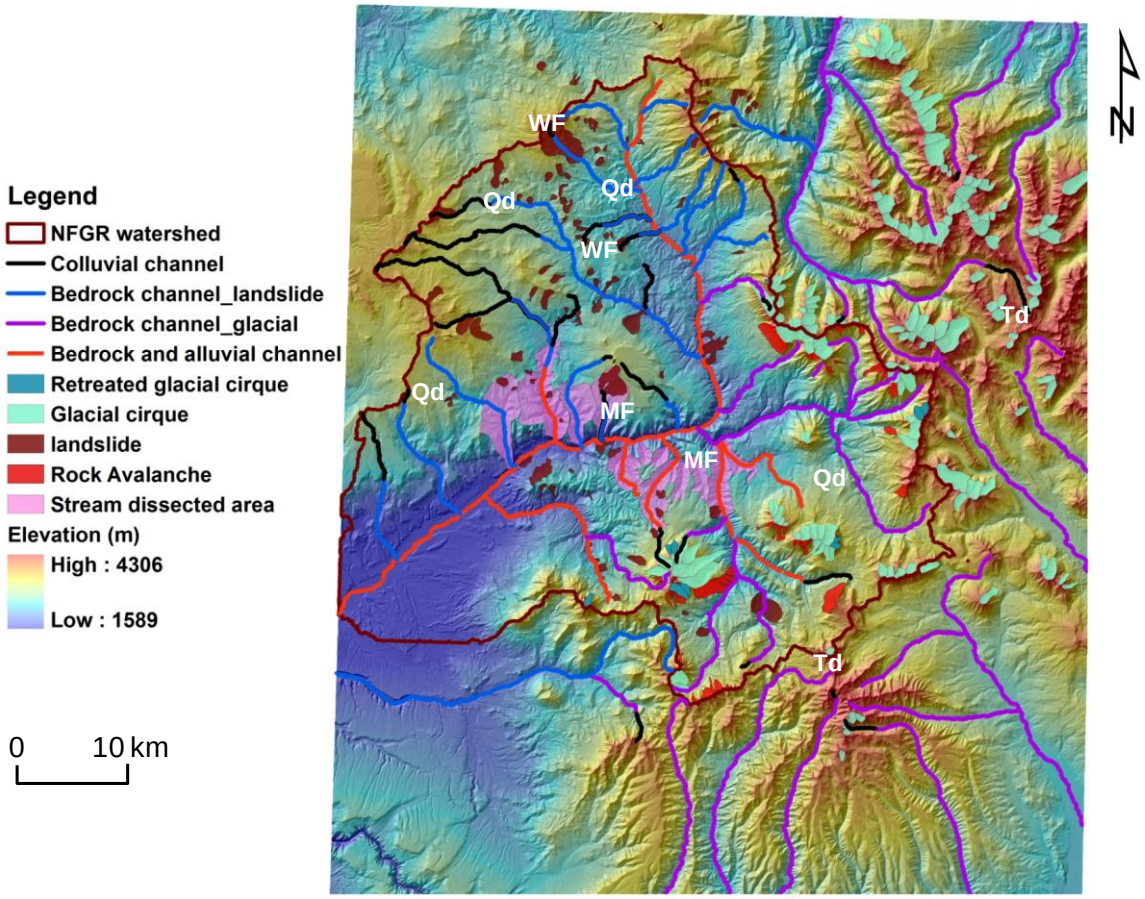

Fig. 2. Distribution of landforms developed by different surface geological processes in and around the North Fork Gunnison River (NFGR) basin. The types of channels were mapped on 1m NAIP color aerial photographs. Colluvial channels are defined as the channels which are in the colluvial deposits and are not deeply incised. Bedrock channels are incised up to the bedrock. Bedrock channels were further classified as influenced by landslides (bedrock channels_landslides) and influenced by glacial processes (bedrock channel_glacial). Landslides (bedrock slides and debris flows), rock avalanches, glacial cirques, and stream dissected areas were mapped. Stream dissected areas are defined as slope units which were mainly developed by the incision of the river and were not affected by glacial processes and large deep-seated landslides. Quaternary deposits (Qd), comprised of unconsolidated colluvium, alluvium and glacial drift. Wasatch Formation (WF), comprised of sandstone and mudstone. The WF rocks are exposed in many localities, where the valley heads are active and producing large deep-seated and shallow landslides, within the upper left section of the map. Mesaverde Formation (MF), comprised of sandstone and mudstone, is exposed around Somerset (see Fig. 1). Tertiary igneous rocks (Td) are exposed on the high elevation mountains. The mountains are carved by the glacial processes.

is known as steepness (k_s), and the power of the equation is known as concavity (θ) of the channel. Steepness and concavity can be determined by the regression of the slope and drainage area (Flint, 1974; Moglen and Bras, 1995; Sklar and Dietrich, 1998; Snyder et al., 2000; Tarboton et al., 1988).

$$S = k_s A^{-\theta} \tag{1}$$

Comparing values of k_s measured on different profiles can be confounded by the inherent scale-dependent co-variance of regression intercept with regression slope. Dependence of k_s on (θ) can be removed by normalizing the drainage area (A) by the representative area (A_r) (Sklar and Dietrich, 1998). Eq. 1 can be rewritten as:

$$S = S_r (A / A_r)^{-\theta} \tag{2}$$

From equations (1) and (2):

$$S_r = k_S A_r^{-\theta} \tag{3}$$

where S_r is a representative slope, considered as an index of steepness. S_r in Eq. 3, is a dimensionless index which depends on the reference area (A_r). To reduce this effect, A_r can be chosen as the representative area of the entire area studied. S_r can be used to check the assumption of uniformity in rate of incision, relief, and lithology within a drainage basin by comparing S_r values obtained from individual sub-basin profiles (Sklar and Dietrich, 1998).

Forty-six glacial cirques, fifty rock avalanches, nine slope units which are finely dissected by streams and less influenced by glacial erosion and large deep-seated mass movements, eighty-one landslides including bedrock slides (45) and debris flows (36),

and seventy-seven channels (17 colluvial channels, 31 bedrock channels influenced by glacial processes, 15 bedrock channels influenced by landslides, and 12 bedrock channel segments) were mapped at 1:12,000 scale from NAIP 1m resolution orthorectified color aerial photograph and 10 m horizontal resolution USGS DEM (Fig. 2). Some of these landforms were verified by the field reconnaissance. Slope and drainage area for each landform (glacial cirque, avalanche, stream dissected slope unit, and landslide) were plotted and indices of concavity and steepness were determined by the random axis regression (RMA) method. Then, these indices were evaluated.

Results

Generalized slope-area plot of the study area

This study developed slope-area curves of the entire North Fork Gunnison River watershed (Fig. 3) and selected landforms within the watershed (Fig. 4). The slope-area plot provided information on the overall location of the points of colluvial channel initiation, bedrock channel initiation, and alluvial channel initiation. Furthermore, the curve provided information on the overall steepness and concavity of the different types of geomorphic zones within the entire watershed and the selected landforms (debris flows and bedrock slides, glacial cirques, rock avalanches, and stream dissected areas) (Fig. 3).

The slope-area plot indicates that five geomorphic zones are present in the study area: hillslopes (A = 0-0.00085 km^2); valley heads (A = 0.00085-0.008 km^2); colluvial

channels (A = 0.008-1 km^2); bedrock channels (A = 1-25 km^2); and alluvial channels (A = 25-2500 km^2). Each geomorphic zone has a characteristic morphology, and one or more surface geological processes were responsible for the development of these geomorphic zones. The steepness, concavity, and relief of these zones depend on the processes operating and the lithology.

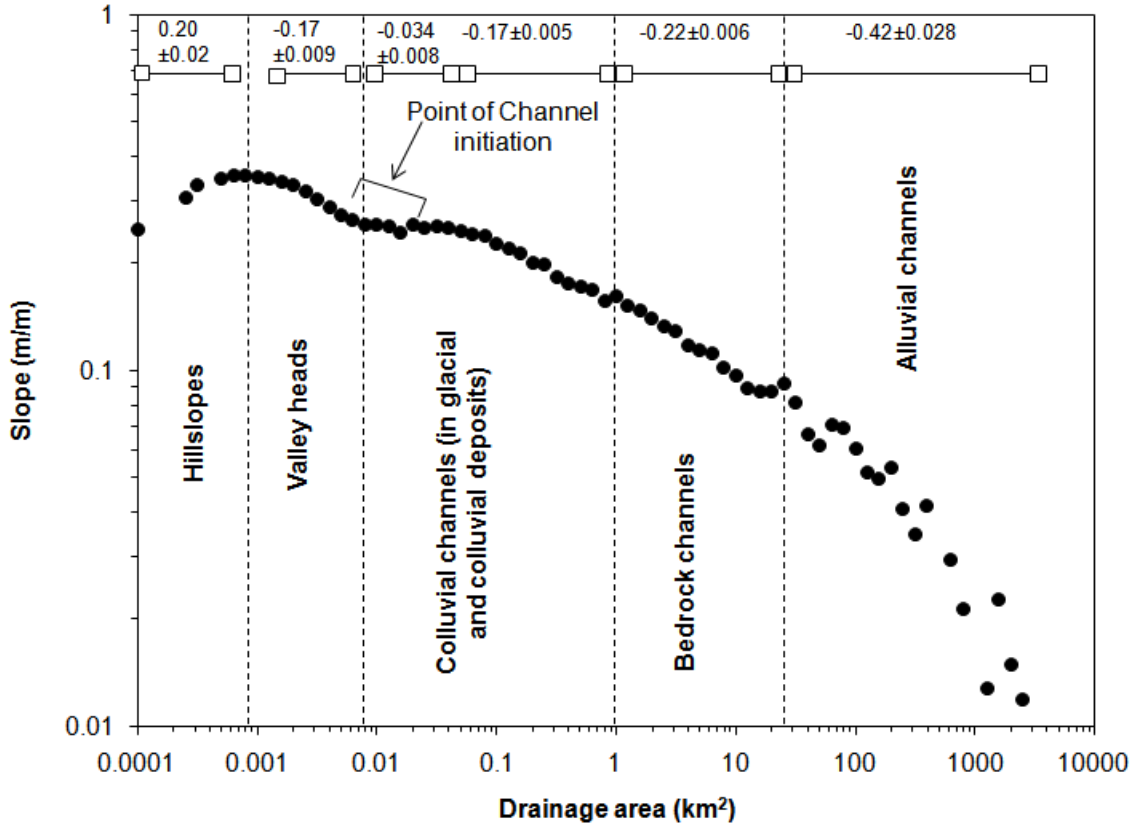

Fig. 3. Plot of log-bin averaged drainage area versus slope for the entire North Fork Gunnison River basin. Data derived from 10 M DEM. The plot shows the mean slope for the individual 10 m grid cells for each 0.1 log interval in drainage area. Numbers shows the exponent for a power function regression of values in the segments of the plots indicated by bars connecting open squares. These values can be considered as generalized indices of concavities of these geomorphic zones. Dashed vertical lines divide the plot into areas considered to reflect different geomorphic zones or the process domain in the study area. The exponent values were determined by the random major axis (RMA) regression.

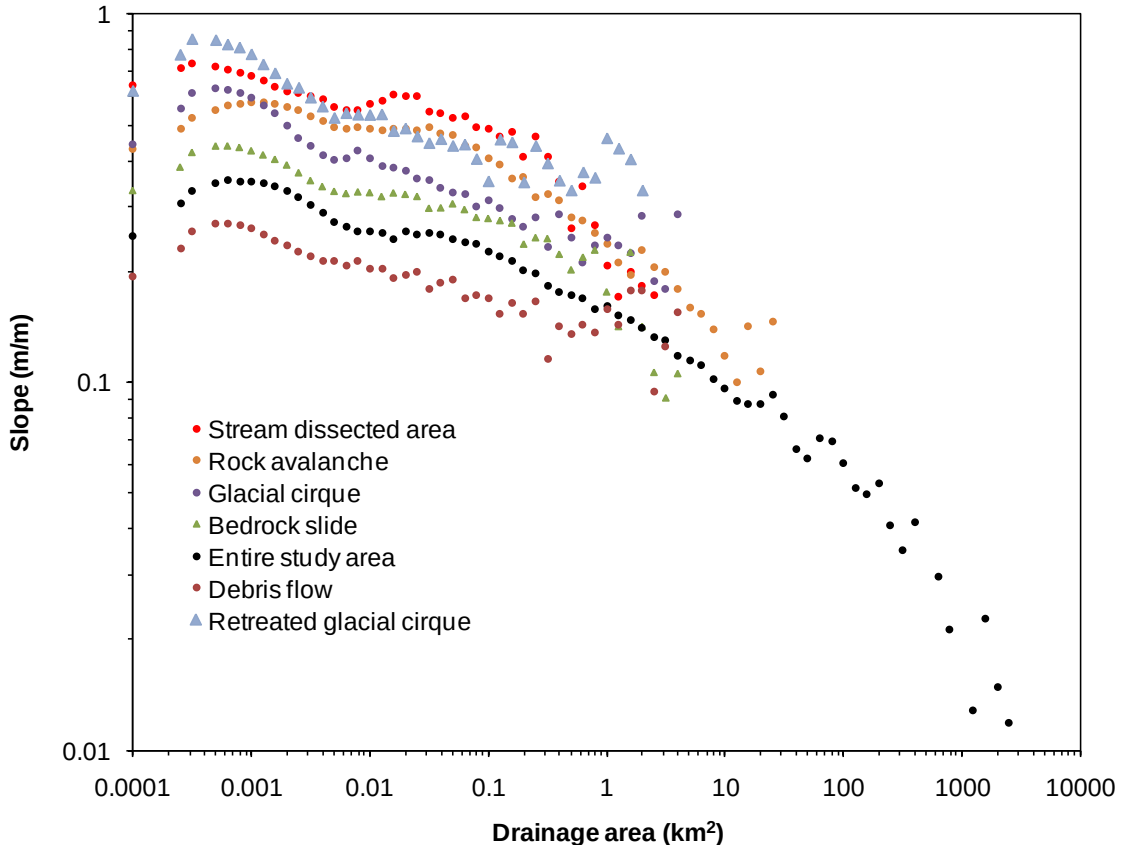

Fig. 4. Plot of log-bin averaged drainage area versus average slope for the entire North Fork Gunnison River and associated landforms. Data were extracted from 10 m USGS DEM. Similar to Fig. 2, the plot shows the mean slope for the individual 10 m grid cells for each 0.1 log interval in drainage area.

I defined the topographic relief as: a difference in elevations of the location of the channel initiation and the head of the landform. The slope-area curves also provided information on topographic relief of different landforms developed by different processes. Assuming the contributing areas needed for the initiation of channels in studied landforms are not significantly different, the steepness of each curve can be used to compare the reliefs of these landforms. Higher the steepness suggests higher the relief. These curves imply that the glacial cirque has the highest relief which is followed by the bedrock slides and rock avalanches. The relief produced by the debris flow is the least.

But these curves do not take into account the frequency and magnitudes of the forces in the geomorphic processes that operated on these landforms. Shallow landslides and rock avalanches occur mostly in a single event, such as an earthquake, or a heavy rainfall, whereas the glacial cirques, and the stream incised slopes are the results of multiple events of glacial erosion and stream erosion, respectively, over a long period of time. This study discusses only large deep-seated landslides and rock avalanches (>160,000 m^2). These landforms are considered as very old, because the landslides are covered by the dense vegetation, and the rock avalanches deposited large amounts of talus at the base of the slope. Furthermore many shallow landslides occur at the headscarps of the large landslides. Although these characteristics imply that the landforms are very old and developed by multiple events, it is still not prudent to compare the relief produced by each of these landforms.

Where do channels begin?

The location of the channel initiation in a landscape depends on many factors, including: contributing area; morphology of the landscape (i.e., concavity, steepness, relief, and slope); lithology; and the processes operating on this landscape. The location of channel initiation controls the overall morphology of the landscape. The closer channels begin to drainage divides, the greater the number of channels that occupy a unit area, and consequently the more finely dissected the landscape becomes. Channels begin closer to the drainage divide in concave landforms because surface water converges and develops a channel right at the base of the valley heads. Channels begin at longer

distances from the drainage divide on planar slopes. Similarly, channels may initiate at significantly different locations in soil mantled landscape and rocky terrain.

Based on the breaks in the slope of area-slope curves (Fig. 4), the locations of channel initiation in different landforms were calculated (Table 1). The data shows that the channel initiation depends on local gradient and contributing area. The contributing area for the beginning of a colluvial channel varies from 0.008± 0.004 km^2 to 0.025± 0.024 km^2. A channel begins at the least contributing area in rock avalanches and at the largest contributing area in glacial cirques. But it is necessary to understand that the locations of channel initiation proposed in this study is only based on the analysis of the DEM. In some cases the approach provides the wrong results; for example, in some rock avalanches the gullies developed by the avalanching of slope material downstream rarely contain water. Similarly, debris flows do not develop well defined gullies at the heads of the debris flow scar but contain water.

Table 1 Concavity, average drainage areas, and the average gradients at the locations of initiations of the colluvial and bedrock channels.

Landform	θ	Colluvial channel initiation		Bedrock channel initiation	
		A	*S*	*A*	*S*
Retreated glacial cirque	0.1761±0.027	0.014±0.009	0.49±0.10	0.19±0.17	0.30±0.12
Glacial cirque with rock glaciers	0.1709±0.056	0.025±0.024	0.34±0.09	NA	NA
Bedrock slides	0.1577±0.11	0.008±0.004	0.36±0.10	0.31±0.24	0.35±0.23
Rock avalanche	0.0852±0.047	0.0086±0.006	0.54±0.14	0.21±0.12	0.50±0.10
Debris flows	0.1385±0.058	0.009±0.006	0.21±0.07	0.48±0.36	0.15±0.076
Stream dissected regions	0.0932±0.041	0.0097±0.003	0.47±0.08	0.50±0.47	0.32±0.11

The average local gradient of the locations of channel initiation in retreated glacial cirques is 0.49±0.10 whereas the average gradient for glacial cirques with rock glaciers is 0.34±0.09. The concavity of the cirque increases and the steepness and relief decreases when the wall of the cirque is incised by the streams. Results show channels begin at a location closer to the crown of the cirque.

The average local gradient of the channel location in a rock avalanche is 0.54±0.14. Rock avalanches occur on steep slopes underlain by resistant rocks. They have higher indices of steepness and lower indices of concavity (0.0852±0.047). Furthermore, the drainage area needed for the initiation of channels is far less than other landforms described in this study. The interpretation is: on steep slopes the soil thickness is low so that the overland flow easily can exceed the water absorbing capacity of the soil and rock and can converge to create a channel. Furthermore, the high frequency of the avalanches create gullies on the slope which help to converge the overland flow.

Table 2 Concavity and steepness of stream channels.

Landform	θ	S_r (A_r = 4 km^2)
Colluvial channel	0.4662±0.36	0.058±0.02
Bedrock and alluvial channels_glacial	0.4768±0.17	0.19±0.09
Bedrock and alluvial channels_landslides	0.3913±0.29	0.19±0.21
Bedrock and alluvial channels	0.4853±0.39	1.92±5.68

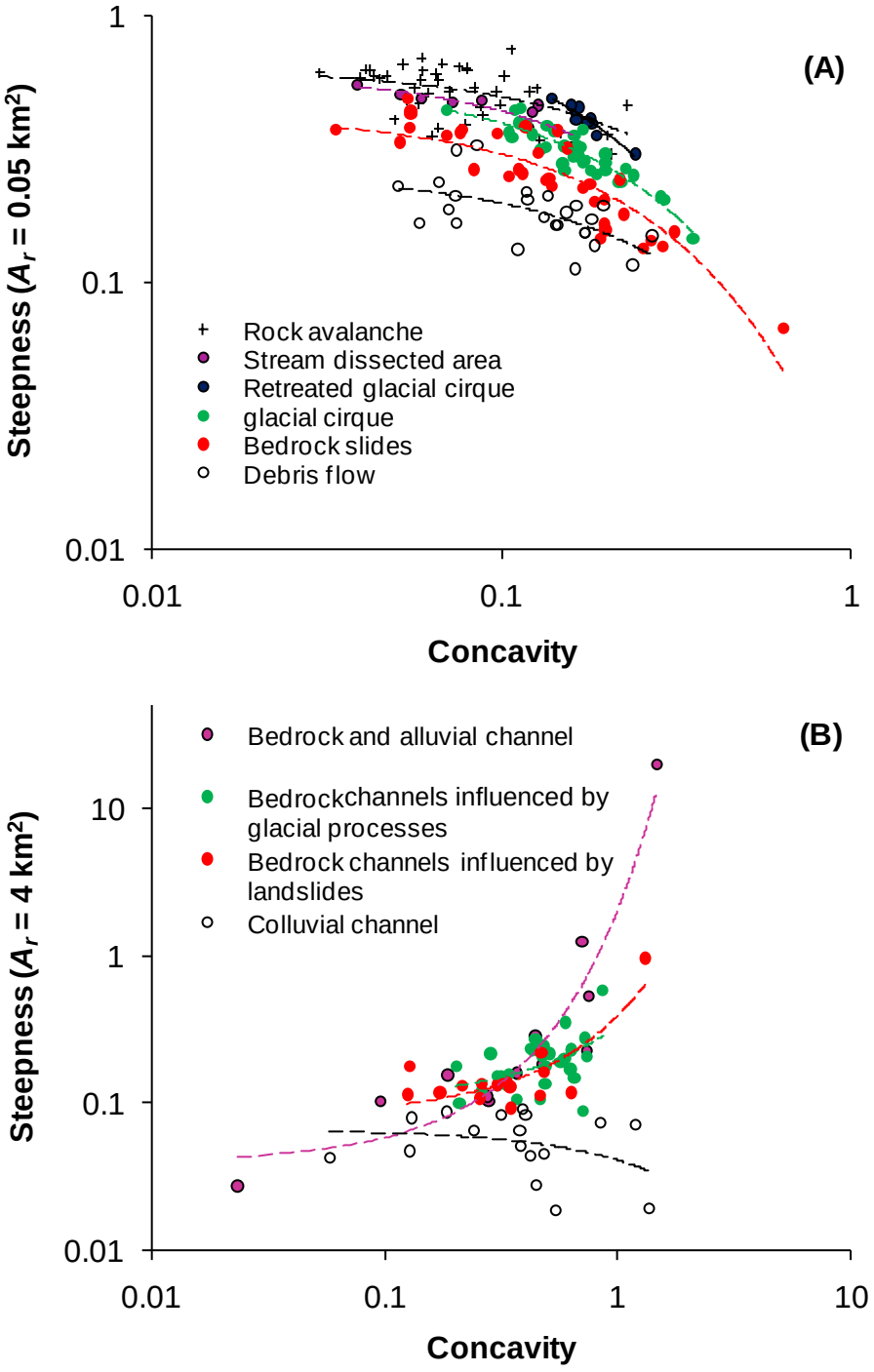

Fig. 5. Steepness and concavity of: A) valley heads and deposits of the selected landforms, and B) channels. The reference area (A_r) for the valley head is taken as 4 km^2 (drainage area of the landforms ranges from 0.001 – 1 km^2).

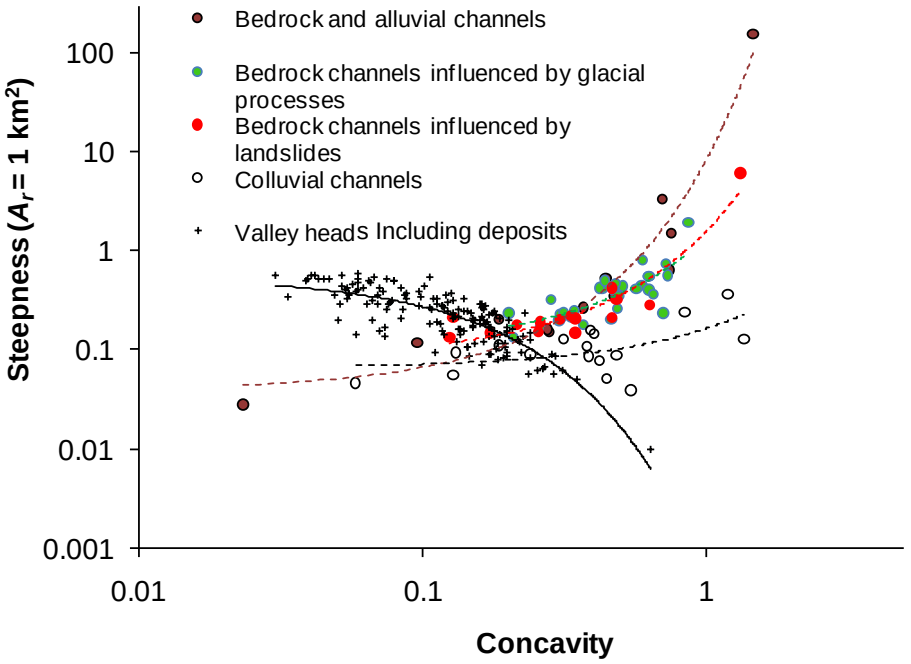

Fig. 6. Steepness and concavity indices of valley heads and deposits of the selected landforms, and different types of channels. The reference area is taken as 1km^2 for the range of the drainage area from 0.01 km^2 to 2500 km^2 (see Fig. 3).

The average of the local gradient required for the initiation of channels in a bedrock slide is 0.36±0.10. The concavity and the steepness of the slopes having bedrock slides are intermediate. Similarly, the drainage area and the local gradient needed for the initiation of the channel in a bedrock slide is intermediate in comparison to other forms. The stream dissected area (Fig. 2) is comprised of the same rock types observed in most of the bedrock slides. The steepness of these landforms is slightly higher than the steepness of the bedrock slides whereas the concavity is slightly lower than that of bedrock slides. The location of the channel initiation is somewhat similar.

Debris flows included in this study are very much younger than the bedrock slides. The concavity and steepness of these landslides are slightly higher than the surrounding stable regions but are the lowest in comparison to other landforms.

Concavity and steepness distribution

The steepness-concavity plots for the channels and the selected landforms indicate that the relationship is exponential (Figs. 5 and 6). Furthermore, each type of the landforms and channels studied have upper and lower boundaries in the relationship. The steepness-concavity relationship for channels obtained in this study (Fig. 5B, and Table 2) is similar to Brocklehurst and Whipple (2002), and Sklar and Dietrich (1998). The relationship can be expressed by:

$$S_r = \beta e^{-\gamma\theta} \quad (4);$$

and

$$S_r = \beta e^{\gamma\theta} \quad (5)$$

In these equations β and γ are non-dimensional parameters. The first parameter is the intercept of the exponential curve controlled by the processes and lithology, whereas the second parameter, the slope of the exponential curve, defines the stability of the form. The steepness-concavity plot of the landforms away from the best-fit line, suggests either the associated process of the landform is changing or the landform is just on the beginning stage of the evolution or changing to an another form. One form can change

into another when the process is changed. Similarly, a change in the form can change the process.

Concavity and steepness of studied landforms

The concavity and steepness of landforms are related by the negative exponential function (Figs. 5 and 6). This suggests that the hillslope with gentle gradient or with a wider drainage basin has higher concavity. Slopes with the steepness-concavity curves for the studied landforms are quite similar whereas the intercepts are different (Fig. 5). This means the processes are different and most of the landforms are stable (Eqs. 4 and 5). For example, glacial cirques which are retreating are unstable and are being modified into another form. The steepness-concavity of these landforms is quite different than the glacial cirque, and indicates that two different processes are operating on them. The result also suggests that a change in a dominant process changes the concavity and steepness of the hillslope.

The generalized steepness-concavity relationships of the different landforms indicate that the steepness of the debris flow is the lowest among all other landforms. Similarly, the steepness of the rock avalanches is the highest among others. Concavities for all landforms, however, are not significantly different.

Concavity and steepness of channels

The concavity and steepness relationship of the channels are significantly different than that of landslides, glacial cirques, and rock avalanches. When the

reference area to calculate steepness index is selected as mean drainage area (A_r = 4 km^2) in the data range (Fig. 3), the steepness-concavity of the bedrock and alluvial channels relate by a positive relationship whereas the steepness-concavity of colluvial channels relate by the negative relationship with a very small negative exponent value. The distribution also shows that the exponent value for the bedrock channels is the highest among all kinds of channels. These graphs indicate that the steepness and the concavity of the colluvial, and bedrock and alluvial channels are significantly different, but when colluvial channels are modified by river incision the steepness increases. In contrary when bedrock channels are loaded by the huge amounts of sediment from the hillslope the concavity of these channels decreases (Fig. 7). The selection of the appropriate representative area (A_r) is very important because S_r depends on A_r. If the reference area increased, the exponent becomes smaller, and for a very high reference area it becomes negative. In contrast, if the reference area decreased, the value of the exponent increases.

Controls of lithology and processes

Hillslope and channel organization are always controlled by the combining effect of processes, geology, and the instability state of the landscape. For example, bedrock slides occur on the rocks with higher discontinuities, debris flows occur at topographic convergence where soil and debris is accumulated, glacial cirques are stable only where hard rock is present, and rock avalanches mostly occur because of the freezing and thawing of rocks on steep slopes. In my study area glacial cirques and rock avalanches are located in Tertiary igneous rocks, rockslides are located in the sandstone and

mudstone of Mesaverde and Wasatch Formations, and debris flows are located in Quaternary unconsolidated deposits.

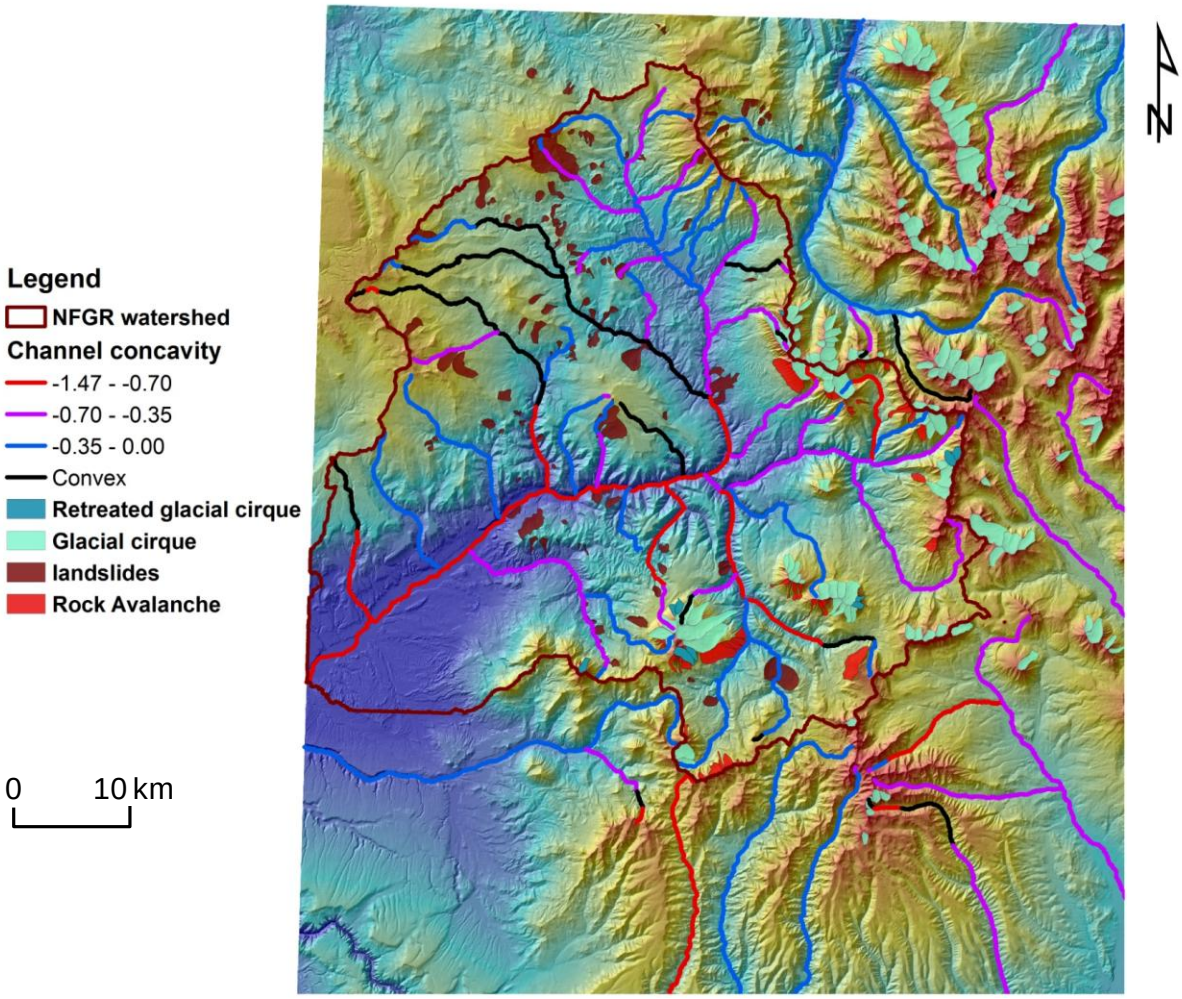

Fig. 7. Concavities of the channels in and around the North Fork Gunnison River (NFGR) watershed.

The instability state of the slope controls the organization of the landform morphology. The distribution of slopes (Fig. 8) suggests that slopes of selected landforms, except debris flows, are almost normally distributed. If the normal

distribution of the slope of a landscape suggests the landscape is in hillslope threshold condition (Burbank et al., 1996), my studied landforms are in hillslope threshold condition. Whereas the bases of the channels are in stable condition, this should be the major reason for difference in the steepness-concavity relationships of these two different geomorphic zones.

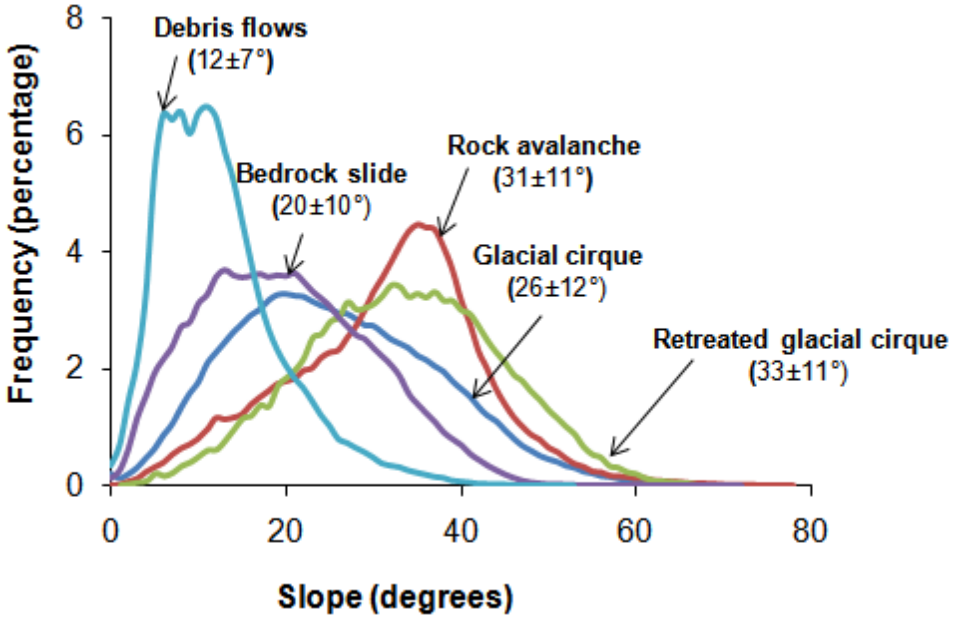

Fig. 8. Smoothed histogram of slopes of debris flow, bedrock slide, rock avalanche, glacial cirque, and retreated glacial cirque. The interval of the data point is 1°. Values in the brackets are the mean and standard deviation of the slopes.

Geology also controls the morphology of the channels. Channels can be convex around knickpoints (Kirby et al., 2003) or at the transition of the hard rock and unconsolidated deposits. In this study some of the convex channels are observed in unconsolidated deposits (Qd) and Meseverde and Wasatch Formations. The density of the landslide is also higher in these regions; therefore, I believe the channels are convex

in these localities because of the large flux of sediments from landslides to the channels as well as the geological complexity. Furthermore, most of the bedrock and alluvial channels in areas affected by glaciation (eastern half of the map) have lower concavity than the bedrock and alluvial channels in North Fork Gunnision River basin. Although major bedrock and alluvial channels in the eastern section are as large as the major rivers in North Fork Gunnison River basin, the concavity is lower. The area has a higher density of glacial cirques, most of which were occupied by rock glaciers. Assuming uniform incision of the river as a response to the uniform tectonic uplift and similar lithology at the lower slope of the river basins in both sections, I concluded that the large amount of the glacial erosion and mass movement derived sediments from hillslopes to the channels is the major factor responsible for the lower concavity of these channels. Overall the clustering of the landslides, rock avalanches, and areas of huge potential for sediment production modified the concavity of the channels.

Discussion and conclusions

Landscape organization in a periglacial environment is quite complicated and very difficult to understand. Change in surface geomorphic processes either because of the change in climate, or tectonic uplift, and or change in base level modifies the shape of the landscape. Intense river incision as a response to the high rate of tectonic uplift creates steep and concave stream channels. Climate change and landscape tendency to achieve isostatic equilibrium increases the frequency of mass movement by different types of surface geological processes, such as glacial erosion, fluvial erosion, and mass

movement. The Paonia-McClure Pass area of western Colorado has a history of a fast rate of uplift during the Quaternary period. Intensely incised channels along with many river terraces reveal the incisional and aggradational history of the area. Presence of glacial valleys suggests that the region also experienced glaciations. Huge amounts of unconsolidated Quaternary deposits, and a large number of scars of large and deep seated landslides, rock glaciers, and glacial cirques suggest that over time sediments moved from the hillslopes to the channels. I have tested an approach to evaluate the effect of all these processes in channels and found that in Paonia-McClure Pass area mass movement contributed to the modification of channel morphology. Furthermore, I evaluated the morphological organization of the different geomorphic zones or process domains in the study area. This study suggests that the steepness-concavity of the valley heads relates by the negative exponential relationship while the steepness-concavity of the channels is related by the positive exponential relationship. The normally distributed slopes in the active valley heads (i.e., rock avalanche landslide, glacial cirque) suggest that these landforms are in a hillslope threshold condition. When the concavity of these landforms increases because of the upslope incision by different surface geological processes, the valley heads decrease the steepness by moving material from the slope to the channels to remain within the threshold condition.

I also observed that the concavity of the streams which received large fluxes of sediment from mass movements is comparatively low. The colluvial and bedrock channels in Quaternary deposits and recent landslide deposits in the study area have low concavities. Similarly the bedrock channels in basins which have higher density of

glacial cirques (eastern half part of the study area) also have comparatively low concavities.

In addition, I have studied the steepness and concavity of the landforms developed by different types of surface geological processes. Rock avalanches have the highest steepness, and debris flows have the lowest steepness. Similarly glacial cirques have the highest concavity and the rock avalanches have the lowest concavity.

CHAPTER III

CHARACTERISTICS OF LANDSLIDES IN PAONIA TO MC-CLURE PASS AREA, COLORADO, USA

Synopsis

Mass movement can be activated by earthquakes, rapid snowmelt, or intense rainstorms in conjunction with gravity. Whereas mass movement plays a major role in the evolution of a hillslope by modifying slope morphology and transporting material from the slope to the valley, it is also a potential natural hazard. Determining the relationships of frequency and magnitude of landslides are fundamental to understanding the role of landslides in the study of landscape evolution, hazard assessment, and determination of the rate of hillslope denudation.

I mapped 735 shallow and active landslides in the Paonia to McClure Pass area of western Colorado from aerial photographs and field surveys. The study area covers ~815 km^2. The frequency-magnitude relationships of the landslides illustrate the flux of debris by mass movement in the area. The comparison of the probability density of the landslides with the double pareto curve, defined by α (power scaling for negative slope), β (power scaling for positive slope) and t (location of rollover), shows that $\alpha = 1.1$, $\beta = 1.9$ and $t = 1{,}600$ m^2 for areas of landslides, and $\alpha = 1.15$, $\beta = 1.8$ and $t = 1{,}900$ m^3 for volumes of landslides. The total area of landslides is 4.8×10^6 m^2 and the total volume of the landslides is 1.4×10^7 m^3. The areas (A) and the volumes (V) of landslides are related by $V = 0.0254\times A^{1.45}$. The frequency-magnitude analysis shows that landslides with areas

ranging in size from 1,600 m^2 - 20,000 m^2 are the most hazardous landslides in the study area. These landslides are the most frequent and also do a significant amount of geomorphic work.

I also developed a conceptual model of hillslope development to upland plateau driven by river incision, shallow landsliding and deep-seated large landslides. The gentle slope to flat upland plateau that dominated Quaternary landscape of the study area was modified to the present steep and rugged topography by the combined action of fluvial incision and glacial processes in response to rock uplift, very frequent shallow landsliding and less frequent deep-seated landsliding.

Introduction

Landslides, complex natural phenomena, are the results of the variety of geomorphic, geologic and hydrologic factors which predispose hillslopes to instability. Events like earthquakes, intense rainfalls, and snowmelt trigger cascading mass from slopes (Keaton, 1988; Santi, 1988). Landslides play a significant role in the modification of the hillslope by transporting sediments from a slope to the base of that slope. Most shallow landslides result from triggering by rainfall and earthquakes and are important tools in contributing to sediment yield (Burton and Bathurst, 1998; Glade, 2003). Landslides and landslide gully complexes in the upland catchment are the sources of the stream deposits in lakes and swamps (Eden and Page, 1998; Hicks et al., 2000; Page et al., 1994). The amount of debris mobilized by landslides depends on a combination of the spatial distribution and frequency of triggering events, the number of failures

triggered in a given event, the probability distribution of landslide volume for such a triggering event and the flux of the debris from landslides into the channel network (Stark and Guzzetti, 2009).

For at least four decades researchers have been investigating the relationships of magnitudes and frequencies of landslides in different lithological and geomorphological terrains to understand the role of landslides in sediment yield, landscape evolution, and as hazards (Fujii, 1969; Whitehouse and Griffiths, 1983; Noever, 1993; Somfai et al., 1994; Hovius et al., 1997; Pelletier, 1997; Crozier, 1999; Crozier and Glade, 1999; Hovius et al., 2000; Dai and Lee, 2001; Stark and Hovius, 2001; Guzzetti et al., 2002; Martin et al., 2002; Brardinoni and Church, 2004; Guthrie and Evans, 2004a, 2004b; Malamud et al., 2004; Korup, 2005; Guthrie and Evans, 2007; Guzzetti et al., 2008; Stark and Guzzetti, 2009). The magnitude of a landslide, defined as the capability to produce change and or the energy associated with the detached mass (Corominas et al., 2003), is represented by the area of a landslide scar (Hovius et al., 1997; Hovius et al., 2000), or the total area of a landslide (Pelletier, 1997; Guzzetti et al., 2002), or the volume of the material displaced by a landslide (Hungr et al., 1999; Dai and Lee, 2001). Frequency of landslides is defined as the number of landslides related to a single event or the various events that occurred in the past. Almost all investigators obtained a power relationship between the frequencies and magnitudes of landslides. Interestingly, a rollover effect appears on a graph of frequencies and magnitudes. A rollover is a point from where the frequency-magnitude relationships of smaller landslides cannot be explained by the power law representing the frequency-magnitude relation of large and

medium sized landslides. Reasons for the rollover have generally been attributed to an inability to consistently resolve and map all small landslides at a given scale (Hungr et al., 1999; Stark and Hovius, 2001; Brardinoni et al., 2003; Brardinoni and Church, 2004), physical condition of the hillslope on which the landslides occur (Pelletier, 1997; Hovius et al., 2000; Guzzetti et al., 2002; Martin et al., 2002; Brardinoni and Church, 2004; Guthrie and Evans, 2004a, 2004b), consequence of material strength limiting the number of small slides and the overall slope geometry that limits the number of very large slides (Pelletier, 1997; Guzzetti et al., 2002), and self organized criticality (Noever, 1993; Hergarten and Neugebauer, 1998). Pelletier (1997) suggested that the rollover might represent the transition from a resistance controlled by friction (large landslides) to a resistance controlled by cohesion (small landslides). The same explanation has been adopted to interpret frequencies and magnitudes of landslides in a study of snowmelt triggered landslides in central Italy (Guzzetti et al., 2002).

The geomorphological expression of the landscape develops by the transfer of mass from unstable zones on steep slopes and highlands to fluvial and coastal lowlands by integrated erosional processes of wind, water or ice, and mass movements. Comparatively, landslides transfer considerable volumes of slope material and play an important role in the shaping the landscape. In many humid upland landscapes, evolution of the hillslope is dominated by landsliding across a wide range of length scales (Anderson, 1994; Gerrard, 1994; Greenbaum et al., 1995; Schmidt and Montgomery, 1995; Burbank et al., 1996). This nature of landslides can be quantified in terms of the geomorphic work. The work performed by a landslide is defined in terms of

destructiveness (Evans, 2003; Malamud et al., 2004), fragmentation energy (Locat et al., 2006), runout (Hungr and Evans, 2004; McClung, 2000), volume (Innes, 1983; Hovius et al., 2000; Martin et al., 2002), combination of volume and expected velocity (Cardinali et al., 2002; Reichenbach et al., 2005), or the product of magnitude and frequency or probability of landslide occurrence (Guthrie and Evans, 2007). Geomorphic work of landslides over time depends on magnitudes (area, volume, runout length, and width), and frequencies of the landslides. Large landslides displace large volumes of materials and leave geomorphic signatures for many years (Korup, 2006). But the frequency of occurrence of large landslides is very low. In contrast, small landslides are frequent but displace only very small amounts of slope material at a time. Furthermore, the signatures of the small landslides disappear in a short period of time (Guthrie and Evans, 2007). Although much research has been done to document the morphology and mechanics, susceptibility and slope stability of landslides, research into the role of frequencies and magnitudes of landslides on the evolution of the landscape is still needed. Recently, a few studies have been conducted on a regional scale to understand the contribution of landslides to landscape evolution (Korup 2006, Guthrie and Evans, 2007).

The primary goals of this study are: (a) to determine the characteristics of the shallow landslides in Paonia-McClure Pass area of western Colorado by using frequency-magnitude relationships; (b) assess the area-volume relationships; and (c) assess the geomorphic work of these landslides. To achieve these goals the following objectives must be met: 1) prepare a landslide inventory map; 2) develop a model that

approximates the hillslopes before the landslides occurred and calculate the volume of soil displaced by the landslides; 3) obtain frequency-magnitude relationship curves and compare the frequency-magnitude relationship curves with a double pareto model to determine the power scaling parameters for small, medium and large sized shallow landslides; and 4) determine the most important range of the sizes of shallow landslides which yielded most of the sediments. Moreover, the study also estimates the rate of hillslope denudation based on the shallow landslides occurring for the last 65 years and discusses the geomorphic evolution of the area in terms of the channel incision, shallow landsliding as a process-response of channel incision, and the upslope steepening of the hillslopes by deep-seated large landslides.

The study area

The study area, located in west-central Colorado (Fig. 9), extends from Paonia to McClure Pass (N 38^{o} 43’ 00”, W 107^{o} 37’ 30” to N 39^{o} 10’ 30” W107 10” 00”) and encompasses ~ 815 km^{2}. General access to Paonia-McClure Pass is gained by Colorado Highway 133. Foot trails and forest roads provide access from the highway.

The climate of the study area has average annual temperatures ranging from 1.8 °C (minimum) to 18°C (maximum) based on the 1905-2005 data of Paonia 1SW climatic station (Western Regional Climate Center, 2009). Precipitation is primarily the result of summer convective thunderstorms. The area also receives winter precipitation in the form of snow. Average annual precipitation is 400 mm based on the 1905-2005 data of Paonia 1SW climatic station (Western Regional Climate Center, 2009).

Vegetation of the area consists of grasses, aspen groves (*Populus tremuloides*), and pines (*Pinus edulis*). The landcover/landuse in the area is forest, grassland, ranching and grazing.

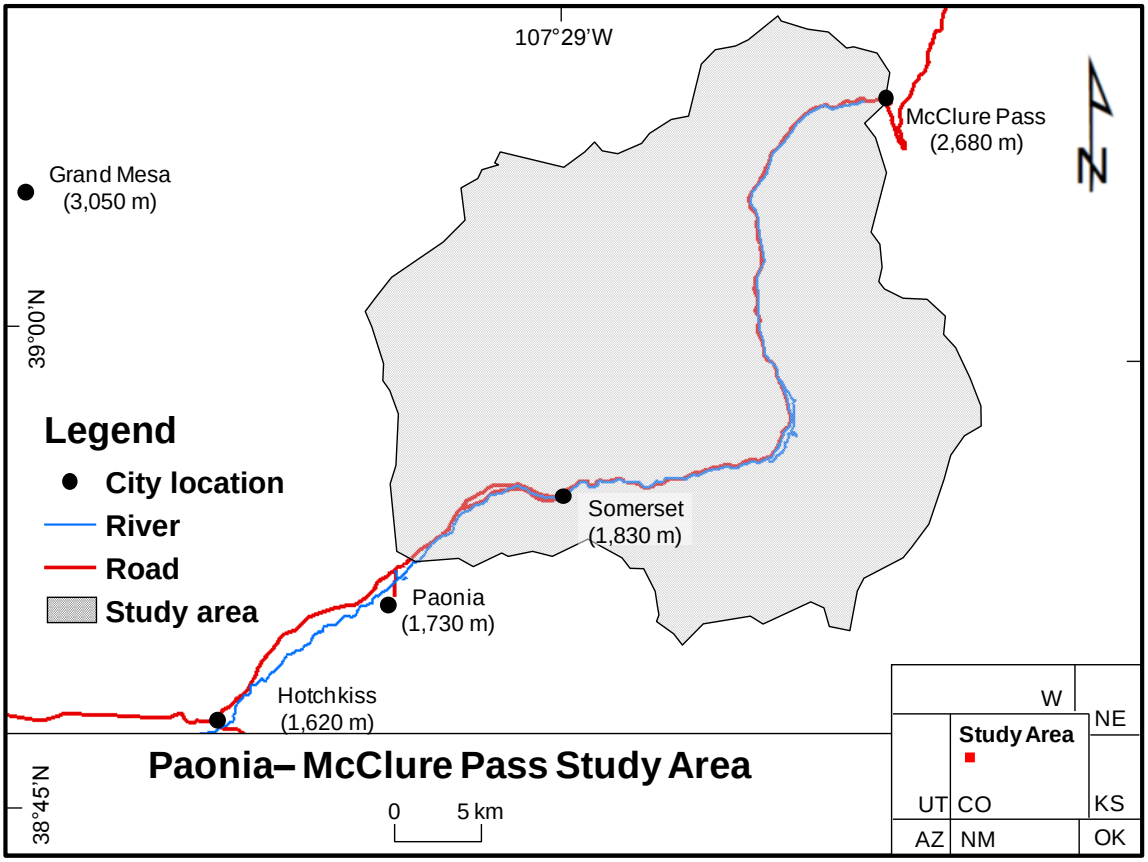

Fig. 9. Paonia-McClure Pass study area. W: Wyoming, NE: Nebraska, UT: Utah, CO: Colorado, KS: Kansas, AZ: Arizona, NM: New Mexico, and OK: Oklahoma.

Very few studies on landslides have been conducted in the study area. Reconnaissance research on mapping landslides and landslide hazards from Paonia to the Hotchkiss area was completed by Junge (1978) and cover part of the study area. A study on human susceptibility to shallow landslides in the area between Paonia and

McClure Pass has been performed by Regmi et al. (2010b). But, no study, has focused on the frequency-magnitude characteristics of the landslides and the contribution to sediment yield and landscape evolution. This study area includes Paonia, the biggest city of the area, and Somerset, a residential area originally settled by coal miners (Fig. 9).

Geomorphology and geology

The area has rugged topography and a dendritic drainage pattern (Fig. 10). The North Fork of the Gunnison River is the major river and drains about 2,500 km^2 of forested mountainous terrain into the Gunnison River (Jaquette et al., 2005). The elevation ranges from 1,712 m to 3,883 m with the lowest elevation on the flood plain of the North Fork of the Gunnison River at Paonia and the highest elevation at Chair Mountain (Fig. 10). The hillslope morphology in the area varies. Slopes are not controlled by the hillslope elevation; gentle slope is dominant. Most of the small mountains have steep slopes and flat mesa like tops, whereas mountain highlands have sharp ridges and steep slopes in the form of horns, arêtes and glacial cirques.

The study area exhibits three different lithologies: 1) sedimentary rocks including shale, mudstone, and sandstone; 2) igneous rocks, including basalt and granodiorites; and 3) various Quaternary deposits all with different geological ages. Limestone and sandstone were deposited during the Cretaceous period and plutonic and volcanic deposits are Tertiary units (Dunrud, 1989). Basalt caps many mountains, whereas rocks adjacent to the basalt cap have been stripped away by glaciation, mass movements, and river erosion. These processes left till and colluvium on most of the lowlands and middle

slopes. Bedrock is dominant along the steep ridges and fluvial deposits fill the valleys. All processes over long geological time formed the river valleys.

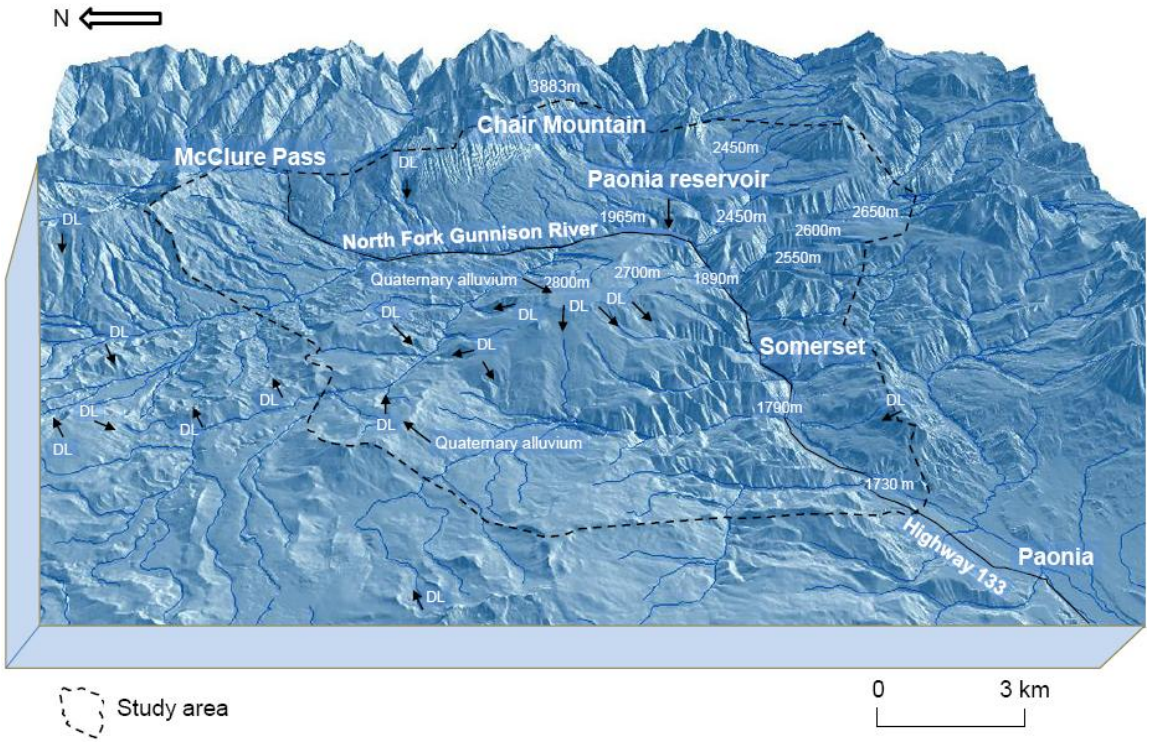

Fig. 10. A hillshaded map showing topography of the study area. The area comprised of river floodplains and upland plateaus, steep slopes in the close proximity of the North Fork Gunnison River and associated tributaries, upland slopes comprised of large deep-seated landslides (DL), and tall and steep mountains. The elevations of the river floodplains at different locations and plateaus are shown.

Landslides

The area exhibits two major groups of landslides: 1) shallow landslides; and 2) large deep-seated landslides. Shallow landslides are defined as modern (<100 years) and have an area of <160,000 m^2. Large deep-seated landslides are defined as paleolandslides (probably hundreds to thousands of years) and have an area of > 160,000 m^2. Only shallow landslides (Fig. 11) were used to study the frequency-magnitude

relationship, area-volume relationship, sediment yield and geomorphic work of landslides. The large deep-seated landslides (Figs. 10 and 12) were excluded because huge uncertainties will be incorporated into the analysis if landslides of ages ranging from a year to thousands of years were analyzed together. In this study, large deep-seated landslides were used only to discuss the contribution of landslides to landscape evolution.

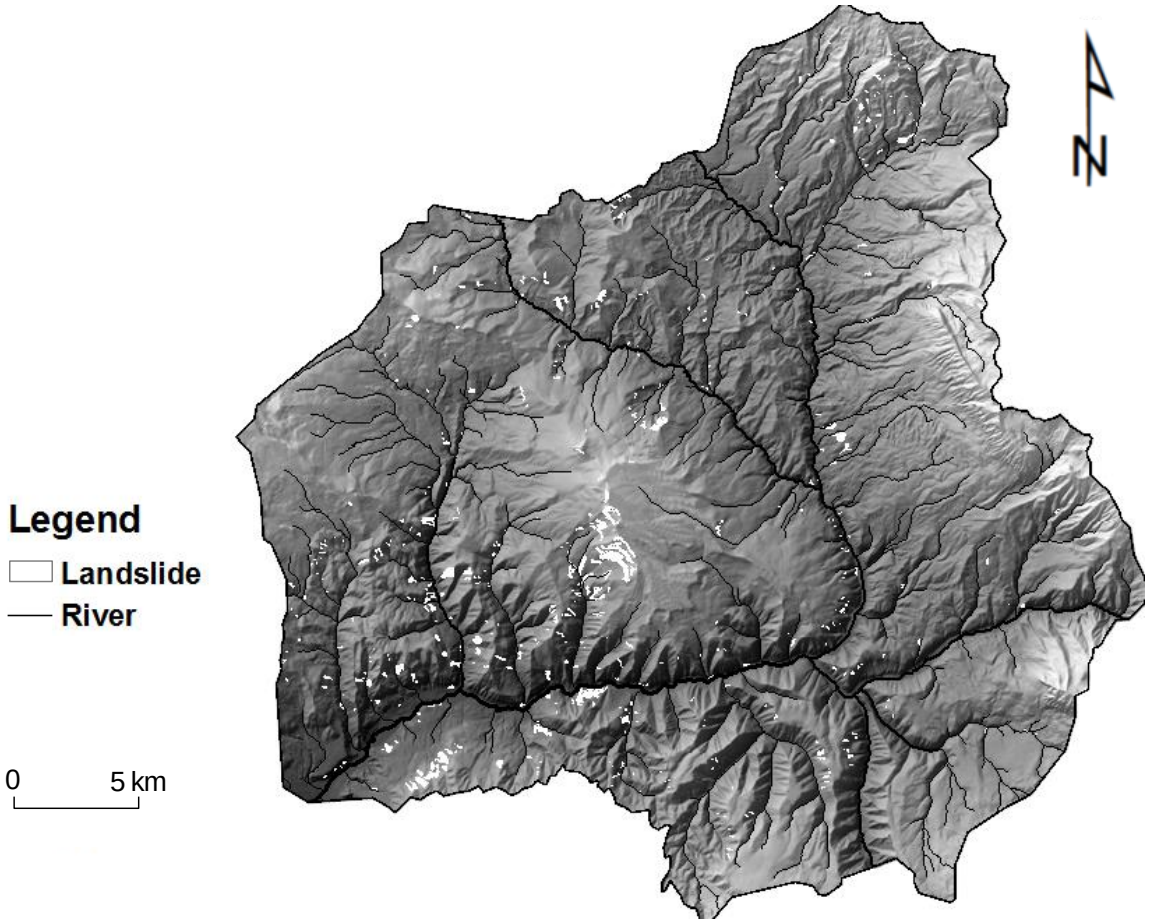

Fig. 11. Distribution of shallow landslides in the study area. The landslides were mapped as polygons.

Shallow landslides (Modern landslides)

I mapped 735 distinguishable boundaries (Fig. 11) of historical shallow landslides (<160,000 m^2) including debris flows, debris slides, soil slides, and rockslides (Fig. 12) from NAIP (National Agriculture Imagery Program) orthorectified color aerial photographs of 1:12,000 scale acquired in 2005 and USGS (United States Geological Survey) black and white orthorectified aerial photographs of 1:12,000 scale acquired in 1993. Small landslides are mostly found on 15° to 40° slopes (Fig. 13), comprised of sandstone, mudstone and colluvial deposits in close proximity to rivers. Small and medium sized landslides occur in divergent and convergent parts of the slopes whereas large landslides occur in almost planar parts of the slopes. Debris flows mostly occur on the convergent parts of the slopes, rock slides and debris slides occur mostly on planar slopes, and soil slides occur everywhere. The area of these landslides ranges from 85 m^2 to 1.6×10^5 m^2. Interestingly, most of the larger landslides are rock slides and most of the smaller landslides are soil slides. Only shallow landslides from these zones were mapped for the analysis. The largest river in the area flowing east–west is the North Fork of the Gunnison River; Colorado Highway 133 trends parallel to the river. The vertical scale of the image is exaggerated twice.

In areas where soil slides, debris slides and debris flows occurred, the thin cover of the regolith above the bedrock moved under the effect of gravity and increased pore-water pressure (Fig. 14). In most of the rock and soil landslides, the boundary between the soil and the underlying bedrock is abrupt. The regolith is cohesionless, has low bulk density, and contains fragments of rocks. The underlying rock is highly fractured, gently

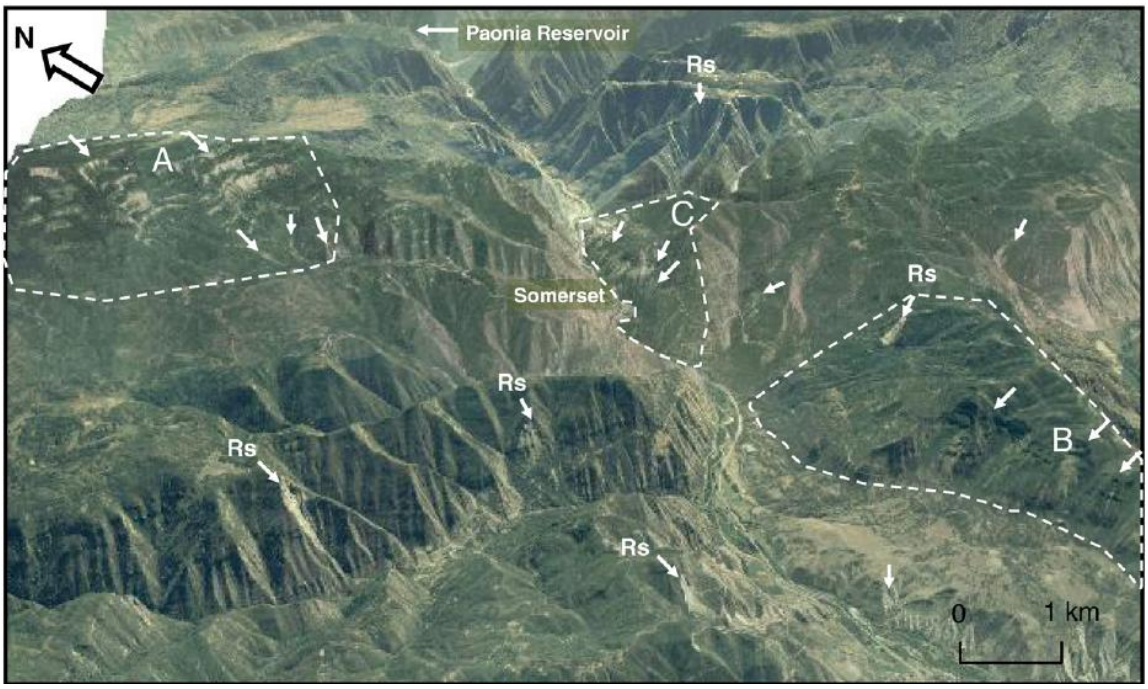

Fig. 12. Shallow and deep-seated landslides around the small community of Somerset. The image shows a 3-D view towards the west. Rockslides (Rs) occur mostly on steep slopes. Zone A is dominated by shallow and deep-seated landslides. The hummocky landform in Zone B and the southern slope of Somerset (Zone C) are dominated by active debris flows. The entire hillslope, shown in A, B and C, is active. Zones A and B also include deep-seated landslides.

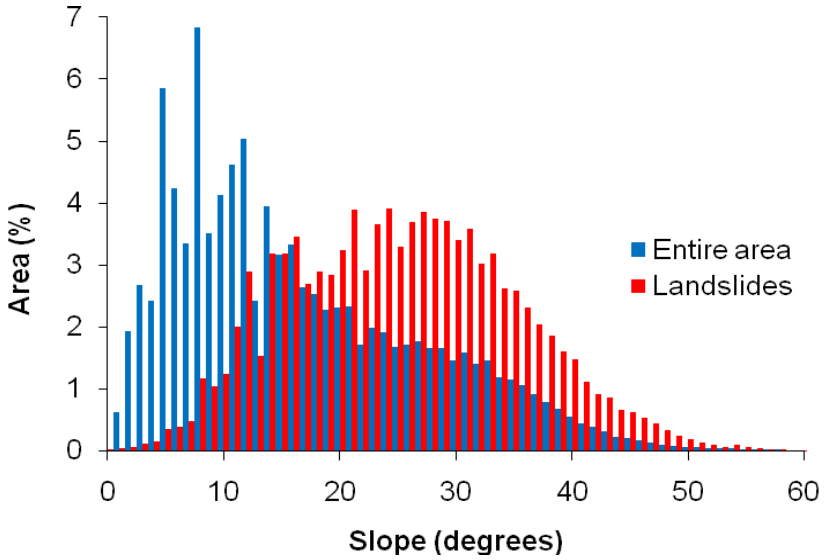

Fig. 13. A map showing the distribution of the slope on the landslide surface and entire area. The average slope of the landslide surface is ~26° and entire area is 21°.

dipping and has considerable cohesion as well as frictional strength. The loose regolith conducts more water than the bedrock. Because the highly fractured underlying bedrock may conduct large amounts of water (Wilson and Dietrich, 1987; Johnson and Sitar, 1990; Montgomery et al., 1997), I consider that the rockslides in the area are probably the result of the weathering and pore-water pressure generated by subsurface flow. The main reason for the rock fractures is sufficient moisture coupled with great depth of the frost penetration in winter. Furthermore, many landslides occurred between the boundary of hard rocks (sandstone and plutonic rock) and soft rocks (mudstone and

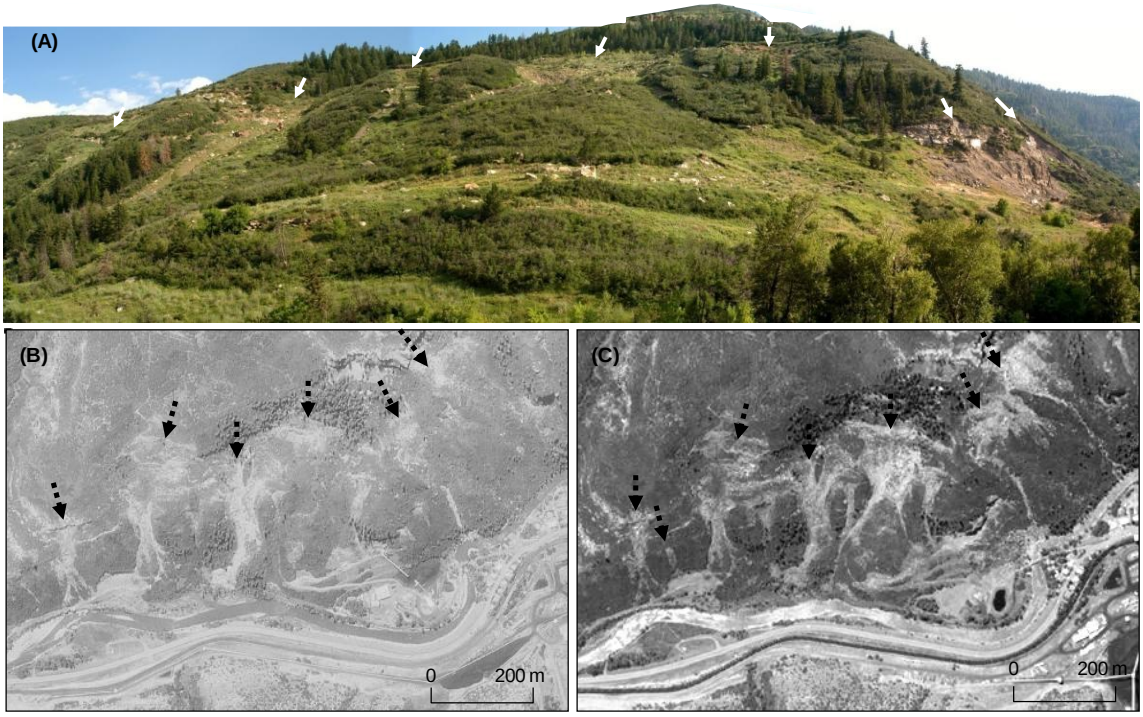

Fig. 14. Distribution of landslides on the southern uphill slope of Somerset on an aerial photograph. A) An aerial photograph acquired in 1993. B) An aerial photograph acquired in 2005. C) A photograph of the part of the area taken in 2006. These photographs indicate the area is quite active. Although the area has very low frequency of new landslide occurrence the photographs show that the old landslides were reactivated and expanded in 12 years of time period.

shale). An interface of differential shear strength and differential rates of weathering also contributed to these landslides.

Only very limited sources describe the occurrence of shallow landslides prior to 1993. Debris flows occurred in many parts of the area during intense rainfalls in 1975, 1983, 1984, 1985, 1986, and 1987 (Rogers, 2003). Based on these events and the lack of vegetation, I assumed many of the medium and small landslides were initiated then. One large shallow landslide in the area has been dated back to the 1940 (Rogers, 2003). I assumed almost all of 735 landslides occurred after 1940.

Large deep-seated landslides (Paleolandslides)

I also identified and mapped locations of large deep-seated landslides (>160,000 m^2) from NAIP orthorectified color aerial photographs 1:12,000 scale acquired in 2005 and USGS DEM of 10 m horizontal resolution (Figs. 10 and 13). These landslides are found on the gentle slope of higher elevations and along the edges of the upland plateaus. The surfaces of these landslides are densely vegetated and indicate the landslides are very old (probably hundreds to thousands of years) and relatively stable now. The headscarps of some of the large landslides are still active and producing shallow landslides. These landslides exhibit how shallow landslides contribute to the upslope propagation of steep edges of upland plateaus and steep heads of rivers and tributaries in the study area. The information on the large and deep-seated landslides was not included in magnitude and frequency analysis but yielded information about landscape evolution.

Materials and methods

The first objective of the study was to map landslides in the study area. Seven hundred and thirty five shallow landslides were mapped by employing a GIS (Geographic Information System) technique on orthorectified aerial photographs of 1:12,000 scale acquired for 1993 and 2005. Landslides were identified visually by distinguishing tone, shape, size and texture and subsequently digitized in an ArcGIS® program. Although landslides occurred as clusters in many locations, individual landslides were mapped by identifying distinct boundaries by employing three-dimensional visualization in ArcGIS® and stereo visualization techniques in Terrain Navigator Pro® programs. The spatial information of landslides and attributes of area, perimeter, volume, length, width, type, activity, position on the hillslope, vegetation, main causes and damage were collected from aerial photographs, historical archives and field surveys. All of these attributes were linked with spatial information from the landslides and stored in ArcGIS®. After extraction of landslide data, the location, type and activity of all landslides were verified by field mapping.

The second objective of this study was to determine the volume of slope material displaced by each landslide. Volume, one of the important aspects in the analysis of geomorphic roles of landslides, can be used as an indicator of the magnitude of a landslide. Furthermore, additional information includes the rate of erosion/denudation, sediment yield, and the degree of hazard and risk of landslides. But, determination of accurate volumes of landslides on a regional scale is quite difficult. Researchers have used length, width, thickness or area of a landslide as a surrogate for volume. The length,

width, and area of a landslide can be measured easily from aerial photographs and topographic maps. Often, however, these parameters may not provide an accurate estimation of volume. Calculation of volume from aerial photographs and topographic map is almost impossible. Volume can be determined by: 1) visual approximation in the field (Simonett, 1967); and 2) analysis using a high resolution digital elevation model (DEM) (Regmi et al., 2007). Acquiring field measurements is expensive, time consuming and depends on the judgment of an expert. Estimating volume from a DEM can create numerous errors, including: 1) the errors in the DEM itself (Claessens et al., 2005); 2) errors caused by algorithms used in the analysis (Wise, 2000); 3) the resolution of DEM; 4) technique used for DEM resampling; and 5) the quality of the available data (Claessens et al., 2005). Use of DEM analysis and expert's judgment based on field observation would be a better approach. The volume of each landslide was calculated by integrating the analysis of the USGS DEM with 10 m horizontal resolution and field observations. The concept behind this approach is: if an elevation surface is created by interpolating elevations of the landslide boundaries, the surface approximates the elevation of the slope prior to the slide. When the elevation of a landslide surface is subtracted from the elevation of slope prior to the slide, the positive value of each pixel gives the depth of depletion for that pixel and the negative value gives the depth of deposit for that pixel. If the depth is multiplied by the cell size, volume of the debris moved onto that pixel can be determined. The summation of the positive and negative values gives the total volume of depletion and accumulation attributable to a landslide.

The third objective of the study was to determine the probability distribution of magnitudes (area and volume) of landslides in the study area. Calculation of the probability of magnitudes for landslide has been discussed in the literature. Widely used techniques are: cumulative probability curve (e.g., Guthrie and Evans, 2004a, 2004b), logarithmic binning (Stark and Hovius, 2001), derivative of cumulative frequency (e.g., Guzzetti et al., 2002), kernel density estimation (e.g., Guzzetti et al., 2008), inverse gamma distribution (e.g., Malamaud et al., 2004) and double pareto distribution model (Stark and Hovius, 2001). In this study, cumulative probability of the landslides and the probability density function (pdf) of landslide magnitudes were determined. The cumulative probability is calculated by dividing the cumulative number of a landslide for each size of landslide in descending order by the total number of landslides. The pdf is calculated based on the Gaussian kernel density estimation method (Eq. 6) in which the estimate of the bandwidth is determined based on the Silverman's Rule of Thumb (Silverman, 1984) (Eq. 7). Then the pdf was plotted against the size of the landslides and the data were fitted with a double pareto curve. The double pareto curve is developed based on Eqs. 8 and 9 (Stark and Hovius, 2001). By using Eq. 8, data for the uniform sizes of landslides, ranging from 1 to m (the maximum size of the landslides), were simulated in which the probability (π) of the simulated sizes of landslides range from 0 to 1. Data for the sizes of simulated landslides were used in Eq. 8 to determine the probability density of given simulated sizes of landslides. The double pareto curve is compared with the pdf curve of the real landslide data. To make a close match between these two curves variables in the double pareto equation as α (positive slope of the

distribution curve), β (negative slope of the distribution curve) and t (rollover of slope) were changed until these curves match.

$$\hat{f}(x;h) = \frac{1}{nh^d}\sum_{i=1}^{n} K\left(\frac{x - x_i}{h}\right) \tag{6}$$

$$\hat{h} = 1.06 \min\left\{\hat{\sigma}, \frac{R}{1.34}\right\} n^{-1/5} \tag{7}$$

where, $\hat{f}$ is the density estimate, n is the number of the population, h is bandwidth, d is the dimension, x is the mean and x_i is the value of i-th population, $k((x\text{-}x_i)/h)$ is the Gaussian function, $\hat{h}$ is the bandwidth estimate, $\hat{\sigma}$ is the estimate of standard deviation, and R is the inter-quartile range.

$$x(\pi) = t\left\{\pi^{-\alpha/\beta}\left[1 + (m/t)^{-\alpha}\right] - 1\right\}^{-1/\alpha} \tag{8}$$

$$p(x) = \eta\left[\frac{\left[1 + (m/t)^{-\alpha}\right]^{\beta/\alpha}}{\left[1 + (x/t)^{-\alpha}\right]^{1+\beta/\alpha}}\right] \times (x/t)^{-\alpha - 1} \tag{9}$$

where, π = randomly selected uniformly distributed probability ranging from δ to 1, $\eta = \frac{\beta}{t(1-\delta)}$, $\delta = \pi(c)$ and c = the minimum size of the landslide.

The fourth objective of the study was to determine the sizes of the landslides which occur frequently and assess how much sediment they moved in the study area. I followed Guthrie and Evans (2007) and used magnitudes and frequencies of landslides

to determine the geomorphic work performed. The logic behind this concept is based on the concept of Wolman and Miller (1960). Processes associated with rivers are mostly continuous in nature, whereas processes associated with landslides are discontinuous (Guthrie and Evans, 2007). In this approach the frequency of landslides is considered as lognormally distributed and the geomorphic work done by a landslide of a certain size is determined by multiplying the probability or frequency and the mean magnitude or size of the given range of sizes. The size of an event is determined by converting the sizes of landslides into logarithmic form and dividing the logarithmic values into equally spaced classes, as done by Wolman and Miller (1960) and Guthrie and Evans (2007). The work and the probability of landslides were plotted together with the magnitude of landslides. This plot is used to evaluate the size range of landslides responsible for observed geomorphic work.

Results

Frequency-magnitude relationships of landslides

The relationships of the frequencies and the magnitudes of the shallow landslides were studied at two different scales. The first is the study of landslides at the local scale (Fig. 15A) and the second is the study of landslides on a regional scale (Fig. 11). Fig. 15A shows the distribution of landslides, including debris flows, debris slides, soil slides and rock slides, on two north facing slopes near Somerset. The distribution of landslides on those slopes indicates that the sizes of landslides vary although the geomorphological

and geological conditions are similar. The lower slope contains predominantly shale and the upper slope contains sandstone over mudstone. Among 31 landslides, only two landslides are relatively large landslides (20,000 m^2 -83,000 m^2), 11 landslides are medium sized landslides (1,600 m^2-20,000 m^2) and 18 landslides are small landslides (<1,600 m^2). The probability distribution of the landslides on these slopes (Fig. 15B) shows that the probability of occurrence or the frequency for large landslides is small than compared to medium and small landslides. The probability of landslide occurrence and the landslide area (i.e. landslide magnitude) are related by a negative inverse power function for landslide areas from 1,600 m^2 to 83,000 m^2 whereas the probability-area relationship for the landslides smaller than 1,600 m^2 is different.

A question regarding the frequency-magnitude relationship is: what causes the difference in the scaling power of the large and small landslides? All resolvable landslides were mapped from the photographs shown in Fig. 15A. The probability curve shows that the scaling is different for small and large landslides with rollover at ~1,600 m^2. The photograph (Fig. 15A) is oblique and represents a very small part of the landscape. It is possible that I could have missed some very small landslides from the upper slope, for example, the white patches indicated by the arrows without "?" symbol. Furthermore, the persistence time of smaller landslides is very low (Guthrie and Evans, 2007), because the hillslope processes and vegetation modifies them very quickly. The topographic depressions shown with "?" symbols possibly are modified landslide scars. Therefore, failing to map all small landslides, a reason for the rollover effect proposed by many authors, could have played a role in the difference of power scaling. Based on

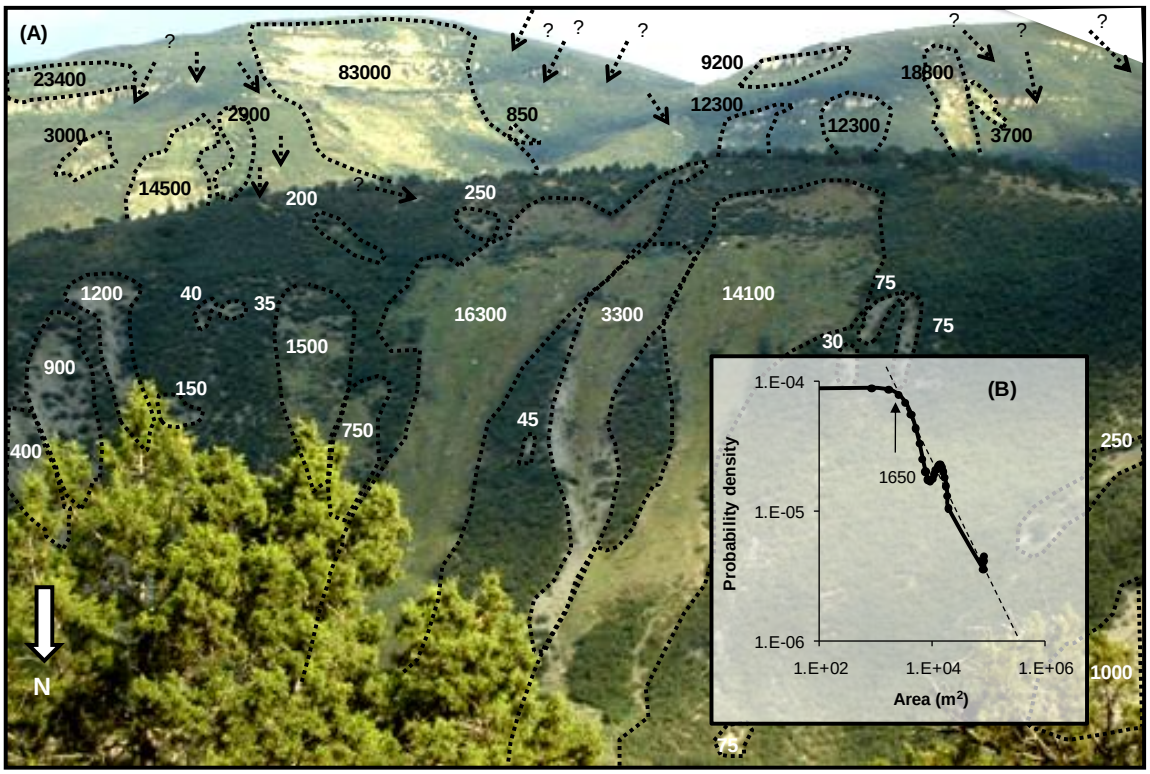

Fig. 15. Distribution of landslides on a slope nearby Somerset. The area shows the variation of the size of the landslides. The bold texts represent the areas of the landslides. Areas indicated by "?" symbols are probably landslide surfaces which were modified by the growth of the vegetation and other surface processes. A graph on the lower right quarter of the photographs is the plot of the probability density of the landslides with magnitudes of the landslides.

my observations and the large value of t (1,650 m^2) in Fig. 15B, I believe undersampling is not the only one reason. In Fig. 15, if the characteristics of the landslides are observed in detail, slope morphology is as a factor that controls the sizes of landslides. Small landslides occur on slopes with relatively smaller slope length and smaller slope angle. Larger landslides occur, however, on relatively steeper slopes with large slope lengths. Similarly, the size of a landslide probably depends on the curvature of the slope. Smaller landslides can be observed on slopes that have small radius of plan curvature or large plan curvature (very convex or very concave). Larger landslides occur on slopes with

large radius of plan curvature or small plan curvature (nearly planar). In this regard it can be inferred that the physical condition of slopes also influences the size of landslides.

Other possible factors that determine the size of landslides can be the characteristics of the slope material and the magnitude and frequency of triggering factors. If the characteristics of the slope material are the major reason, as described by Pelletier (1997), a question arises about the spatial variation of the soil characteristics. Evaluating the evenly distributed sizes of the landslides in each slope unit of Fig. 15, a local area having relatively similar lithologies, provides suspicion about the sole dependency of magnitude of landslides on the characteristics of regolith (cohesive or frictional). Magnitude of a landslide is the response of the coupling effect of the spatial variability of the soil characteristics and the geometric characteristics of the slope.

Following this example I studied the distribution of the areas and volumes of 735 landslides in the region from Paonia to McClure Pass (Fig. 16A) and developed frequency-magnitude curves (Fig. 8). Fig. 8A shows the cumulative percentage distribution of sizes of landslides (area and volume). Fig. 8B shows the plot of cumulative probability versus the sizes of landslides. Figs. 16C and 16D show the plot of pdf versus the sizes of landslides. All curves show the rollover effect, but the curves developed by plotting pdf versus the sizes of landslides show negative power scaling for medium to large landslides and positive power scaling for small landslides separated by a rollover point. The cumulative distribution curve flattens rapidly and could be described by several relations. I observed in the field that the sizes of the most of

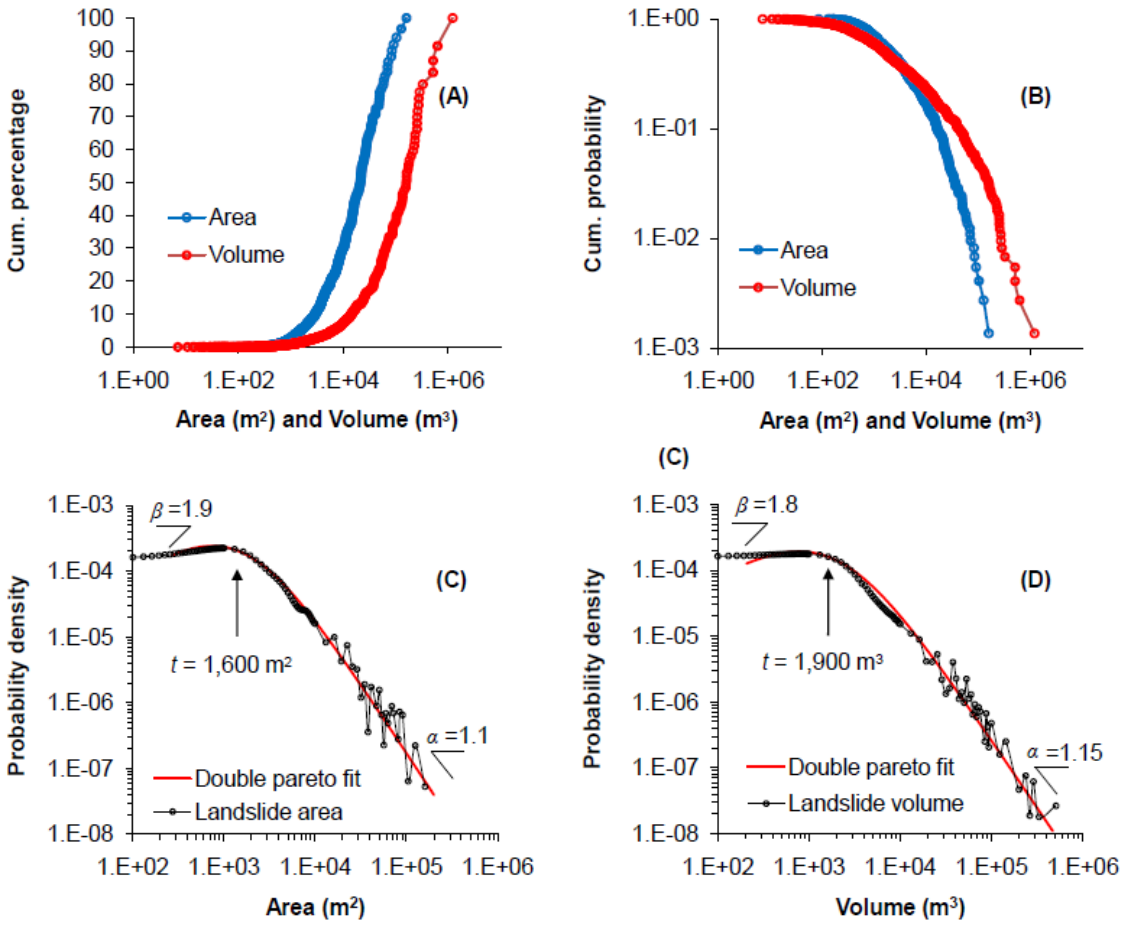

Fig. 16. Probability distribution of landslide areas and volumes. A) A graph showing the distribution of the landslide volume and the area in terms of the cumulative percentage. B) A graph showing the cumulative probability distribution of landslide areas and volume. C) A graph showing the distribution of the probability density of landslide areas. D) A graph showing the distribution of the probability density of landslide volumes.

landslides are controlled by the slope length, curvature of the slope, and the characteristics of the materials. The change in the slope profile from steeper to gentle slopes causes most of the landslides to stop on the slope and immediately deposit the displaced material. Many landslides ended in the rivers and on roads. Zones of convergence are the sites of the frictional regolith where most of the medium and large

sized debris flows and debris slides occur. Large rockslides and debris slides occur on nearly planar slopes having shattered rocks and frictional regolith. Soil slides, mostly small events, occur on all kinds of slope curvatures (convex, concave and planar) with soils of slightly cohesive nature.

Figs. 16C and 16D show that the double pareto models fit well with the probability distribution curves for the areas and volumes of landslides. The probability curve for landslide area rolls at t = 1,600 m^2, with power scaling for large and medium landslides as α = 1.1 and for small landslides as β = 1.9. The probability plot for landslide volume rolls at 1,900 m^3 with the power scaling value for large and medium landslides as α = 1.15 and the scaling for smaller landslides as β = 1.9. Both curves show similar trends of power scaling. A small value of α and a large value of β indicate that the distribution has a long tail, which means the mass movement process in the area is debris dominated. Although 328 landslides have an area less than the area at rollover point (1,600 m^2), the total area of these landslides is only 6% of the total area of all landslides and the total volume of the material displaced by these landslides is only 1.5% of the total volume of debris mobilized by all landslides (Fig. 16A). This indicates that the slope material mobilized by small landslides is very insignificant in comparison to the amount of slope material mobilized by medium and large landslides.

Area-volume relationship of shallow landslides

Precise or even approximate calculation of the volume of landslides is quite difficult in the study area. Mountainous regions of western Colorado are densely forested

and inaccessible. The best way to estimate the volumes of landslides is by the analysis of aerial photographs and DEMs. Similar to the other studies, this study shows that the areas and the volumes of landslides are related by a power relationship (Table 3 and Fig. 17). An empirical equation was obtained (Eq. 10) to estimate the volumes of landslides based on the least square regression ($R^2 = 0.87$) of areas (A) and the estimated volumes (V) of 735 landslides.

$$V = 0.0254 \times A^{1.45} \quad (10)$$

The area-volume relationships of landslides described in six articles (Table 3) are compared with my results (Fig. 17B). The result is not significantly different from Hovius et al., (1997), Guzzetti et al. (2008), Innes, (1983) and Simonett, (1967) whereas the result is significantly different than those obtained by Korup (2005) and Guthrie and Evans (2004a) (Table 3 and Fig. 17B). The equation obtained by Korup (2005) is for very large landslides ($A>1$ km^2) and may be the reason for results different than this study.

The areas of recorded landslides ranged from 85 m^2 to 1.6×10^5 m^2. The total area eroded by all landslides is 4.8×10^6 m^2 with the average area of 6,600 m^2 and a standard deviation of 1.36×10^4 m^2. The average thickness of the landslides studied is 1.9 m and the total volume of the soil displaced by all landslides is 1.4×10^7 m^3 with the average volume of 20,000 m^3 and standard deviation of 7×10^4 m^3. This is a lower estimate of the total volume of landslides because only distinguishable landslides were considered in the

analysis. Only 36 landslides have a volume large than 1×10^5 m^3 and these landslides contribute 62% of the total volume of all landslides. The three largest landslides (landslide area 1×10^5– 1.6×10^5 m^2) mapped in the area (~0.4% of total number) account for ~17% of the total landslide volume; 58 landslides (landslide area 20,000 – 1×10^5 m^2) mapped in the area (~8 % of total number) account for ~54% of the total landslide

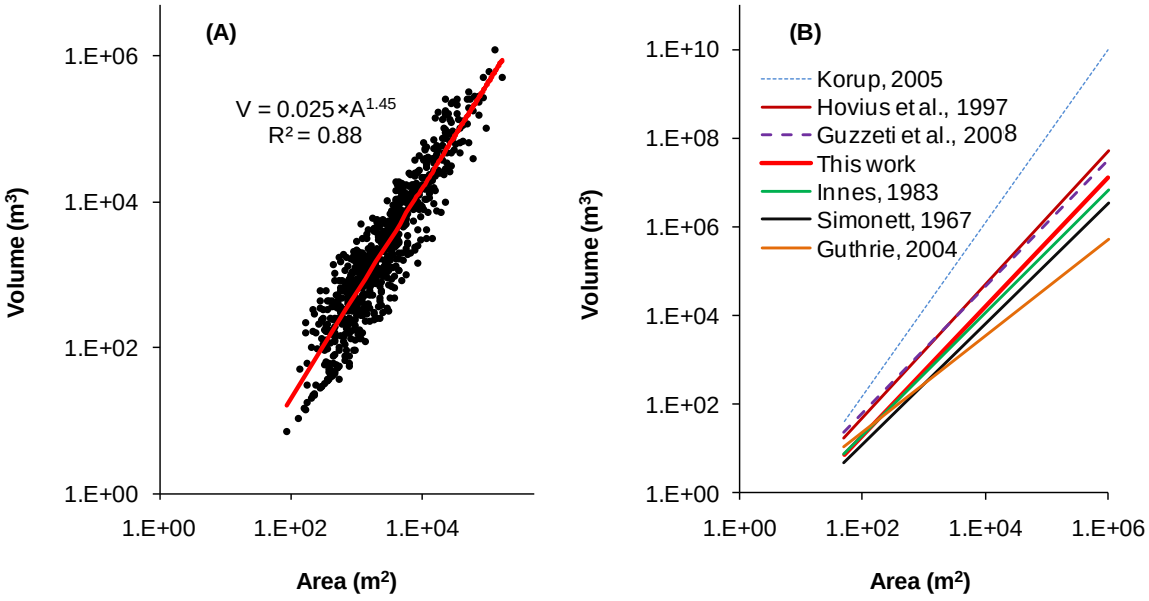

Fig. 17. A) A graph showing the relationship of the landslide volumes and the landslide areas. B) Figure showing the relationships of landslide area and volume obtained by different authors.

volume; 346 landslides (landslide area 1,600 - 20,000 m^2) mapped in the area (~47 % of total number) account for 28 % of the total landslide volume and 328 landslides (landslide area 85 – 1,600 m^2) mapped in the area (~44 % of total number) account for ~1.4 % of the total landslide volume. These data confirm the importance of large landslides in determining the total volume of landslide material in the study area.

Table 3 Comparison of the statistical values of the landslide volumes and areas with the results obtained by many researchers around the world.

Equation	Landslide area range (m^2)	Source	Area of study	Mean volume (m^3)	Landslide type
$V= 0.0254\times A^{1.45}$	$85\text{-}1.6\times10^5$	This study	western Colorado	2×10^4	Shallow
$V = 0.0844\times A^{1.43}$	$170 - 5.5\times10^6$	Guzzetti et al., 2008	central Italy	3.9×10^5	Shallow and large
$V = 0.024\times A^{1.36}$	NA	Simonett, 1967	central Italy	3.2×10^5	Shallow and large
$V= 0.05\times A^{1.5}$	$100 -1\times10^6$	Hovius et al., 1997	central Italy	5.4×10^5	Shallow and large
$V = 0.02\times A^{1.95}$	$5\times10^4\text{-}5\times10^6$	Korup, 2005	central Italy	1.43×10^5	Large
$V = 0.0329\times A^{1.39}$	30-900	Innes, 1983	Scottish Highlands	NA	Shallow
$V = 0.1549\times AL^{1.09}$	$1124\text{-}4.09\times10^6$	Guthrie, 2004a,b	British Columbia	NA	Shallow and large

The geomorphic work performed by the shallow landslides of different sizes

The probability and work curves indicate that smaller landslides have higher probability of occurrence and do less work while larger landslides have lower probability of occurrence and perform more work (Fig. 18). These curves show that the size of a landslide ~1,600 m^2 (3.2 in log value) has the highest probability of occurrence but the landslide size ~20,000 m^2 (4.3 in log value) creates the most work. A range of sizes of landslides which have high probability and high work are the important landslides for geomorphic effectiveness. This means the landslides with the range of sizes lying between these two peaks have potential roles in creating significant geomorphic change from sediment yield in Paonia-McClure Pass area. About 226 landslides are found within the area range of 1,600 m^2 to 20,000 m^2. These landslides, the medium sized landslides, mobilized about 30% of the total volume attributed to landslides.

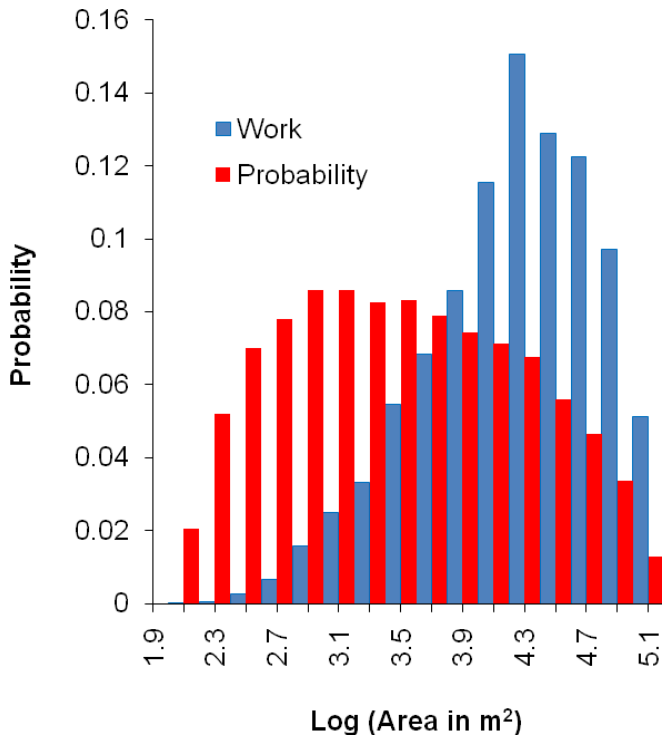

Fig. 18. Histograms showing the probability distribution of the landslide areas in logarithmic intervals and the work performed by the landslides of each logarithmic interval.

Spatial distribution of shallow landslides and sediment yield

Landslides are not distributed uniformly in the study area but are clustered in 60 regions among which only eight zones are major (Fig. 19). Major areas of the landslides are A to G in Fig. 19A. Shallow landslides in zone A and B are influenced by the deep-seated landslides. The flow structures in zones C, D, E and G indicate that the landslides were triggered by intense rainstorms. Landslides in zone F are related to the weathered and highly fractured rocks. Landslides in zone H occur in colluvium, glacial till and highly weathered rocks. The maximum density of landslide is 13 landslides per square kilometer (Fig. 19A). In terms of the area, the maximum density of a landslide is 0.347

sq km of landslide area per sq km of the study area (Fig. 19B). Similarly, maximum volume of material displaced is 1.3×10^6 m^3 from one sq. km area (Fig. 19C).

A map showing the standard deviation of the elevation (*SDE*) for each pixel within the circle of 100 m diameter implies that the geomorphic expression of the area can be differentiated into four categories (Fig. 20). Zone I, the area of low relief variability (*SDE* = 0-2 m), is comprised of river floodplains and upland plateaus. Zone II is the rough and steep zone in close proximity to the streams and is defined by a contributing area > 10 km^2 (*SDE* = 5-20 m). The slopes of the zone result from river incision, erosion and toe cutting of the slopes. Furthermore, the height and the width of the zone increase downstream. Most of the shallow landslides in the study area occur in this zone. The geology of the zone II is sandstone and mudstone that are highly fractured and weathered. The average slope of this zone is 25.6°±10° whereas the average slope of the entire study area is 17°±11°. This indicates that many of the slopes within zone III are more unstable than the slopes of other areas. Zone III, the upland gentle slope (*SDE* = 2-5 m), contributes to deep-seated large landslides. Zone IV is the steep slopes formed by the rocks and the tall mountains developed by the igneous intrusions (*SDE* = >20 m). Rock glaciers, horns and arêtes are the characteristic landforms of this zone. Figs. 20A and 20B show that a relief variability map alone can be used to predict the landslides in the area with 75% accuracy because most of the shallow landslides in the study area occurred on steep slopes in close proximity to the rivers and associated tributaries. Most of the small and medium sized debris flows occurred on the convergent zones of the first order tributaries whereas rock slides and

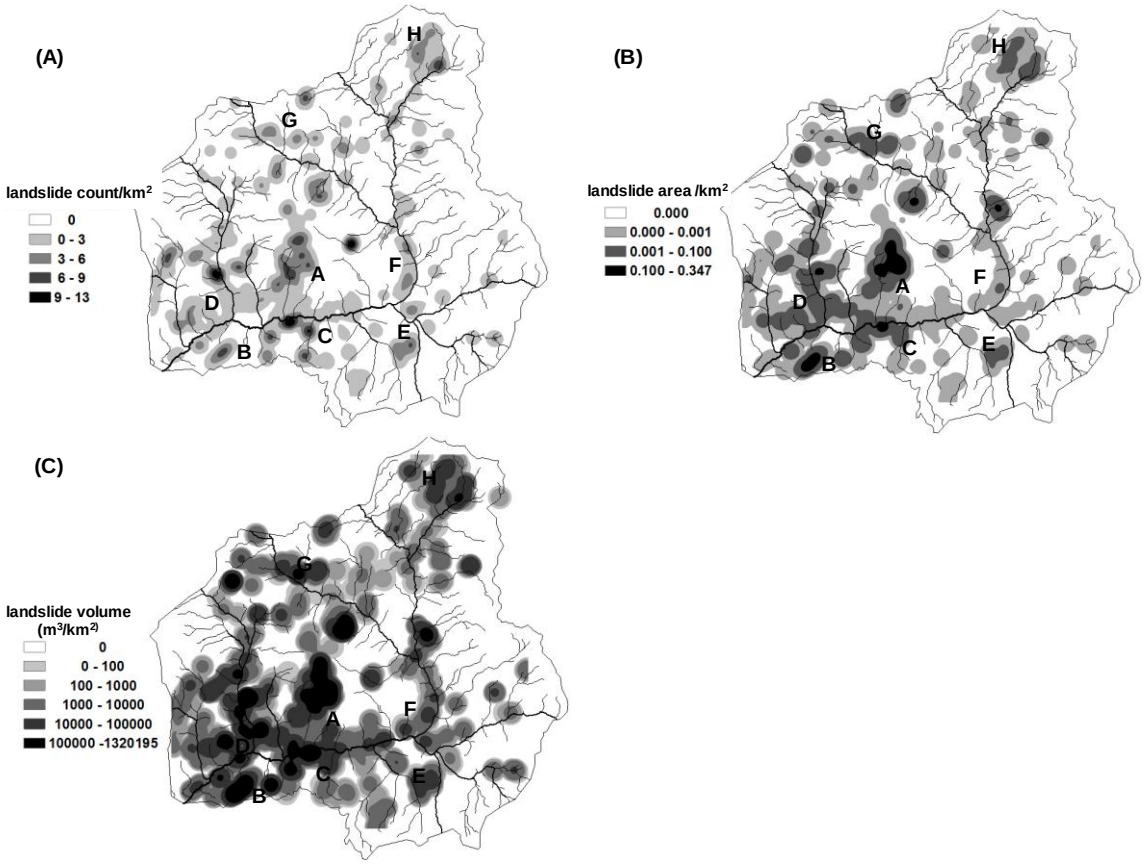

Fig. 19. Spatial distribution of the landslides in the study area. A) The density of the landslides. B) The density of the landslide area. C) The density of the landslide volume.

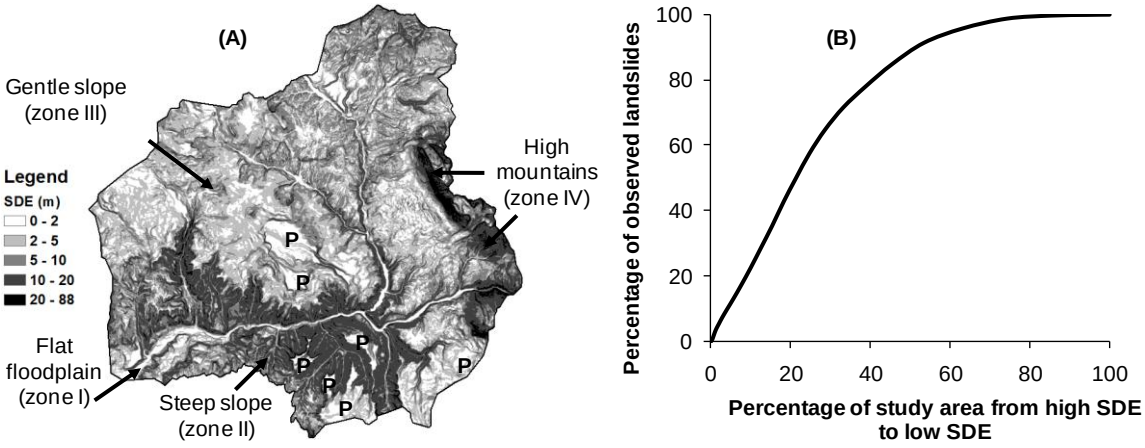

Fig. 20. A) A map showing the standard deviation of the elevation (SDE) within a roving circular window of 100 m. B) The map A is quite effective in predicting existing landslides with 75% of prediction accuracy.

debris slides occurred on the nearly planar steep slopes.

The shallow landslides studied are historical and almost all of those landslides occurred after 1940 and as recent as 2005. The shallow landslides that occurred before 1940 were either modified by the surface processes or covered by dense vegetation. Based on the analysis of the shallow landslides that occurred from 1940 to 2005, the volume of the soil displaced by landslides each year is $\sim 2.2 \times 10^5$ m^3 and the contribution of shallow landslides to the rate of denudation for the entire area is at least 0.27 mm yr^{-1}. The calculated overall rate of denudation yields a very rough estimate based on a number of assumptions: 1) each year the same number of landslides occurred, which is not true, because most of the rainstorm influenced landslides occurred during 1980s and only 35 landslides occurred after 1993; 2) The landslides are distributed uniformly within the study area, which is also false because landslides are clustered in many locations; and 3) all landslides were not mapped because of the scale of the study and modification of some landslides by vegetation and erosional processes.

As mentioned above, the approximated rate of denudation in the entire area is 0.27 mm yr^{-1}. Whereas most of the landslides occur in zone II, the rate of denudation from this zone is 0.33 mm yr^{-1}. This suggests that zone II is very unstable in comparison to the other areas.

Contribution of landslides to landscape evolution

In addition to the frequency-magnitude relationship, geomorphic work, and sediment yield of landslides, this study briefly describes the evolution of the landscape

in the study area from incision of the North Fork of Gunnison River and associated streams and the contribution of shallow and deep-seated landslides in the appearance of the landscape. Fluvial geomorphology in western Colorado is largely characterized by climatically controlled cycles of aggradation and incision (Darling et al., 2009). Cycles of aggradation and incision are generally linked to the glacial and interglacial oscillations (Sinnock, 1981, Dethier, 2001, Sharp et al., 2003) and result in a series of terraces. Older terraces are higher in elevation than younger terraces (Bull 1991). The study area, comprised of many upland plateaus, shows relict topography of the Quaternary Period. Some of the plateaus exhibit Quaternary fluvial deposits (probably the deposits of the ancient Colorado River). The total relief of one of the plateaus near Somerset, with respect to the nearest point at the North Fork of Gunnison River, is ~ 800 m which indicates that the river incised at least 800 m during the Quaternary period and the response of the incision is zone II type of geomorphic form. The rate of incision of the Gunnison River, based on the study at and around the Black Canyon of Gunnison and Unaweep Canyon in western Colorado, varies from 61 to 142 m/Ma (Aslan et al., 2008). Similarly, the study assessed the incision of the Gunnison River as ~1,550 m based on the elevation of the 10 Ma old basalt capped Grand Mesa and Delta (Fig. 9) which indicates that the rate of incision of the Gunnison River is at least 155 m/Ma.

Based on the field observations of landslides and the history of incision by rivers in the study area, I developed a simple conceptual model of the landscape evolution contributed by the incision and toe cutting of the North Fork Gunnison River and associated tributaries, shallow landslides and the deep-seated landslides (Fig. 21).

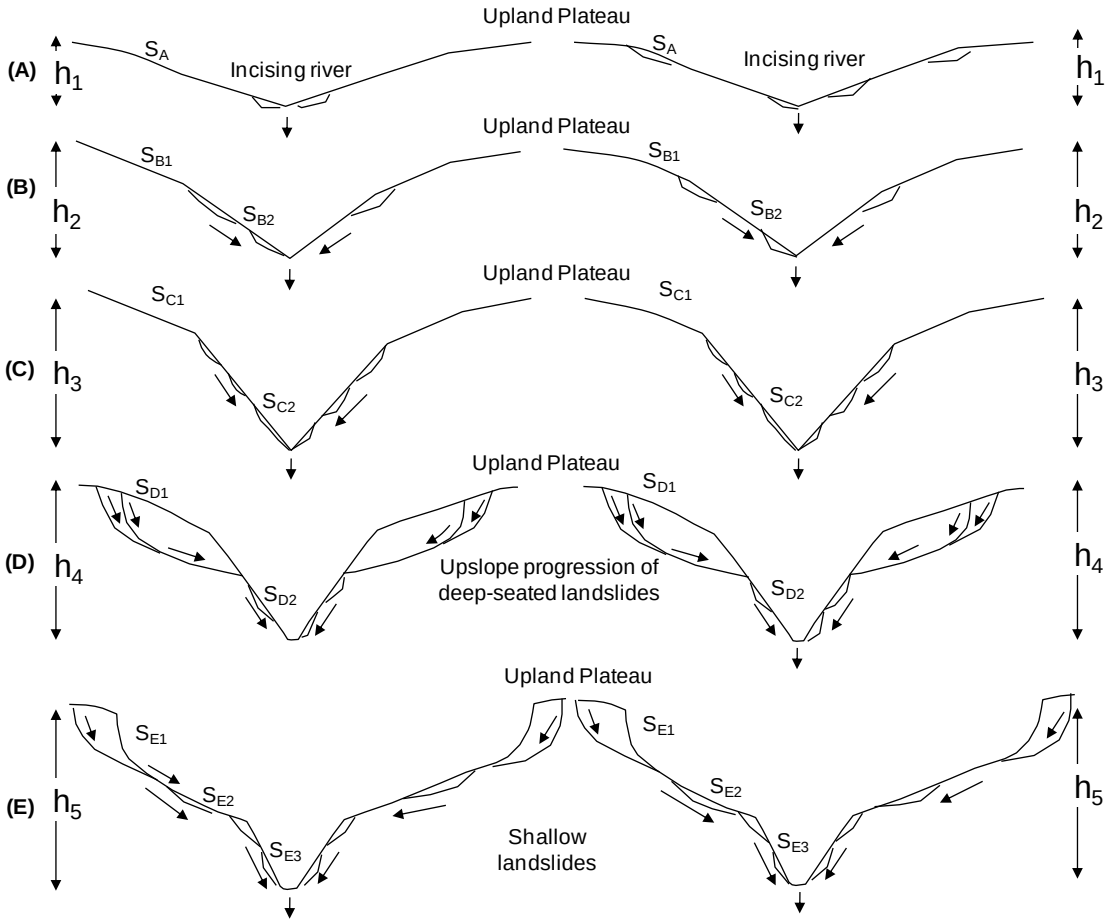

Fig. 21. A simple model of landscape evolution in Paonia-McClure Pass area. Although the present slopes in the area around the rivers and tributaries are not perfectly symmetrical as shown in the figure, the sketches present a concept of how the landscape in the area was modified over time from Quaternary to present. A) Figure shows the beginning of the river incision with a large region of upland plateau. B) As rivers undergo incision the regions in close proximity to the rivers develop steep slopes and the slopes tend to stabilize by the shallow landslides. C) The relief of the upland plateaus increases ($h_3>h_2$) with two distinct slopes ($S_{C2}>S_{C1}$). The steep slopes retreats by the shallow landslides and the upland slopes reach to the instability threshold because of the high potential energy. D) Because the incision processes are continuous, the high potential energy upland exceeds the instability threshold and under the effect of the gravity produces deep-seated large landslides. E) These deep-seated landslides steepened the upland gentle slope by propagating upslope. Figure E is the recent condition of the topography nearby Somerset.

Although the present slopes around the rivers and tributaries of the study area are not perfectly symmetrical, as shown in Fig. 21, the sketches present a concept of how the landscape was modified during the Quaternary to the present time. It is hypothesized that

during Quaternary Period the topography of the area was very gentle with large plateaus most probably developed by the incisional and aggradational nature of Ancient Colorado River (?) from Early Miocene to the Quaternary time (Epis et al., 1980). This concept is supported by a 10 Ma basalt flow and the existence of ancient fluvial deposits capping many plateaus (e.g., Grand Mesa) around the study area. The first figure (Fig. 21A) shows the beginning of the river incision into a large region of upland plateau. The second figure (Fig. 21B) shows river incision in close proximity to steep slopes ($S_{B2}>S_{B1}$) because of the base level being lowered. These slopes also tend to be stabilized by shallow landslides. The upslope regions change to a more unstable condition because of the increasing energy (Energy = mgh_2) on steeper slopes. The shallow landslides are a process-response reaction to river incision and frequent toe cutting. With continuous lowering of the base level, the area develops two distinct slopes ($S_{C2}>S_{C1}$) and the relief of the upland plateaus increases ($h_3>h_2$) (Fig. 21C). The steep slopes retreat as shallow landslides occur and the upland slopes reach an instability threshold because of the high energy (mgh_3). Because incision processes are continuous, the high levels of energy present in the uplands exceeds ($mgh_1<mgh_2<mgh_3$) the instability threshold. Under the effect of the gravity deep-seated large landslides are produced (Fig. 21D). These deep-seated landslides steepen the upland gentle slope by propagating upslope (Fig. 21E) and form three types of slopes ($S_{E1}>S_{E2}<S_{E3}$). Fig. 21E is similar to the topographic profile of the recent topography nearby Somerset and areas around the center of the study area. This model suggests that the frequency of the shallow landslides is larger than the frequency of deep-seated large landslides. The dense

vegetation on the surface of the deep-seated landslides also suggests that the frequency of these landslides is very small in comparison to the frequency of shallow landslides. No deep-seated large landslides occur on some of the plateaus in the study areas (e.g., upper right center of Fig. 10). Low relief (h) and hard rock lithology, i.e. sandstone and mudstone, contribute to this condition. In contrast, this model supports deep-seated large landslides along the edges of the Grand Mesa and other mesas having relatively high relief.

The geology of the study area also plays a major role in the present physiographic expression of the area. Zone II is comprised of fractured and weathered sandstone and mudstone, whereas zone III is underlined by thick colluvium and glacial till. Geology, also, supports the model. Further study is needed to enhance and confirm these observations and this model.

Discussion and conclusions

Seven hundred and thirty five shallow landslides were analyzed to evaluate the frequency-magnitude relationship and geomorphic work of landslides. These landslides were mapped on aerial photographs acquired in 1993 and 2005. Seven hundred landslides were identified on the aerial photographs from 1993 and 35 more landslides were identified on the aerial photographs acquired in 2005. Many landslides were reactivated between 1993 and 2005 (e.g., Fig. 14). The slope varies with the lithology. Most of the medium to gentle slopes are observed in mudstone and shale whereas steep slopes are observed in sandstone and intrusive rocks. The distribution of the slope angles

of the landslide surfaces is different than the distribution of slopes in the total area (Fig. 13). Slope zone 10°-20° is dominant in the entire area whereas slope zone 20°-30° is dominant on landslide surfaces. Most of the landslides were observed on slopes ranging from 15°-40° with mean value of 26°. Many of the landslide scars connect to the sediment deposited at the toe. The total volume deposited for all landslides, however, is lower than the total volume transported, which indicates that the sediments were washed down the slope. The ratio of the mass moved down slope to the mass accumulated on the toe of landslides for small landslides is less than for large landslides.

All curves of probability and magnitude of landslides show a rollover effect. The double pareto model of the relationship of landslide frequency and magnitude (landslide area) shows that the value of power law scaling for larger landslides is $\alpha = 1.12$ and power law scaling for smaller landslides is $\beta = 1.90$ and the rollover in slopes of power curves is at $t = 1{,}600\ \mathrm{m}^2$ (Fig. 16C). Similarly, values of these parameters for volume of mass moved as magnitudes of landslides are: $\alpha = 1.15$, $\beta = 1.80$ and $t = 1{,}900\ \mathrm{m}^3$ (Fig. 16D). In both cases, values of power law scaling parameters are quite similar. These values along with the relationship of areas and volumes of landslides (Fig. 17) first indicate that the calculation of volume is acceptable. Second, the curves with high values of the scaling for smaller and relatively low values of power scaling for larger landslides indicate that the movement of the mass is dominated by debris rather than erosion. The methodology used to determine the volume is appropriate for medium sized landslides, but is inappropriate for very small and very large landslides. The prior slope of these landslides may not be smooth and the resolution of DEM is not sufficient to detect the

signature of very small landslides. Furthermore, if the landslide surface is reactivated, the method gives the volume transported for the history of the slide. This problem was corrected based on the field observation of landslide volumes. Landslide area and depleted volume are also related by power function (Fig. 17). The result is consistent and not significantly different from the result determined in other studies around the world (Table 3).

Landslides contributing major amounts of work for the geomorphic effectiveness in the area are mostly medium landslides (size ranging from 1,600 m^2 to 20,000 m^2) which have medium probability of occurrence (0.6-0.8) or medium frequency (Fig. 18). Landslides falling within this range have higher probability and perform more work compared to landslides of other sizes. The total volume displaced by the landslides is 1.4×10^7 m^3. Assuming most of these landslides occurred after 1940 and based on the total volume of materials displaced by the landslides, the average rate of denudation of the hillslope is 0.27 mm yr^{-1}. This amount is based on the volume of the soil mass displaced by 735 landslides. Although only 735 landslides were observed in the last 65 years, this total cannot be true. The study failed to map many landslides which occurred after 1940 because the landslides were either modified by the surface processes or covered by the dense vegetation so that the signature of these landslides on aerial photographs and a DEM is not extractable. Therefore, the rate of denudation should be higher than the observed value.

First, comparison of the equation for area-volume relationships of landslides with the equations obtained by others suggests that the approach used to calculate volume for

landslides is valid. Second, the double pareto relationship of frequencies and magnitudes of landslides in Paonia-McClure Pass area indicates that the mass movement in the area is debris dominated. Although the frequency of the landslides is low (735 landslides in ~65 years or ~11 landslides in a year on average), they produce debris that is fluxed into the rivers. Landslides of sizes ranging from 1,600 m^2 to 20,000 m^2 are the most hazardous because they occur frequently and play a major role in the modification or evolution of landscape.

The model describing the contribution of landslides to the evolution of landscapes in Paonia-McClure Pass area is supported by the location of the observed deep-seated landslides, observed and predicted shallow landslides, and the landslides doing much of the geomorphic work. Most of the deep-seated landslides are located on the circumference of the upland plateau. The observed and predicted shallow landslides along with the landslides doing much of the geomorphic work are found on the steep slopes in close proximity to the rivers and tributaries, slopes of inner gorges and heads of the first order streams as well as circumference of the plateaus. The characteristics of these landslides demonstrate how landslides contribute to the conversion of a large plateau or mesa into a rugged mountainous topography by upslope propagation of steep slopes. Furthermore, these landslides are well-clustered and indicate areas that are currently unstable. Toward the center of the study area, landslides cluster on the slopes of inner gorges around a plateau. Evidence suggests that the landscapes evolve by river incision and the dominance of the low frequency deep-seated large landslides towards

the upper portion of the slopes whereas the middle and the lower portion of the slopes tend to reach stabilization by frequent shallow landslides.

CHAPTER IV

MODELING SUSCEPTIBILITY TO LANDSLIDES USING THE WEIGHT OF EVIDENCE APPROACH: WESTERN COLORADO, USA*

Synopsis

The Paonia-McClure Pass area of Colorado is well known for active mass movements. I examined 735 active shallow movement features, including debris flows, debris slides, rock slides and soil slides, in this area. Identification of the hazardous areas is a fundamental component of disaster management and an important basis for promoting safe human occupation and infrastructure development in landslide prone areas. Bayes' theorem, based on the weight-of-evidence (WOE), was used to create a map of landslides that could be hazardous. The modeling was accomplished by employing a geographical information system (GIS) and a statistical package.

Seventeen factors that cause landslides were measured and weighted using the WOE method to create a map of areas susceptible to landslides. The maps of weighted factors were summed on a pixel-by-pixel basis after performing chi-square tests to determine factors that are conditionally independent of each other. By combining factors that represent topography, hydrology, geology, land cover, and human influences, six models were developed. The performance of each model was evaluated by the distribution of the observed landslides. The validity of the best map was checked against

---

*Reprinted with permission from "Modeling susceptibility to landslides using the weight of evidence approach: Western Colorado, USA" by Regmi N.R., Giardino J.R., and Vitek J.D., 2010. *Geomorphology*, 115, 172-187, Copyright (2010) by Elsevier B.V.

landslides, which were not entered in the analysis. The resulting map of areas susceptible to landslides has a prediction accuracy of 78%.

Introduction

Landslides on steep slopes are always a major concern because of the affect on human lives and economic losses. In the US, landslides alone have an estimated annual economic cost of more than $2 billion (Spiker and Gori, 2003). Landslides are among the most damaging natural hazards in the Rocky Mountains of Colorado (Rogers, 2003). Identification of the hazardous areas associated with landslides is an important geomorphological component of disaster management and an important basis for promoting safe human occupation, infrastructure development and environmental protection in these mountains. This study maps landslides and identifies areas susceptible to landslides in the Paonia-McClure Pass area of western Colorado.

In this study, landslide is defined following Varnes (1978). Mass movements like soil slides, debris slides, rock slides and debris flows are incorporated into the term landslides. A landslide hazard is defined, according to Varnes (1984, pp. 10), as "the probability of a landslide occurrence within a specified time and within a given area of potentially damaging phenomenon".

Many studies have been undertaken to assess susceptibility to landslides through heuristic, deterministic, and statistical approaches (Carrara et.al, 1995; Wu and Sidle, 1995; Gökceoglu and Aksoy, 1996; Van Westen and Terlien, 1996; Atkinson and Massari, 1998; Pachauri et al., 1998; Van Westen, 2000; Dai et al., 2001; Van Westen et

al., 2003; Xie, 2004; Zêzere et al., 2004; Concha-Dimas et al., 2007; Neuhäuser and Terhorst, 2007; Dahal et al., 2008a). A heuristic approach is a direct or qualitative approach based on field observations and an expert's *priori* knowledge. In this approach, an expert uses geomorphological and topographical maps to identify landslides and then makes *a priori* assumptions about those sites where movement has occurred and is likely to occur again. In this way, the expert develops decision rules or assigns weighted values for the classes of index maps and overlays them to develop a map of hazards. Deterministic approaches are based on slope stability analyses (Wu and Sidle, 1995; Gökceoglu and Aksoy, 1996; Xie, 2004), and are applicable when the ground conditions across a study area are relatively homogeneous and the types of landslides are known and relatively simple (Dahal et al., 2008a). Statistical approaches are indirect and are based partly on field observations and expert's *priori* knowledge and partly on statistical computation of the weight or probabilities of occurrence of a landslide. This approach uses statistical methods and/or map algebra to assess the role of various factors that cause landslides. The importance of each factor is determined on the basis of observed relationships with landslides.

The current study evaluates the susceptibility to landslides through GIS techniques using Bayes' theorem based on weights-of-evidence (WOE). The WOE method was initially applied to non-spatial, quantitative, medical diagnoses to combine evidence from clinical diagnoses to predict diseases (Lusted, 1968; Spiegelhalter and Knill-Jones, 1984). In geosciences the method is applied extensively. Within the GIS environment, it was used in assessing mineral potentials (Bonham-Carter et al., 1988,

1989; Agterberg, 1992; Agterberg et al., 1993; Emmanuel et al., 2000; Harris et al., 2000; Bonham-Carter, 2002; Carranza and Hale, 2002), predicting the locations of flowing wells (Cheng, 2004) and groundwater springs (Corsini, et al., 2009), determining spatial associations between faults and seismicity (Goodacre et al., 1993; Daneshfar and Benn, 2002), mapping cliff instabilities associated with land subsidence (Zahiri et al., 2006) and mapping of landslide hazard and susceptibility (Lee et al., 2002; Van Westen et al., 2003; Lee and Choi, 2004; Lee and Sambath, 2006; Neuhäuser and Terhorst, 2007; Dahal et al., 2008a). For mapping susceptibility to landslides, the WOE method calculates weight for each causative factor of a landslide based on the presence or absence of landslides within the area. The fundamental assumption of this method is that future landslides will occur under conditions similar to those contributing to previous landslides. It also assumes that causative factors for the mapped landslides remain constant over time.

The times of the occurrences of all the landslides in this study were not identified. Based on the report of Rogers (2003), most of the landslides occurred in the 1980s and one of the old landslides occurred in 1940. The study included intrinsic and anthropogenic factors in the analysis of landslides. Intrinsic variables include bedrock geology, topography, soil depth, soil type, slope gradient, slope aspect, slope curvature, elevation, engineering properties of the slope material, land cover, and drainage. The anthropogenic factors include roads and settlements. Although landslide triggers, like rainfall and snowmelt, are generally related to mass movements, this study does not use these factors in the analysis. A study of forty precipitation related landslides all over

Colorado suggests that 50% of them occurred during periods of intense rainfall and 50% occurred because of snowmelt. Because of the insufficient numbers of exactly dated landslides, I was unable to determine what rainfall (mean, max or min) for what period is appropriate to include in this analysis. Furthermore, I was unable to include snow as a factor because snowmelt occurs over a long period of time, and the landslide occurs by the coupling effect of runoff from snowmelt and ground water hydrology.

The study area

The study area is located in west-central Colorado (Fig. 22). The area extends from Paonia to McClure Pass (N 38^{o} 43' 00", W 107^{o} 37' 30" to N 39^{o} 10' 30" W 107 10" 00") and encompasses ~ 815 km^{2}. Access to Paonia-McClure Pass is gained by Colorado Highway 133. Foot trails and forest roads provide direct access off the highway.

The climate of the study area is predominantly semi-arid with average annual temperatures ranging from 1.8°C to 18°C based on the 1905-2005 data of Paonia 1SW climatic station (Western Regional Climate Center, 2009). Precipitation is primarily the result of summer convective thunderstorms. The area does receive snow as winter precipitation. Average annual precipitation is 400 mm based on the 1905-2005 data of Paonia 1SW climatic station (Western Regional Climate Center, 2009). Vegetation of the area consists of grasses, aspen groves *(Populus tremuloides),* and pines (*Pinus edulis*). The land cover in the area is forest and grassland, with landuse dominated by ranching and grazing.

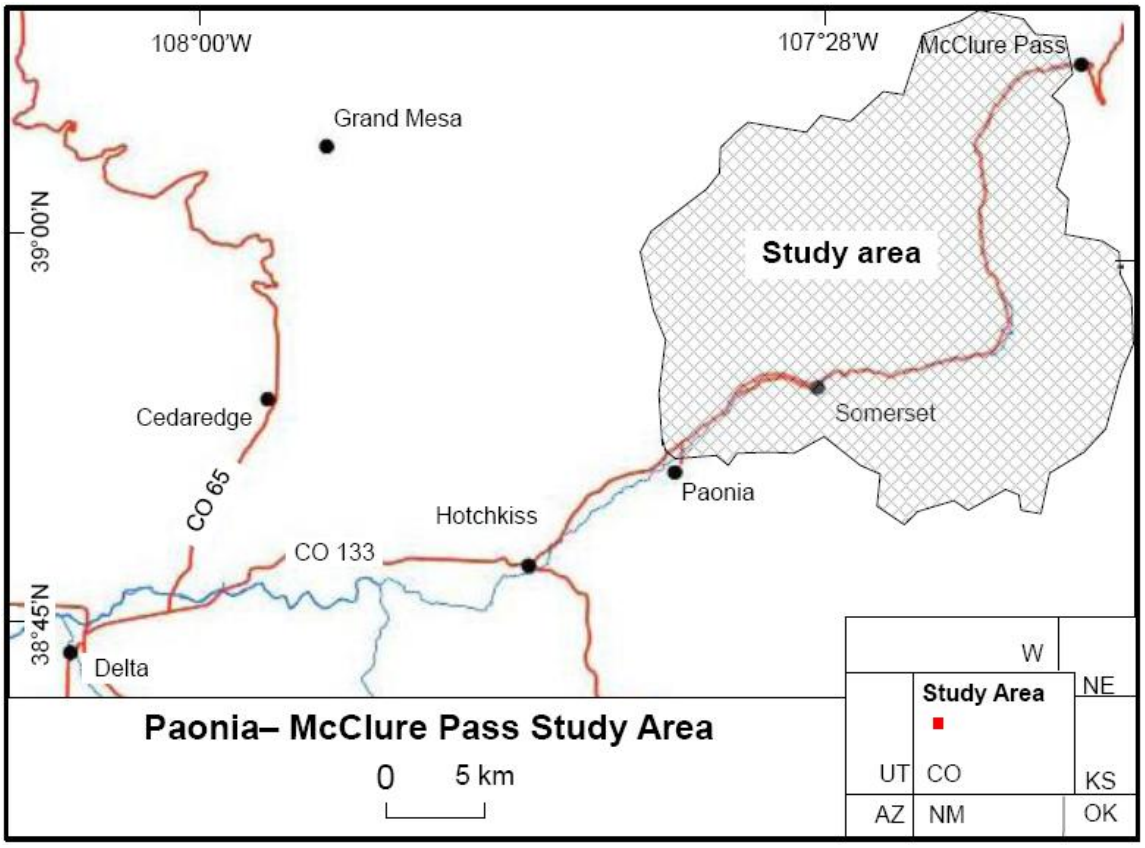

Fig. 22. The study area. W: Wyoming, NE: Nebraska, UT: Utah, CO: Colorado, KS: Kansas, AZ: Arizona, NM: New Mexico, and OK: Oklahoma.

The area has rugged topography and a dendritic drainage pattern. The North Fork of the Gunnison River is the major river that drains ~2,500 km^2 of forested mountainous terrain (Jaquette et al., 2005) into the Gunnison River. Elevations in the study area range from 1,712 m to 3,883 m. The lowest elevation is along the flood plain of North Fork of the Gunnison River at Paonia, and the highest elevation is Chair Mountain. The hillslope morphology in the area varies. Slope angles are not controlled by hillslope elevation; slopes are mainly controlled by geology. The terrain consists of igneous intrusive rocks, dikes of basalt and gabbros, and sandstone and has steeper slopes than the terrain

comprised of mudstone, shale and Quaternary deposits of glacial, colluvial, alluvial and mixed origin (Dunrud, 1989). Most of the hills have steep slopes and flat mesa like tops, whereas the highland areas have sharp ridges and steep slopes with horns, arêtes and glacial cirques developed during Pleistocene glaciation (Fig. 23). Key controls on the evolution of these hillslopes are the incision of the North Fork of the Gunnison River and its associated tributaries, Pleistocene glaciation and mass movement attributed to the coupling effect of snowmelt, rainfall and river erosion.

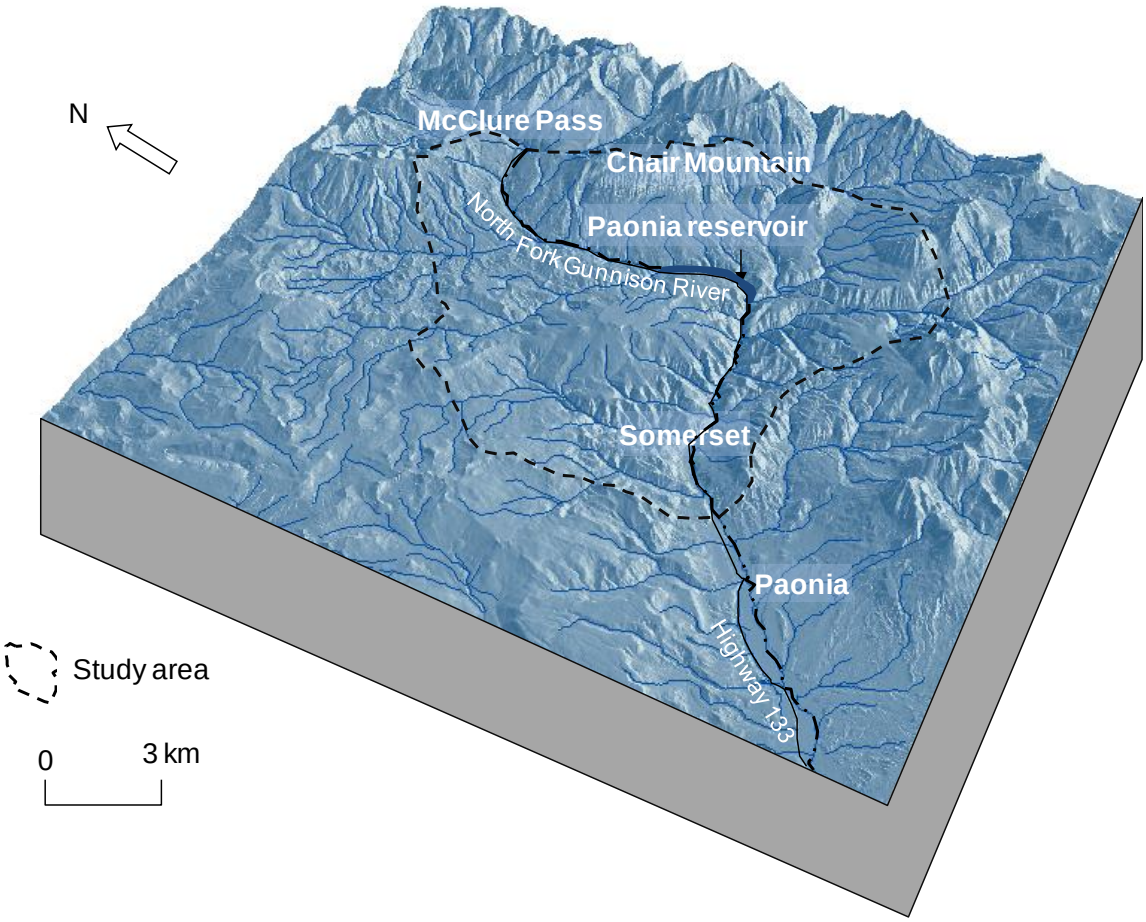

Fig. 23. A hillshaded map of the study area showing variations in topography.

The matrix of the landslides consists mainly of sandstone, mudstone and shale. Shallow translational and rotational landslides, the subject of the present study, dominate; deep seated landslides, rock falls, topple blocks and rock glaciers are also present. The gentle slopes of the area are mostly covered by glacial moraine, colluviums and alluvium deposits. Stream flow is primarily driven by the snowmelt, which is greatest in May (Jaquette et al., 2005).

Theory of weights-of-evidence (WOE)

WOE is a data-driven method (Bonham-Carter, 1994), which is basically the Bayesian approach in a log-linear form (Spiegelhalter, 1986) and uses prior (unconditional) probability and posterior (conditional) probability. The method is applicable when sufficient data are available to estimate the relative importance of evidential themes via statistical means (Bonham-Carter, 1994). The prior probability is the probability of an event, determined by the same types of events that occurred in the past, for a given period of time. For example, the probability of a unit area (or pixel) of land sliding in the future can be estimated based on the frequency of the unit area (or pixel) of land that moved in the past. This can be determined by taking the ratio of the area or the total number of landslide pixels to the area or the total number of the pixels in the study area. The prior probability can be modified using other sources of information or evidence. This revised probability of past events, based on new evidence, is called posterior probability. In this way, the prior probability can be successively updated with the addition of new evidence, so that the posterior probability from adding one piece of

evidence can be treated as the prior for adding a new piece of evidence. For example, if a landslide causing factor "*F*" exists (Fig. 24A), the probability of occurrence of landslides based on this factor might change. Then, the favorability for predicting the landslides,

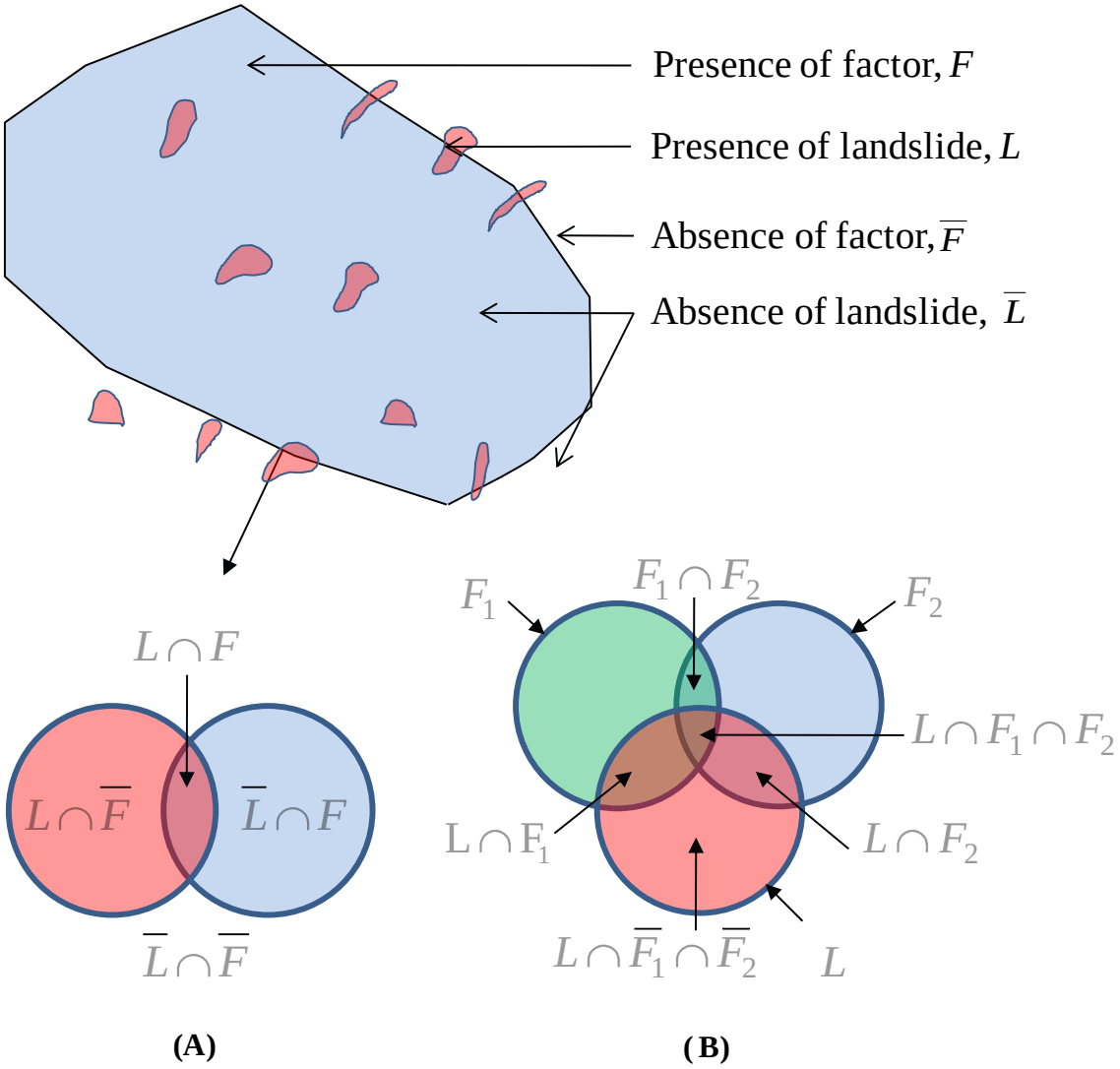

Fig. 24. Figures illustrating the relationships of landslides and factors used in WOE. A) Illustrating the presence and absence of a factor in relation to the landslide (Modified after Bonham-Carter, 2002). B) A Venn diagram showing the relationship of a landslide and two factors F_1 and F_2 (Modified after Bonham-Carter, 2002).

given the presence of the evidence factor, can be expressed by the conditional probability ($P\{L|F\}$) (Bonham- Carter, 2002):

$$P\{L \mid F\} = \frac{P\{L \cap F\}}{P\{F\}} \tag{11}$$

In terms of the number (N) of the cells occupied by L and F, the equation can be rewritten as:

$$P\{L \mid F\} = \frac{N\{L \cap F\}}{N\{F\}} \tag{12}$$

Similarly, the conditional probability of landslides based on factor F is:

$$P\{F \mid L\} = \frac{P\{L \cap F\}}{P\{L\}} \tag{13}$$

$P\{F \cap L\}$ and $P\{L \cap F\}$ are same, so from Eqs. (11) and (13)

$$P\{L \mid F\} = P\{L\}\frac{P\{F \mid L\}}{P\{F\}} \tag{14}$$

This states that the conditional (posterior) probability of a landslide, given the presence of the factor F, equals the prior probability of the landslide $P\{L\}$ multiplied by the factor $P\{F|L\}/P\{F\}$. Similarly, the posterior probability of a landslide, given the absence of the factor, can be determined as:

$$P\{L \mid \overline{F}\} = P\{F\}\frac{P\{\overline{F} \mid L\}}{P\{\overline{F}\}} \tag{15}$$

A similar model can be expressed in an odds form, the ratio of $P/(1\text{-}P)$. The odds of a landslide is expressed as:

$$O\{L\} = \frac{\text{Probability that an event will occur}}{\text{Probability that an event will not occur}} = \frac{P\{L\}}{1 - P\{L\}} = \frac{P\{L\}}{P\{\overline{L}\}} \tag{16}$$

Likewise,

$$\mathrm{O}\{\mathrm{L} \mid \mathrm{F}\} = \frac{P\{L \mid F\}}{1 - P\{L \mid F\}} = \frac{P\{L \mid F\}}{P\{\bar{L} \mid F\}} \tag{17}$$

Dividing both sides of the Eq. (14) by $P\{\bar{L} \mid F\}$

$$\frac{P\{L \mid F\}}{P\{\bar{L} \mid F\}} = \frac{P\{L\}P\{F \mid L\}}{P\{\bar{L} \mid F\}P\{F\}} \tag{18}$$

Similar to Eqs. (11) and (14), from the definition of the conditional probability is:

$$P\{\bar{L} \mid F\} = \frac{P\{\bar{L} \cap F\}}{P\{F\}} = \frac{P\{F \mid \bar{L}\}P\{\bar{L}\}}{P\{F\}} \tag{19}$$

Substituting the value of $P\{\bar{L} \mid F\}$ in the right side of Eq. (18), produces:

$$\frac{P\{L \mid F\}}{P\{\bar{L} \mid F\}} = \frac{P\{L\}P\{F \mid L\}}{P\{\bar{L}\}P\{F \mid \bar{L}\}} \tag{20}$$

From Eqs. (16), (17), and (20), it can be rewritten as:

$$O\{L \mid F\} = O\{L\}\frac{P\{F \mid L\}}{P\{F \mid \bar{L}\}} \tag{21}$$

where $O\{L|F\}$ is the conditional (posterior) odds of L given F, and $O\{L\}$ is the prior odds of F. $P\{F \mid L\}/P\{F \mid \bar{L}\}$ is known as the sufficiency ratio LS (Bonham- Carter, 2002). In WOE, the natural logarithm of the sufficiency ratio is W^+.

Thus,

$$W^+ = \log_e\left(\frac{P\{F \mid L\}}{P\{F \mid \bar{L}\}}\right) \tag{22}$$

Similarly, taking the natural log of Eq. (21) on both sides, produces:

$$W^{+} = \log_e\left(\frac{O\{L \mid F\}}{O\{L\}}\right) \tag{23}$$

Similar algebraic manipulation leads to the derivation of an odds expression for the conditional probability of *L* given the absence of the factor. Thus,

$$O\{L \mid \overline{F}\} = O\{L\}\frac{P\{\overline{F} \mid L\}}{P\{\overline{F} \mid \overline{L}\}} \tag{24}$$

The term $P\{\overline{F} \mid L\}/P\{\overline{F} \mid \overline{L}\}$ is known as the necessity ratio, *LN* (Bonham- Carter, 2002). W^{-} is the natural logarithm of *LN*.

Thus,

$$W^{-} = \log_e \frac{P\{\overline{F} \mid L\}}{P\{\overline{F} \mid \overline{L}\}} \tag{25}$$

Similarly, taking the natural log of Eq. (21) on both sides gives:

$$W^{-} = \log_e \frac{O\{L \mid \overline{F}\}}{O\{L\}} \tag{26}$$

LN and *LS* are also referred to as likelihood ratios. If the pattern is positively correlated, *LS* is greater than 1 (W^{+} = positive) and *LN* ranges from 0 to 1 (W^{-} = negative). If the pattern is negatively correlated, *LN* would be greater than 1 (W^{-} = positive) and *LS* ranges from 0 to 1 (W^{+} = negative). If the pattern is uncorrelated with a landslide, then *LS = LN = 1 (*$W^{+} = W^{-} = 0$*)* and the posterior probability would equal the prior probability, and the probability of a landslide would be unaffected by the presence or absence of the factor. I used Eqs. (23) and (25) to calculate weights of the factors. When more than one factor occurs, it is necessary to combine weights of all the factors.

For example,

$$P\{L \mid F_1 \cap F_2\} = \frac{P\{L \cap F_1 \cap F_2\}}{P\{F_1 \cap F_2\}} \tag{27}$$

Based on the Bayes' theorem, if factors F_1 and F_2 are assumed conditionally independent, Eq. (27) can be rewritten as:

$$P\{L \mid F_1 \cap F_2\} = \frac{P\{F_1 \cap F_2 \mid L\} \quad P\{L\}}{P\{F_1 \cap F_2\}} = \frac{P\{F_1 \cap F_2 \mid L\} \quad P\{L\}}{P\{F_1 \cap F_2 \mid L\}P\{L\} + P\{F_1 \cap F_2 \mid \bar{L}\}P\{\bar{L}\}} \tag{28}$$

Again if F_1 and F_2 are conditionally independent

$$P\{F_1 \cap F_2 \mid L\} = P\{F_1 \mid L\}P\{F_2 \mid L\} \tag{29}$$

Thus, from Eqs. (28) and (29),

$$P\{F_1 \cap F_2 \mid L\} = P(L)\frac{P\{F_1 \mid L\}}{P(F_1)}\frac{P\{F_2 \mid L\}}{P(F_2)} \tag{30}$$

For the odds formulation:

$$O\{L|F_1 \cap F_2\} = O\{L\}\frac{P\{F_1 \cap F_2|L\}}{P\{F_1 \cap F_2|\bar{L}\}}$$

$$= O\{L\}\frac{P\{F_1 \mid L\}P\{F_2 \mid L\}}{P\{F_1 \mid \bar{L}\}P\{F_2 \mid \bar{L}\}} = O\{L\} * LS_1 * LS_2 \tag{31}$$

$$Logit\{L|F_1 \cap F_2\} = Logit\{L\} + W_1^{+} + W_2^{+} \tag{32}$$

Therefore, the general expression for combining i =1, 2, .n maps containing data on factors is:

$$Logit\{L|F_1 \cap F_2 \cap F_3 \cap .....F_n\} = Logit\{L\} + \sum_{i=1}^{n} W^{+} \tag{33}$$

In this equation, if the *i*-th pattern is absent instead of present, the W^{+} becomes W^{-}

where the data are missing in any layer, the weight values for the missing part are set to 0. All of these equations are similar to the equations derived by Bonham-Carter (2002) and Dahal et al. (2008a).

Based on Eq. (26), the WOE method requires only the factors conditionally independent of each other. The meaning of the conditional independence is that if two factors (F_1 and F_2) are conditionally independent with respect to a set of landslides (Fig. 24B), Eq. (29) should be satisfied. The equation can also be written in terms of the number of pixels (N) as:

$$N\{F_1 \cap F_2 \mid L\} = \frac{N\{L \cap F_1\} N\{L \cap F_2\}}{N\{L\}} \tag{34}$$

The left hand side of the equation is the observed number of cells where factors F_1 and F_2 and landslides are present and the right hand side of the equation is the predicted or expected number of landslides in this overlap zone, which should equal the number of landslide on F_1 times on F_2 divided by the total number of landslide, if the two parameters are conditionally independent.

Different types of statistical tests can be employed to test the dependency of the factors with respect to the landslides. Pairwise comparison, principal component analysis and logistic regression are some of the tests commonly used in landslide studies. Among them, pairwise comparison is the most employed method for testing conditional independence in the modeling approach using WOE.

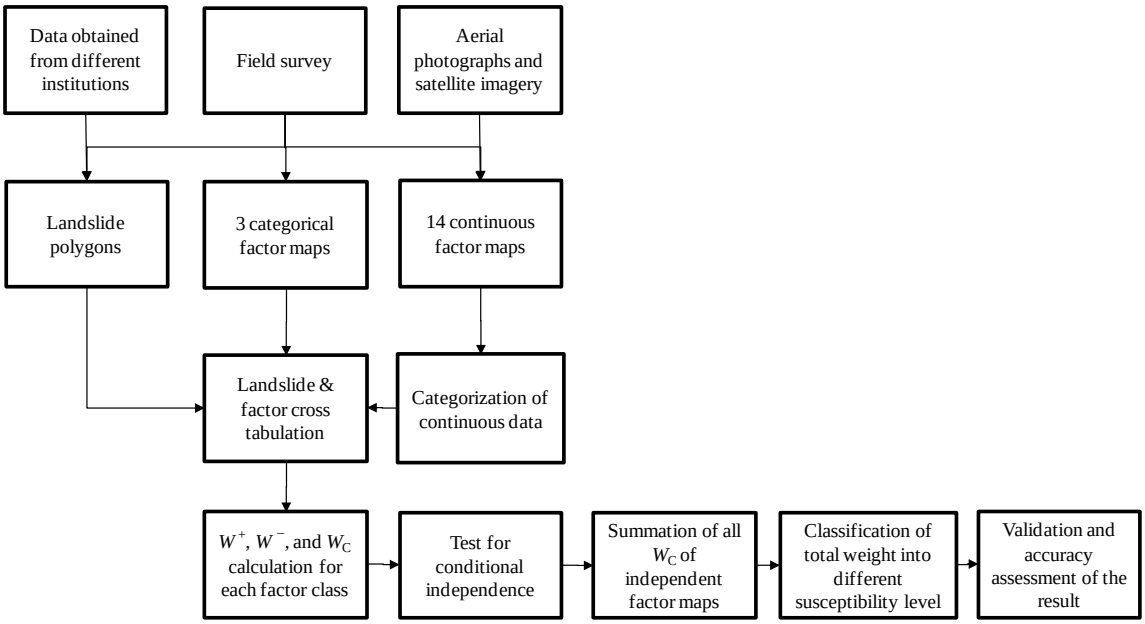

Fig. 25. Flow chart of methodology.

Materials and methods

Data preparation

The first phase of this study entailed collection and preparation of landslide related spatial and attribute data. This step was followed by the assessment of areas susceptible to landslides using the relationship between landslides and causative factors, and the final phase was the accuracy assessment, verification, and validation of the results (Fig. 25). The landslide related spatial and attribute data were collected from USGS topographic maps of 1:24,000 scale, 1 m resolution NAIP (National Agriculture Imagery Program) aerial photographs, a 1:50,000 scale USGS geological map (Dunrud, 1989), 10 m resolution USGS digital elevation model (DEM), ETM+ (Enhanced

Thematic Mapper Plus) satellite data provided by University of Maryland and USDA (United States Department of Agriculture) and USFS (United States Forest Service) soil data. Field surveys were carried out for verification of the existing data and collection of additional data. These data sources were used to generate 17 thematic layers using ArcGIS® (Table 4).

Table 4 Sources and significances of the factors used in the analysis. TWI: Topographic Wetness Index, SPI: Stream Power Index, FA: Flow Accumulation, FL: Flow Length.

Data Type	Factors	Source	Significance
Geologic	Geological map	USGS	Characteristics of the slope material
	Proximity to Fault	USGS	Co-seismic landslide triggering
Land cover	Land cover	Landsat ETM+	Root reinforcement of soil, surface runoff regulation
Soil	Soil plasticity index, coarseness	USDA, USFS	Shear strength of soil
Topographic	Elevation	DEM	Climate, vegetation, potential energy
	Slope	DEM	Overland and subsurface flow velocity
	Aspect	DEM	Solar insolation, evapo-transpiration, flora and fauna distribution and abundance
	Plan Curvature	DEM	Converging, diverging flow, soil water content, soil characteristics
	Profile Curvature	DEM	Flow acceleration, erosion/deposition, geomorphology
	Tangent Curvature	DEM	Erosion/deposition
	Solar Radiation	DEM	Weathering, soil moisture, flora and fauna distribution and abundance
	FL	DEM	Runoff velocity, potential energy
	FA	DEM	Runoff velocity, runoff volume, potential energy
Water-related	SPI	DEM	Erosive power of water flow
	TWI	DEM	Soil water content
	Proximity to rivers	DEM	Susceptible to hillslope undercutting
Anthropogenic	Highway and roads	Aerial photo	Landslide triggering by the road cutting and vibration generated by the vehicles
Landslides	Landslide inventory	Aerial photographs, field surveys	Spatial pattern of unstable zones

Landslide characteristics and inventory maps

In mapping the susceptibility of landslides using the WOE approach many researchers (e.g., Neuhäuser and Terhorst, 2007; Dahal et al., 2008a) commonly use point locations of landslides, as shown by either the center of the polygon or the scarp, and represent the area of the landslide by the size of the unit pixel at that location. In this scenario, the probability of a landslide occurrence is the ratio of one landslide pixel from each existing landslide to the total number of the pixels in the entire area. This calculation ignores the sizes or magnitudes of the existing landslides. Furthermore, if the analysis does not have sufficient locations of landslides, the results obtained, based on the analysis of the parameters at the center of the landslides, might yield a biased result. These uncertainties can be reduced by entering the number of the pixels covered by the landslide polygons. I use this approach in this study.

Seven hundred and thirty five shallow landslide polygons were mapped on 1991 and 2005 orthorectified aerial photographs of 1:12,000 scale using GIS (Geographic Information System). The aerial photographs are 1 meter ground sample distance ortho imagery rectified to a horizontal accuracy of within ± 5 m of reference digital ortho quarter quads (DOQQS) from the National Digital Ortho Program (NDOP). The positional accuracy of the landslide polygons is within ± 5 m of the aerial photograph. Landslides were identified visually based upon distinguishing tone, shape, size and texture of landslides on aerial photograph (Fig. 26), and then digitized and entered into ArcGIS®. Although landslides were clustered in many locations, individual landslides were mapped by identifying the distinct boundary of each (Fig. 27). Three-dimensional

visualization techniques and stereo-visualization techniques were employed to determine the types of landslides. These techniques help to identify landslides from features having a landslide appearance on a two-dimensional non-stereo visualization of an aerial photograph. For example, an observer may have difficulty distinguishing between a snow-avalanche track and a landslide when observing Fig. 28A and between a landslide and a non-vegetated slope when observing Fig. 28B.

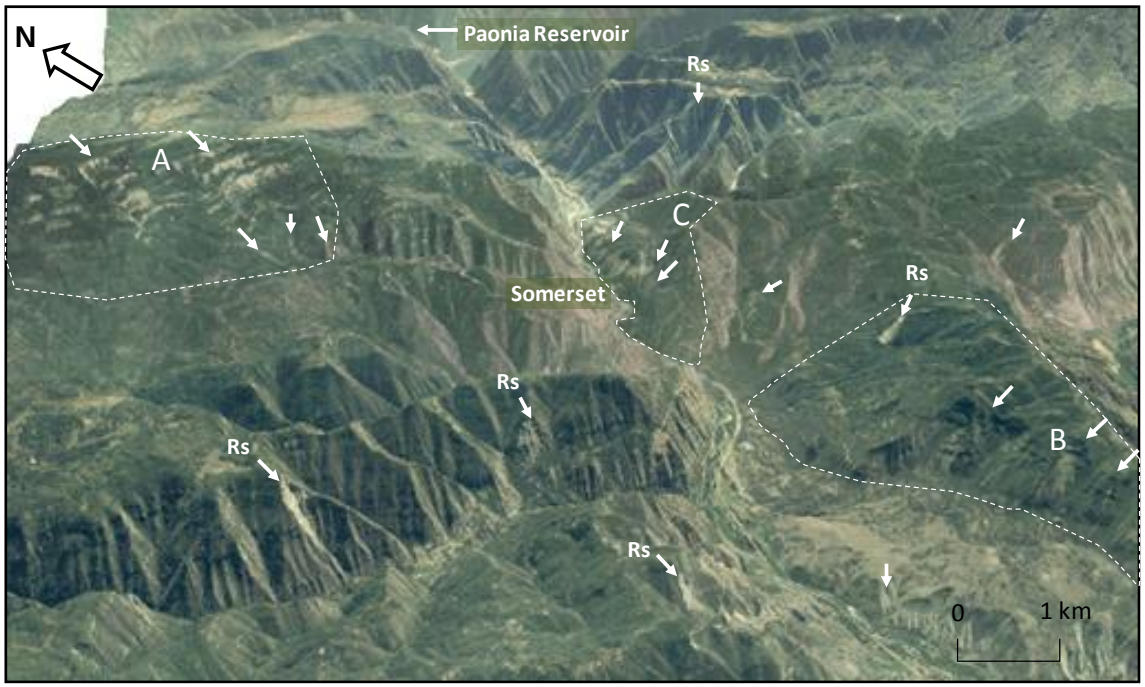

Fig. 26. Landslides around the small community of Somerset on a 2005 aerial photograph. The image shows a 3-D view towards west. Rockslides (Rs) occur mostly on steep slopes. Zone A is dominated by shallow and deep seated landslides. Hummocky landform in Zone B and southern slope of Somerset (Zone C) are dominated by active debris flows. The entire hillslope, shown in A, B and C, is active. Zone A and B also includes deep-seated landslides. Only shallow landslides from these zones were mapped for the analysis. The largest river in the area flowing east-west is the North Fork of Gunnison River; Colorado Highway 133 trends parallel to the river. The vertical scale of the image is exaggerated twice.

After mapping locations of landslides on aerial photographs, field mapping verified the data. Most of the attributes of the landslides were collected from aerial

photographs, historical archives and field surveys. The attribute data of a landslide includes area, perimeter, volume, length, width, type, activity, position on the hillslope, vegetation, main causes, damage, and preventive measures taken. All these attributes were linked with the spatial information of the landslides. The landslides mapped range in area from 85 m^2 to 160,000 m^2 with average area of 6,600 m^2; about 50% of the landslides are smaller than 2,000 m^2. Based on the analysis of the profiles of 735 landslides developed from DEM, the average depth of the landslides is calculated as 1.9 m; the mean slope of the landslide surface is 26°.

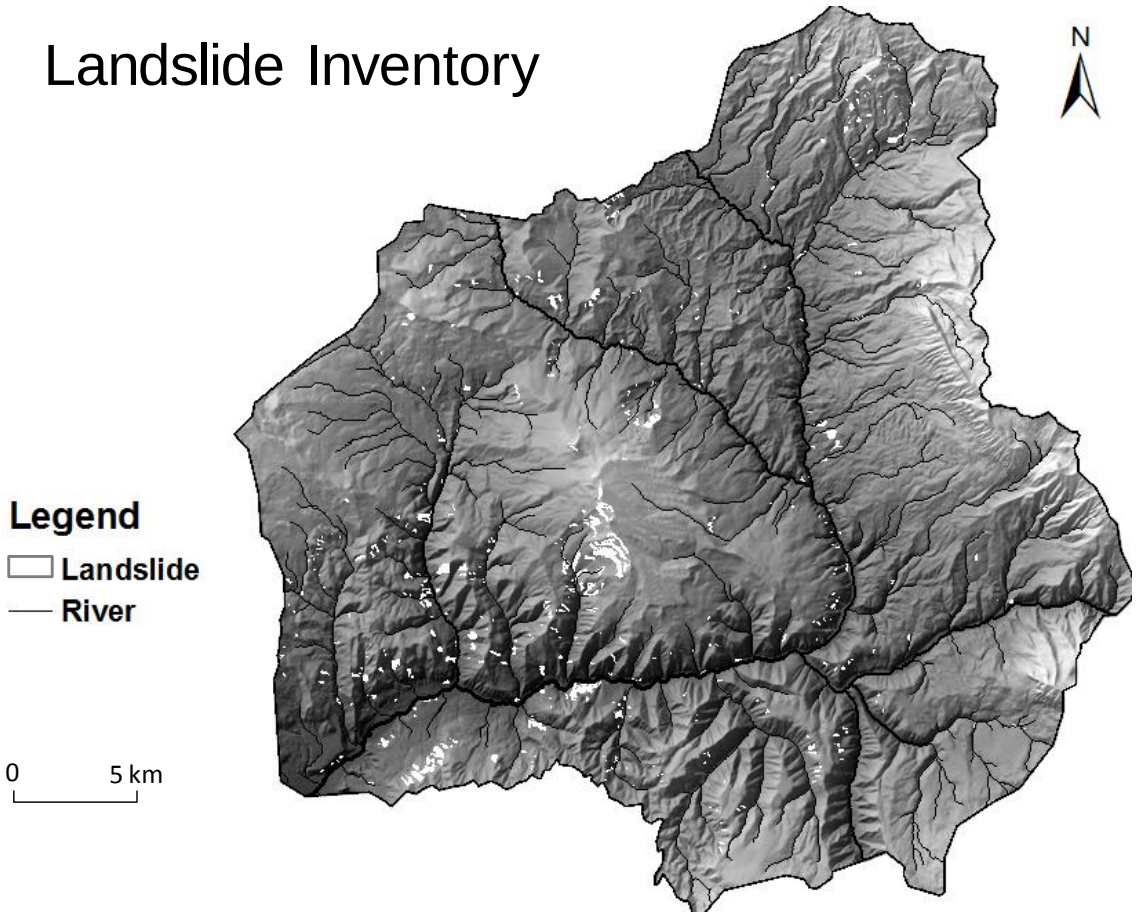

Fig. 27. Distribution of shallow landslides in the study area.

Fig. 28. A panoramic view of the SE slope near Somerset. The entire slope is moving downslope. The topography indicates mass movement is the major process that modified the slope. Landslides comprised of unconsolidated materials. B) A large slump indicated by a dashed line in the photograph is comprised of Mancos Shale. Arrows without "?" symbols also represent landslides. Arrows with "?" symbol indicate the unvegetated part of the landscape which looks like landslides in non-stereo two-dimensional visualization of an aerial photograph. C) A landslide (debris slide) in the study area. The entire slope is moving downslope. The landslides are comprised of unconsolidated materials.

Geological factors

The study area is mainly comprised of only five types of rocks but the geology of the area is differentiated into 13 classes of lithology based on the dominance of the types of rocks and deposits. Using the geological map of Dunrud (1989), some of the geological formations were combined to simplify the relationship of geology to characteristics and frequencies of landslides. Most of the landslides were observed in

interbedded sandstone, shale and mudstone and unconsolidated colluvial, alluvial and glacial deposits (Fig. 28).

Twenty surface and subsurface faults were mapped. Many landslides are found in the close proximity of these faults. The distances from these faults are divided into different categories (Table 5) based on the variation in weight contrast values ($W_C = W_i^+ - W_i^-$) with distances (Fig. 29A).

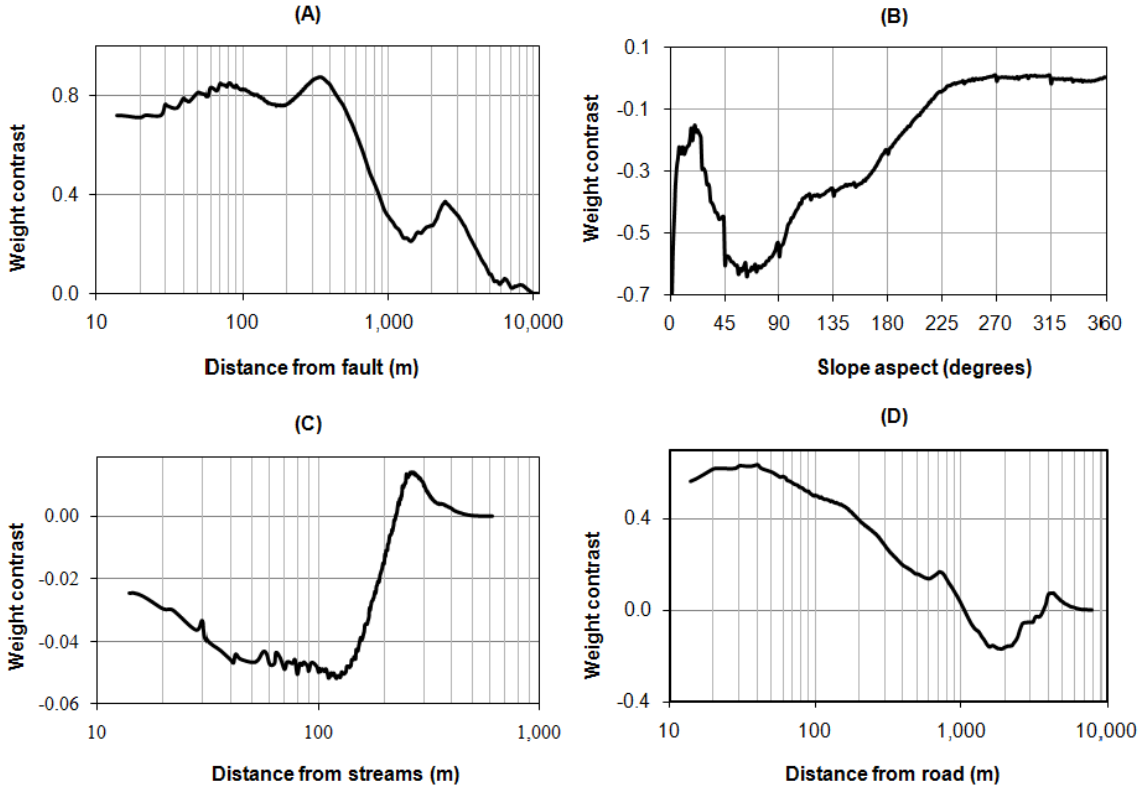

Fig. 29. Approach of categorizing continuous factor data. The continuous data were categorized using the values of continuous data at which the slope of the weight contrast graph breaks. The graph shows weight contrasts for the cumulative values of the continuous data. A) Graph showing the variation of weight contrasts with distances from fault. The weight contrast is maximum at 350 m distance from a fault. B) Graph showing the variation of weight contrasts with slope aspects. C) Graph showing the variation of weight contrasts with distances from river. The weight contrast is maximum at 250 m distance from a river. D) Graph showing the variation of weight contrasts with distances from road. The weight contrast is maximum at 40 m distance from a road.

Table 5 Factors, factor classes, number of factor class pixels and landslide pixels and weights of the factor classes. Weights represented by the bold text are underestimated values. During the analysis, these values were replaced by 0 to reduce the effect of the underestimation. Acronyms: sst: sandstone, mst: mudstone and clst: claystone.

Factor	Class	Class pixels	Landslide pixels	% Class	% Landslide	W^+	W^-	W^+-W^-
Slope (SL)	<10°	2,631,299	1,868	32	4	-2.10	0.40	-2.50
	10-20°	2,778,671	12,566	34	26	-0.30	0.10	-0.40
	20-30°	1,532,209	17,400	19	36	0.70	-0.20	0.90
	30-40°	956,744	12,703	12	26	0.80	-0.20	1.00
	40-50°	216,809	3,513	3	7	1.00	0.00	1.00
	50-60°	31,890	377	0	1	0.70	0.00	0.70
	>60°	7,189	21	0	0	-0.70	0.00	-0.70
Aspect (AS)	Flat (-1°)	68,073	12	1	0	-3.52	0.01	-3.53
	North (337-360°, 0-22°)	806,660	5,048	10	10	0.05	-0.01	0.06
	North East (22-67°)	998,178	2,239	12	5	-0.98	0.08	-1.06
	East (67-112°)	1,054,092	5,565	13	11	-0.12	0.02	-0.14
	South East (112-157°)	961,195	4,509	12	9	-0.24	0.03	-0.27
	South (157-202°)	1,033,415	8,776	13	18	0.36	-0.06	0.42
	South West (202-247°)	1,136,000	9,866	14	20	0.38	-0.08	0.46
	West (247-292°)	1,157,728	7,316	14	15	0.06	-0.01	0.07
	North West (292-337°)	939,470	5,117	12	11	-0.09	0.01	-0.10
Elevation (EL)	<1,800 m	59,546	250	1	1	-0.35	0.00	-0.35
	1800-2000 m	381,734	4,941	5	10	0.79	-0.06	0.85
	2000-2200 m	1,067,871	9,356	13	19	0.39	-0.07	0.47
	2200-2400 m	2,426,731	13,029	30	27	-0.10	0.04	-0.14
	2400-2600 m	2,178,609	10,621	27	22	-0.20	0.06	-0.26
	2600-2800 m	1,133,622	7,378	14	15	0.09	-0.02	0.11
	2800-3800 m	906,698	2,873	11	6	-0.63	0.06	-0.69
Solar radiation (SR)	<600 kwh/m^2	2,168	0	0	0	0.00	0.00	0.00
	600-800 kwh/m^2	15,980	84	0	0	-0.12	0.00	-0.12
	800-1000 kwh/m^2	119,325	1,809	1	4	0.95	-0.02	0.97
	1000-1200 kwh/m^2	371,934	5,883	5	12	0.99	-0.08	1.07
	1200-1400 kwh/m^2	830,039	7,373	10	15	0.41	-0.06	0.46
	1400-1600 kwh/m^2	2,378,225	9,975	29	21	-0.35	0.11	-0.46
	1600-1800 kwh/m^2	3,865,732	16,697	47	34	-0.32	0.22	-0.54
	>1800 kwh/m^2	571,408	6,627	7	14	0.67	-0.07	0.75
Profile curvatur (PRC)	<-5 m^{-1}	26,531	335	0	1	0.76	0.00	0.76
	-5--2 m^{-1}	299,059	2,998	4	6	0.53	-0.03	0.55
	-2-0 m^{-1}	3,039,226	18,117	37	37	0.00	0.00	0.01
	0 m^{-1}	1,406,670	4,617	17	10	-0.60	0.09	-0.69
	0-2 m^{-1}	3,085,047	18,854	38	39	0.03	-0.02	0.05
	2-5 m^{-1}	265,601	3,101	3	6	0.68	-0.03	0.71
	>5 m^{-1}	32,677	426	0	1	0.79	0.00	0.80
Plan curvature (PLC)	<-5 m^{-1}	29,897	298	0	1	0.52	0.00	0.52
	-5--2 m^{-1}	219,985	2,586	3	5	0.69	-0.03	0.72
	-2-0 m^{-1}	2,726,472	18,226	33	38	0.12	-0.07	0.18
	0 m^{-1}	1,911,300	6,600	23	14	-0.55	0.12	-0.67
	0-2 m^{-1}	3,123,923	19,288	38	40	0.04	-0.02	0.06
	2-5 m^{-1}	127,701	1,306	2	3	0.55	-0.01	0.56
	>5 m^{-1}	15,533	144	0	0	0.45	0.00	0.45
Tangential curvature (TC)	<-5 m^{-1}	151,092	1,875	2	4	0.74	-0.02	0.76
	-5--2 m^{-1}	1,426,520	9,754	17	20	0.14	-0.03	0.17
	-2-0 m^{-1}	1,392,935	8,072	17	17	-0.03	0.01	-0.03
	0 m^{-1}	2,109,470	10,237	26	21	-0.20	0.06	-0.27
	0-2 m^{-1}	2,590,590	14,151	32	29	-0.08	0.04	-0.12
	2-5 m^{-1}	417,858	3,633	5	7	0.38	-0.03	0.41
	>5 m^{-1}	66,346	726	1	1	0.62	-0.01	0.62
Distance to road (DR)	<20 m	139,258	1,518	2	3	0.61	-0.01	0.63
	20-40 m	105,648	1,208	1	2	0.66	-0.01	0.67
	40-100 m	300,766	2,607	4	5	0.38	-0.02	0.40
	100-350 m	971,971	6,040	12	12	0.05	-0.01	0.05
	>350 m	6,637,168	37,075	81	77	-0.06	0.23	-0.30

Table 5 continued.

Factor	Class	Class pixels	Landslide pixels	% Class	% Landslide	W^+	W^-	W^+-W^-
Geology (GEO)	Glacial Drift	112,072	786	1	2	0.17	0.00	0.17
	Alluvial Terrace	73,624	84	1	0	-1.65	0.01	-1.66
	Colluvium	37,250	960	0	2	1.49	-0.02	1.50
	Talus and Rock Glacier Deps.	127,298	1	2	0	**-6.63**	**0.02**	**-6.65**
	Unconsolidated alluvium	172,579	458	2	1	-0.81	0.01	-0.82
	Mixed Alluvium and colluvium	781,043	3,256	10	7	-0.36	0.03	-0.39
	Landslide and Mudflow Deps.	1,453,863	17,902	18	37	0.74	-0.27	1.00
	Unconsolidated Deps. (mixed)	878,963	4,304	11	9	-0.19	0.02	-0.22
	Basalt and gabbros	1,486	97	0	0	2.46	0.00	2.46
	Plutonic rock (granodiorite)	264,197	2	3	0	**-6.67**	**0.03**	**-6.70**
	Wasatch Fm. (clst, mst, sst)	2,651,560	6,606	33	14	-0.87	0.25	-1.12
	Mesavarde Fm. (sst, mst, shale)	1,534,501	13,192	19	27	0.37	-0.11	0.48
	Mancos Shale	51,216	800	1	2	0.98	-0.01	0.99
Distance to fault (DF)	<25 m	45,726	556	1	1	0.72	-0.01	0.73
	25-75 m	78,361	1,151	1	2	0.91	-0.01	0.93
	75-150 m	121,788	1,421	1	3	0.68	-0.01	0.70
	150-350 m	342,546	5,211	4	11	0.95	-0.07	1.02
	350-10,653 m	7,566,390	40,109	93	83	-0.11	0.88	-0.99
Land cover (LC)	Forest	3,378,384	11,581	41	24	-0.55	0.26	-0.82
	Shrub/bush	3,236,247	30,241	40	62	0.46	-0.48	0.93
	Grassland	711,441	1,677	9	3	-0.93	0.06	-0.98
	Woodland	395,505	3,514	5	7	0.41	-0.03	0.43
	Agriculture	209,061	123	3	0	-2.32	0.02	-2.34
	Rock cliff and barren land	176,481	1,273	2	3	0.20	-0.01	0.20
	Water	28,305	0	0	0	0.00	0.00	0.00
	Residential	19,557	26	0	0	-1.50	0.00	-1.50
Soil plasticity (SP)	Rock	96,412	1,139	1	2	0.70	-0.01	0.71
	Non-plastic-very low plastic	815,150	18,633	10	38	1.36	-0.38	1.75
	Low plastic	4,710,787	21,313	58	44	-0.27	0.28	-0.56
	Medium Plastic	2,282,552	7,864	28	16	-0.55	0.15	-0.70
	High plastic	227,026	595	3	1	-0.82	0.02	-0.84
	Water	21,122	43	0	0	-1.08	0.00	-1.08
Flow length (FL)	<11 m	2,023,344	7,664	25	16	-0.45	0.11	-0.57
	30 m	1,131,536	5,468	14	11	-0.21	0.03	-0.24
	300 m	4,224,709	29,171	52	60	0.15	-0.19	0.34
	1000 m	631,820	5,341	8	11	0.36	-0.04	0.39
	75,158 m	143,402	804	2	2	-0.06	0.00	-0.06
Flow acc. (FA)	1 Cells	1,606,771	5,760	20	12	-0.51	0.09	-0.60
	3 Cells	1,445,479	7,093	18	15	-0.19	0.04	-0.23
	7 Cells	1,532,847	8,939	19	18	-0.02	0.00	-0.02
	50 Cells	2,729,873	20,425	33	42	0.23	-0.14	0.37
	700 Cells	655,731	5,101	8	11	0.27	-0.03	0.30
	16,262,011 Cells	184,110	1,130	2	2	0.03	0.00	0.03
Stream power index (SPI)	0-3	1,514,627	1,991	19	4	-1.52	0.17	-1.69
	3-12	1,905,600	8,183	24	17	-0.33	0.08	-0.42
	12-50	2,485,090	15,513	31	32	0.04	-0.02	0.06
	50-400	1,814,457	18,641	22	38	0.54	-0.23	0.78
	400-5000	268,044	3,450	3	7	0.77	-0.04	0.81
	5,000-97,269,664	99,050	658	1	1	0.10	0.00	0.11
Topographic wetness index (TWI)	0-2	3,338	18	0	0	-0.11	0.00	-0.11
	2-4	1,189,006	10,042	15	21	0.35	-0.07	0.42
	4-6	4,173,081	23,860	52	49	-0.05	0.05	-0.10
	6-8	1,935,985	10,944	24	23	-0.06	0.02	-0.08
	8-10	536,021	2,500	7	5	-0.25	0.02	-0.27
	10-12	143,660	686	2	1	-0.23	0.00	-0.23
	12-23	105,777	386	1	1	-0.50	0.01	-0.50
Distance to stream (DS)	<25 m	1,386,867	8,004	17	17	-0.03	0.01	-0.04
	25-50 m	1,253,719	6,983	15	14	-0.06	0.01	-0.08
	50-100 m	1,923,620	10,858	24	22	-0.05	0.02	-0.07
	100-250 m	3,055,075	19,942	37	41	0.09	-0.06	0.16
	250-614 m	535,530	2,661	7	5	-0.18	0.01	-0.19

Land cover

Land cover is also one of the key factors responsible for landslides in the study area. Vegetated areas are less prone to shallow landslides (Greenway, 1987; Styczen and Morgan, 1995) because vegetation prevents erosion through the natural anchorage provided by roots. Based on the unsupervised classification of the ETM satellite image acquired in 2002, evaluation of aerial photograph acquired in 2005 and field surveys, seven land cover classes were mapped: forest (41%), woodland (5%), shrub (40%), grassland (9%), agricultural land (3%), rock cliffs and barren land (2%), and human settlement (0.2%). Among these classes, shrubland and woodland are the classes where most of the landslides occurred.

Soil

Grain size and plasticity index of the soil or regolith up to a depth of about 1.5 m were collected. Grain size of the soil is classified based on the percentage of soil passing through number 200 sieve (0.075 mm). The soil size is classified in to three classes as fine grained, medium grained and coarse grained. Fine soil is classified if more than 66% passes through the sieve, medium grained if 33% to 66% passes through the sieve and the coarse grained with 0 to 33 % passing through the number 200 sieve. Soil plasticity index is classified as non-plastic, low plastic (PI = 0-5), medium plastic (PI = 5-20), and high plastic (PI >20). Most of the landslides are observed in medium to coarse and non-plastic to low plastic soils. The spatial pattern of the classes of both

factors is quite similar. Therefore, only the plasticity index is used in the analysis of the susceptibility to landslides.

Topographic factors

DEMs with a horizontal resolution of ten meters have been used to derive various topographic factors including slope, aspect, elevation, profile curvature, plan curvature, tangential curvature, and mean hourly solar radiation using inbuilt algorithms in ArcGIS®. All of these data were initially continuous, but were converted into different categories based on the variation in weight contrast values with values of the topographic data (e.g., Fig. 29B) as well as the frequency distribution of different topographic values on the surface of the landslides and for the entire area. Both approaches provided similar results.

Water-related factors

Surface water, sub-surface water and groundwater are the major hydrological causes of landslides. Surface water promotes landslides by undercutting and eroding slopes. Fluctuation of sub-surface water and groundwater changes the pore water pressure in soil and changes the stability of the slope. The factors of drainage network, topographic wetness index (*TWI*), stream power index (*SPI*), flow accumulation and upstream flow length, were derived from a DEM as a measure of surface water, sub-surface water and groundwater. Topographic wetness index and stream power index can be defined by Eqs. (35) and (36), where A (m^2) is the upstream catchment area or flow

accumulation, b (m) is the width of a cell through which water flows and β (radian) is the slope.

$$TWI = \log_e (A/b \tan \beta) \quad (35)$$

$$SPI = A \tan \beta / b \quad (36)$$

Researchers suggest that soil moisture can be estimated by topographic wetness index (Moore et al., 1991; Beven, 1997; Blyth et al., 2004). The stream power index is a measure of the erosive power of water flow based on the assumption that discharge is proportional to specific catchment area (Moore et al., 1991). Flow accumulation in its simplest form is the number of upslope cells that flow into each cell. The flow length is the longest upslope distance along the flow path from each cell to the top of a drainage divide. The flow accumulation and flow length were created using inbuilt algorithms in ArcGIS®. The algorithm uses an eight direction (D8) flow model proposed by Jenson and Domingue (1988).

I observed many landslides in the proximity of the North Fork of the Gunnison River and its associated tributaries. To include the effect of the stream in the assessment of susceptibility to landslides, the drainage map of the study area, which consists of drainage orders up to the 8th order based on Strahler (1957), was created from the DEM. A cell is considered to have a stream if more than 500 upslope cells (50,000 m^2 catchment) flow through it. Distances from the streams were calculated and the map was divided into different categories (Table 5) based on the variation in weight contrast values with distances (Fig. 29C). Similarly, topographic wetness index, stream power index, flow accumulation and flow length were divided into different classes (Table 5).

Distance to road

Excavating slopes for the construction of roads and frequent vibrations generated by vehicles predispose hillslopes to failure (Ayalew and Yamagashi, 2005; Mittal et al., 2008). Around the Paonia-McClure Pass area numerous landslides were observed along Colorado Highway 133 and various forest roads. To include the role of roads in the assessment of hazardous landslides, Highway 133 and the forest roads were mapped within ± 5 m positional accuracy of the aerial photograph and distances from these roads were calculated. The distances from roads are divided into different categories based on the variation in weight contrast values with distances (Fig. 29D and Table 5). Some roads, including those around residential areas, on flat terrains, and in areas with little potential for landslides, were excluded from this study.

Calculation of weighted values

Weighted values for the classes of 17 factors were calculated using Eqs. (37) and (38) which are derived from Eqs. (22) and (25):

$$W^{+} = Log_e \left(\frac{\frac{A_1}{A_1 + A_2}}{\frac{A_3}{A_3 + A_4}} \right) \tag{37}$$

$$W^{-} = Log_e \left(\frac{\frac{A_2}{A_1 + A_2}}{\frac{A_4}{A_3 + A_4}} \right) \tag{38}$$

where, A_1 is the number of the landslide pixels present on a given factor class, A_2 is the number of the landslide pixels not present in the given factor class, A_3 is the number of the pixels in the given factor class in which no landslide pixels are present and A_4 is the number of the pixels in which neither landslide nor the given factor is present.

The calculation is performed in ArcGIS 9.2® by using the spatial analysis tool. A positive weight (W_i^+) indicates presence of the causative factor in the landslide, and the magnitude of this weight is an indication of the positive correlation between presence of the causative factor and landslides. A negative weight (W_i^-) indicates an absence of the causative factor, and the magnitude indicates negative correlation. The difference between the two weights is known as the weight contrast, W_C ($W_C = W_i^+ - W_i^-$), and the magnitude of the contrast reflects the overall spatial association between the causative factor and landslides. If the weight contrast is positive, the factor is favorable for the landslides, and if it is negative, it is unfavorable for the landslides. If the weight contrast is close to zero, this indicates that the factor shows little relation to the landslides. A problem with this method is that when very few pixels of a landslide are present in a given factor class, the weighted value of the class becomes very low. While summing this value with the weighted values of other factors, the high negative values might cause the region to fall into a low susceptibility category, although the weighted values of other factors imply that the zone is hazardous. In this case it is better to assign a zero weighted value to this class or combine the class with other classes.

Test for conditional independence

The conditional independence of the factors assigned to given landslides was tested before the integration of the weighted map to create a total weight map by pairwise comparison using chi-square statistics.

First, for the ease of the analysis, all of the factors causing landslides were converted into a binary pattern (presence or absence of landslides) based on weight contrast and expert's knowledge. Categorical data, like geology, land cover, soil size and soil plasticity index, were first separated into the binary pattern based on the expert's judgment and the weight contrasts of each factor class. Continuous data, like slope, aspect, elevation, curvature, wetness index, stream power index, were first divided into classes and then categorized into binary patterns based on the weight contrasts of each class. In both cases, mostly the factor classes having positive values of weight contrasts, were assigned as presence and factor classes having negative weight contrast values were assigned as absence. These binary classes were cross-verified by a *priori* judgment based on the personal evaluation of the hazards and the distribution of the landslides. Continuous data, like distance to roads, drainage, and faults, have different meanings. If these features are responsible for the landslides, the weighted values should be relatively higher nearby these features. I classified distance to faults, roads and drainage into the binary pattern based on the maximum value of weight contrast from the cumulative weight contrast curve (Fig. 29). Areas within 350 m of faults are categorized as presence, and the areas beyond this distance are categorized as absence. The areas within 40 m of the roads are categorized as presence and the areas beyond this distance are

categorized as absence. Likewise, the areas within 250 m of the drainage are categorized as presence and the areas beyond this distance are categorized as absence.

Table 6 2×2 contingency table showing observed frequencies (O_i) and expected frequencies (E_i) of landslides (L) in binary factors F_1 and F_2. The expected frequencies (E_i) are determined by multiplying the marginal frequencies together and dividing by the total.

		Binary pattern F_1		
		Present	Absent	Totals
Binary pattern F_2	Present	$O_1 = \{F_1 \cap F_2 \cap L\}$ $(E_1 = \{F_2 \cap L\} * \{F_1 \cap L\} / \{L\})$	$O_3 = \{\overline{F}_1 \cap F_2 \cap L\}$ $(E_3 = \{F_2 \cap L\} * \{\overline{F}_1 \cap L\} / \{L\})$	$\{F_2 \cap L\}$
	Absent	$O_2 = \{F_1 \cap \overline{F}_2 \cap L\}$ $(E_2 = \{\overline{F}_2 \cap L\} * \{F_1 \cap L\} / \{L\})$	$O_4 = \{\overline{F}_1 \cap \overline{F}_2 \cap L\}$ $(E_4 = \{\overline{F}_2 \cap L\} * \{\overline{F}_1 \cap L\} / \{L\})$	$\{\overline{F}_2 \cap L\}$
	Totals	$\{F_1 \cap L\}$	$\{\overline{F}_1 \cap L\}$	$\{L\}$

Second, 2×2 contingency tables for all possible pairs of 17 binary factors (similar to Table 6) were prepared and chi-square tests were performed with 1 degree of freedom. The observed chi square value for each pair is compared with the table value for 1 degree of freedom at the 99% confidence level (6.64). Chi-square values, greater than the table values, suggest that the pairs are not significantly different, given the occurrence of landslides. Chi-square values were determined by employing Eq. (39), in which the observed frequencies (O_i) and the expected frequencies (E_i) are determined from the contingency table (Table 6). One hundred and thirty six pairs were tested. Among 136 pair-wise comparisons, 103 of the pair-wise comparison couples were found independent of each other for all the landslides examined (Table 7).

$$\chi^2 = \sum_{i=1}^{i=n} \frac{(O_i - E_i)^2}{E_i} \quad (39)$$

The chi-square test evidenced relationships of different factors. Geology, distance to a fault, and soil plasticity index are conditionally dependent on each other. Slope and soil plasticity index are dependent on land cover. Slope is dependent on its derivatives solar radiation, profile curvature and plan curvature. Likewise hydrologic factors, soil plasticity index, topographic wetness index, flow accumulation and flow length are related to each other. Therefore, a major question to be answered from the WOE method of mapping susceptibility of landslides is what factors are important to prepare an accurate map of susceptibility to landslides? To answer this question, I designed six models, which include combinations of different independent factors representing topographic, hydrologic, geologic, land cover and anthropogenic factors (Table 8).

Combination of weighted maps and selection of the best model

Maps of susceptibility to landslides were prepared from each model by summing the weight contrast values of different factors pixel by pixel (e.g. Figs. 30A, 30B). The accuracy of each model was tested using the observed landslides (Fig. 30C).

In addition, the validity of the models was tested by creating maps of susceptibility to landslides (e.g., Figs. 31A, 31B) based on randomly selected 368 observed landslides (training sets) and checking the accuracy of these models using training sets (Fig. 31C) and validity of these models (Fig. 31D) against the remaining

367 landslides (validation sets). The prediction capability of each model is determined by the area under the curve (Table 9). Based on these values, model 1 and model 2 are

Table 7. Pairwise chi-square statistics of 17 factors. GEO: Geology, DF: Distance From Faults, SP: Soil Plasticity, LC: Land cover, SL: Slope, AS: Aspect, EL: Elevation, SR: Solar Radiation, PRC: Profile Curvature, PLC: Plan Curvature, TC: Tangential Curvature, FL: Flow Length, FA: Flow Accumulation, SPI: Stream Power Index, TWI: Topographic Wetness Index, DS: Distance From Streams, and DR: Distance From Roads.

	GEO	**DF**	**LC**	**SP**	**SL**	**AS**	**EL**	**SR**	**PRC**	**PLC**	**TC**	**FL**	**FA**	**SPI**	**TWI**	**DS**	**DR**
GEO		8.5	0.2	**9.3**	6.2	0.0	0.8	2.0	1.6	1.9	6.0	6.5	**10.4**	7.3	0.7	2.2	0.5
DF			**21.2**	**9.0**	2.5	**19.3**	**15.5**	2.9	0.2	0.0	0.0	1.2	**11.2**	0.2	0.9	0.5	**34.3**
LC				**10.8**	**24.4**	6.6	2.5	6.5	1.7	0.0	0.8	0.2	0.0	0.1	3.7	3.8	**10.3**
SP					6.0	0.0	**37.0**	4.6	3.3	4.9	**7.7**	0.0	1.5	0.2	1.9	0.8	1.0
SL						4.6	0.0	**28.8**	**12.7**	**14.2**	3.2	1.5	0.0	**31.6**	**16.5**	0.2	1.2
AS							0.0	2.1	0.0	0.1	0.8	0.7	4.3	0.5	4.4	0.9	3.1
EL								**37.6**	0.3	0.3	1.9	**89.0**	1.0	0.0	0.5	**8.1**	**128**
SR									**24.5**	0.3	0.2	0.4	0.6	0.6	0.7	0.1	3.5
PRC										**347**	**30.8**	0.1	0.1	0.3	1.1	0.2	0.3
PLC											**27.7**	1.6	0.0	1.9	1.3	1.7	0.0
TC												0.6	0.0	0.7	0.1	4.6	2.2
FL													**288**	**372**	**443**	0.4	0.4
FA														**187**	**236**	0.1	0.0
SPI															**237**	0.3	0.0
TWI																3.1	0.3
DS																	0.2
DR																	

Table 8 Six possible combinations of the factors based on the chi-square statistics. Acronyms same as table 6.

Factors	Model 1	Model 2	Model 3	Model 4	Model 5	Model 6
Geology/ soil/land cover	SP	GEO	SP	GEO LC	GEO	
Topographic	SL AS TC	SL AS TC	SR AS PLC	SR AS TC/*PLC	SL AS TC EL	SL AS TC
Hydrologic	*FA/FL DS	FL DS	*SPI/TWI/FA/FL DS	TWI DS	DS	SPI/TWI/*FA/FL DS
Anthropogenic	DR	DR	DR			DR

considered as accurate models. These two models have five factors in common; and only two factors are different. Although most of the distribution patterns of the total weight in these two models (Figs. 30A, 30B) are quite similar, the difference results from two factors in each model. Flow accumulation and flow length are measuring the same topographic character as shown by the very high chi-square statistics of this pair. Thus, the difference in these models solely depends on the difference in the patterns of

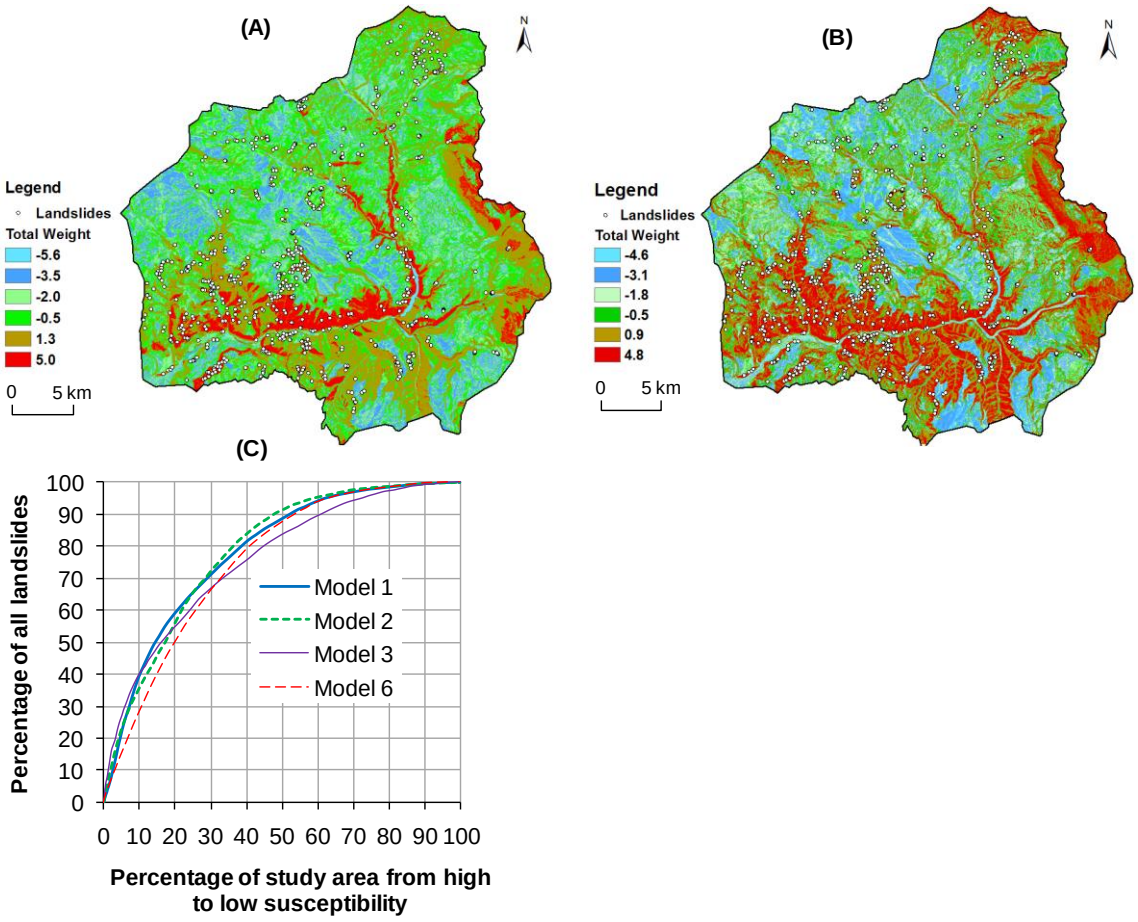

Fig. 30. Accuracy assessment of the models. A) Total weight map developed using model 1 factors and 735 landslides. B) Total weight map developed using model 2 factors and 735 landslides. C) Accuracy assessment of the four models of susceptibility to landslides. The total weights for these models were based on 735 landslides and the performance of the models was evaluated by all 735 landslides.

classes between geology and soil plasticity. A prudent judgment to obtain a better result would be the combination of these two factors, but in the WOE method the combination of these factors is logically impossible because they are conditionally dependent on each other.

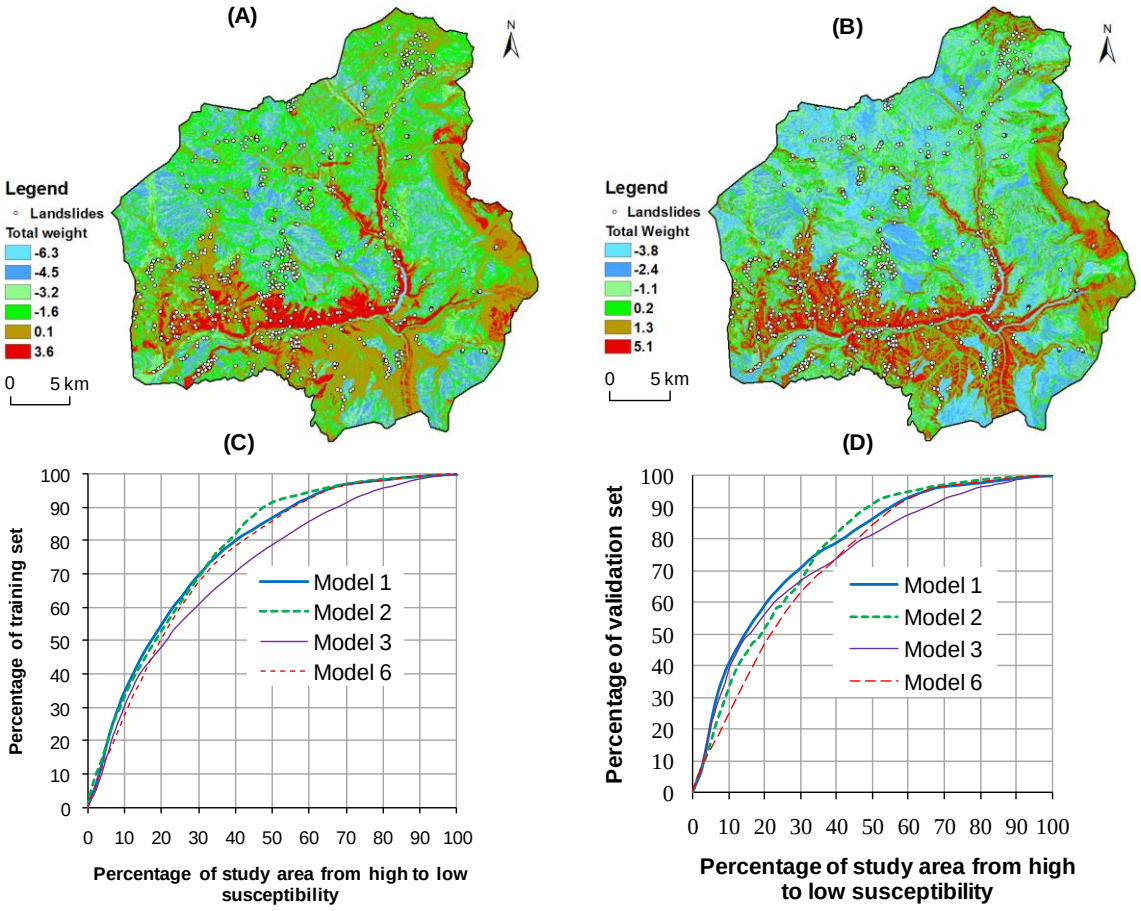

Fig. 31. Validity assessment of the models. A) Total weight map developed using model 1 factors and 368 landslides (training set). B) Total weight map based on model 2 factors and 368 landslides (training set). C) Accuracy assessment of the four models of susceptibility to landslides. The total weights for these models were based on 368 landslides (training set) and the performance of the models was evaluated by all 368 landslides. D) Test of validity of the four models. The total weight maps were based on the 368 landslides (training set) and the accuracy is assessed by using the remaining 367 landslides (validation set). Models 1 and 2 predict more landslides in zones of high susceptibility than the other models.

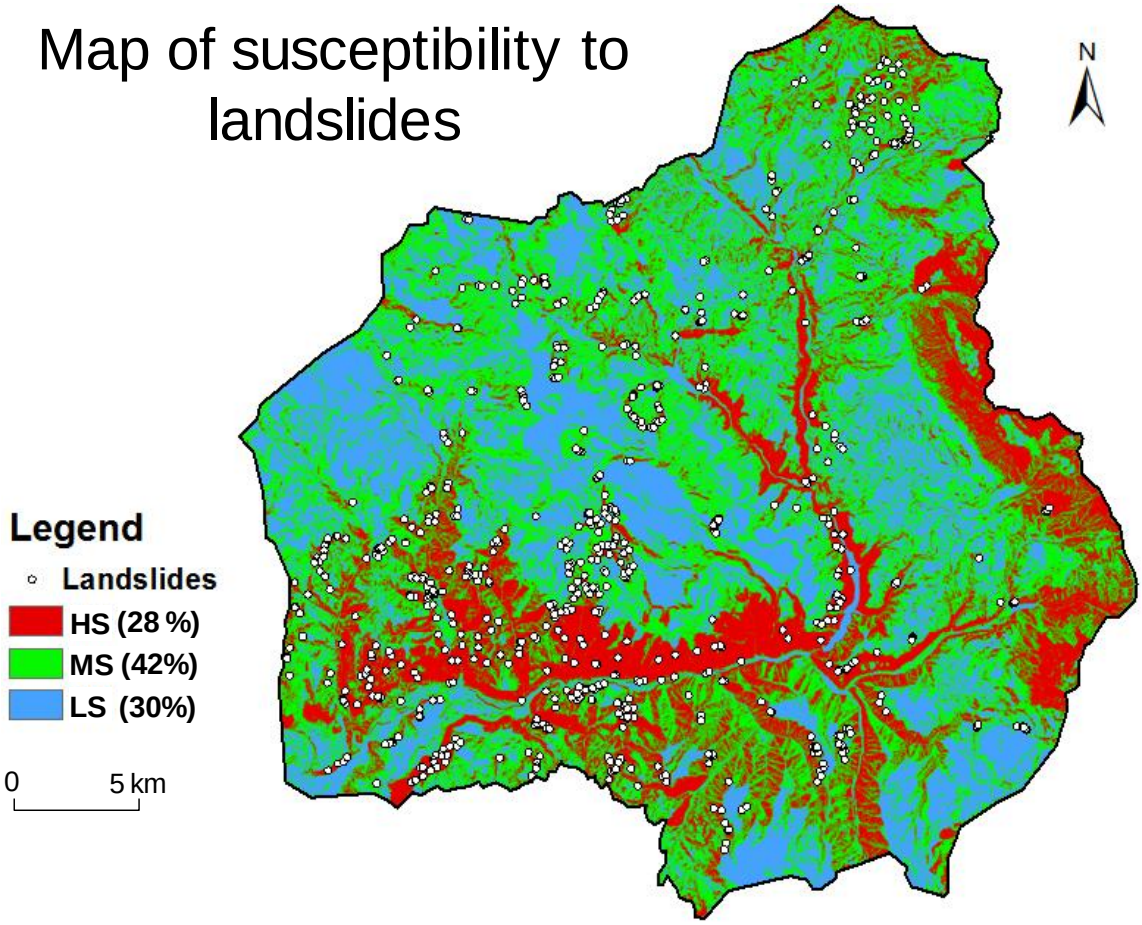

Fig. 32. Susceptibility to landslides based on model 1 factors and 735 landslides. This model has the highest rate of prediction. The high susceptibility (HS) area consists of 28% of the study area; it includes 70% of the total area of landslides. The medium susceptibility (MS) area, consists of 42% of the study area and comprises 27% of the total area of landslides. The low susceptibility (LS) area, consists of 30% of the study area and contains 3% of the total area of landslides.

Test of validity implies that model 1 is the best model. The total weighted map of model 1 was converted into three classes representing high susceptibility, medium susceptibility and low susceptibility (Fig. 32). The classification is based on the natural break in the frequency distribution curve of the total weight (Fig. 33). These values were slightly modified so that optimum amount of landslides falls into zones of high

susceptibility and flat terrain like river floodplain and upland plateau falls into zones of low susceptibility.

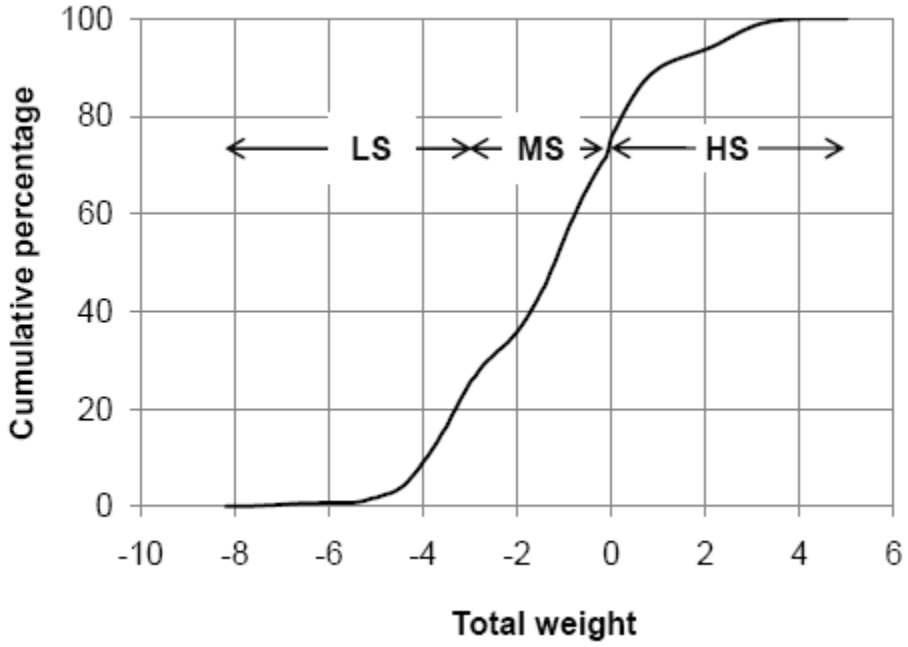

Fig. 33. The frequency distribution of the total weight values. Natural breaks of the curve were used to classify the total weight map (Fig. 30A) into a map of susceptibility (Fig. 32). The high susceptibility zone has a value of weight ranging from 5 to 0, the medium susceptibility has a value of weight ranging from 0 to -2.5 and the low susceptibility has a value of weight ranging from -2.5 to -8.2.

Table 9 Accuracy assessments of the six models of susceptibility to landslides based on the area under the curve approach. Case A) the prediction accuracy of the models represented by the curves in Fig. 30C. Case B) the prediction accuracy of the models represented by the curves in Fig. 31C. Case C) the prediction accuracy of the models represented by the curves in Fig. 31D.

Models	Predicted area % under the curve (Case A)	Predicted area % under the curve (Case B)	Predicted area % under the curve (Case C)
1	78.3	77.4	78.4
2	78.7	77.2	77.6
3	75.7	72.3	75.0
4	77.0	72.5	73.8
5	79.0	76.5	77.0
6	75.2	76.9	73.9

Results and discussion

The predictive capability of model 1 for known and unknown landslides (Table 9) suggests that slope, aspect, tangential curvature, soil plasticity index, flow accumulation, distance to streams and distance to roads are sufficient to create an optimum and valid map of susceptibility to landslides of the study area. The high susceptibility zone has a value of weight ranging from 5 to 0, the medium susceptibility has a value of weight ranging from 0 to -2.5 and the low susceptibility has a value of weight ranging from -2.5 to -8.2. On the susceptibility map, 28% of the area is shown as high susceptibility, 42% is shown as medium susceptibility and 30% is shown as low susceptibility (Fig. 32). Most of the high susceptibility zones are primarily located in the areas adjacent to streams and roads, have steep slopes with shrubland and woodland vegetative covers and consist of non-plastic to low plastic soils. Observed and predicted landslides are found on the slopes of the inner gorges of North Fork Gunnison River and its associated streams which are incising into plateaus upland. These characteristics of landslides represent potential for the first order prediction of the landslides in this landscape.

Based on my results, some of the pros-and-cons of the WOE method in predicting zones of landslide susceptibility are as follows. Advantages of the method are: 1) the method calculates the weighted value of the factor based on the statistical formula, i.e. Eqs. (22) and (25), and avoids the subjective choice of weighting factors; 2) in GIS these multiple weighted maps can be combined by a writing GIS script; 3) weighted values, calculated from Eqs. (22) and (25), can be used to categorize the continuous data;

4) input maps with missing data (incomplete coverage) can be accommodated in the model; 5) undersampled landslide data does not significantly impact the results; and 6) the method provides a technique to avoid the use of data that are intercorrelated.

The WOE method has three major disadvantages: 1) Because the weight is dependent on the number of landslide pixels used on the modeling, the method overestimates or underestimates weights if the area of a factor class is very small and the landslides are not evenly distributed. 2) The method creates a number of possible combinations of the conditionally independent factors. To determine what combination of factors is appropriate, assessment of the performance of each combination is necessary, which is a lengthy process. 3) The weight values calculated for different areas are not comparable in terms of the degree of susceptibility. This is possible only if the weights are standardized or converted to the probability. The effect of overestimation and underestimation of weights can be reduced either by excluding the factor class from the analysis by assigning 0 weight value or by reclassifying the factor maps. In this study I excluded two classes of geology (plutonic rock and talus and rock glacier deposits) from the analysis by assigning them 0 weight value. The cutoff values of weight depend on the *priori* knowledge of the study area. The commonly used method for the test of the conditional independence in the WOE method is pair-wise comparison. When the analysis consists of a large number of factors and factor classes, the pairwise comparison becomes complicated because of the numerous possible combinations of the classes of the factors. For example, I observed only seven factors being conditionally independent of each other, but we can combine the factors in different ways to develop different

models (Table 8). So which model performs better? A solution is to assess the prediction capabilities of the possible models based on the landslides considered in the analysis, as well as landslides not considered in the analysis. I observed that model 1 is the best model for my study area. In this regard, this method is more complicated than variable selection by factor analysis or linear and non-linear regression analyses. Other limitations of the method are: 1) the method is only applicable in areas where the landslides are fairly well known, and 2) it is impossible to enter the interaction of two different factors in the analysis.

I think this method can provide a better result if the landslides are classified into different types, and a map of weighted values is created for each landslide type. For example, using the WOE method Neuhäuser and Terhorst (2007) obtained ~95% prediction accuracy for a single type of landslide in south-west Germany; Dahal et al. (2008a) obtained 85.5% prediction accuracy for newly formed debris flows in the Lesser Himalaya of Nepal; Dahal et al. (2008b) obtained 80.7% and 77.6% prediction accuracy for landslides comprising the translational and flow types of slides in the Moriyuki and Monnyu catchments in Japan, respectively. Although a WOE-based map of susceptibility to a single type of landslide performs better then a map of susceptibility to various types of landslides, a map showing zones of susceptibility to all kinds of landslides would be the choice of the decision makers. Combination of maps of susceptibility to landslides of different types into a single map would be a solution, but in the WOE method the combination of two or more maps of weighted values is impossible because the weighted values are not comparable.

Nevertheless, the map of susceptibility to landslides developed by this method is effective in predicting known and unknown landslides. The prediction accuracy of my best model is 78.4%. The model predicts 70% of the known as well as unknown landslides in high susceptibility zones when 28% of the study area is defined as high susceptibility (Figs. 30C, 31D). The performance of my model is slightly different than the performance of the models suggested by other investigators (e.g., Lee et al., 2002, 2004; Van Westen et al., 2003; Mathew et al., 2007; Dahal et al., 2008a, 2008b). It should be understood that model performance depends on the correct identification of the major factors of landslides, quality of the data collected, number of landslides, scale and size of the study and uncertainties associated with the digitization of the data. Moreover, highly generalized data, like geology and the soil plasticity index, do not distinguish individual soil and rock types, which may introduce large amounts of uncertainties in the analysis. The study consisted of a large area and highly generalized geology and soil data. Furthermore, I was unable to evaluate the role of rainfall and snowmelt in landslides of my study area. Many rainfall and snowmelt induced landslides have been reported in Colorado (Rogers, 2003). In spite of not being able to evaluate the role of rainfall and snowmelt in my area, I think the result I obtained from the analysis is satisfactory for a regional-scale (815 km^2) study.

CHAPTER V

ASSESSING SUSCEPTIBILITY TO LANDSLIDES: USING MODELS TO UNDERSTAND OBSERVED CHANGES IN SLOPES*

Synopsis

A map of landslide susceptibility is a necessary tool for proper planning and selection of sites for agriculture, infrastructure and other human developments. The Paonia-McClure Pass area of Colorado, USA, is well known for active mass movements. Large losses of property and risks to people highlight the need to accurately map susceptibility to shallow landslides and to identify safe locations for infrastructure and residential development.

The study mapped 735 active mass movements and 17 factors about each one. The weights of evidence, frequency ratio of landslides, and fuzzy-logic method were used to create an optimum map of landslide susceptibility. Weights of the evidence were used to categorize continuous factor data, frequency ratios of shallow landslides were used to assign the membership values for the categories of the factors, and the fuzzy-logic method was used to integrate the membership values. Four models from the fuzzy-inference network of mapping susceptibility to shallow landslides were developed based on the combination of factors using five types of fuzzy operators. The first inference-

---

*Reprinted with permission from "Assessing susceptibility to landslides: Using models to understand observed changes in slopes" by Regmi N.R., Giardino J.R., and Vitek J.D., 2010. *Geomorphology*, 122, 25-38, Copyright (2010) by Elsevier B.V.

network model was comprised of the combination of factors, which are independent of each other. The second, third and the fourth inference-network models were developed such that factors are not necessarily independent of each other. These models combine all dependent and independent factors, based on the expert's knowledge. Intermediate steps in the second, third and fourth models were developed by combining the fuzzy factors in the first step by fuzzy-OR, fuzzy-AND, and fuzzy-OR plus fuzzy-AND operations, respectively.

All models predicted similar percentages of observed shallow landslides with the fuzzy-gamma operation. Although the prediction capabilities of all the models are not significantly different, the fourth model is the best because it is the only model that accommodates the undersampled and missed landslide data and the effect of increasing and decreasing gamma values. The first and third models create a problem if a category of a factor has a 0 membership value because of the absence or under-sampling of shallow landslides. The second model incurs the highest increasing effect of gamma values, and the third model incurs the highest decreasing effect of gamma values. The approaches described in this chapter reduce the uncertainties associated with the categorization of continuous data, determination of fuzzy-membership values, and the combination of factors that cause shallow landslides.

Introduction

Maps of landslide hazards/susceptibilities and risks are necessary tools for engineers, earth scientists, engineering geologists, planners and decision makers to select

appropriate sites for development of agriculture, construction and other human activity. Numerous articles have been published on mapping hazards and susceptibilities to landslides. The methods of mapping landslide susceptibility can be categorized into qualitative or knowledge-based (Carrara and Merenda, 1976; Kienholz, 1978; Fenti et al., 1979; Ives and Messerli, 1981; Rupke et al., 1988, Regmi et al., 2010a), quantitative or statistical (Carrara, 1983; Carrara et al., 1991, 1999; Anbalagan, 1992; Juang et al., 1992; Maharaj, 1993; Gokceoglu and Aksoy, 1996; Van Westen et al., 1997; Atkinson and Massari, 1998; Pachauri et al., 1998; Guzzetti et al., 1999; Rautela and Lakhera, 2000; Gritzner et al., 2001; Sakellariou and Ferentinou, 2001; Gorsevski et al., 2003; Cevik and Topal, 2003; Tangestani, 2004; Lee, 2004; Ayalew and Yamagishi, 2005; Regmi et al., 2010a,b) and deterministic methods (Chowdhury, 1976; Chowdhury and Bertoldi, 1977; Wu and Sidle, 1995; Gokceoglu and Aksoy, 1996). In summary, qualitative or knowledge-based methods are based on field observations and *a priori* knowledge of the expert, in which the expert identifies landslides and makes *a priori* assumptions about those sites where movement has occurred and is likely to occur again. The expert then develops decision rules or assigns weighted values for the classes of index maps and overlays them to develop a map of landslide susceptibility.

The quantitative-based methods are mostly statistical analyses, neural networks and fuzzy logic. Deterministic methods mainly focus on slope geometry, shear strength data (cohesion and angle of internal friction), and pore-water related data. A deterministic approach considers angle of slope, strength of the slope material, structure (rock discontinuities, rock and soil stratification), moisture content of the slope material,

and depth of the groundwater table in a physics-based equation to determine an index of the stability of the slope such as the factor of safety. This method usually ignores climatic and human induced factors, which also can contribute to landslides. Furthermore, this method only determines the stability of a slope at the time of data collection. It does not account for the changes or modifications of the factors that cause landslides, the spatial and temporal frequency of the landslides, and the magnitudes of the landslides. A method that analyzes the environment of the failed slope, based on the relationship between past landslides and the factors that cause landslides, and calculates the probability/index of the slopes to fail in the future is more appropriate for planners and decision makers.

This study made some assumptions to develop an appropriate method of mapping susceptibility to landslides in a fuzzy-logic framework. These assumptions are: 1) the past environmental conditions at the time of a landslide can be used as indicators for the identification of potential sites for future landslides; and 2) the factors responsible for landslides can be quantified and spatially overlaid to prepare a map of landslide susceptibility. Thus, the objectives of the study are to: 1) prepare an inventory map of landslides and maps of the factors causing landslides; 2) categorize continuous data using the weight of evidence approach; 3) use a bivariate chi-square test to determine dependency of the factors; 4) calculate fuzzy-membership values for each factor; 5) apply fuzzy operators and a GIS (Geographic Information System) to develop models of susceptibility to landslides; 6) validate an accuracy assessment of each model; and 7) identify the best model that creates an optimum map for landslide susceptibility.

The study area

The study area, located in west-central Colorado (Fig. 34), covers ~815 km^2 area between Paonia and McClure Pass (N 38^o 43’ 00”, W 107^o 37’ 30” to N 39^o 10’ 30”, W107^o 10’ 00”). The area is accessible via Colorado Highway 133 and forest roads. In addition to rugged topography the area possesses a dendritic drainage pattern. The North Fork Gunnison River is the major river of the area. Elevations in the study area range from 1712 to 3883 m with the lowest elevation being the flood plain of the North Fork

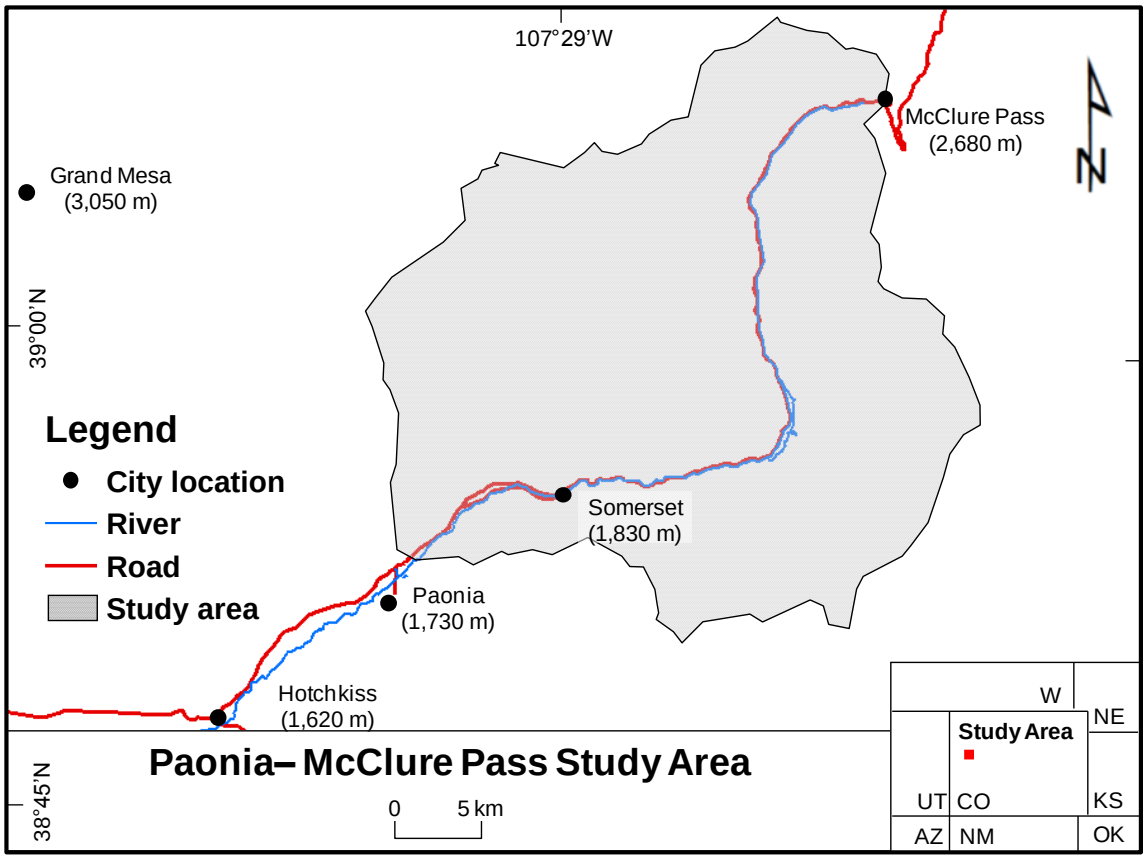

Fig. 34. Location of the study area. W: Wyoming, NE: Nebraska, UT: Utah, CO: Colorado, KS: Kansas, AZ: Arizona, NM: New Mexico, and OK: Oklahoma.

Gunnison River at Paonia, and the highest elevation is Chair Mountain. The morphology of the hillslopes varies with most of the lower elevations having steep slopes and gentle to flat tops whereas mountains at higher elevations have sharp ridges and steep slopes with horns, arêtes and cirques attributable to glacial processes (Fig. 35). Slopes are controlled by geology rather than elevation. Sandstone and plutonic rocks have steep slopes, and the mudstone, shale, alluvial and colluvial deposits have medium and gentle

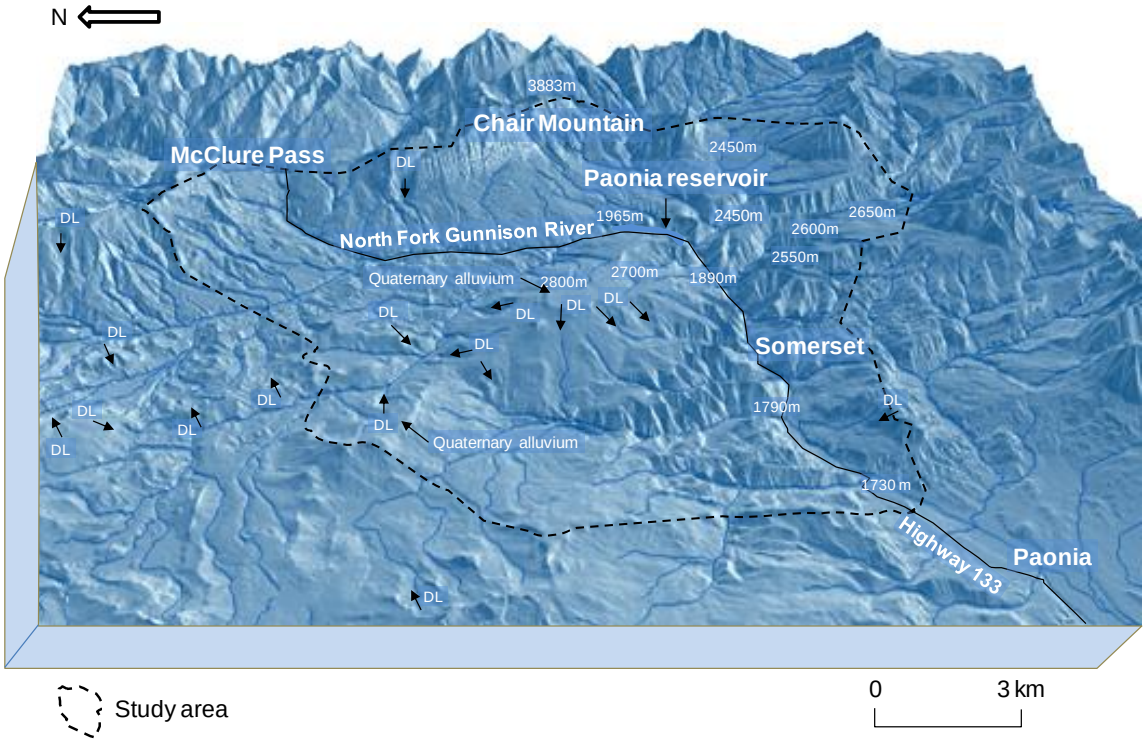

Fig. 35. A three-dimensional hillshade map of the study area showing variation in the topography. The geomorphic expression of the area can be divided into four forms. The first form is the flat topography of the river floodplains and upland plateaus. The elevations of the river floodplains at different locations and plateaus are shown. The second form is the steep slopes in the close proximity of the North Fork Gunnison River and associated tributaries. The third form is the gentle upland slopes comprised of large deep-seated landslides (DL). The fourth form is the tall and steep mountains. The vertical scale is exaggerated twice. Large deep-seated landslides (DL) were not considered for the study.

slopes. Major geomorphic processes, involved in the evolution of the hillslopes and in the incision of the North Fork Gunnison River and its associated tributaries, include Pleistocene glaciation and mass movement from the coupling effect of snowmelt, rainfall and river erosion. The area frequently receives intense rainfall and snowstorms. Stream flow is primarily driven by the snowmelt, which is greatest in May (Jaquette et al., 2005). Shallow translational slides dominate; rotational slides, deep-seated slides, rock falls, topple blocks and rock glaciers are also present in the area. The gentle slopes of the area are covered mostly by glacial till and colluvium.

Characteristics of landslides

Varieties of mass movements, ranging from imperceptibly slow moving rock glaciers and soil creep to rapidly moving rockslides and debris flows, are present in the Paonia−McClure Pass study area. The landslides, defined according to Varnes (1978), contain mainly sandstone, mudstone, shale, alluvial, colluvial and mixed deposits. The shallow landslides are mostly found in steep and convergent parts of the landscape. These landslides occur in sandstone, mudstone and colluvial deposits, shrubland and woodland, non-plastic to low plastic soil, 20° to 40° slopes, and in close proximity to rivers and roads. Lack of vegetation suggests that these landslides are recent and active. Large deep-seated landslides, mostly found on the edges of the upland plateau (Fig. 35), are related to the structural failure of bedrock as opposed to the failure of surficial deposits, including soil, colluvium, glacial till and outwash, and weathered bedrock. Deep-seated events occur rarely in contrast to the rapidity at which shallow landslides

occur. The surfaces of these landslides are densely vegetated and indicate that the landslides are very old and relatively stable now. The headscarps of some of the large deep-seated landslides contain active shallow landslides. This study focuses only on the mapping and analysis of the shallow landslides (Fig. 36). I have selected this focus because of the different processes responsible for the shallow landslides versus deep-seated events. The average depth of the slip surface of the shallow landslides is ~1.9 m. The average slope, area, transported volume, length, width and height of these landslides

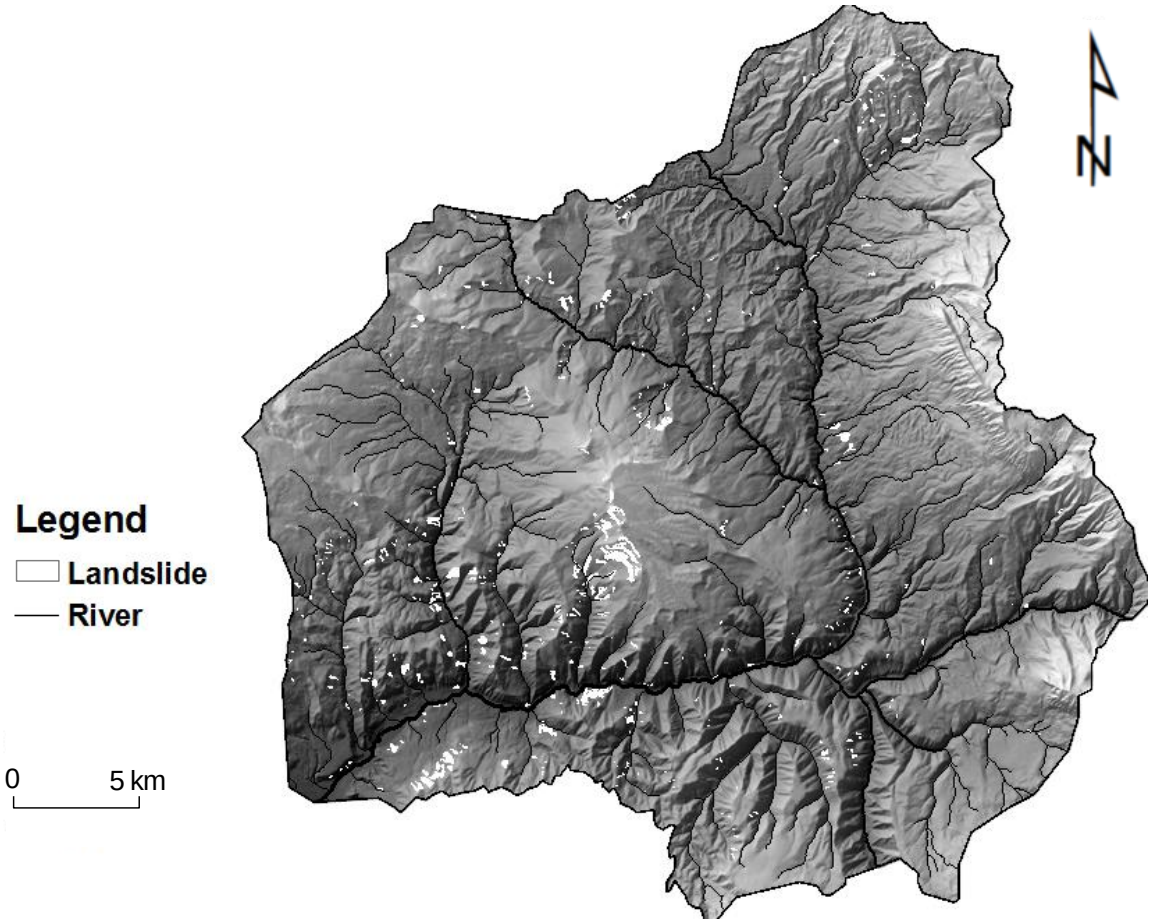

Fig. 36. An inventory map of shallow landslides in the Paonia-McClure Pass study area.

are calculated as 26°, 6600 m^2, 33,500 m^3, 120 m, 85 m, and 60 m, respectively.

This study shows that most of the shallow landslides are smaller than 1000 m^2, and none exceed 160,000 m^2. In most of the areas where soil slides, debris slides and debris flows occurred, the thin cover of the regolith/soil above the bedrock moved under the influence of gravity and increased pore-water pressure (Fig. 37A-C). In most of the landslides, the boundary between soil and the underlying bedrock is abrupt (Fig. 37D). The soil/regolith is cohesionless, has low bulk density, and contains fragments of rocks. The underlying rock is highly fractured, gently dipping and has considerable cohesion as well as frictional strength. The loose soil is more conductive than the bedrock. Because highly fractured underlying bedrock may conduct large amounts of water (e.g., Wilson and Dietrich, 1987; Johnson and Sitar, 1990; Montgomery et al., 1997), the rock slides in the area are probably the result of the weathering and pore-water pressure generated by subsurface flow. The main reason for the rock fractures probably is frost shattering because the area receives sufficient snow in the winter and the temperature fluctuates above and below freezing. Furthermore, many landslides occurred between the boundary of hard rocks (sandstone and plutonic rock) and soft rocks (mudstone and shale). An interface of differential shear strength and differential rates of weathering are also possible contributing factors for these shallow landslides.

Fig. 37. Photographs of landslides in the study area. A) Landslides on west-facing slopes located between Paonia and Somerset. B) Shallow landslides (mostly debris flows) on the north-west facing slopes nearby Somerset Village. C) A rockslide on a north-facing slope near Somerset, Co. Weathered and highly fractured bedrock is covered by a thin regolith. D) A close up view of a rockslide at Somerset. Thin regolith has an abrupt contact with weathered and fractured bedrock.

Fuzzy set theory and fuzzy operators

The fuzzy set theory, introduced by Zadeh (1965), facilitates analysis of non-discrete natural processes or phenomenon (Zimmermann, 1996). It employs the concept of a membership function, which expresses the degree of membership with respect to some attributes of interest. It is flexible, allows for combinations of the categorical and continuous data, and deals with the uncertainties (fuzziness, vagueness, and imprecision) inherent in the ways experts approach a problem. The attribute of interest is measured over discrete intervals, and the membership function of a discrete category can be

expressed in terms of membership values. For example, if x is the number of landslides in a category of a given factor, then $\mu(x)$ is the fuzzy-membership function. Every value of x is associated with a value of $\mu(x)$, and the ordered pairs $[x,\mu(x)]$ are collectively known as a fuzzy set. This theory is different from the classical set theory. Whereas, the classical set theory defines an object as a member of a set if it has a membership value of 1, or is not a member if it has a membership value of 0, the membership of a fuzzy set is expressed on a continuous scale from 1 (full membership) to 0 (full-non-membership). Membership values for a factor causing landslides can be chosen based on the data-driven method (relationship of the past landslides with factors causing landslides) or by expert-based judgments (use of if-then rules). A single map can have more than one fuzzy-membership value and several maps can have membership values for the same proposition or hypothesis (Bonham-Carter, 1994). No practical constraints limit the choice of fuzzy-membership values; values are chosen to reflect the degree of membership of a set. Furthermore, values need not increase or decrease monotonically with class number (Bonham-Carter, 1994).

The fuzzy-logic method allows flexible combinations of weighted maps derived from any measurement scale. Given two or more maps with fuzzy-membership functions for the same set, five fuzzy operators, namely: 1) fuzzy OR, 2) fuzzy AND, 3) fuzzy algebraic sum, 4) fuzzy algebraic product, and 5) fuzzy gamma, can be employed to combine membership values (An et al., 1991; Bonham-Carter, 1994; Chung and Fabbri, 2001). The method has been used in various fields within the geosciences. For example,

it has been used to map gold potential (Bonham-Carter, 1994) and landslide hazards (Anabalgan, 1992; Gorsevski et al., 2003, 2006; Tangestani, 2004; Lee, 2007).

A script can be written in GIS to employ this method. Five fuzzy operators can be expressed mathematically as:

$$\mu_{\text{OR}} = \text{MAX}(\mu_A, \mu_B, \mu_C, ...) \quad \text{(Fuzzy OR)} \quad (40)$$

$$\mu_{\text{AND}} = \text{MIN}(\mu_A, \mu_B, \mu_C, ...) \quad \text{(Fuzzy AND)} \quad (41)$$

$$\mu_{\text{sum}} = 1 - \prod_{i=1}^{n} (1 - \mu_i) \quad \text{(Fuzzy algebraic sum)} \quad (42)$$

$$\mu_{\text{product}} = 1 - \prod_{i=1}^{n} \mu_i \quad \text{(Fuzzy algebraic product)} \quad (43)$$

$$\mu_{\text{gamma}} = [\text{Fuzzy algebric sum}]^{\gamma} \times [\text{Fuzzy algebric product}]^{1-\gamma} \quad \text{(Fuzzy gamma)} \quad (44)$$

where, μ_i is the fuzzy-membership function for the *i*-th map, and *i* = 1, 2, ..., n. Output membership values are controlled by various pieces of evidence.

In the fuzzy OR operator (Eq. 40), the combination output membership value for any particular location is controlled by the maximum fuzzy-membership value of the input maps occurring at that location. In the fuzzy-AND operator (Eq. 41), the output membership value for any particular location is controlled by the smallest fuzzy-membership value of the input maps occurring at that location. These operators are appropriate if the combined membership value at a location is controlled by the most suitable evidence maps. If two pieces of evidence favor a hypothesis so that the

combined evidence is more supportive than one piece of evidence, then the fuzzy algebraic sum, fuzzy algebraic product, and fuzzy-gamma operators are appropriate.

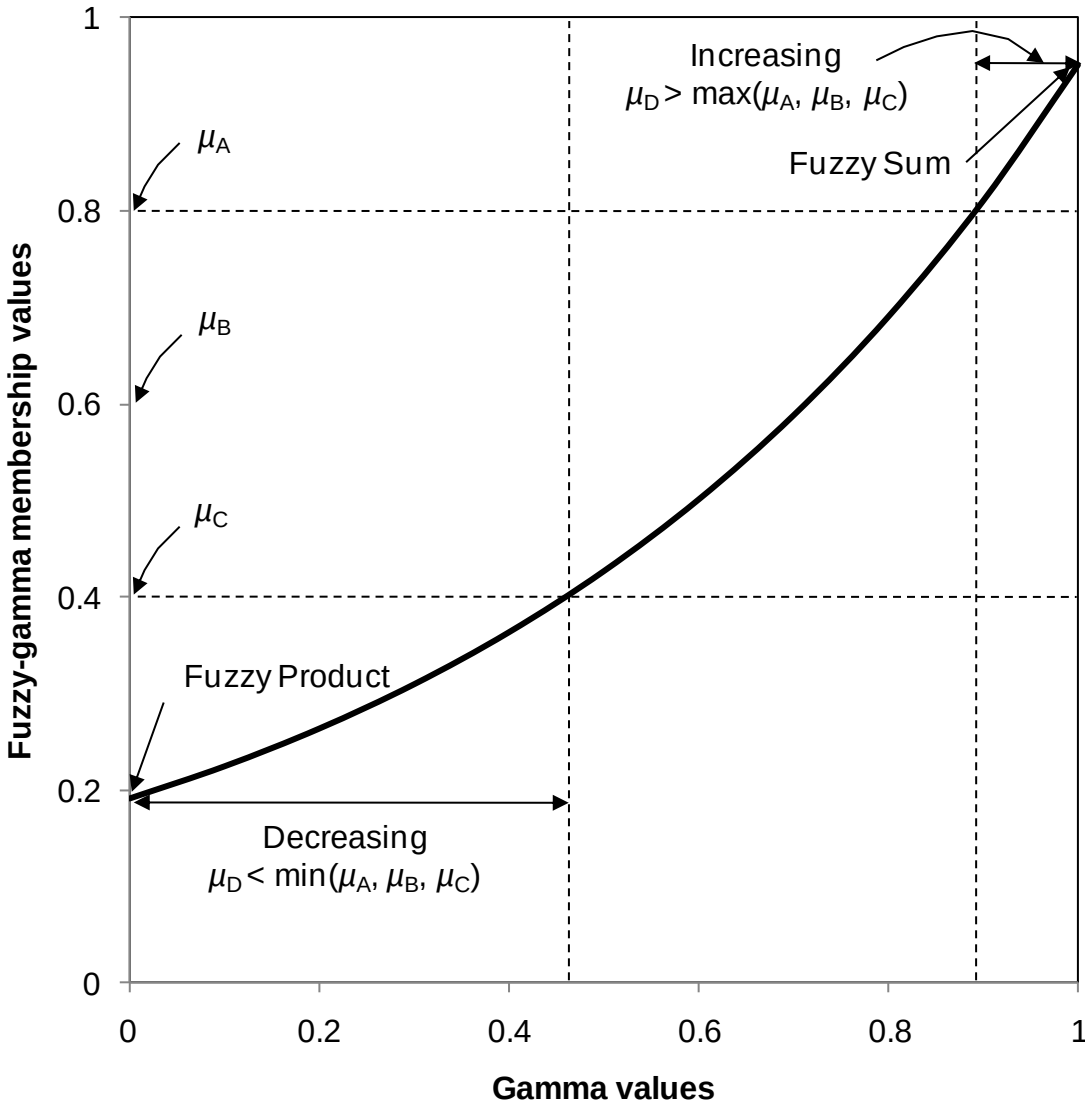

Fig. 38. A graph showing an example of combination of three fuzzy factors ($\mu_A = 0.8$, $\mu_B = 0.6$, $\mu_C = 0.4$) by fuzzy-gamma operation. The decreasing effect is the zone where the result of fuzzy-gamma operation is smaller than the minimum membership value of the factors and the increasing effect is the zone where the result of the fuzzy-gamma operation is larger than the maximum value of the fuzzy factors.

In the fuzzy algebraic sum (Eq. 42), the output value is always larger than or equal to the largest contributing fuzzy-membership value (Fig. 38). The maximum limit of the output value is 1.0. The fuzzy algebraic product is complementary to the fuzzy algebraic sum (Eq. 43), and the output value is always smaller than or equal to the smallest contributing fuzzy-membership value (Fig. 38). The maximum limit of the value is 1.0. The fuzzy-gamma operation is defined in terms of the fuzzy algebraic sum and the fuzzy algebraic product (Eq. 44). In the fuzzy-gamma operation, when gamma is 1, the combination is the same as the fuzzy algebraic sum, and when gamma is 0 the combination equals the fuzzy algebraic product. Therefore, the appropriate choice of gamma produces output values that ensure a flexible compromise between effects of the fuzzy algebraic sum and the effects of the fuzzy algebraic product (Fig. 38).

Materials and methods

The method proposed here is time-consuming and requires attention to detail, but facilitates differentiation of complex landslide landscapes. The overall method includes: 1) mapping landslides and factors causing landslides; 2) categorizing continuous data based on the weight of evidence (Regmi et al., 2010b); 3) calculating frequency ratios of landslides for each category of factors; 4) implementing frequency ratio to fuzzy-membership values of each category; and 5) combining all factors based on fuzzy operators to create maps of susceptibility to landslides.

To prepare spatial and non-spatial databases of landslides and landslide related factors, aerial photographs and available data sources were collected. This step was

followed by extensive field work. A handheld GPS was used to map the location and the dimensions of landslides easily accessible. In addition, slope angle, direction of movement, soil and rock characteristics, and length, width and area of each landslide were measured in the field. Similar characteristics of landslides inaccessible in the field were determined from interpretation of orthorectified NAIP (National Agricultural Program) aerial photographs and a USGS (United States Geological Survey) digital elevation model (DEM). Other characteristics such as land use, vegetation cover, aspect and curvature of slope, and mode of failure were documented, and all data were recorded on landslide inventory sheets. Ten-meter resolution USGS DEMs were used to extract topographic factors and water-related factors. Geologic factors were extracted from a USGS geological map (Dunrud, 1989) of the area as well as from field work, and soil factors were extracted from soil data collected by the USDA (United States Department of Agriculture) and the USFS (United States Forest Service). Data for land cover were extracted from an ETM+ (Enhanced Thematic Mapper Plus) satellite image. Anthropogenic factors, such as road network, were extracted from aerial photographs.

GIS database of landslides and landslide causing factors

An inventory of landslides was created to show the distribution of observable landslides. Although some researchers prefer to represent locations of landslides by points on a regional scale, I mapped all landslides as polygons. I mapped via polygons because an inventory map of landslides, which consisted of location of a landslide represented by a point either in the center of the whole landslide or in the center of

landslide scarp only provides information about the frequency of landslides, but not the magnitude. An inventory map, in which all landslides are represented by polygons, represents the frequency and magnitude of landslides.

Seven hundred and thirty five landslide polygons were mapped (Fig. 36) using 1991 and 2005 aerial photographs with scales of 1:12,000. Landslides were identified visually by distinguishing tone, shape, size and texture and were then digitized in ArcGIS®. The identification of types of landslides was facilitated by a 3D visualization technique in ArcGIS® and a stereo-visualization technique in Terrain Navigator Pro®. All landslides were classified based on the classification scheme of Varnes (1978). After extraction of landslides, the location, type and movement activity of all landslides were verified by field mapping. Attribute information of all landslides was also collected from aerial photographs, historical archives and field surveys. For each landslide, the attribute data include: area, perimeter, volume, length, width, type of slide, current activity, position on hillslope, percent vegetation cover, main causes of movement, damage to infrastructure, and preventive measures taken. All these attributes were linked with the spatial information of each landslide and stored in ArcGIS®.

The study area contains three different lithologies: 1) sedimentary rocks including shale, mudstone, claystone and sandstone; 2) igneous rocks including basalt and batholiths of granodiorite; and 3) various Quaternary deposits. Shale, mudstone, claystone and sandstone are Cretaceous and volcanic deposits are Tertiary (Dunrud, 1989). Bedrock is dominant along the steep ridges; till and colluvium cover most of the middle slopes and lowlands; and fluvial deposits fill the stream valleys. Twenty surface

and subsurface faults were mapped using the USGS geological map and field work data. Numerous landslides are found in close proximity to these faults.

Land cover of the area is separated into eight categories: 1) forest (41%), 2) shrub/bush (40%), 3) woodland (5%), 4) grassland (9%), 5) agricultural land (2.8%), 6) barren land (2%), and 7) settlement (0.2%). Most of the landslides occur in shrubland and woodland. Shrub land cover has the highest percentage of landslides and settlement land cover has the lowest percentage.

USDA and USFS have geotechnical information for the soils; these data are compiled to a depth of ~1.5 m. Soil data was categorized based on the plasticity index (*PI*). The soil plasticity index includes four classes: non-plastic to very low plastic, low plastic (*PI* = 0−5), medium plastic (5−20), and high plastic (>20). Most of the landslides occur in non-plastic to low plastic soils.

Topographic factors such as slope, aspect, measures of curvature and slope heating from solar radiation, were developed in ArcGIS® from USGS DEMs of 10 m resolution. Profile curvature affects the acceleration and deceleration of flow and, therefore, influences subsequent erosion and deposition; whereas, the plan and tangential curvatures control the convergence or divergence of landslide material and water in the direction of landslide motion (Carson and Kirkby, 1972; Mitasova and Hofierka, 1993, Ohlmacher, 2007). Solar radiation directly or indirectly relates to the landslides because it contributes to variations in microclimate, including factors like patterns of snowmelt and soil moisture. The variation in solar radiation depends on elevation, orientation of the slopes (slope and aspect of slope), and shadows cast by upslope topographic features.

Water-related factors, such as flow accumulation, flow length, topographic wetness index (*TWI*), and stream power index (*SPI*) were developed from a USGS DEM using ArcGIS®. *TWI* and *SPI*, are steady-state indices of wetness and stream power (Moore et al., 1991), which are a function of slope and the upstream contributing area per unit width orthogonal to the flow direction:

$$TWI = \ln(A/b\tan\beta) \tag{45}$$

$$SPI = A\tan\beta/b \tag{46}$$

where A is the upstream contributing area expressed as m^2, b is the width of a cell expressed as m, and β is the slope angle of that cell expressed as radians.

TWI correlates with soil moisture (Moore et al., 1991; Beven, 1997; Blyth et al., 2004), and *SPI* is a measure of the erosive power of water flow based on the assumption that discharge is proportional to catchment area (Moore et al., 1991). Moore et al. (1988) found the ephemeral gullies could be predicted from the magnitude of these indices.

Flow accumulation and upstream length of flow can also be taken as predictors of landslides. Streams and associated tributaries are important factors in the occurrence of landslides. Streams and gullies in a basin can erode the surface and undercut the slope toe, which, in turn, causes surficial mass movement in areas adjacent to drainage channels (Barredo et al., 2000). In the study area, I observed many landslides initiated by streams undercutting slopes.

Human influence is one of the major factors causing landslides world-wide. Road-cuts are usually sites of anthropologically-induced instability. Landslides may occur on the slopes adjacent to the roads (Pachauri and Pant, 1992; Pachauri et al., 1998;

Table 10 Area of landslides and landslide-causing factors, frequency ratio and fuzzy-membership values.

Factor	Class	Class pixels	Landslide pixels	% Class	% Landslide	Frequency ratio	Membership value
Flow length (*FL*)	<11 m	2,023,344	7,664	25	16	0.64	0.45
	30 m	1,131,536	5,468	14	11	0.81	0.57
	300 m	4,224,709	29,171	52	60	1.16	0.82
	1000 m	631,820	5,341	8	11	1.42	1.00
	75,158 m	143,402	804	2	2	0.94	0.66
Flow accumulation (*FA*)	1 Cells	1,606,771	5,760	20	12	0.60	0.46
	3 Cells	1,445,479	7,093	18	15	0.83	0.63
	7 Cells	1,532,847	8,939	19	18	0.98	0.75
	50 Cells	2,729,873	20,425	33	42	1.26	0.96
	700 Cells	655,731	5,101	8	11	1.31	1.00
	16,262,011 Cells	184,110	1,130	2	2	1.03	0.79
Distance to stream (*DS*)	<25 m	1,386,867	8,004	17	17	0.97	0.88
	25-50 m	1,253,719	6,983	15	14	0.94	0.85
	50-100 m	1,923,620	10,858	24	22	0.95	0.86
	100-250 m	3,055,075	19,942	37	41	1.10	1.00
	250-614 m	535,530	2,661	7	5	0.84	0.76
Stream power index (*SPI*)	0-3	1,514,627	1,991	19	4	0.22	0.10
	3-12	1,905,600	8,183	24	17	0.72	0.33
	12-50	2,485,090	15,513	31	32	1.04	0.48
	50-400	1,814,457	18,641	22	38	1.72	0.80
	400-5000	268,044	3,450	3	7	2.15	1.00
	5,000-97,269,664	99,050	658	1	1	1.11	0.52
Topographic wetness index (*TWI*)	0-2	3,338	18	0	0	0.90	0.64
	2-4	1,189,006	10,042	15	21	1.41	1.00
	4-6	4,173,081	23,860	52	49	0.95	0.68
	6-8	1,935,985	10,944	24	23	0.94	0.67
	8-10	536,021	2,500	7	5	0.78	0.55
	10-12	143,660	686	2	1	0.80	0.57
	12-23	105,777	386	1	1	0.61	0.43
Geology (*GEO*)	Mesavarde Fm. (sst, mst, shale)	1,534,501	13,192	19	27	1.45	0.26
	Unconsolidated deps. (mixed)	878,963	4,304	11	9	0.82	0.15
	Unconsolidated alluvium	172,579	458	2	1	0.45	0.08
	Mixed alluvium and colluvium	781,043	3,256	10	7	0.70	0.12
	Colluvium	37,250	960	0	2	4.34	0.77
	Landslide and mudflow deps.	1,453,863	17,902	18	37	2.07	0.37
	Mancos shale	51,216	800	1	2	2.63	0.46
	Glacial drift	112,072	786	1	2	1.18	0.21
	Alluvial terrace	73,624	84	1	0	0.19	0.03
	Wasatch Fm. (clst, mst, sst)	2,651,560	6,606	33	14	0.42	0.07
	Basalt and gabbros	1,486	50	0	0	5.66	1.00
	Plutonic rock (granodiorite)	264,197	0	3	0	0.00	0.00
	Talus and rock glacier deps.	127,298	0	2	0	0.00	0.00
Soil plasticity index (*SP*)	Rock	96,412	1,139	1	2	1.99	0.52
	Non-plastic-very low plastic	815,150	18,633	10	38	3.85	1.00
	Low plastic	4,710,787	21,313	58	44	0.76	0.20
	Medium plastic	2,282,552	7,864	28	16	0.58	0.15
	High plastic	21,122	43	0	0	0.34	0.09
	Water	227,026	595	3	1	0.44	0.11
Distance to fault (*DF*)	<25 m	45,726	556	1	1	2.05	0.80
	25-75 m	78,361	1,151	1	2	2.47	0.97
	75-150 m	121,788	1,421	1	3	1.96	0.77
	150-350 m	342,546	5,211	4	11	2.56	1.00
	350-10,653 m	7,566,390	40,109	93	83	0.89	0.35
Land cover (*LC*)	Shrub/bush	3,236,247	30,241	40	62	1.57	1.00
	Grassland	711,441	1,677	9	3	0.40	0.25
	Forest	3,378,384	11,581	41	24	0.58	0.37
	Woodland	395,505	3,514	5	7	1.50	0.95
	Agriculture	209,061	123	3	0	0.10	0.06
	Residential	19,557	26	0	0	0.22	0.14
	Rock cliff and barren land	176,481	1,273	2	3	1.21	0.77
	Water	28,305	0	0	0	0.00	0.00

Table 10 continued.

Factor	Class	Class pixels	Landslide pixels	% Class	% Landslide	Frequency ratio	Membership value
Slope (*SL*)	<10°	2,631,299	1,868	32	4	0.12	0.04
	10-20°	2,778,671	12,566	34	26	0.76	0.28
	20-30°	1,532,209	17,400	19	36	1.91	0.70
	30-40°	956,744	12,703	12	26	2.23	0.82
	40-50°	216,809	3,513	3	7	2.73	1.00
	50-60°	31,890	377	0	1	1.99	0.73
	>60°	7,189	21	0	0	0.49	0.18
Aspect (*AS*)	Flat (-1°)	68,073	12	1	0	0.03	0.02
	North (337-360°, 0-22°)	806,660	5,048	10	10	1.05	0.72
	North East (22-67°)	998,178	2,239	12	5	0.38	0.26
	East (67-112°)	1,054,092	5,565	13	11	0.89	0.61
	South East (112-157°)	961,195	4,509	12	9	0.79	0.54
	South (157-202°)	1,033,415	8,776	13	18	1.43	0.98
	South West (202-247°)	1,136,000	9,866	14	20	1.46	1.00
	West (247-292°)	1,157,728	7,316	14	15	1.06	0.73
	North West (292-337°)	939,470	5,117	12	11	0.92	0.63
Elevation (*EL*)	<1,800 m	59,546	250	1	1	0.71	0.32
	1800-2000 m	381,734	4,941	5	10	2.18	1.00
	2000-2200 m	1,067,871	9,356	13	19	1.47	0.68
	2200-2400 m	2,426,731	13,029	30	27	0.90	0.41
	2400-2600 m	2,178,609	10,621	27	22	0.82	0.38
	2600-2800 m	1,133,622	7,378	14	15	1.10	0.50
	2800-3800 m	906,698	2,873	11	6	0.53	0.24
Solar radiation (*SR*)	<600 kwhm^{-2}	2,168	0	0	0	0.00	0.00
	600-800 kwh m^{-2}	15,980	84	0	0	0.88	0.33
	800-1000 kwh m^{-2}	119,325	1,809	1	4	2.55	0.96
	1000-1200 kwh m^{-2}	371,934	5,883	5	12	2.66	1.00
	1200-1400 kwh m^{-2}	830,039	7,373	10	15	1.50	0.56
	1400-1600 kwh m^{-2}	2,378,225	9,975	29	21	0.71	0.27
	1600-1800 kwh m^{-2}	3,865,732	16,697	47	34	0.73	0.27
	>1800 kwhm^{-2}	571,408	6,627	7	14	1.95	0.73
Profile curvature (*PRC*)	<-0.05m^{-1}	26,531	335	0	1	2.13	0.97
	-0.05--0.02 m^{-1}	299,059	2,998	4	6	1.69	0.77
	-0.02-0 m^{-1}	3,039,226	18,117	37	37	1.00	0.46
	0 m^{-1}	1,406,670	4,617	17	10	0.55	0.25
	0-0.02m^{-1}	3,085,047	18,854	38	39	1.03	0.47
	0.02-0.05 m^{-1}	265,601	3,101	3	6	1.97	0.90
	>0.05 m^{-1}	32,677	426	0	1	2.19	1.00
Plan curvature (*PLC*)	<-0.05 m^{-1}	29,897	298	0	1	1.68	0.85
	-0.05--0.02 m^{-1}	219,985	2,586	3	5	1.98	1.00
	-0.02-0 m^{-1}	2,726,472	18,226	33	38	1.13	0.57
	0 m^{-1}	1,911,300	6,600	23	14	0.58	0.29
	0-0.02 m^{-1}	3,123,923	19,288	38	40	1.04	0.53
	0.02-0.05 m^{-1}	127,701	1,306	2	3	1.72	0.87
	>0.05 m^{-1}	15,533	144	0	0	1.56	0.79
Tangential curvature (*TC*)	<-0.05 m^{-1}	151,092	1,875	2	4	2.09	1.00
	-0.05--0.02 m^{-1}	1,426,520	9,754	17	20	1.15	0.55
	-0.02-0 m^{-1}	1,392,935	8,072	17	17	0.98	0.47
	0 m^{-1}	2,109,470	10,237	26	21	0.82	0.39
	0-0.02 m^{-1}	2,590,590	14,151	32	29	0.92	0.44
	0.02-0.05 m^{-1}	417,858	3,633	5	7	1.46	0.70
	>0.05 m^{-1}	66,346	726	1	1	1.84	0.88
Distance to road (*DR*)	<20 m	139,258	1,518	2	3	1.83	0.95
	20-40 m	105,648	1,208	1	2	1.92	1.00
	40-100 m	300,766	2,607	4	5	1.46	0.76
	100-350 m	971,971	6,040	12	12	1.05	0.54
	>350 m	6,637,168	37,075	81	77	0.94	0.49

Ayalew and Yamagishi, 2005) because slope excavation for construction of the road and vibrations generated by vehicles results in unstable slopes. In this study, many landslides occur adjacent to Colorado Highway 133 and the various forest roads. I used field mapping and GIS to measure the distances from roads to the various landslides. The distances were grouped into five categories (Table 10).

Categorization of the continuous data

All continuous data were categorized by employing the weight of evidence approach (Bonham-Carter, 1994, Dahal et al., 2008, Regmi et al., 2010b). The weight of evidence approach calculates the weight for a certain category of a factor map based on the following equations:

$$W^{+} = \log_e\left(\frac{P\{F \mid L\}}{P\{F \mid \overline{L}\}}\right) \tag{47}$$

$$W^{-} = \log_e\left(\frac{P\{\overline{F} \mid L\}}{P\{\overline{F} \mid \overline{L}\}}\right) \tag{48}$$

$$\text{Weight contrast } (W_C) = W^{+} - W^{-} \tag{49}$$

A positive weight (Eq. 47) is the logarithmic ratio of probability of a factor category (F) in the area where a landslide is present (L) to F in the area where a landslide is absent ($\overline{L}$). A negative weight (Eq. 48) is the logarithmic ratio of the probability of a factor class not present ($\overline{F}$) in the area where a landslide is present (L) to $\overline{F}$ in the area where a landslide has not occurred ($\overline{L}$). The categorization was performed based on the variation in the weight contrast values (Eq. 49) of the continuous

data with cumulative values of the continuous data. The natural breaks in the weight contrast distribution curves were used to categorize the continuous data (Fig. 39).

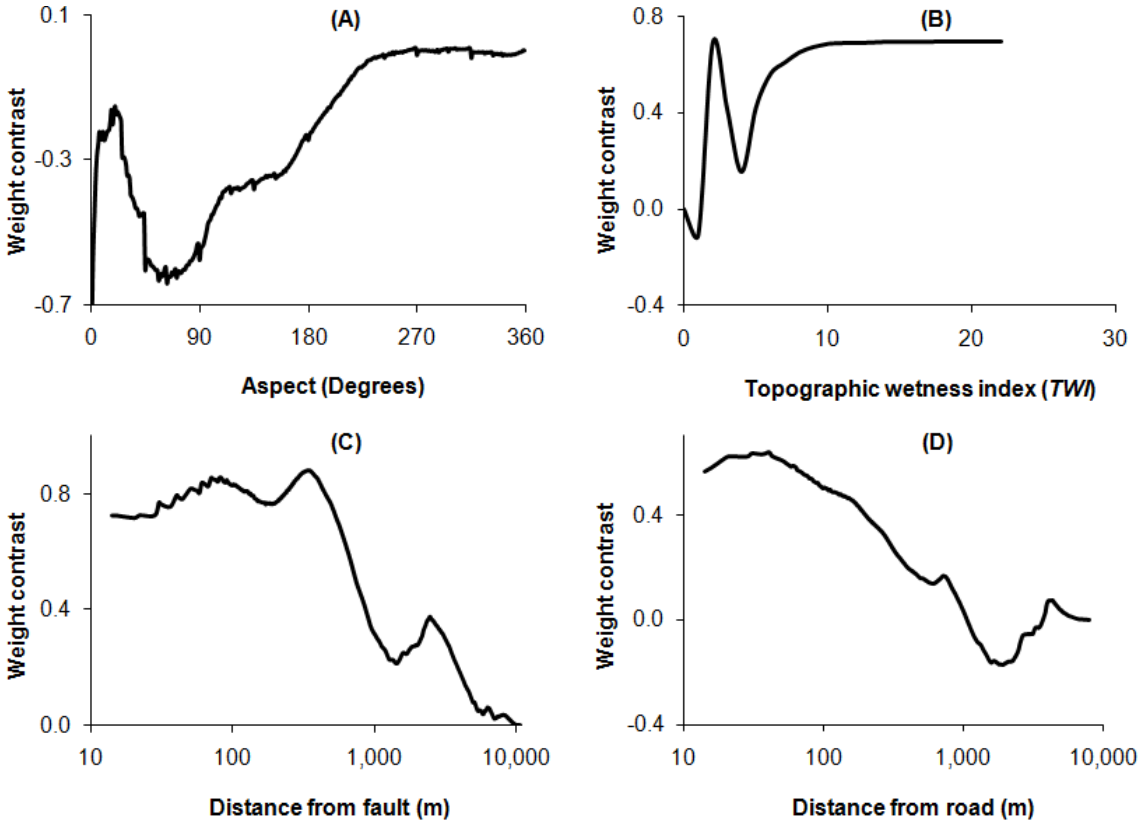

Fig. 39. Plots of cumulative distribution of weight contrast vs. factor value for classes of very narrow ranges of the continuous data. A) Cumulative weight contrast for aspect. B) Cumulative weight contrast graph for topographic wetness index. C) Cumulative weight contrast graph for distance from fault. D) Cumulative weight contrast graph for distance from road. These four continuous data were categorized based on the natural breaks on these graphs (see Table 10 for the categories). Cumulative weight contrast graphs for other continuous data are not shown here.

Assignment of membership value

The frequency ratio of landslides was used to calculate the membership value for each factor category (Table 10). It is the ratio of the percentage of the landslides in each category to the percentage of each category in the study area:

$$\text{Frequency ratio} = \frac{\text{Landslide density in predictor class}}{\text{landslide density for the entire map}} = \frac{N_{\text{cell}}(L_i)/N_{\text{cell}}(C_i)}{\sum N_{\text{cell}}(L_i)/\sum N_{\text{cell}}(C_i)} \quad (50)$$

where $N_{\text{cell}}(L_i)$ = Number of cells of landslides in a given predictor category, and $N_{\text{cell}}(C_i)$ = Total number of cells in a given predictor category.

The frequency ratio explains the relationships of factor categories and landslides. If the ratio for a category is >1, the density of landslides in this category is higher than the norm (density for the entire map) and, if the ratio is <1, the density of landslides in this category is lower than the norm. Then, the frequency ratio was normalized between 0 and 1 by dividing the frequency ratio of each factor by the maximum frequency ratio. These values, ranging from 0 to 1, were termed membership values. The category having the highest value of the membership has a major role in landslide occurrence, and the category having the lowest value of membership has a minor role in landslide occurrence.

Fuzzy-inference network models

In cases of mapping landslide susceptibility by using fuzzy operators, an important question arises: how should the factors be combined to achieve an optimum result? Depending on the number of factors available, a number of combinations can be established using the five types of fuzzy operators (Eqs. 40-44). This study introduces the use of four different combinations of factors. Among these, the inference-network model 1 (Fig. 40A) uses only those factors that are independent of one another. Models 2, 3 and 4 (Similar to Fig. 40B) combine the factors in such a way that the dependency

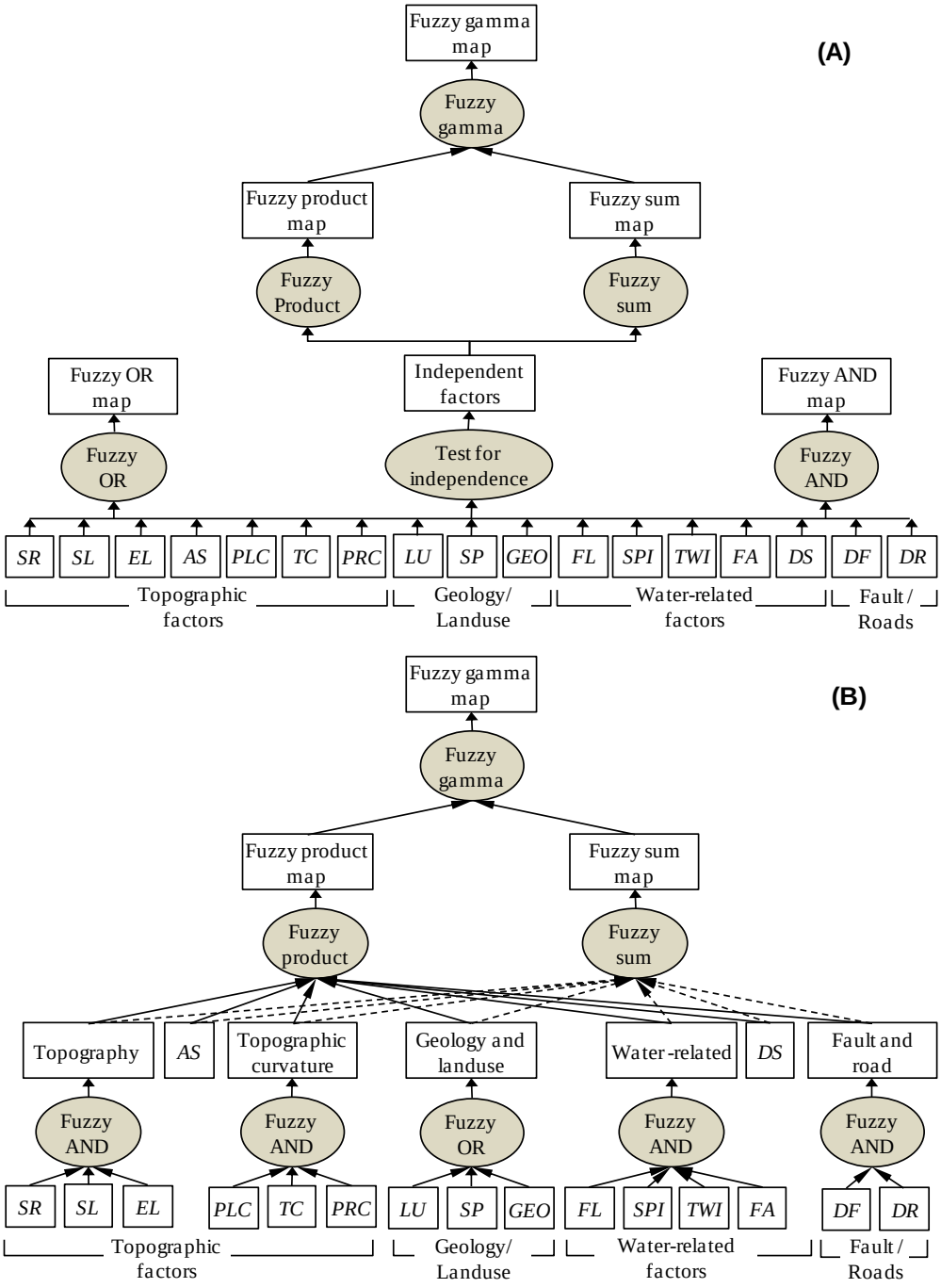

Fig. 40. Fuzzy-inference network for A) Model 1, and B) Model 4. Models 2 and 3 are not shown. These models are similar to the model 4, except the fuzzy operators used in the first step to combine the raw factors. In model 2 only fuzzy AND is used in the first step, and in model 3 only fuzzy OR is used in the first step. *SL*: slope, *AS*: aspect, *EL*: elevation, *SR*: solar radiation, *PRC*: profile curvature, *PLC*: plan curvature, *TC*: tangential curvature, *GEO*: geology, *DF*: distance from faults, *SP*: soil plasticity, *LC*: land cover, *FL*: flow length, *FA*: flow accumulation, *SPI*: stream power index, *TWI*: topographic wetness index, *DS*: distance from streams, and *DR*: distance from roads.

of factors does not have a major significant impact on the results. In each model, 11 maps of susceptibility to landslides were created based on the fuzzy-OR, fuzzy-AND, fuzzy algebraic sum, fuzzy algebraic product and fuzzy-gamma operators. Fuzzy OR and fuzzy AND maps are the same for all models because these operations combine all 17 factors together at one time. Furthermore, these operations do not require the factors to be independent of each other because these operations assign the minimum or the maximum of the membership values of all the factors in a cell (pixel). A cell defines the susceptibility of a landslide based on the minimum or maximum value of all the factors in that cell. The fuzzy-sum, fuzzy-product and fuzzy-gamma operations are based on the multiplication of the membership values of all the factors in that cell. Therefore, the factors, combined using these operators, need to be independent of each other, otherwise the effect of one factor can be counted more than once.

The first model uses the fuzzy-product, fuzzy-sum and fuzzy-gamma operators. This model only considers the factors, which are independent of each other. Thus, dependency of all 17 factors were tested by employing pair-wise comparison by making a 2×2 contingency table and using chi-square statistics in one degree of freedom and 99% confidence ($\chi^2 = 6.64$). To perform this step, first, all the factors were converted into binary forms based on the frequency ratios (Table 10). Classes having a frequency ratio ≥ 1 were assigned to one class, and classes having frequency ratios <1 were assigned to another class. Then, the number of landslides were counted within the four combination zones of each pairs of factors combined. These numbers were used to develop a 2×2 contingency table. Out of 136 pairs of factors, 103 pairs were found

independent of each other. Of the 17 factors, only seven factors were found independent of each other. These seven factors, slope, aspect, tangential curvature, flow accumulation, soil plasticity index, distance from streams and distance from roads, were used for mapping susceptibility to landslides based on model 1.

The second model was developed from the combination of the factors without determining dependency. In this approach, first, all the factors were grouped in such a way that each group was comprised of factors that were likely dependent on each other, based on the expert's a prior knowledge (similar to Fig. 40B). Factors from each group were combined by the fuzzy-OR operation to create a new fuzzy map from each group. Then, newly developed fuzzy maps were combined by the fuzzy product and fuzzy sum operators. Lastly, the fuzzy product and fuzzy sum maps were combined by a fuzzy-gamma operator with values of gamma as 0.1, 0.2, 0.3, 0.4, 0.5, 0.6, 0.7, 0.8, 0.9, and 0.95.

In the third model, factors from each group were combined by the fuzzy-AND operator in the first step. Then, similar to the second model, newly created fuzzy maps were combined by the fuzzy-sum, fuzzy-product, and fuzzy-gamma operators.

The fourth model was the combination of the second and third models in which all the groups, except geological and land cover, were combined in the first step by the fuzzy-OR operator, and geology and land cover group were combined by the fuzzy-AND operator. Other processes are similar to those used in the second and third models.

Results

Performance of the models of landslide susceptibility

Forty-four maps of landslide susceptibility were created from the four models. All of the maps predicted similar percentages of observed landslides with fuzzy-gamma

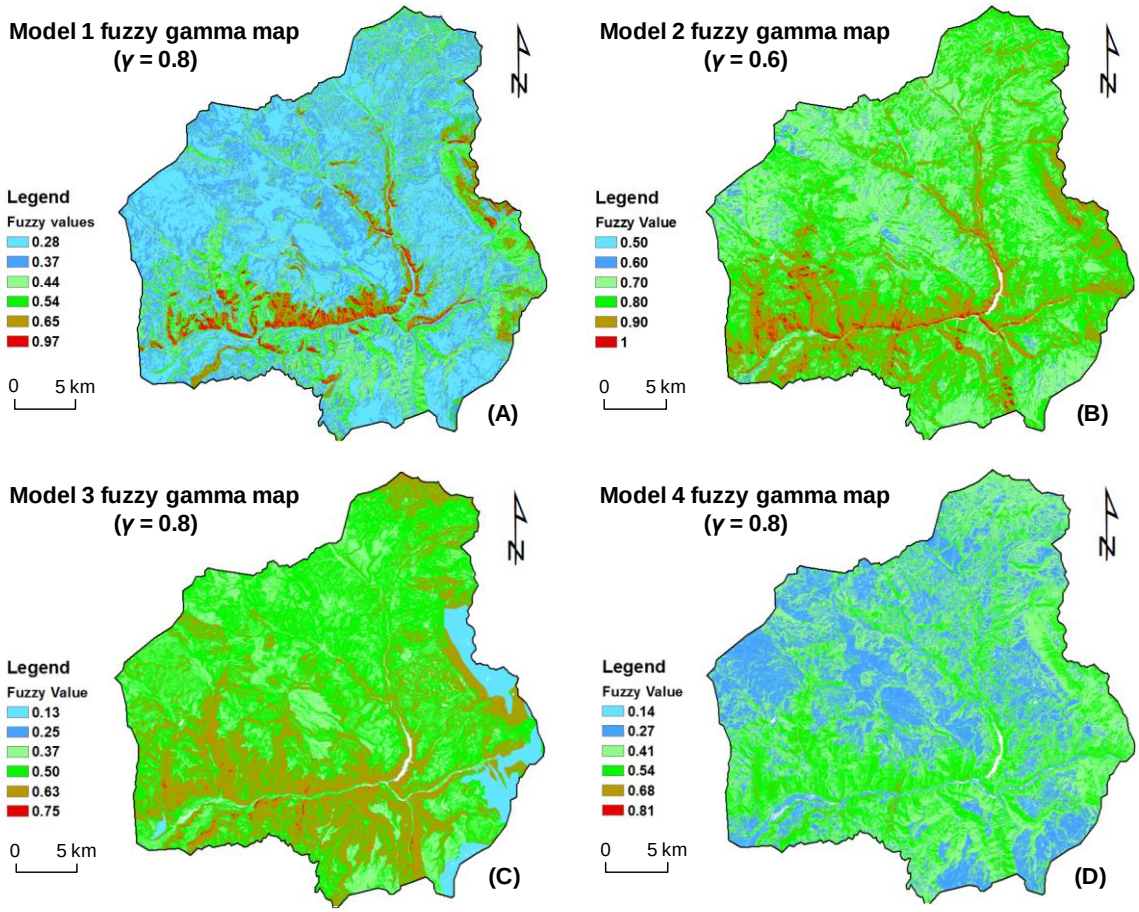

Fig. 41. Results of fuzzy-gamma operation based on 735 landslides and different fuzzy-inference network models. A) Fuzzy gamma map (γ = 0.8) for model 1 combination. B) Fuzzy gamma map (γ = 0.5) for model 2 combination. C) Fuzzy gamma map (γ = 0.8) for model 3 combination. The white zone in the eastern end of the map occurs because of the 0 membership value of one of the geological categories that results from the undersampling of landslides. D) Fuzzy gamma map (γ = 0.8) for model 4 combination.

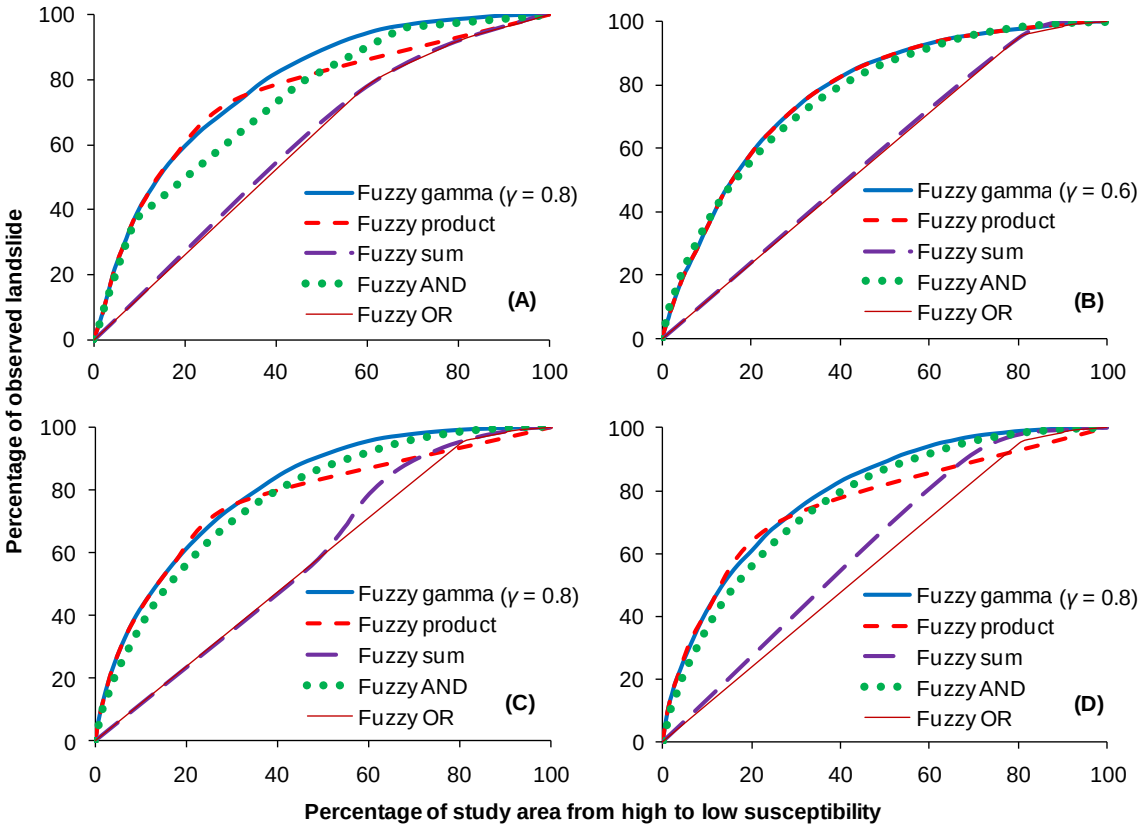

Fig. 42. Accuracy assessment of the four models based on 735 landslides. A) model 1, B) model 2, C) model 3, D) model 4. In all maps the fuzzy product and fuzzy sum graphs show smaller percentage of prediction than fuzzy-gamma operation (Table 11), because of the decreasing and increasing effects of fuzzy-product and fuzzy-sum operations. The percentage calculation is based on the analysis of fuzzy values only in two decimal places.

operation (Fig. 41 and Table 11). The approach of area under the curve (*AUC*), in which percentage of the predicted landslides was plotted along the *x*-axis and the percentage of the observed landslides was plotted along the *y*-axis, was used to assess the performance of each model (Fig. 42). For all models the fuzzy-gamma operation is the best for predicting observed landslides (Table 11). The first model has a 78.6% prediction accuracy with fuzzy-gamma operation (γ = 0.8); the second model has a 77.7% prediction accuracy with fuzzy-gamma operation (γ = 0.5); the third model has an 80.2%

prediction accuracy with fuzzy-gamma operation (γ = 0.8); and the fourth model has a 79.4 % prediction accuracy with fuzzy-gamma operation (γ = 0.8) (Table 11).

Table 11 Accuracies of the maps of landslide susceptibility developed based on the four models.

Operation		Model 1 (%)	Model 2 (%)	Model 3 (%)	Model 4 (%)	Validity of model 4 (%)
Fuzzy product		74.66	77.68	75.80	74.17	72.60
Fuzzy gamma	0.1	76.94	77.68	78.00	76.85	75.89
	0.2	78.10	77.70	79.86	78.29	77.30
	0.3	78.40	77.72	80.15	78.94	78.01
	0.4	78.55	77.70	80.16	79.21	78.30
	0.5	78.60	**77.71**	80.16	79.27	78.32
	0.6	78.62	77.71	80.17	79.32	78.36
	0.7	78.64	77.71	80.19	79.32	78.40
	0.8	**78.64**	77.71	**80.21**	**79.35**	**78.42**
	0.9	78.63	77.69	80.10	79.34	78.37
	0.95	78.60	77.60	80.16	79.30	78.29
Fuzzy sum		59.09	57.33	56.95	61.16	60.91
Fuzzy AND		71.47	71.47	71.47	71.47	71.47
Fuzy OR		57.46	57.46	57.46	57.46	57.46

Whereas the first model requires independent factors as input, the second, third and fourth models do not require factors to be independent of each other. The third model combines factors based on fuzzy AND at first. This approach does not work if a category of a factor has a 0 membership value because of the absence or under-sampling of landslides. In this case, the model is inappropriate. Similarly, the first model also has the same problem with missed and under-sampled data. The second model has the highest increasing effect of gamma values and the third model has the highest decreasing effect of gamma values. The fourth model has relatively moderate effect of increasing

and decreasing gamma values and is appropriate to deal with missed or under-sampled landslide data. Other characteristics of the models are listed in Table 12. After evaluating all the models, the fourth model was considered the best model because it accommodates the undersampled and missed landslide data as well as the effect of increasing and decreasing gamma values.

Table 12 Comparison of the four models based on seven characteristics. The fourth model is considered as the best.

Characteristics	Model 1	Model 2	Model 3	Model 4
Factors needed to be independent	Yes	No	No	No
Expert's choice of factor combination	No	Yes	Yes	Yes
Increasing effect of gamma values	Moderate	High	Low	Moderate
Decreasing effect of gamma values	Moderate	Low	High	Moderate
Problems with undersampled/missed landslide data	Yes	No	Yes	No
Time for data processing and analysis	High	Low	Low	Low

Validity of the best model and the final map of landslide susceptibility

The validity of the best model (model 4) was assessed by dividing the 735 landslides into training and validation sets. The training data consisted of 367 landslides and the validation data consisted of 368 landslides. The frequency ratios of each landslide-causing factor were calculated based on the training data. Maps of landslide susceptibilities were created based on training data and five fuzzy operators. The predictive capabilities of these maps were tested using a validation set of landslides. The susceptibility map developed by fuzzy-gamma operation with the value of gamma as 0.8 indicates that the model has a 78.4 % predictive capability (Table 11). The map of

susceptibility to landslides, based on the training landslides, is quite similar to the susceptibility map based on the 735 landslides (Figs. 41D and 43). This suggests that this method of mapping susceptibility to landslides, based on the integration of weight of evidence, frequency ratio and fuzzy operators, is accurate and applicable to the study area.

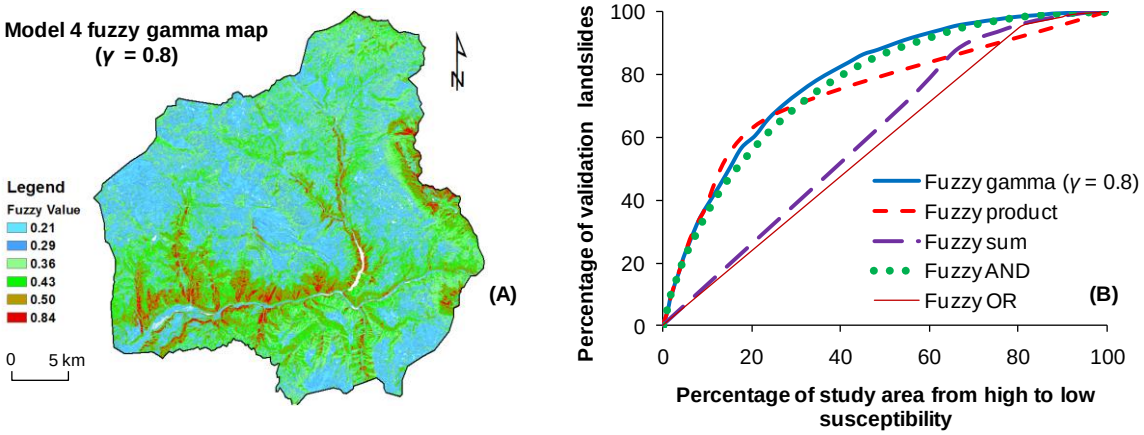

Fig. 43. Accuracy assessment of the map of landslide susceptibility developed based on model 4 combination and 367 landslides (training landslides). A) fuzzy-gamma (γ = 0.8) map, B) assessment of the prediction of the 368 landslides (validation landslides).

The fuzzy gamma map (Fig. 41D) based on model 4 was used to classify the study area into three zones of landslide susceptibility (Fig. 44). The classification is based on the frequency distribution of the fuzzy-gamma values (Fig. 45). The fuzzy-gamma value from 0.38 to 0.81 is classified as high susceptibility, 0.26 to 0.38 as medium susceptibility and 0 to 0.26 as low susceptibility.

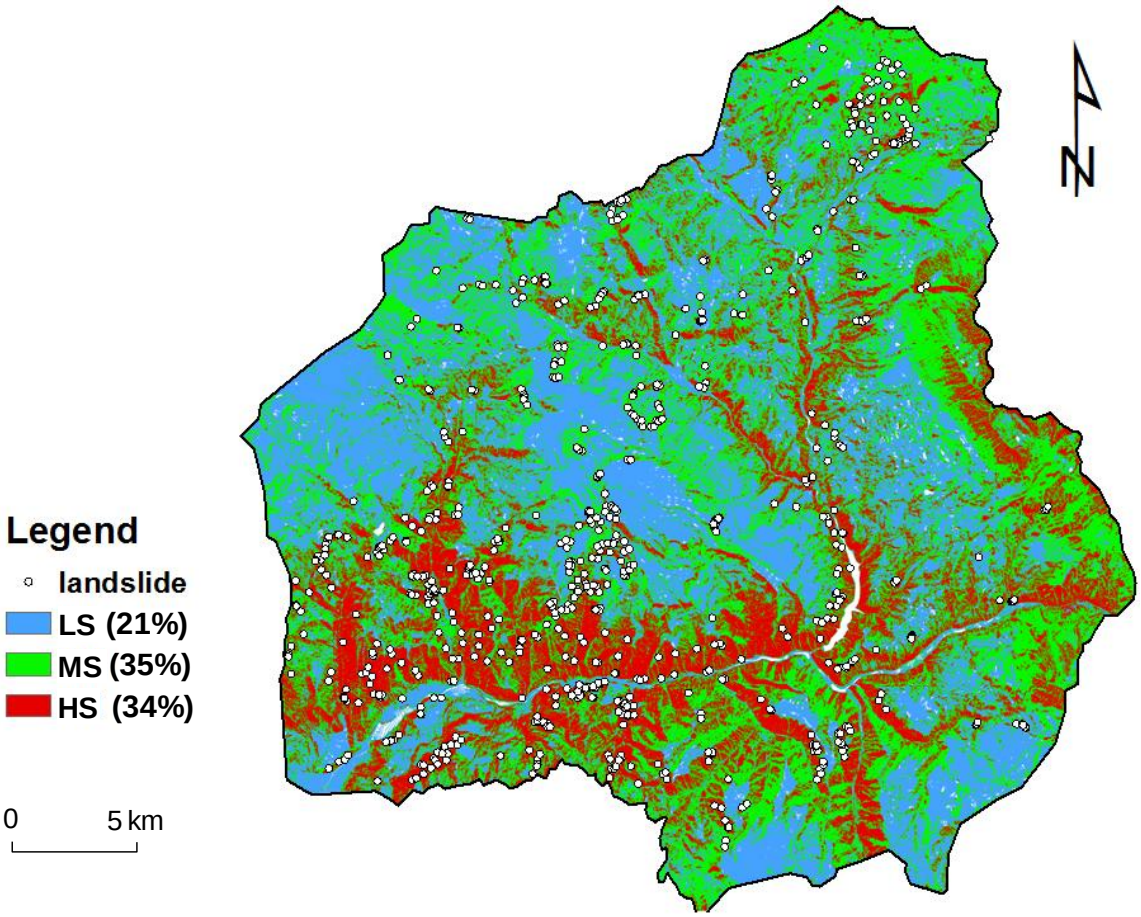

Fig. 44. A map of landslide susceptibility based on 735 shallow landslides and the combination of the landslide causing factors according to model 4 fuzzy network inference. This model has the highest rate of prediction. The high susceptibility area consists of 34% of the study area; it includes 78% of the total area of landslides. The medium susceptibility area, consists of 35% of the study area and comprises 19% of the total area of landslides. The low susceptibility area, consists of 21% of the study area and contains 3% of the total area of landslides.

Discussion and conclusions

The approach in this research divides the continuous data into different categories and calculates membership values for each category of the factors based on the frequency ratio. The first model is a method only appropriate when an expert tests the dependency of the factors. The other models do not require independent factors, if

the combinations of the factors are based on the expert's knowledge and appropriate choice of the fuzzy operators (Table 12). All of the four models developed are acceptable for the assessment of landslide susceptibility. The maps of landslide susceptibility developed by this method are effective in predicting known and unknown landslides. The prediction accuracy of the best model is ~80%. The methodology described in this paper reduces the uncertainties associated with the determination of fuzzy-membership values and manipulation of the continuous data. This method can provide better results if the landslides are classified into different types; a map of landslide susceptibility is created for each landslide type, and all maps of landslide susceptibility are combined in a single map using fuzzy operators.

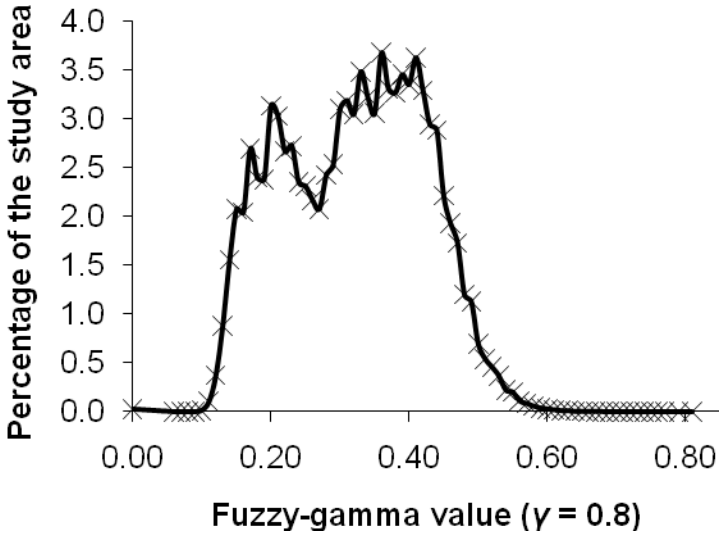

Fig. 45. Distribution of the fuzzy-gamma ($\gamma = 0.8$) based on model 4. The fuzzy-gamma value from 0.38 to 0.81 is classified as high susceptibility (HS), 0.26 to 0.38 as medium susceptibility (MS), and 0 to 0.26 as low susceptibility (LS).

The selection of the fuzzy operators is one of the most important aspects of fuzzy logic. An evidence map can be combined in a series of steps, as depicted in Fig. 40. Thus, instead of combining all the maps in one operation, it is appropriate to link some maps with different kinds (fuzzy OR or fuzzy AND) of fuzzy operators to support different intermediate hypotheses and finally linking raw evidence and intermediate hypotheses with a fuzzy-gamma operation. Many combinations are possible, and a quite complex inference network can be implemented. The inference network becomes an important means of simulating the logical thought process of an expert.

Thus, from this study it is apparent that the fuzzy operator approach to landslide mapping is a positive step in mapping landslide susceptibility. I believe this approach has world-wide application. Although the approach used was applied to a specific geographic location, it is suggested that the approach should be tried in other locations to validate its applicability.

The corridor of the North Fork Gunnison River has a history of serious and frequent landslides along its entire length. Observed and predicted shallow landslides are found on the slopes of the inner gorges of the North Fork Gunnison River and its associated streams, which are incising into upland plateaus. Furthermore, numerous, large deep-seated landslides are found on the edges of the upland plateaus. These characteristics of landslides represent potential for a first-order prediction of the landslides in this landscape.

Landslides in the study area have occurred in the past and activity continues. Landslides in the area have damaged Colorado Highway 133 and the D&RGW Railroad

(now Union Pacific). A possibility exists of landslides damming the North Fork Gunnison River, which could cause potential serious problems to communities downstream. The river flows parallel to Colorado Highway 133 and has been affected by landslides from the high hazard zones several times in the past. This hazard will exist into the future and all land use decisions should consider the potential destruction that may result.

CHAPTER VI

MAPPING LANDSLIDES WITH LOGISTIC REGRESSION

Synopsis

The area between Paonia and McClure Pass in Colorado was evaluated by coupling geographic information system (GIS) and logistic regression methods to assess susceptibility to landslides. Seven hundred and thirty five shallow landslides including debris dominated flows, debris dominated slides, rock dominated slides and soil dominated slides were mapped. Seventeen factors, as predictor variables of landslides, were mapped from aerial photographs, available public data archives, ETM+ satellite data, published literature and frequent field surveys. Landslides are shown on a binary map in which landslide cells were represented by 1 and non-landslide cells were represented by 0. A logistic regression model was run using landslides as dependent factor and landslide causing factors as covariates (independent factors).

Different techniques of sampling landslide and non-landslide data were developed and the capabilities of this information to assess landslide susceptibility were evaluated. Landslide data were collected from the landslide masses, landslide scarps, landslide mass centers, landslide scarp centers, and an equal amount of data were collected from areas free of landslides. First, with all landslides, models of susceptibility to landslides for each sampling technique were developed. Second, landslides were classified as debris dominated flows, debris dominated slides, rock dominated slides and soil dominated slides and then models of susceptibility to landslides were created for

each type of landslide. For this study landslide data were collected from the landslide masses and landslide scarps. Fourteen models of susceptibility to landslides were created from both parts of the study. The prediction accuracies of each model were compared using the ROC curve technique.

The model using samples from landslide scarps has the highest prediction accuracy and the model using samples from centers of the landslide masses has the lowest prediction accuracy among models developed from the four techniques of data sampling to assess susceptibility to landslides. Likewise, the model developed for debris dominated slides has the highest prediction accuracy and the model developed for soil dominated slides has the lowest prediction accuracy among four types landslides. Furthermore, prediction of the model developed by combining four models of four types of landslides is better than the prediction from the model developed by using all landslides together.

Introduction

Landslides, complex natural phenomenon, pose a serious natural hazard and play a significant role in the evolution of the hillslope. Landslides modify slope morphologies by transporting sediments from a slope toward the base of the slopes. Landslides represent ~9% of the worldwide natural disasters that occurred during 1990s (Gomez and Kavzoglu, 2005). Landslides, a major geologic hazard in the United States, occur in all 50 states and U.S. territories; cause $1-2 billion in damages and more than 25 fatalities on average each year (USGS, 2010). In Colorado, landslides are one of the

major natural hazards, which cause large economic losses (Rogers, 2003). The study area, the basin of North Fork of Gunnison River, is one of the areas affected by landsliding in Colorado. The Colorado Geological Survey listed the basin as sixth on the 2002 priority list for the Colorado landslide hazard mitigation plan (Rogers, 2003). The total cost of direct landslide losses and excess maintenance in this corridor is estimated to be at least $1 million a year (Rogers, 2003).

Landslides mostly result from triggering events, like earthquakes, intense rainfall, and snow melt. Besides triggering factors, other factors can be responsible for the instability of the hillslopes, including: geology, landcover, slope geometry, solar radiation, surface and subsurface hydrology, and the role of people. When assessing susceptibility to landslides, the role of each of these factors needs to be evaluated. Besides these factors, landslide frequency and magnitude are also necessary in an assessment. Frequency and magnitude of landslides are rarely introduced in the assessment of susceptibility to landslides.

Maps of the susceptibilities and risks of landslides are necessary tools to select appropriate sites for development of agriculture, construction and other human endeavors. Engineers, Earth scientists, planners and decision makers can use this information. Maps for susceptibility to landslides can be prepared in three ways: 1) deterministic approach; 2) probabilistic approach; and 3) qualitative or heuristic approach. A deterministic model considers slope geometry, characteristics of slope materials, and pressure generated by surface and subsurface water in a physical equation. The approach is commonly used to map slope instability (Chowdhury and Bertoldi,

1977; Chowdury, 1976; Gokceoglu and Aksoy, 1996; Wu and Sidle, 1995). The probabilistic approach, establishes statistical relationships among the preexisting landslides with the factors responsible for the occurrence and assumes future landslides will occur in similar environments where landslides occurred in the past (Anbalagan, 1992; Atkinson and Massari, 1998; Ayalew and Yamagashi, 2005; Carrara et al., 1991; Carrara et al., 1999; Cevik and Topal, 2003; Gokceoglu and Aksoy, 1996; Gorsevski et al., 2000; Gorsevski et al., 2003; Gritzner et al., 2001; Guzzetti et al., 1999; Juang et al., 1992; Lee, 2004; Maharaj, 1993; Pachauri et al., 1998; Tangestani, 2004; Van Westen et al., 1997). The qualitative or heuristic approach, in which an expert differentiates zones susceptible to landslides based on his/her *priori* knowledge of landslide instability, is also employed in many studies (Fenti et al., 1979; Ives and Messerli, 1981; Kienholz, 1978; Rupke et al., 1988).

The primary goals of this study are to evaluate the effect of data sampling and landslide types on the prediction accuracy of the models. To achieve these goals the major objectives were: 1) prepare maps of landslides and landslide causing factors; 2) develop database for landslides and non-landslide areas; 3) Develop probabilistic models of susceptibility to landslides in a logistic regression framework and evaluate the accuracy of the models using an ROC curve approach; and 4) test the validity of the best model.

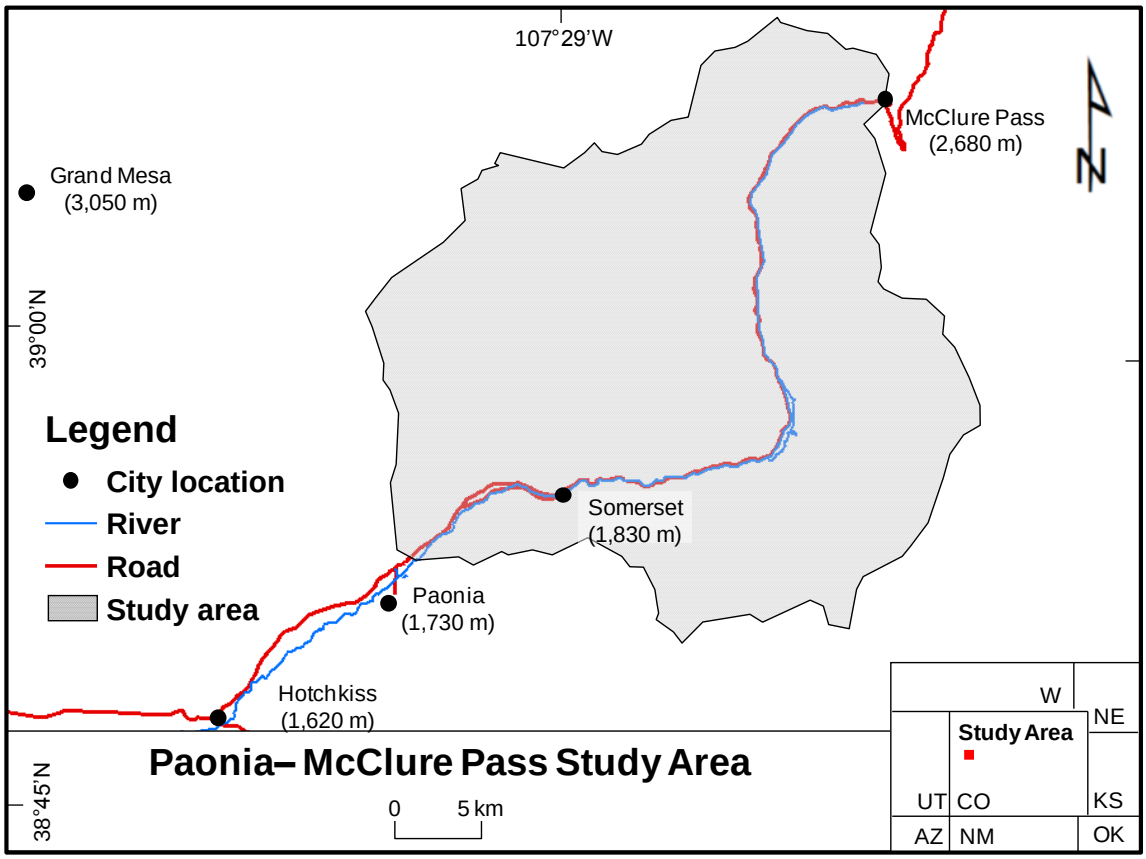

Fig. 46. Location map of the study area. W: Wyoming, NE: Nebraska, UT: Utah, CO: Colorado, KS: Kansas, AZ: Arizona, NM: New Mexico, and OK: Oklahoma.

Location and the geomorphology

The study area, located in west-central Colorado (Fig. 46), extends from Paonia to McClure Pass and encompasses ~ 815 km^2. General access to Paonia-McClure Pass is gained by Colorado Highway 133. Foot trails and forest roads provide direct access around the highway. The climate of the study area is predominantly semi-arid with 1.8 °C (minimum) to 18°C (maximum) average annual temperatures, 400 mm average annual precipitation and 1,220 mm average annual snowfall based on the 1905-2005 data

of Paonia 1SW climatic station (Western Regional Climate Center, 2010). Precipitation is primarily the result of summer convective thunderstorms.

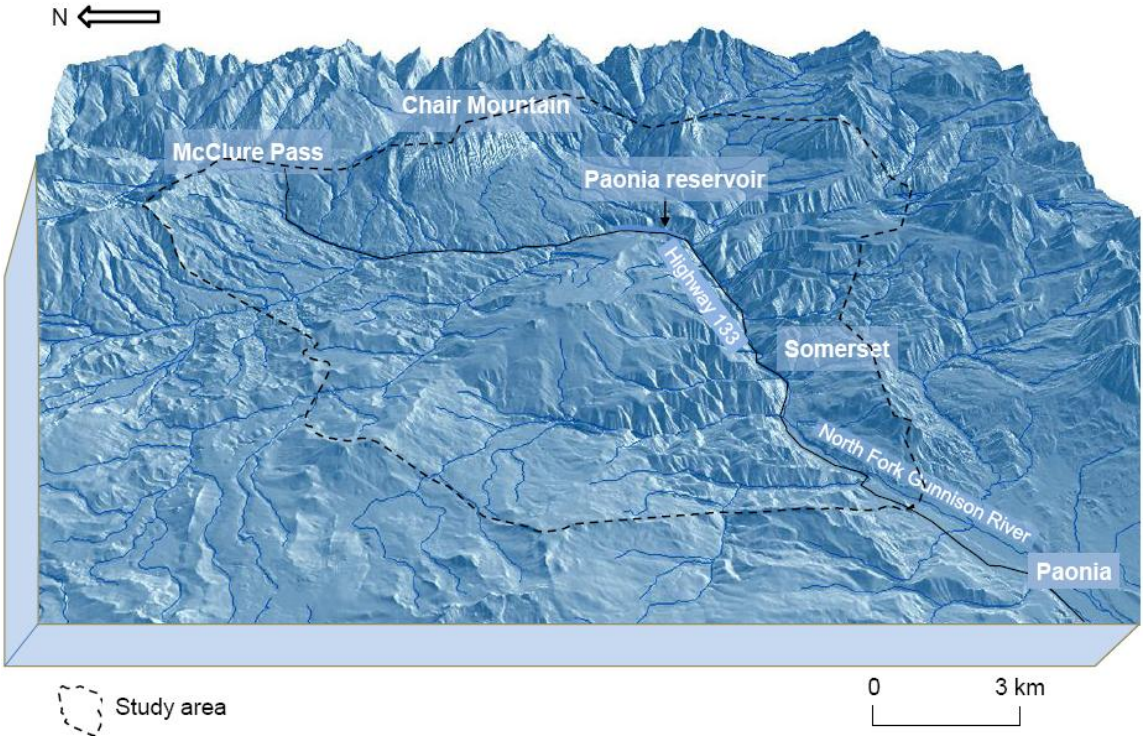

Fig. 47. A hill shadow image of the study area showing rugged topography. In some places the top of some hills can be seen as flat.

The area has rugged topography and a dendritic drainage pattern. The North Fork of Gunnison River drains the area into the Gunnison River. The elevation in the study area ranges 1,712 m to 3,883 m. The lowest elevation is the flood plain of North Fork of Gunnison River at Paonia and the highest elevation is Chair Mountain. The hillslope morphology is controlled by geology rather than elevation. Sandstone and plutonic rocks have steep slopes and the mudstone, shale, alluvial and colluvial deposits have medium

and gentle slopes. Most of the small mountains have steep slopes and flat mesa like tops, whereas tall mountain highlands have sharp ridges and steep slopes sculpted into horns, arêtes and cirques developed by alpine glaciers (Fig. 47). Major processes involved in the evolution of these hillslopes are the incision of the North Fork of Gunnison River and its streams and tributaries, Pleistocene glaciation, and mass movement from the coupling effects of snowmelt, rainfall and river erosion. Stream flow is primarily driven by the snow melt, which is greatest in May (Jaquette et al., 2005).

Landslides

In Colorado frequent landslides are widely distributed in the study area. Seven hundred and thirty five shallow landslides (Fig. 48) were mapped by employing a GIS (Geographic Information System) technique on 1991 and 2005 aerial photographs with a scale of 1:12,000. Landslides were identified visually by the distinguishing tone, shape, size and texture and digitized in ArcGIS® by identifying the scarp or zone of landslide material source and zone of transportation and deposition A three-dimensional visualization technique in ArcGIS® and stereo-visualization technique in Terrain Navigator Pro® were employed to determine the type of landslides; debris dominated flows, debris dominated slides, rock dominated slides and soil dominated slides. After mapping landslides on aerial photographs, the location, type and activity of all landslides were verified by field mapping. Other data such as area, perimeter, volume, length, width, position on the hillslope, vegetation, main causes, damage and preventive

measures taken were also collected from aerial photographs and field surveys. All these attributes were linked with spatial information of the landslides and stored in ArcGIS®.

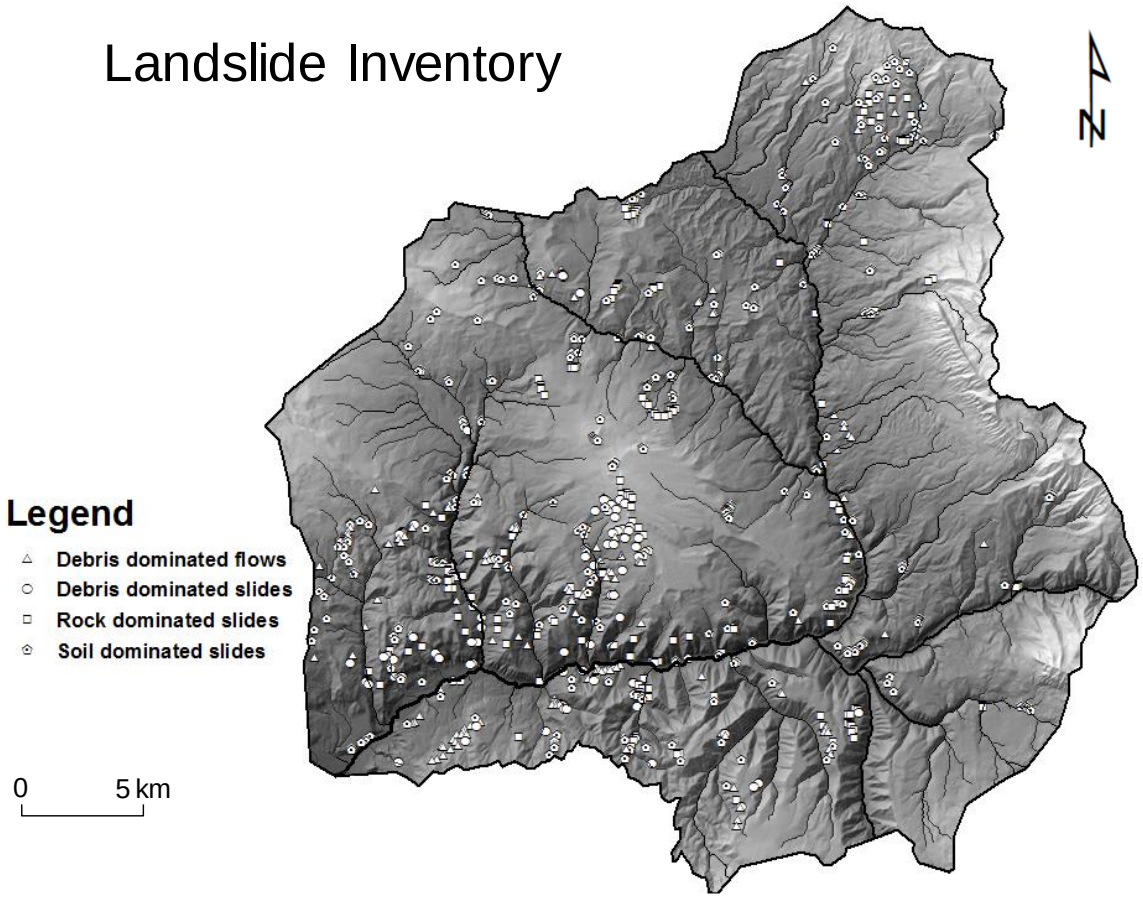

Fig. 48. A map showing distribution of different types of landslides in the study area. Soil slides are evenly distributed and other types of landslides are clustered in some places.

Among 735 landslides, 155 landslides were identified as debris dominated flows, 86 landslides were identified as debris dominated slides, 139 landslides were identified as rock dominated slides, and 324 landslides were identified as soil dominated slides. The smallest landslide mapped is 85 m^2 and the largest landslide mapped is 160,300 m^2.

Debris dominated flows mostly occur in topographic convergence covered by unconsolidated deposits. Debris dominated slides mostly occur in planar and concave slopes covered by unconsolidated alluvium and colluvium. Rock dominated slides mostly occur in steep and convex to planar slopes (Fig. 49). Soil dominated slides, the most dominant type of landslde, are distributed everywhere, but are smaller in size in comparison to the other types.

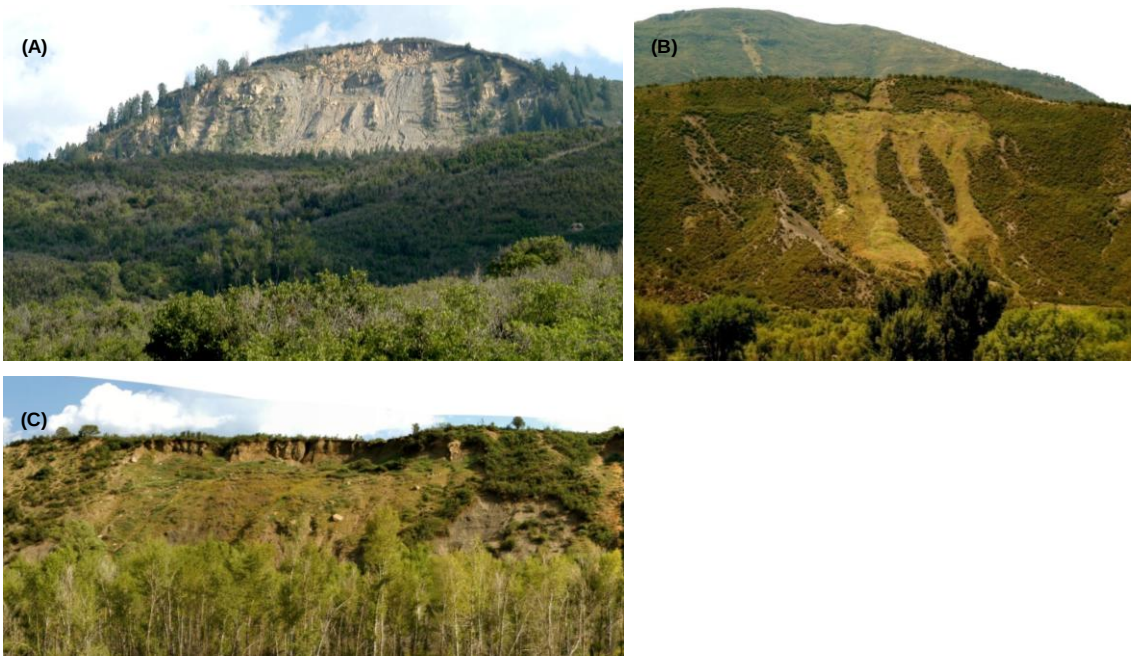

Fig. 49. Photographs of typical landslides in the study area. A) A debris flow on the north facing slope lying west of Somerset Village. The landslide is located on a concave slope. B) A rock dominated slide on north facing slope lying southeast of Somerset Village. The landslide occurred on a convex slope. C) A soil dominated slide on a north facing slope located about 6 km downstream from Somerset Village.

Materials and methods

Two major assumptions are made in a probabilistic approach of mapping the susceptibility of landslides: 1) landslides will occur in similar environments in which

landslides occurred in the past; and 2) the areas which are predicted as having landslide potential are only true if the factors used in the analysis will not significantly change in the future.

The methodology of this study can be classified broadly into three steps. First, landslide and landslide causing factors were collected and converted into GIS formats. Second, sampling techniques of data were developed; landslides were classified; and landslide and non-landslide data were extracted from maps of landslide causing factors. Third, logistic regression was run for different scenarios of data sampling and types of landslides.

GIS data layers

First step in mapping susceptibility to landslides is to identify factors responsible for the existing landslides. Extensive field work was completed to evaluate the roles of geologic, hydrologic, geomorphic and anthropogenic factors in the formation of landslides. Furthermore, the values of these factors on landslide and non-landslide areas were statistically compared. Most of the landslides are observed in sandstone and mudstone, shrubland and woodland, fine to medium grained loose regolith having non-plasticity index to low plasticity index, 20° to 40° slopes, south facing slopes, topographic convergence, and close proximity of rivers faults and roads. Based on the field survey, major factors of the landslides were determined as slope, the aspect of slope, solar radiation, streams, roads, geology, landcover and soil. Minor factors were

topographic curvature, geological structure, the topographic wetness index and the stream power index.

Geology and landcover

Cretaceous sedimentary rocks, including shale, mudstone and sandstone; Tertiary igneous rocks, including basalt and batholiths of granodiorite; and various Quaternary deposits including alluvium, colluvium and mixed deposits are the main lithologies of the study area. The basalt, formed by extensive volcanic eruption, capped many mountains. Colluvium and moraines occur on gentle mountain slopes, bedrock is dominant along the steep ridges, and the fluvial deposits occupy the stream valleys.

Movements along faults weakens rocks and soil and triggers landslides. I mapped 20 exposed and unexposed (sub-surface) fault lines from a USGS geological map prepared by Dunrud (1989). Many landslides are located in the close proximity to these fault lines.

Soil data, obtained from USDA (United States Department of Agriculture) and US Forest Service, contains information about the soil or regolith up to a depth of 1.5 m. I classified the soil based on the plasticity index (*PI*) as non-plastic, low plastic (*PI* = <5), medium plastic (*PI* = 5-15), high plastic (*PI* = 15-20), and very high plastic (*PI* = >20). Most of the landslides are observed in non-plastic to low plastic soils.

Vegetation in the area consists of grasses, aspen groves (*Populus tremuloides*), and pines (*Pinus edulis*). The landcover of the area, extracted from a LANDSAT ETM+ satellite image acquired in 2002, was categorized into: 1) forest, 2) woodland, 3)

shrubland, 4) grassland, 5) agricultural land, 6) barren land, and 7) settlement. Most of the landslides occurred in shrubland.

Hillslope geometry and solar radiation

Slope, aspect of slope and curvature of slope are geomorphic attributes of landslides in the study area. All of these factors were developed in ArcGIS® from USGS DEM of 10 m horizontal resolution.

Total annual global solar radiation was calculated for each pixel in the study area by using the inbuilt algorithm in ArcGIS®. The total global solar radiation is the summation of the total direct solar radiation, total diffuse solar radiation and total reflected solar radiation. Direct solar radiation is defined as the unimpeded interception of the solar radiation directly from the sun. Diffuse radiation is defined as the radiation scattered by atmospheric constituents, such as clouds and dust. Reflected solar radiation is defined as the radiation reflected from surface features. Direct radiation is the largest component of total radiation, and diffuse radiation is the second largest component. Reflected radiation generally constitutes only a small proportion of total radiation, except for locations surrounded by highly reflective surfaces such as snow cover. The reflected radiation is ignored in this study.

Water-related factors

Flow accumulation, flow length, topographic wetness index (*TWI*) and stream power index (*SPI*) are water-related factors derived from the DEMs and used as

predictors of landslides in this study. Flow accumulation is the number of cells flowing through a point. It provides information on upstream contributing area of that point. Flow length is defined as the length of stream from drainage divide to the point of interest. *TWI*, a steady state wetness index (Beven and Kirkby, 1979), is a function of the slope and the upstream contributing area per unit width orthogonal to the flow direction. This index is used in this study as a predicting factor of landslides because it correlates in some degree with the groundwater condition and soil moisture, areas with the higher values of *TWI* are most likely to become saturated during a rain or snowmelt event (Moore et al., 1991). The topography index was created from a DEM using Eq. 51.

$$TWI = \ln\left(\frac{A}{b\tan\beta}\right) \tag{51}$$

where A is the upstream contributing area expressed as m^2, b is the width of a cell expressed as m and and β is the slope angle of that cell expressed as radians. The variable was created from DEM using Eq. 51.

SPI, a steady state index, assumes that every point in the catchment has reached sub-surface drainage equilibrium, and the upslope contributing area can be quite large. When a steep slope has a large upstream contributing area, the *SPI* value becomes larger. The higher value of *SPI* is generally found at the foot of the slope and it seems reasonable to believe that higher values of *SPI* at the foot of slopes make the triggering of landslides much more probable (Conoscenti et al., 2008). *SPI* is calculated from DEM using Eq. 52 (Moore et al., 1991).

$$SPI = \frac{A\tan\beta}{b} \tag{52}$$

Irregular flow regimes of the streams and gullies can be the cause of intense, superficial mass movement phenomena in areas adjacent to drainage channels (Barredo et al., 2000). Rivers induce failure of banks because of slope undercutting. I observed many landslides in the study area caused by rivers undercutting banks. To include the role of rivers in the assessment of susceptibility, a map showing distances from rivers was created.

Human related factors

Worldwide, human influence is one of the major factors causing landslides. Road-cuts are usually sites of anthropologically induced instability (Ayalew and Yamagashi, 2005; Pachauri et al., 1998; Pachauri and Pant, 1992). Construction of a road on a hillslope increases the slope above the road and stress on the back of the slope. Furthermore, the hillslope that was in equilibrium before the road is constructed may become unstable because of water ingress. In the study area many landslides occurred in close proximity to roads. Because of these reasons, proximity to roads is also considered as landslide causing factor. Roads and residential areas were extracted from aerial photographs and an ETM satellite map. A map showing distance from roads was created and the relationships of the number of landslide cells and the distance from roads were evaluated. I observed that the density of landslide cells is the highest in close proximity to roads. The distance map was considered as one of the independent factors of landslides in this study.

Variable selection and model development using logistic regression

Logistic regression is generally used when the predictor variables are not normally distributed (Allison, 1999; Johnson, 1998). The dependent variable in this approach is sampled as a binary variable (i.e. presence or absence of landslide). Therefore, the method determines the probability of the presence or absence of landslides. Logistic regression fits a s-shaped curve by taking a linear regression, between binary dependent variable and continuous or categorical independent variables (covariates). The logistic regression equation can be expressed as:

$$p(y=1|x)=\frac{exp(\beta_0+\beta_1x_1+\beta_2x_2.....\beta_nx_n)}{1+exp(\beta_0+\beta_1x_1+\beta_2x_2.....\beta_nx_n)} \quad (53)$$

where x is the data vector of an independent variable, β is the coefficient(s) of the independent variable(s), and y is the value of the binary outcome variable.

Preparation of the database for logistic regression includes collection of the independent data at the selected locations of landslide and non-landslide experimental units. Mainly three types of selection of landslide and non-landslide experimental units are common. First one is collecting data from each cell of the entire study area, which undoubtedly leads to unequal proportions of landslide and non-landslide cells (Guzzetti et al., 1999; Ohlmacher and Davis, 2003). A large volume of data is included in this method. The second method is random selection of unequal proportion of landslide and non-landslide cells (Garcia-Rodriguez et al., 2008). Third method is using all or part of the landslide cells and equal number of randomly selected non-landslide cells (Ayalew and Yamagashi, 2005; Duman et al., 2006; Mathew et al., 2009). This may decrease data

number and eliminate bias in the sampling process. In this study the third approach was applied.

A forward likelihood ratio method was employed to select important variables of landslides. In this method, the covariates (landslide independent variables) specified on forward logistic regression were tested for entry into the model one by one based on significance level. A variable with a significance value less than 0.05 was entered into the model. After each entry, variables that were already in the model were tested for possible removal based on the significance of the likelihood ratio. In the likelihood ratio, the variables with the largest probability greater than 0.1 were removed, and the model was re-estimated. The final model was achieved when no more variables met entry or removal criteria.

Effect of data sampling

Use of an appropriate technique of sampling landslide data is always essential to create an accurate map of susceptibility to landslides. A very difficult problem is the identification of the location on the slope where the value of the landslide causing factor exceeded the threshold value of stability and caused the slope to become unstable. A landslide can possibly occur at any location on the slope. For example, 1) seeding of landslides is possible at the toe of the slope because of the unloading of the slope toe by road cutting or river undercutting; 2) seeding of a landslide is possible at the head of the slope because of the steep slope; 3) likewise, the seeding of a landslide is possible at the center of the slope because of the loading of slope materials and increase in pore-water

pressure. Wherever the seeding occurs, a landslide can extend upslope, downslope and sidewise from the seeding location regardless of the characteristics of the factors causing the landslide. This creates a difficult problem for an expert to identify the exact location of landslide seeding. Furthermore, for a large region with a large number of landslides, it is almost impossible to determine such locations either by field work or by the analysis of remotely sensed images. Therefore, when assessing susceptibility to landslides, an expert should be aware of uncertainties associated with the sampling technique. In many studies of assessing landslides this uncertainty is commonly ignored. Only a few studies described the effectiveness of the sampling techniques. Some studies used data from centers of the landslide masses and landslide scarps or source regions (Dahal et al., 2008; Neuhauser and Terhorst, 2007). In some studies landslides are differentiated into body rupture areas or source areas and the deposition areas or runout zones (Atkinson and Massari, 1998; Dai and Lee, 2003). In some studies only depositional areas of landslides are analyzed to determine susceptible zones of landslides (Fernandez et al., 2003; Remondo et al., 2003). Likewise, some studies considered only zones of rupture or the upper edges of main scarp to evaluate susceptibility to landslides (Clerici et al., 2006; Santacana et al., 2003). Moreover, undisturbed morphological conditions from the close vicinity of the landslide polygons were also used to sample landslide data (Suzen and Doyuran, 2004), pre-landslide hillslope was constructed to extract pre-landslide slope angle (den Eeckhaut et al., 2006) and a seed cell approach was used (Nefeslioglu et al., 2008). Results show all of these methods are reliable in mapping the susceptibility of

a surface to landslides. But a question still exists is: did these studies collect the data in the same proportion of size or magnitudes of the landslides?

To show the difference in results of different sampling techniques, four techniques to sample landslide and non-landslide data were employed (Fig. 50): A) samples from each cell of the landslide mass and an equal number of random samples from areas free of landslides; B) samples from each cell of the landslide scarps and an equal number of random samples from areas free of landslides; C) samples from the centers of the landslide masses and an equal number of random samples from areas free of landslides; D) samples from centers of the landslide scarps and an equal number of random samples from areas free of landslides. Number 1 does not ignore the information on landslide magnitude. Number 2 also does not ignore the information on landslide magnitude because the scarp area of a landslide relates to the area of landslide mass (Fig. 51A). Number 3 and number 4 ignore information on the magnitude of landslides.

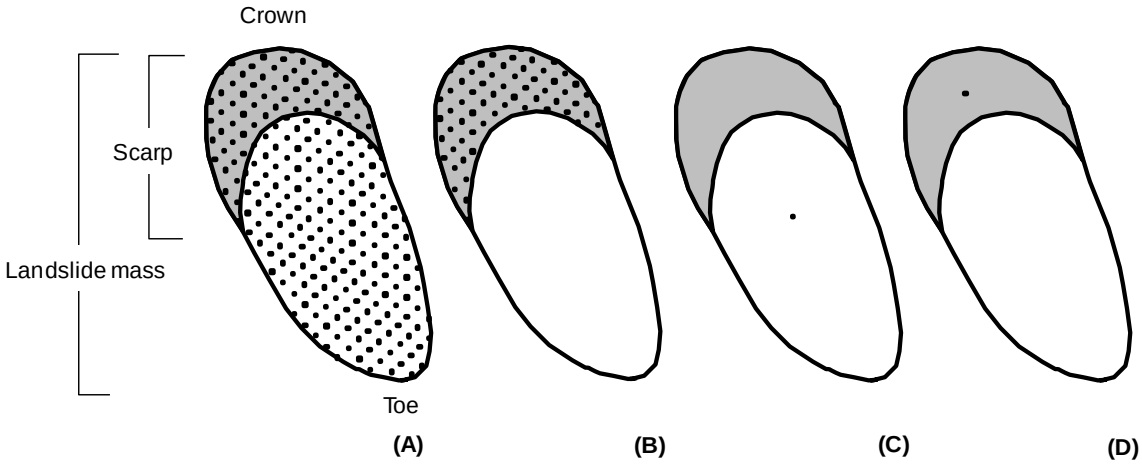

Fig. 50. Techniques of landslide data sampling. A) From landslide mass; B) from landslide scarp; C) landslide mass center; D) landslide scarp center.

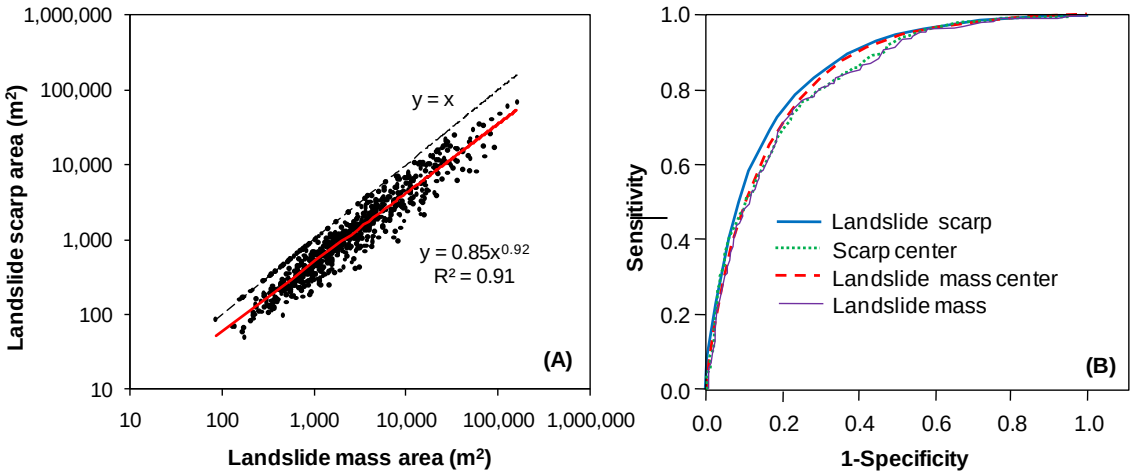

Fig. 51. Figures showing A) ROC curves for models developed based on the four techniques of data sampling, and B) the relationships of landslide scarp areas and landslide mass areas.

Effect of landslide types

The sampling techniques and the type of landslides may cause inconsistency in the result of mapping the susceptibility to landsides. Different mechanisms cause different types of landslides. A factor mostly responsible for one type of landslide can be different than for another type of landslide. For example, intense rainfall or snowmelt can induce saturation of soil or regolith and cause the slope to experience debris dominated flow or mud dominated flow. An unfavorable condition of the orientation of rock discontinuities can be a major cause of a rock dominated slide. Similarly, debris slides and soil slides can have different major causes. Therefore, a map of susceptibility, created for each type of landslides, should be more accurate than a map created based on the analysis of landslides not differentiated by factors of formation. Furthermore, if these individual maps are then combined into a single map of susceptibility, the prediction

accuracy of the combined map should be better than the prediction accuracy of a map prepared by analyzing all landslides together.

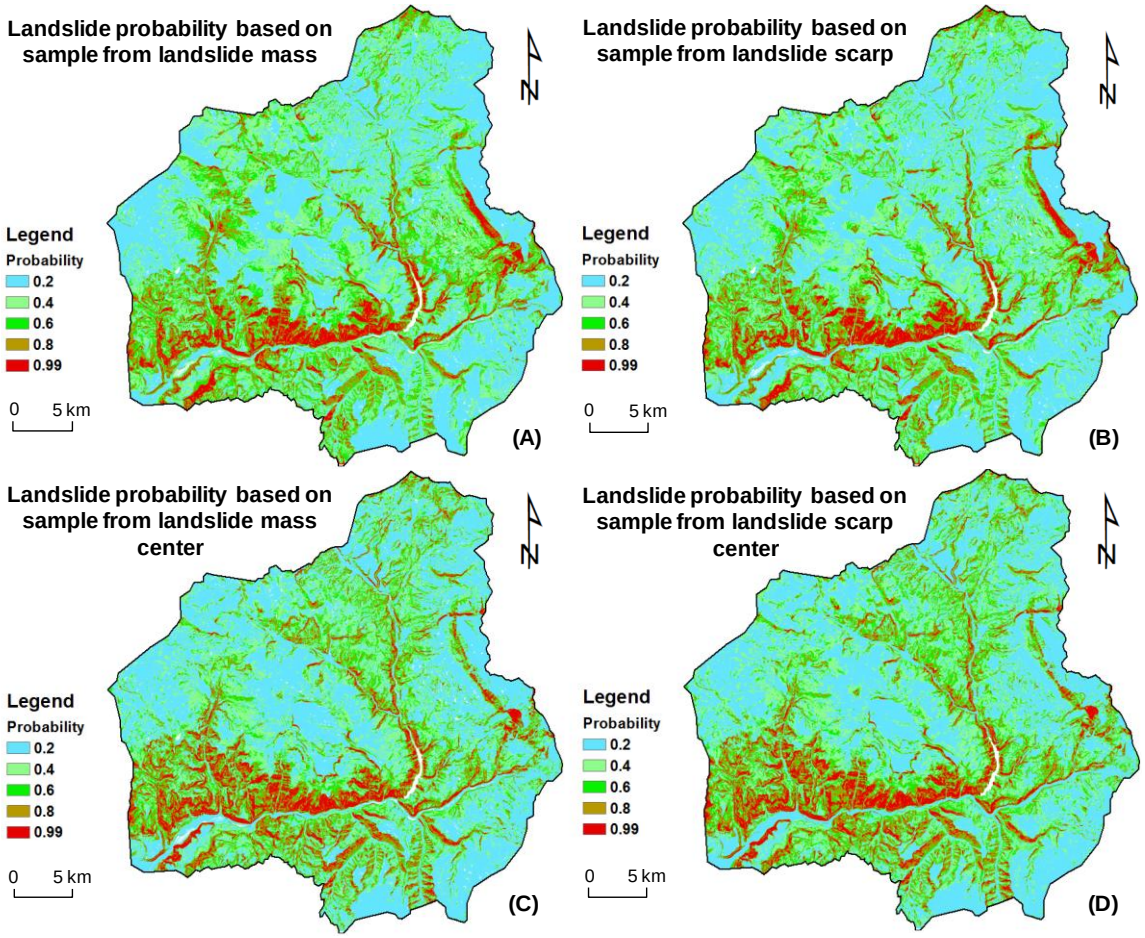

Fig. 52. Maps of landslide probability developed based on the four techniques of data sampling. A) Sampling from the landslide masses; B) sampling from the landslide scarps; C) sampling from landslide mass centers; D) sampling from landslide scarp centers.

Models of susceptibility to landslides

Among four techniques of data sampling (Fig. 50), the first model consisted of 48,000 (100%) data points collected from landslide masses and 48,000 (~0.5 %) data

points collected from areas free of landslides. The second model consisted of 22,000 (100%) data points collected from landslide scarps and 22,000 (0.025%) data points collected from areas free of landslides. The third model consisted of 735 landslide data points collected from centers of landslide masses and 735 non-landslide data points collected from areas free of landslides. Similarly, the fourth model consisted of 735 landslide data points collected from centers of the landslide scarps and 735 non-landslide data points collected from areas free of landslides. Using these data, four maps of landslide probability were created (Fig. 52) and the validity of these maps were tested (Fig. 53).

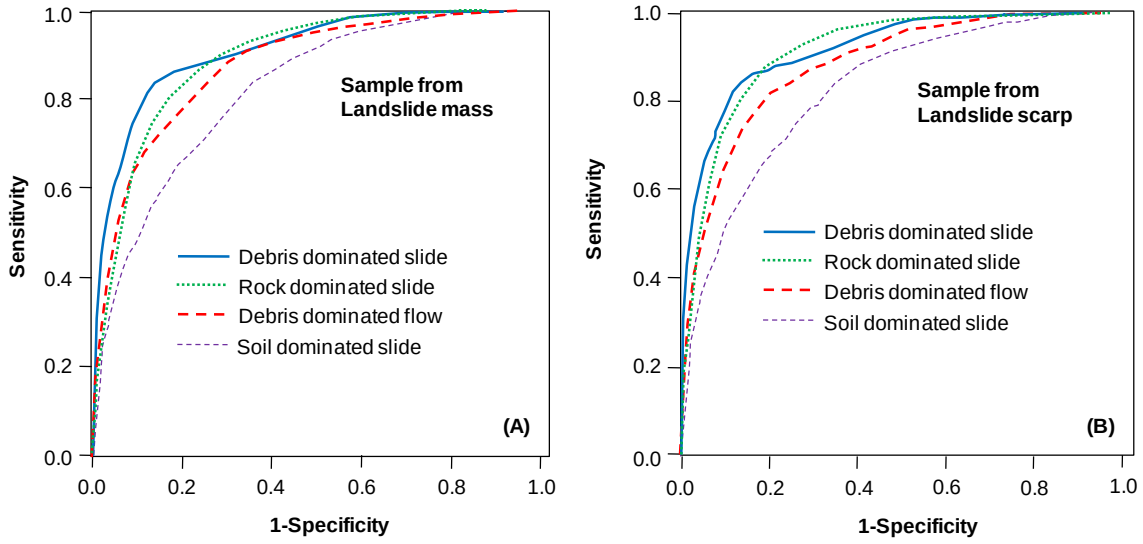

Fig. 53. ROC curves for different types of landslides. A) Landslide data were sampled from the landslide masses, and B) landslide data were sampled from the landslide scarps.

To evaluate the effect of landslide type, landslides were classified as debris dominated flows, debris dominated slides, rock dominated slides and soil dominated

slides. Then, a landslide and non-landslide database for two techniques of sampling were developed for each type of landslide. The samples for landslide data were collected from the landslide masses and landslide scarps and non-landslide data were randomly collected from areas free of landslides. Four maps of landslide probability were created for each technique of sampling. As an example, probability maps created based on the data sampled from the landslide scarps are shown in Fig. 54. Finally, all of four landslide

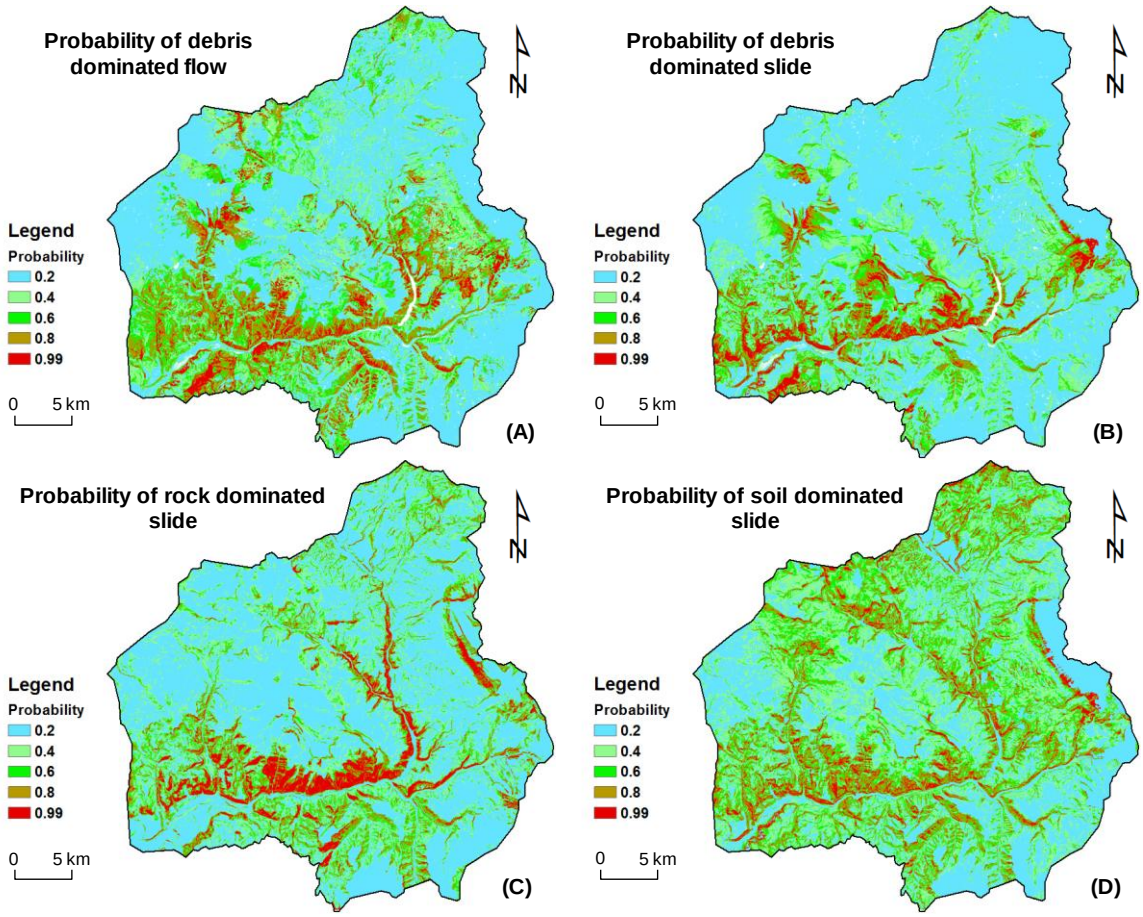

Fig. 54. Probability maps of A) debris dominated flows; B) debris dominated slides; C) rock dominated slides; and D) soil dominated slides. Landslide data were sampled from the landslide scarps.

Table 13 Selected factors, logistic regression coefficients and significance of Wald statistics for four techniques of sampling landslide data. G1: Tertiary igneous rock (Td and Tmi), G2: Wasatch Formation (Tw), G3: Quaternary alluvial, glacial, and talus deposits (Qac, Qa, Quwa, Qtr, Qg, Qd, Qdo), G4: Mesaverde Formation (Kmv, Kmvr, Kmvo, Kmvb, Kmvc), G5: Quaternary unconsolidated colluvial deposits (Quwe, Quwi, Qc, Qls), G6: Mancos shale (Km), G7:Qa L1: forest, L2: water, L3: agricultural land, L4: grassland, L5: rock, L6: woodland, L7: shrub/bush, S1: high plastic soil, S2: medium plastic soil, S3: low plastic soil, S4: rock, S5: non-plastic to very low plastic soil.

Independent Factors		Landslide mass			Scarp centroid			landslide mass			Landslide scarp		
		model factors	*B*	*p*	model factors	*B*	*p*	model factors	*B*	*p*	model factors	*B*	*p*
slope		×	0.14	0.00	×	0.12	0.00	×	0.11	0.00	×	0.11	0.00
aspect								×	0.00	0.00			
elevation								×	0.00	0.00	×	0.00	0.00
Profile Curvature								×	-0.03	0.04	×	-0.02	0.00
Plan Curvature													
Tangential curvature								×	-0.04	0.00			
Solar Radiation		×	0.00	0.00	×	0.00	0.00	×	0.00	0.00	×	0.00	0.00
Wetness Index		×	0.09	0.01				×	0.07	0.00	×	0.03	0.00
Stream Power Index													
Flow Accumulation											×	0.00	0.02
Flow Length													
Distance to road								×	0.00	0.00	×	0.00	0.00
Distance to stream					×	0.00	0.01				×	0.00	0.00
Distance to fault								×	0.00	0.00	×	0.00	0.02
Landuse		×		0.00	×		0.00	×		0.00	×		0.00
	L1		-1.34	0.00		-1.26	0.00		-1.02	0.00		-0.91	0.00
	L2		-	-		-	-		-1.02	0.00		-1.36	0.02
	L3		-1.47	0.17		-1.24	0.24		-1.71	0.00		-3.72	0.00
	L4		0.13	0.64		-0.01	0.96		-0.46	0.00		-0.43	0.00
	L5		-2.35	0.00		-2.11	0.00		-0.28	0.00		-0.36	0.00
	L6		-0.35	0.25		-0.39	0.21		-0.47	0.00		-0.49	0.00
	L7		**	**		**	**		**	**		**	**
Geology		×		0.00	×		0.00	×		0.00	×		0.00
	G1		-4.96	0.00		-4.24	0.00		-5.07	0.00		-5.94	0.00
	G2		-2.51	0.02		-2.35	0.03		-0.98	0.00		-0.96	0.00
	G3		-2.63	0.02		-2.53	0.02		-0.54	0.00		-0.93	0.00
	G4		-3.12	0.00		-2.81	0.01		-0.99	0.00		-1.15	0.00
	G5		-2.21	0.04		-2.11	0.05		0.37	0.00		0.04	0.75
	G6					**	**		**	**		**	**
soil plasticity index		×		0.00	×		0.00	×		0.00	×		0.00
	S1		-0.37	0.40		-0.34	0.43		-1.87	0.00		-1.51	0.00
	S2		-0.66	0.00		-0.74	0.00		-1.37	0.00		-1.51	0.00
	S3		-0.16	0.45		-0.21	0.31		-0.91	0.00		-1.07	0.00
	S4		-2.95	0.00		-3.71	0.00		-0.29	0.00		-0.86	0.00
	S5		**	**		**	**		**	**		**	**
Constant		×	-2.31	0.07	×	-1.35	0.27	×	-0.22	0.10		-1.61	0.00

** reference category

Table 14 Selected factors, logistic regression coefficients and significance of Wald statistics for four types of landslides. Acronyms same as table 13.

Independent Factors	Debris dominated flow			Debris dominated slide			Soil dominated slide			Rock dominated slide		
	model factors	*B*	*p*	model factors	*B*	*p*	model factors	*B*	*p*	model factors	*B*	*p*
slope	×	0.06	0.00	×	0.12	0.00	×	0.13	0.00	×	0.14	0.00
aspect	×	0.00	0.00							×	0.00	0.00
elevation	×	0.00	0.00	×	0.00	0.00	×	0.00	0.00	×	0.00	0.00
Profile Curvature	×	-0.11	0.00				×	0.05	0.01			
Plan Curvature	×	-0.21	0.00	×	-0.07	0.02						
Tangential curvature										×	0.05	0.00
Solar Radiation	×	0.00	0.00	×	0.00	0.00	×	0.00	0.00	×	0.00	0.00
Wetness Index	×	0.10	0.00	×	0.12	0.00				×	-0.15	0.00
Stream Power Index												
Flow Accumulation												
Flow Length												
Distance to road	×	0.00	0.00	×	0.00	0.00				×	0.00	0.00
Distance to stream	×	0.00	0.00	×	0.00	0.00				×	0.00	0.00
Distance to fault	×	0.00	0.00	×	0.00	0.00	×	0.00	0.00	×	0.00	0.00
Landuse	×		0.00	×		0.00	×		0.00	×		0.00
L1		-2.27	0.00		-0.01	0.93		-0.78	0.00		-0.65	0.00
L2		-20.10	1.00		-0.75	0.51		0.23	0.74		-19.02	1.00
L3		-2.90	0.00		-18.35	1.00		-20.18	1.00		-18.94	0.99
L4		-1.10	0.00		-0.13	0.36		-0.21	0.05		-0.30	0.01
L5		-20.80	0.99		-20.45	0.99		-21.50	0.99		0.46	0.00
L6		-1.24	0.00		0.52	0.00		-0.16	0.21		-1.07	0.00
L7		**	**		**	**		**	**		**	**
Geology	×		0.00	×		0.00	×		0.00	×		0.00
G1		-21.14	0.99		-22.24	0.99		-22.72	0.99		-4.24	0.00
G2		-1.86	0.00		-2.28	0.00		-0.91	0.01		0.95	0.01
G3		-2.12	0.00		-2.77	0.00		-0.55	0.09		1.18	0.00
G4		-0.67	0.01		-2.29	0.00		-1.99	0.00		0.46	0.21
G5		-0.10	0.68		-0.47	0.11		-0.73	0.02		0.53	0.15
G6		**	**		**	**		**	**		**	**
soil plasticity index	×		0.00	×		0.00	×		0.00	×		0.00
S1		-3.58	0.00		-21.98	0.99		0.74	0.00		-0.57	0.00
S2		-0.58	0.00		-1.74	0.00		-0.37	0.00		-1.84	0.00
S3		-0.24	0.00		-1.19	0.00		0.11	0.25		-1.51	0.00
S4		-20.53	1.00		-21.10	1.00		0.03	0.97		-0.32	0.06
S5		**	**		**	**		**	**		**	**
Constant		3.66	0.00		-1.99	0.00		-3.52	0.00		-4.95	0.00

** reference category

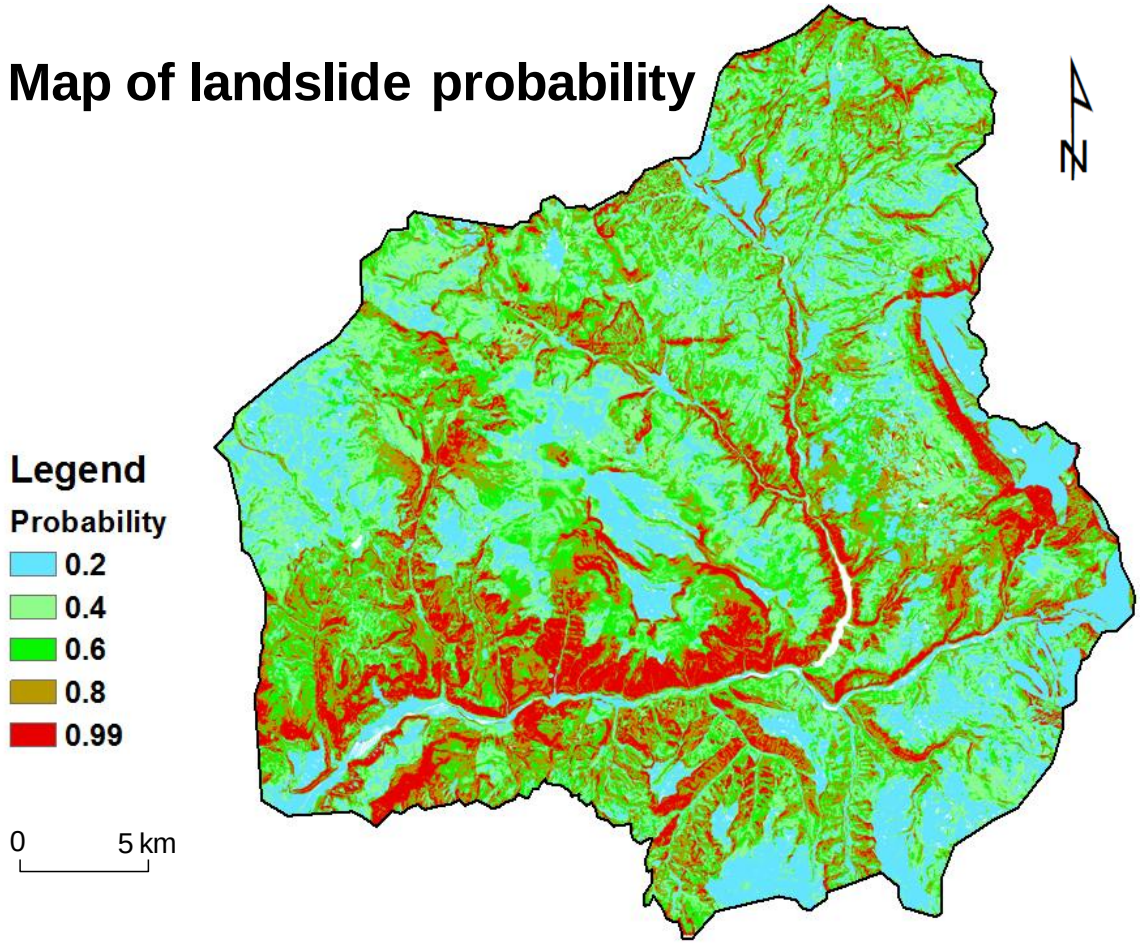

Fig. 55. Landslide probability map prepared by combining all probability maps shown in Fig. 54.

probability maps for each technique of data sampling were combined in such a way that each cell was represented by the maximum landslide probability of four maps at that cell. A combined probability map, developed from landslide data sampled from scarps of landslides, is shown in Fig. 55. The final combined map of landslide probability is classified into three types of susceptibility based on the classification scheme as areas having probability greater than 0.6 is high susceptibility, 0.2 to 0.6 is medium susceptibility and less than 0.2 is low susceptibility. The final map of susceptibility to

landslides from the techniques of sampling landslide data from scarps of landslides is shown in Fig. 56.

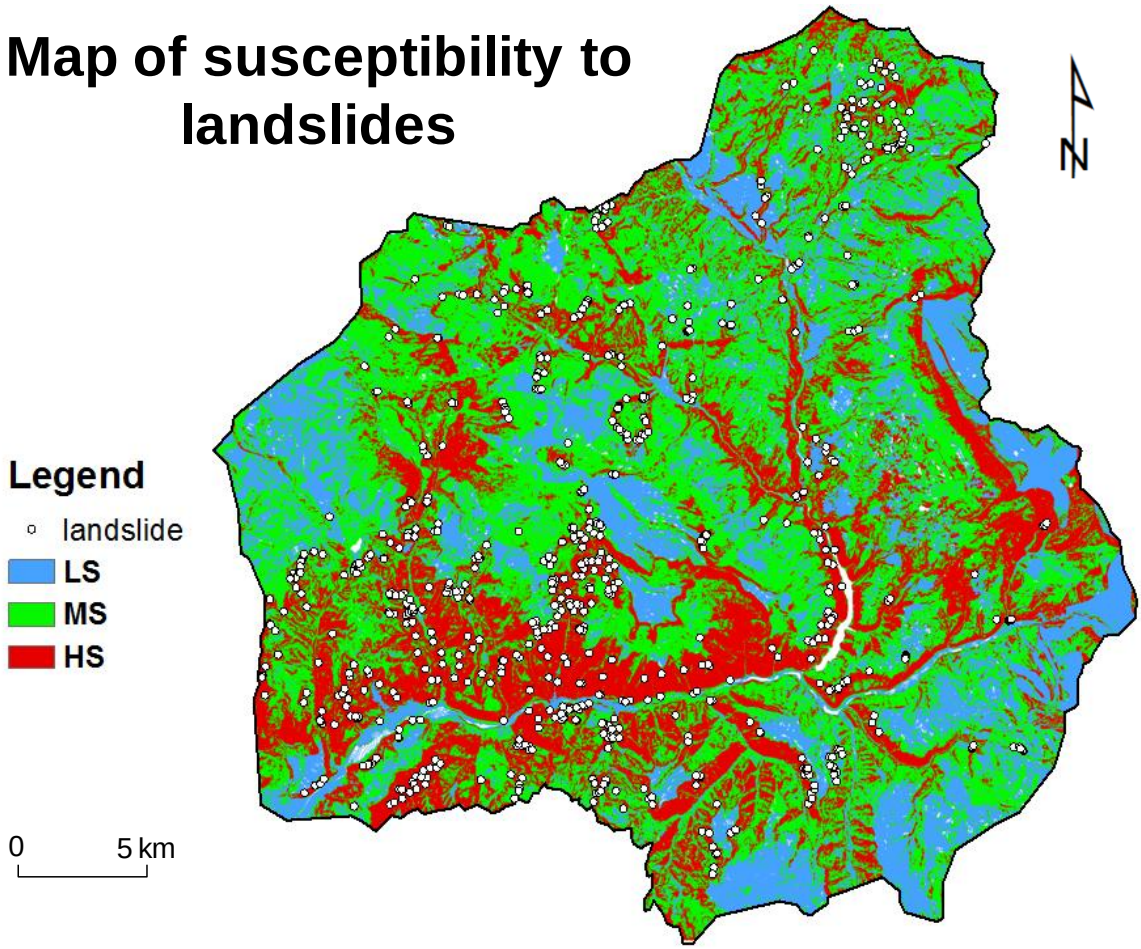

Fig. 56. A map of susceptibility to landslides. The map is developed by classifying Fig. 55. High susceptibility is classified as landslide probability >0.6, medium susceptibility is classified as landslide probability 0.2 – 0.6, and low susceptibility is classified as landslide probability <0.2.

In all cases, the probabilities of landslides were calculated for each cell of the study area by using Eq. 53, where β_0 is constant, β_1, $\beta_2 \ldots \beta_n$ are the coefficients of independent factors (Tables 13 and 14) and $x_{1,}\, x_2 \ldots x_n$ are the values of the independent

factors. A common assumption is: the distributions of the non-landslide database of all factors in all cases are similar to each other and similar to the non-landslide database for the entire area. The variability of all databases, the distribution curve and the mean values of each factor are not significantly different.

Accuracy assessment by ROC curve

ROC (Receiver Operating Characteristic) curve analysis is a commonly used method for assessing the accuracy of a diagnostic test (Egan, 1975; Søreide, 2009; Swets, 1988; Williams et al., 1999). It provides a diagnostic statistic that may be used to distinguish between two classes of events. The curve is a plot of the probability of a correctly predicted event response (true positive) versus the probability of a falsely predicted event response (false positive) as the cut-off probability varies. For example, a correctly predicted event response is a prediction of a landslide for a location where a landslide occurred, whereas a falsely predicted event response is a prediction of a landslide for a location where a landslide did not occur. If all landslides are correctly predicted, the area under the curve would equal 1. The ROC curve also helps an expert to make decisions. Each point on the ROC curve may be associated with a specific decision criterion for how much risk the user is willing to take regarding the accuracy of the prediction (Gorsevski et al., 2006). In modeling based on logistic regression, ROC curves are very useful for evaluating the predictive accuracy of the model. The predicted probabilities generated for a binary response variable can be viewed as a continuous indicator and plot as a ROC curve to determine the prediction accuracy of the model

(Gorsevski et al., 2006). Although ROC analysis provides an overall value of accuracy independent of a cutoff value and occurrence, it does not provide the optimal cutoff value nor does it illustrate how occurrence affects cutoff selection (Mcfall, 1999).

Results

Table 13, the important factors needed to prepare an accurate model of susceptibility to landslides, depends on sampling techniques. For example, factors selected for models relying on landslide data sampled from the landslide masses and landslide scarps are not similar to the factors selected for models relying on the landslide data collected from centers of the landslide masses and landslide scarps. Similarly, ROC curves and prediction accuracies, shown in Fig. 51B and Table 15 imply that the accuracy of the model depends on techniques of sampling the landslide data. The model depending on landslide data sampled from the landslide scarps has the highest prediction accuracy (85%) and the model depending on landslide data sampled from centers of the landslide masses has the lowest prediction accuracy (83%).

Table 14 shows that important factors needed to prepare an accurate model of susceptibility of landslides also depends on the types of landslides. Factors selected for the models created by different types of landslides are not same. The ROC curve and prediction accuracies (Figs. 54A and 54B and Table 15) of different kinds of landslides are also different. In both cases of sampling, the model for the debris dominated slide has the highest prediction accuracy (91% for sampling from mass and 92% for sampling

from scarp) and the model for soil dominated slides has the lowest prediction accuracy (92% for sampling from mass and 93% for sampling from scarp).

In all cases the prediction of the models developed by sampling data from the landslide scarps is better than others (Figs. 51B, 54A, 54B and Table 15). The areas of the landslide scarps preserve the magnitude of the landslides (Fig. 51A). Therefore, this technique of sampling is considered to be the best.

If the probability maps of different landslides are combined, the prediction of the final map (Figs. 55 and 56) is better than the prediction of the probability map prepared by using all landslides together (Fig. 52 and Table 15).

Table 15 Prediction accuracies of 14 models of susceptibility to landslides based on area under ROC curves.

Landslides	Models	Sample from landslide	Prediction accuracy (%)
All Landslides	1	mass	83.78
	2	scarp	84.95
	3	scarp center	83.34
	4	mass center	82.83
Debris dominated flows	5	mass	87.51
	6	scarp	88.08
Debris dominated slides	7	mass	91.00
	8	scarp	91.79
Rock dominated slides	9	mass	88.76
	10	scarp	91.30
Soil dominated slides	11	mass	82.06
	12	scarp	82.72
Combination of models 5, 7, 9, and 11	13	mass	85.09
Combination of models 6, 8, 10, and 12	14	scarp	86.34

Validity test

The validities of the combined models were tested by dividing each type of landslide into training data (50% of each landslide types) and validation data (50% of

each landslide types). Using training data and the same factors used in models 13 and 14, four maps of landslide probability were created for each type of sampling technique. All maps of same sampling techniques were combined. The ROC curves of the final maps were developed and compared with the ROC curves of models 13 and 14. The comparison of ROC curves (Fig. 57) suggests that both models 13 and 14 were valid and provided similar results.

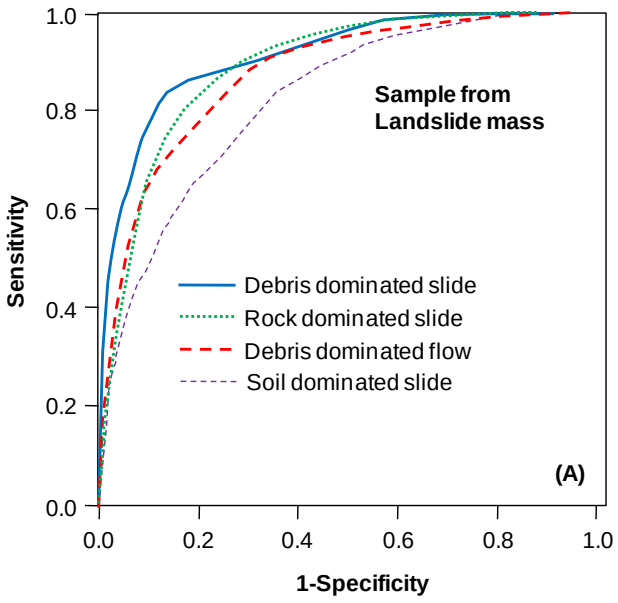

Fig. 57. ROC curves for the final landslide probability map developed by data sampling from the landslide masses and landslide scarps; and ROC curves for the assessment of validity.

Discussion and conclusions

The literature shows variations in the techniques of sampling landslides in most of the probabilistic approaches to mapping susceptibility to landslides. In this study, the inconsistencies in maps of susceptibility to shallow landslides based on the commonly

used techniques of sampling landslide data were evaluated. Differences in the prediction accuracies of the maps were noted, although the accuracy values are not significantly different. It is concluded that this inconsistency is the result of uncertainty associated with the techniques employed to sample the data. What sampling technique is best is a difficult question yet appropriate. Samples from landslide masses and landslide scarps yield better data than samples from centers of the landslide masses and landslide scarps. Data from centers of the landslide masses and landslide scarps definitely incurs uncertainty because of the insufficient number of landslides and non-landslides in the database. Furthermore, data from centers of the landslide masses and scarps do not provide information on the magnitude of landslides although this factor can be represented by landslide area. The area of a scarp is directly proportional to the area of a landslide mass; therefore, sampling from scarps of landslides preserves the magnitude of landslides. In this aspect sampling from the landslide masses and scarps are equally appropriate for mapping susceptibility to shallow landslides. But prediction accuracy of the model is best when developed based on samples obtained from the scarp. With this result, it was assumed that most of the shallow landslides in the study area occurred because of an unfavorable condition at the slope heads. Therefore, collection of the data from the scarps reduced uncertainties.

The map of debris dominated slides has the highest prediction accuracy (92 %) and the map of soil dominated slides has the lowest prediction accuracy (83 %) (Fig. 53). I believe prediction of debris dominated slides is the highest because these slides mostly occur in concave to planar steep slopes covered by unconsolidated deposits. Prediction

of rock dominated slides and debris dominated slides are also excellent because rock dominated slides are mostly found in steep slopes, region of convex to planar curvature, and they are larger in size. Debris dominated flows predominantly occur in zones of topographic convergence and areas covered by unconsolidated soil/regolith. The prediction accuracy for soil dominated slides is the lowest because they are smaller in size and occur in diverse environments. This implies that landslide types which have well defined environments of occurrence are easier to predict.

The study also suggests that classification of landslides, creation of probability maps for each type of landslide and combination of these maps is a better method to prepare an accurate map of potential susceptibility to landslides. This study shows, the prediction of the susceptibility map is 84.95 % when all landslides were used together and 86.34% when landslides were classified into different types and maps of susceptibility for each type of landslide were combined (Table 15).

A better result can be achieved if an expert is able to approximate a database for pre-failure conditions of the slopes. In a simple way this can be achieved by buffering certain distances around scarps of landslides and collecting landslide data from the buffer zone. This approach still needs to be tested; future work will focus on this approach.

CHAPTER VII

CONCLUSIONS AND FUTURE DIRECTIONS

Conclusions

Conclusions for the present research and directions for future research are discussed in this chapter. In the previous chapters, the entire research was motivated by the major deficiencies in the understanding of the contribution of mass movements to the modification of mountain hillslopes. I have added more information on how landscape is modified by different surface geological processes and where landslides occur in a periglacial landscape based on the analysis of DEMs and the mass movement and associated features in Paonia-McClure Pass area. The study focused primarily on three topics of mass movement. The first study established an understanding of how different types of mass movements modify the morphology of hillslopes and channels. The second established the frequency-magnitude relationships and relationships of the morphometrric parameters of the shallow landslides. This study established an empirical equation to determine the volume of the landslides given the area of the landslides. The third study developed and tested the performance and validity of four probabilistic (quantitative) approaches of mapping susceptibility to landslides in a regional scale in western Colorado.

The study of the drainage area and the local slope of the hillslopes in Paonia-McClure Pass area suggest that: 1) the drainage area and local slope in a landscape is related by an inverse power relationship, 2) the slope-area plot is a viable technique to

evaluate and compare the morphologic characteristics of different geomorphic zones of a landscape, and 3) the plot is very effective in determining the locations of colluvial, bedrock and alluvial channel initiation; evaluating the response of channels to the tectonic upliftment; and determining the flux of the hillslope materials to the channels. Results from the study of Paonia-McClure Pass area suggest that the colluvial channels in the area are initiated at the location of ~0.008 km^2 contributing area. Similarly the colluvial channels are transformed into bedrock channels at ~0.7 km^2 contributing area and the bedrock channels are modified into alluvial channels at ~25 km^2 contributing area. The location of the colluvial channels are found just at the base of the valley head where most of the shallow landslides occurred. Furthermore, the study suggests that the steepness and concavity of the landforms at the valley heads developed by major mass movement processes and are related by the negative exponential relationship whereas the steepness and the concavity of the bedrock and alluvial channels are related by the positive exponential relationships. The study also suggests that each landforms developed by a specific surface geological process has an upper and lower boundary of steepness-concavity relationship. I hypothesized that the steepness and the concavity of the landscape are controlled by the processes and the lithology. The glacial cirques have the highest index of concavity (0.17±0.02) whereas the rock avalanche has the lowest index of concavity (0.08±0.04). Similarly, the landforms developed by rock avalanches have the highest index of steepness and the debris flows have the lowest index of steepness. I further concluded that the valley heads are in a hillslope threshold condition. When the concavity of the valley heads increases because of upslope incision by mass

movement and streams, steepness decreases. The increase in concavity tends to increase the steepness of the valley heads but because of exceeding the hillslope threshold, the valley heads dominate the mass movement processes and result in sediments from the valley heads being deposited at the base of the slope, steepness, therefore decreases. This does not apply for bedrock and alluvial channels. The steepness and the concavity of the bedrock and alluvial channels are higher than colluvial channels because of the higher energy associated with higher flow of water and more stable base. But the concavity and steepness of these channels changes if the hillslopes deliver huge amounts of materials to the channels. Many of the bedrock channels in the study area have lower indices of concavity and steepness because of the deposit of huge amount of the sediments from landslides, rock avalanches and glacial processes.

The third chapter of this dissertation focused on the frequency-magnitude relationships of shallow landslides in Paonia-McClure Pass area. The results from this study suggest that the frequency (probability of occurrence of a landslide of a given size) and the magnitude (area or volume) of shallow landslides are related by an inverse-power relationship with a rollover of the power at 1600 m^2 or 1900 m^3. The relationship can be described by the double pareto curves. The higher value of the power for the large sized shallow landslides in the study area indicates that the area is dominated by the flux of large amounts of debris. The response of these characteristics is distinctly observed in many bedrock channels. Bedrock channels of the basin, where the density of landslides is high, have either convex or very low values of concavity indices. The frequency-magnitude analysis also suggests that the size of the landslides which are frequent and

perform more geomorphic work ranges from 1,600 m^2 to 20,000 m^2. Moreover, this study established the relationship of area-volume, length-width, length-area, and width-area of the landslides. All of these relationships can be expressed by positive power equations.

The fourth, fifth, and sixth chapters of this dissertation focused on the identification of the major landslide causing factors and development of an optimum model of mapping susceptibility to shallow landslides. These studies made extensive progress in the pre-existing techniques of mapping landslides. Among three quantitative methods of mapping landslides introduced in this dissertation, the logistic regression method predicted most of the landslides. The first approach of mapping susceptibility to landslides, the weight of evidence (WOE) approach, determines the weight of the landslide contributing factors based on the probability of the landslides occurring in the given category of the factor and the probability of the landslides not occurring in the given category of the factor. This approach is based on the prior probability, posterior probability and Bayes' theory. The approach take into account the magnitude and frequency of the landslides but it overestimates or underestimates if not enough landslide data are collected. A method to deal with the undersampled landslides in WOE framework has been explained in this dissertation. The additional techniques of the WOE method introduced in this dissertation are: a technique of categorizing continuous data and development of the models of susceptibility to landslides based on the results from the test of independence of the factors. In this study six models, comprising different combinations of factors, were developed and an optimum model which has the

best prediction of landslides has been proposed. The best model predicted 78% of the observed landslides. The model includes six factors that cause landslides: soil plasticity index, slope, aspect, tangential curvature, flow accumulation, distance to stream, and distance to road.

The second approach of mapping susceptibility to landslides, the fuzzy-logic approach, is excellent because data need not be independent from each other. The method is compared with the weight of evidence method and I found that both approaches have similar prediction performance (~78%). The method also needs the continuous data to be categorized and is the major deficiency of the method. This deficiency has been solved by integrating weight of evidence approach with the fuzzy logic. Another major disadvantage of the approach is that the approach does not provide information on what minimum factors are necessary to obtain an optimum model of mapping landslides.

The third approach of mapping susceptibility to landslides is logistic regression. The method has two advantages over other methods: the continuous data does not need to be categorized, and the output value is the probability rather than a summed value of weights or fuzzy memberships. The method determines the minimum number of factors required to achieve an optimum model for mapping landslides. The performance of the model primarily depends on the techniques of landslide and non-landslide data sampling. In this study four techniques of data sampling were introduced. The first technique samples an equal number of landslides from the center of the landslide body and areas free of landslides. The second technique samples an equal number of landslides and non-

landslide data from the center of the scarps of the landslides and areas free of landslides. The third technique samples data from the entire body of the landslides and areas free of landslides. The fourth technique samples an equal number of landslides and non-landslide data from the entire scarp of the landslides and areas free of landslides. The performance of the model based on the approach of sampling data from the entire scarp of the landslides is the best (86%). Furthermore, maps of susceptibility to landslides were developed for different types of landslides. The model with debris slides predicted 92% of the observed landslides whereas the model with soil dominated slides predicted 83% of the observed landslides.

All models of mapping susceptibility to landslides suggest that the major factors of the landslides are: slope, landuse, soil plasticity index, solar radiation, curvature, distance to stream, distance to fault, distance to road, and wetness index. The majority of the observed and predicted landslides occur on 20-30° slopes, with south and southwest facing aspect, slightly concave and slightly convex slopes, within 300 m of flow length, 5000 (50 cells) m^2 contributing area, <400 stream power index, 4-6 topographic wetness index, landslide and mudflow deposits, non-plastic to low plastic soils and shrub and bush landcover.

Future directions

Although the research described in the second chapter of this dissertation has added more information on the current understanding of the characteristics of the geomorphic zones of a landscape and characteristics of the landforms developed by

different surface geological processes, information is lacking on how a landform responds with change in process. Similarly, does a process changes with change in a landform for example rock avalanches can occur on slopes of the glacial cirque and completely change the characteristics of the glacial landform. Again an important question is the validity of my results of the steepness-concavity relationship. Is this relationship is consistent in other periglacial landscapes of Colorado and even other periglacial areas of the world?

Although the present study of the landslide frequency-magnitude relationships and study of the relationships of landslide morphologic parameters supported current knowledge of landslide dynamics, understanding is lacking on why the frequency-magnitude relation curve rolls and what are the major controlling factors? The study showed that undersampling of the landslides is not the only reason, the size of the shallow landslides also controls by the morphology of the topography, such as plan curvature, slope length, and slope concavity. Geotechnical properties of the associated slope materials were not studied in this research. This is a possible direction for future research. Furthermore, the proposed range of sizes of the landslides which are frequent and perform more geomorphic work is only applicable for shallow landslides. Frequency-magnitude study of large landslides is needed to fully understand the total geomorphic work of all landslides.

The distribution of the observed and predicted landslides in this study suggest that the shallow landslides tends to occur on the slopes of river gorges and valley heads and the deep seated large landslides tend to occur on the edges of the upland plateau and

ridges. This study did not include the frequency-magnitude relationships and the geomorphic work of the large deep-seated landslides. The next step in this research is to understand such relationship for the large deep seated landslides and evaluate again what size of landslides are frequent and perform more geomorphic work. Furthermore, it is necessary to fill the gap in the understanding and linking of landslide frequency and magnitude, persistence, and geomorphic work in the context of the evolution of landscape as well as input of these variables in the model of mapping landscape susceptibility to landslides. One more question needs an answer: what process of mass movement does more geomorphic work and produces more hillslope relief over a specific period of time?

REFERENCES

Allison, P.D., 1999. Logistic Regression Using the SAS System: Theory and Application. SAS Institute Inc. Cary, North Carolina.

Agterberg, F.P., 1992. Combining indicator patterns in weights of evidence modeling for resource evaluation. Natural Resources Research 1, 39-50.

Agterberg, F.P., Bonham-Carter, G.F., Cheng, Q., Wright, D.F., 1993. Weights of evidence modeling and weighted logistic regression for mineral potential mapping. In: David, J.C., Herzfeld, U.C. (Eds.), Computers in Geology, 25 Years of Progress. Oxford University Press, Oxford, New York, pp. 13-32.

Ahnert, F., 1970. Functional relationships between denudation, relief, and uplift in large mid-latitude drainage basins. American Journal of Science 268, 243-263.

Anbalagan, R., 1992. Landslide hazard evaluation and zonation mapping in mountainous terrain. Engineering Geology 32, 269-277.

Anderson, R.S., 1994. Evolution of the Santa-Cruz Mountains, California, through tectonic growth and geomorphic decay. Journal of Geophysical Research-Solid Earth 99, 20161-20179.

An, P., Moon, W.M., Rencz, A., 1991. Application of fuzzy set theory for integration of geological, geophysical and remote sensing data. Canadian Journal of Exploration Geophysics 27, 1-11.

Aslan, A., Karlstrom, K., Hood, W.C., Cole, R.D., Oesleby, T.W., Betton, C., Sandoval, M.M., Darling, A., Kelley, S., Hudson, A., Kaproth, B., Schoepfer, S., Benage, M., Landman, R., 2008. River incision histories of the Black Canyon of the Gunnison and Unaweep Canyon: Interplay between late Cenozoic tectonism climate change, and drainage integration in the western Rocky Mountains. In: Raynolds, R.G. (Ed.), Roaming the Rocky Mountains and environs: Geological Field Trips: Geological Society of America Field Guide 10, 175-202.

Atkinson, P.M., Massari, R., 1998. Generalized linear modeling of susceptibility to landsliding in the central Appenines, Italy. Computational Geosciences, 24, 373-385.

Ayalew, L., Yamagashi, H., 2005. The application of GIS based logistic regression for landslide susceptibility mapping in Kakuda-Yahiko Mountains, Central Japan. Geomorphology 65, 15-31.

Barredo, J.I., Benavidesz, A., Herhl, J., Van Westen, C.J., 2000. Comparing heuristic landslide hazard assessment techniques using GIS in the Tirajana basin, Gran Canaria Island, Spain. International Journal of Applied Earth Observation and Geoinformation 2, 9-23.

Beven, K., 1997. TOPMODEL: a critique. Hydrological Processes 11, 1069-1085.

Beven, K., Kirkby, M.J., 1979. A physically based, variable contributing area model of basin hydrology. Hydrological Processes 5, 1993-2011.

Blyth, E.M., Finch, J., Robinson, M., Rosier, P., 2004. Can soil moisture be mapped onto the terrain? Hydrology and Earth System Sciences 8, 923-930.

Bonham-Carter, G.F., 1994. Geographic Information Systems for Geoscientists: Modeling with GIS. Pergamon/Elsevier, London.

Bonham-Carter, G.F., 2002. Geographic information systems for geoscientist: Modelling with GIS. In: Merriam, D.F. (Ed.), Computer Methods in the Geosciences. Pergamon/Elsevier, New York, pp. 302-334.

Bonham-Carter, G.F., Agterberg, F.P., Wright, D.F., 1988. Integration of geological datasets for gold exploration in Nova-Scotia. Photogrammetric Engineering and Remote Sensing, 54, 1585-1592.

Bonham-Carter, G.F., Agterberg, F.P., Wright, D.F., 1989. Weights of evidence modeling: a new approach to mapping mineral potential. In: Agterberg, F.P., Bonham-Carter, G.F. (Eds.), Statistical Applications in the Earth Science. Geological Survey of Canada Paper, 89-9, pp. 171-183.

Brardinoni, F., Church, M., 2004. Representing the landslide magnitude-frequency relation: Capilano River Basin, British Columbia. Earth Surface Processes and Landforms 29, 115-124.

Brardinoni, F., Slaymakerl, O., Hassan, M.A., 2003. Landslide inventory in a rugged forested watershed: a comparison between air-photo and field survey data. Geomorphology 54, 179-196.

Brocklehurst, S.H. and Whipple, K.X., 2002. Glacial erosion and relief production in the Eastern Sierra Nevada, California. Geomorphology 42, 1-24.

Bull, W.B., 1991. Geomorphic responses to climate change. Oxford University Press, New York, 326 pp.

Burbank, D.W., Leland, J., Fielding, E., Anderson, R.S., Brozovic, N., Reid, M.R., Duncan, C., 1996. Bedrock incision, rock uplift and threshold hillslopes in the northwestern Himalayas. Nature 379, 505–510.

Burton, A., Bathurst, J.C., 1998. Physically based modeling of shallow landslide sediment yield at a catchment scale. Environmental Geology 35, 89-99.

Cardinali, M., Reichenbach P., Guzzetti F., Ardizzone F., Antonini G., Galli M., Cacciano M., Castellani M., Salvati P., 2002. A geomorphologic approach to estimate landslide hazard and risk in urban and rural areas in Umbria, central Italy. NHESS 2, 57-72.

Carranza, E.J.M., Hale, M., 2002. Spatial association of mineral occurrences and curvilinear geological features. Mathematical Geology 34, 203-221.

Carrara, A., 1983. Multivariate models for landslide hazard evaluation. Journal of the International Association for Mathematical Geology 15, 403-426.

Carrara, A., Cardinali, M., Guzzetti, F., Reichenbach, P., 1995. GIS-based techniques for mapping landslide hazard. In: Carrara, A., Guzzetti, F. (Eds.), Geographical Information Systems in Assessing Natural Hazards. Kluwer Publications, Dordrecht, pp. 135-176.

Carrara, A., Cardinali, M., Detti, R., Guzzetti, F., Pasqui, V., Reichenbach, P., 1991. GIS techniques and statistical-models in evaluating landslide hazard. Earth Surface Processes and Landforms 16, 427-445.

Carrara, A., Guzzetti, F., Cardinali, M., Reichenbach, P., 1999. Use of GIS technology in the prediction and monitoring of landslide hazard. Natural Hazards 20, 117-135.

Carrara, A., Merenda, L., 1976. Landslide inventory in Northern Calabria, Southern Italy. Geological Society of America Bulletin 87, 1153-1162.

Carson, M.A., Kirby, M.J., 1972. Hillslope Form and Process. Cambridge University Press, Cambridge.

Carson, M.A. and Petley, D.J., 1970. Existence of threshold hillslopes in denudation of landscape. Transactions of the Institute of British Geographers 49, 71-95.

Cevik, E., Topal, T., 2003. GIS-based landslide susceptibility mapping for a problematic segment of the natural gas pipeline, Hendek (Turkey). Environmental Geology 44, 949-962.

Cheng, Q., 2004. Application of weights of evidence method for assessment of flowing wells in the Greater Toronto area, Canada. Natural Resource Research 13, 77-86.

Chowdhury, R., 1976. Initial stresses in natural slope analysis, rock engineering for foundations and slopes. Geotechnical Engineering Division Specialty Conference, American Society of Civil Engineers (ASCE), pp. 404–415.

Chowdhury, R.N., Bertoldi, C., 1977. Residual shear tests on soil from two natural slopes. Australian Geomechanics Journal G7, 1-9.

Chung, C.F., Fabbri, A.G., 2001. Prediction models for landslide hazard using fuzzy set approach. In: Marchetti, M., Rivas, V. (Eds.), Geomorphology and Environmental Impact Assessment. A.A. Balkema, Rotterdam, pp. 31-47.

Claessens, L., Heuvelink, G.B.M., Schoorl, J.M., Veldkamp, A., 2005. DEM resolution effects on shallow landslide hazard and soil redistribution modeling. Earth Surface Processes and Landforms 30, 461-477.

Clerici, A., Perego, S., Tellini, C. and Vescovi, P., 2006. A GIS-based automated procedure for landslide susceptibility mapping by the Conditional Analysis method: the Baganza valley case study (Italian Northern Apennines). Environmental Geology 50, 941-961.

Concha-Dimas, A., Campos-Vargas, M., Lopez-Miguel, C., 2007. Comparing heuristic and bivariate GIS-based methods for refining landslide susceptibility maps in northern Mexico City. Environmental & Engineering Geoscience 13, 277-287.

Conoscenti, C., Di Maggio, C. and Rotigliano, E., 2008. GIS analysis to assess landslide susceptibility in a fluvial basin of NW Sicily (Italy). Geomorphology 94, 325-339.

Corominas, J., Copons, R., Vilaplana, J.M., Altimir, J., Amigo, J., 2003. Integrated landslide susceptibility analysis and hazard assessment in the principality of Andorra. Natural Hazards 30, 421-435.

Corsini, A., Cervi, F., Ronchetti, F., 2009. Weight of evidence and artificial neural networks for potential groundwater spring mapping: an application to the Mt. Modino area (Northern Apennines, Italy). Geomorphology 111, 79-87.

Crozier, M.J., 1999. Prediction of rainfall-triggered landslides: A test of the antecedent water status model. Earth Surface Processes and Landforms 24, 825-833.

Crozier, M.J. and Glade, T. (Eds.), 1999. The frequency and magnitude of landslide activity. Magnitude and Frequency in Geomorphology, 115. Zeitschrift fur Geomorphologie Supplementbund, 141-155 pp.

Dahal, R.K., Hasegawa, S., Nonomura, A., Yamanaka, M., Dhakal, S., Paudyal, P., 2008a. Predictive modelling of rainfall-induced landslide hazard in the Lesser Himalaya of Nepal based on weights-of-evidence. Geomorphology 102, 496-510.

Dahal, R.K., Hasegawa, S., Nonomura, A., Yamanaka, M., Masuda, T., Nishino, K., 2008b. GIS-based weights-of-evidence modelling of rainfall-induced landslides in small catchments for landslide susceptibility mapping. Environmental Geology 54, 311-324.

Dai, F.C., Lee, C.F., 2001. Frequency-volume relation and prediction of rainfall-induced landslides. Engineering Geology 59, 253-266.

Dai, F.C. and Lee, C.F., 2003. A spatiotemporal probabilistic modelling of storm-induced shallow landsliding using aerial photographs and logistic regression. Earth Surface Processes and Landforms 28, 527-545.

Dai, F.C., Lee, C.F., Li, J., Xu, Z.W., 2001. Assessment of landslide susceptibility on the natural terrain of Lantau Island, Hong Kong. Environmental Geology, 40, 381-391.

Daneshfar, B., Benn, K., 2002. Spatial relationships between natural seismicity and faults, southeastern Ontario and north-central New York State. Tectonophysics 353, 31-44.

Darling, A.L., Karlstrom, K.E., Aslan, A., Cole, R., Betton, C., Wan, E., 2009. Quaternary incision rates and drainage evolution of the Uncompaghre and Gunnison Rivers, western Colorado, as calibrated by the Lava Creek B ash. Rocky Mountain Geology 44, 71-83.

Den Eeckhaut, M., Vanwalleghem, T., Poesen, J., Govers, G., Verstraeten, G., Vandekerckhove, L., 2006. Prediction of landslide susceptibility using rare events logistic regression: A case-study in the Flemish Ardennes (Belgium). Geomorphology 76, 392-410.

Dethier, P., 2001. Pleistocene rates in the western United States calibrated using Lava Creek B tephra. Geology 29, 783-786.

Duman, T.Y., Can, T., Gokceoglu, C., Nefeslioglu, H.A. and Sonmez, H., 2006. Application of logistic regression for landslide susceptibility zoning of Cekmece Area, Istanbul, Turkey. Environmental Geology 51, 241-256.

Dunrud, R.C., 1989. Geologic map and coal stratigraphic framework of the Paonia area, Delta and Gunnison counties, Colorado, U.S. Geological Survey, Coal Investigations Map C-115, scale 1:50,000.

Eden, D.N., Page, M.J., 1998. Palaeoclimatic implications of a storm erosion record from late Holocene lake sediments, North Island, New Zealand. Palaeogeography Palaeoclimatology Palaeoecology 139, 37-58.

Egan, J.P., 1975. Signal Detection Theory and ROC Analysis. Academic Press, New York.

Emmanuel, J., Carranza, M., Hale, M., 2000. Geologically constrained probabilistic mapping of gold potential, Baguio district, Philippines. Natural Resource Research 9, 237-253.

Epis, R.C., Scott, G.R., Taylor, R.B., Chapin, C.E., 1980. Summary of Cenozoic geomorphic, volcanic, and tectonic features of central Colorado and adjoining areas. In: Kent, H.C., Porter, K.W. (Eds.), Colorado Geology: Denver, Colorado, Rocky Mountain Association of Geologists, p. 135–156.

Ercanoglu, M., Gokceoglu, C., 2002. Assessment of landslide susceptibility for a landslide-prone area (north of Yenice, NW Turkye) by fuzzy approach. Environmental Geology 41, 720–730.

Evans, S.G., 2003. Characterizing landslide risk in Canada. 3rd Canadian Conference on Geotechnique and Natural Hazards. Canadian Geotechnical Society, Edmonton, AB, pp. 35-50.

Fenti, V., Silvano, S., Spagna, V., 1979. Methodological proposal for an engineering geomorphological map. Forecasting rockfalls in the Alps. Bulletin of the International Association of Engineering Geology 19, 134-138.

Fernandez, T., Irigaray, C., El Hamdouni, R., Chacon, J., 2003. Methodology for landslide susceptibility mapping by means of a GIS. Application to the Contraviesa area (Granada, Spain). Natural Hazards 30, 297–308.

Flint, J.J., 1974. Stream gradient as a function of order, magnitude, and discharge. Water Resources Research 10, 969-973.

Fujii, Y., 1969. Frequency distribution of landslides caused by heavy rainfall. Journal Seismological Society of Japan 22, 244-247.

Garcia-Rodriguez, M.J., Malpica, J.A., Benito, B., Diaz, M., 2008. Susceptibility assessment of earthquake-triggered landslides in El Salvador using logistic regression. Geomorphology 95, 172-191.

Gerrard, J., 1994. The landslide hazard in the Himalayas - geological control and human action. Geomorphology 10, 221-230.

Glade, T., 2003. Landslide occurrence as a response to land use change: a review of evidence from New Zealand. Catena 51, 297-314.

Gokceoglu, C., Aksoy, H., 1996. Landslide susceptibility mapping of the slopes in the residual soils of the Mengen region (Turkey) by deterministic stability analyses and image processing techniques. Engineering Geology 44, 147-161.

Gomez, H. and Kavzoglu, T., 2005. Assessment of shallow landslide susceptibility using artificial neural networks in Jabonosa River Basin, Venezuela. Engineering Geology 78, 11-27.

Goodacre, A.K., Bonham-Carter, G.F., Agterberg, F.P., Wright, D.F., 1993. A Statistical-analysis of the spatial association of seismicity with drainage patterns and magnetic-anomalies in Western Quebec. Tectonophysics 217, 285-305.

Gorsevski, P.V., Gessler, P.E., Foltz, R.B., 2000. Spatial prediction of landslide hazard using logistic regression and GIS, 4th International Conference on Integrating GIS and Environmental Modeling (GIS/EM4): Problems, Prospects and Research Needs, Banff, Alberta, Canada.

Gorsevski, P.V., Gessler, P.E., Jankowski, P., 2003. Integrating a fuzzy k-means classification and a Bayesian approach for spatial prediction of landslide hazard. Journal of Geographical Systems 5, 223-251.

Gorsevski, P.V., Jankowski, P., Gessler, P.E., 2006. An heuristic approach for mapping landslide hazard by integrating fuzzy logic with analytic hierarchy process. Control and Cybernetics 35, 121-146.

Greenbaum, D., Tutton, M., Bowker, M., Browne, T., Buleka, J., Greally, K., Kuna, G., McDonald, A., Marsh, S., O'Connor, E., Tragheim, D., 1995. Rapid Methods of Landslide Hazard Mapping: Papua New Guinea Case Study. British Geological Survey Technical Report WC/95/27.

Greenway, D.R., 1987. Vegetation and slope stability. In: Anderson, M.G., Richards, K.S. (Eds.), Slope Stability. Wiley, New York, pp. 187-230.

Gritzner, M.L., Marcus, W.A., Aspinall, R., Custer, S.G., 2001. Assessing landslide potential using GIS, soil wetness modeling and topographic attributes, Payette River, Idaho. Geomorphology 37, 149-165.

Guthrie, R.H., Evans, S.G., 2004a. Analysis of landslide frequencies and characteristics in a natural system, Coastal British Columbia. Earth Surface Processes and Landforms 29, 1321-1339.

Guthrie, R.H., Evans, S.G., 2004b. Magnitude and frequency of landslides triggered by a storm event, Loughborough Inlet, British Columbia. Natural Hazards and Earth System Sciences 4, 475-483.

Guthrie, R.H., Evans, S.G., 2007. Work, persistence, and formative events: The geomorphic impact of landslides. Geomorphology 88, 266-275.

Guzzetti, F., Ardizzone F., Cardinali, M., Galli, M., Reichenbach, P., Rossi, M., 2008. Distribution of landslides in the Upper Tiber River basin, central Italy. Geomorphology 96, 105-122.

Guzzetti, F., Carrara, A., Cardinali, M., Reichenbach, P., 1999. Landslide hazard evaluation: A review of current techniques and their application in a multi-scale study, Central Italy. Geomorphology 31, 181-216.

Guzzetti, F., Malamud, B.D., Turcotte, D.L., Reichenbach, P., 2002. Power-law correlations of landslide areas in central Italy. Earth and Planetary Science Letters 195, 169-183.

Harris, J.R., Wilkinson, L., Grunsky, E.C., 2000. Effective use and interpretation of lithogeochemical data in regional mineral exploration programs: application of

Geographic Information Systems (GIS) technology. Ore Geology Reviews 16, 107-143.

Hergarten, S., Neugebauer, H.J., 1998. Self-organized criticality in a landslide model. Geophysical Research Letters 25, 801-804.

Hicks, D.M., Gomez, B., Trustrum, N.A., 2000. Erosion thresholds and suspended sediment yields, Waipaoa River Basin, New Zealand. Water Resources Research 36, 1129-1142.

Hooke, R.L., 2003. Time constant for equilibration of erosion with tectonic uplift. Geology 31, 621-624.

Hovius, N., Stark, C.P., Allen, P.A., 1997. Sediment flux from a mountain belt derived by landslide mapping. Geology 25, 231-234.

Hovius, N., Stark, C.P., Chu, H.T., Lin, J.C., 2000. Supply and removal of sediment in a landslide-dominated mountain belt: Central Range, Taiwan. Journal of Geology 108, 73-89.

Hungr, D., Evans, S.G., 2004. Entrainment of debris in rock avalanches: An analysis of a long run-out mechanism. Geological Society of America Bulletin 116, 1240-1252.

Hungr, O., Evans, S.G., Harzard, J., 1999. Magnitude and frequency of rock falls and rock slides along the main transportation corridors of southwestern British Columbia. Canadian Geotechnical Journal 36, 224-238.

Innes, J.L., 1983. Lichenometric dating of debris-flow deposits in the Scottish Highlands Earth Surface Processes and Landforms 8, 579-588.

Ives, J.D., Messerli, B., 1981. Mountain hazard mapping in Nepal: Introduction to an Applied Mountain Research Project. Mountain Research and Development 1, 223-230.

Jaquette, C., Wohl, E., Cooper, D., 2005. Establishing a context for river rehabilitation, North Fork Gunnison River, Colorado. Environmental Management 35, 593-606.

Jenson, S.K., Domingue, J.O., 1988. Extracting topographic structure from digital elevation data for geographic information-system analysis. Photogrammetric Engineering and Remote Sensing 54, 1593-1600.

Johnson, D.E., 1998. Applied Multivariate Methods for Data Analysis. Duxbury Press, Belmont, California.

Johnson, K.A., Sitar, N., 1990. Hydrologic conditions leading to debris-flow initiation. Canadian Geotechnical Journal 27, 789-801.

Juang, C.H., Lee, D.H., Sheu, C., 1992. Mapping slope failure potential using fuzzy-sets. Journal of Geotechnical Engineering-ASCE 118, 475-494.

Junge, W.R., 1978. Geologic hazards, North Fork Gunnison River Valley, Delta and Gunnison Counties, Colorado: Colorado Geological Survey, Open-File Report 78-12, explanation sheet, 6 maps.

Keaton, J.R., 1988. A probabilistic model for hazards related to sedimentation processes on alluvial fans in Davis County, Utah. PhD Dissertation, Texas A&M University, College Station, Texas.

Kienholz, H., 1978. Maps of geomorphology and natural hazard of Griendelwald, Switzerland, scale 1: 10.000. Arctic and Alpine Research 10, 169-184.

Kirby, E., Whipple, K.X., Tang, W.Q. and Chen, Z.L., 2003. Distribution of active rock uplift along the eastern margin of the Tibetan Plateau: Inferences from bedrock channel longitudinal profiles. Journal of Geophysical Research-Solid Earth, 108, 2217, 24pp.

Kirkbride, M. and Mathews, D., 1997. The role of fluvial and glacial erosion in landscape evolution: The Ben Ohau Range, New Zealand. Earth Surface Processes and Landforms 22, 317-327.

Korup, O., 2005. Distribution of landslides in southwest New Zealand. Landslides 2, 43-51.

Korup, O., 2006. Effects of large deep-seated landslides on hillslope morphology, western Southern Alps, New Zealand. Journal of Geophysical Research-Earth Surface 111, F01018, 18 pp.

Kuhni, A. and Pfiffner, O.A., 2001. The relief of the Swiss Alps and adjacent areas and its relation to lithology and structure: topographic analysis from a 250-m DEM. Geomorphology 41, 285-307.

Lague, D. and Davy, P., 2003. Constraints on the long-term colluvial erosion law by analyzing slope-area relationships at various tectonic uplift rates in the Siwaliks Hills (Nepal). Journal of Geophysical Research-Solid Earth 108, 2129.

Lee, S., 2007. Application and verification of fuzzy algebraic operators to landslide susceptibility mapping. Environmental Geology 52, 615-623.

Lee, S., Choi, J., 2004. Landslide susceptibility mapping using GIS and the weights-of-evidence model. International Journal of Geographical Information Science 18, 789-814.

Lee, S., Choi, J., Min, K., 2002. Landslide susceptibility analysis and verification using the Bayesian probability model. Environmental Geology 43, 120-131.

Lee, S., Sambath, T., 2006. Landslide susceptibility mapping in the Damrei Romel area, Cambodia using frequency ratio and logistic regression models. Environmental Geology 50, 847-855.

Locat, P., Couture, R., Leroueil, S., Locat, J., Jaboyedoff, M., 2006. Fragmentation energy in rock avalanches. Canadian Geotechnical Journal 43, 830-851.

Lusted, L.B., 1968. Introduction to medical decision making. Charles C. Thomas, Springfield III, 271 pp.

Maharaj, R.J., 1993. Landslide processes and landslide susceptibility analysis from an upland watershed - a case-study from St-Andrew, Jamaica, West-Indies. Engineering Geology 34, 53-79.

Malamud, B.D., Turcotte, D.L., Guzzetti, F., Reichenbach, P., 2004. Landslide inventories and their statistical properties. Earth Surface Processes and Landforms 29, 687-711.

Martin, Y., Rood, K., Schwab, J.W., Church, M., 2002. Sediment transfer by shallow landsliding in the Queen Charlotte Islands, British Columbia. Canadian Journal of Earth Sciences 39, 189-205.

Mathew, J., Jha, V.K., Rawat, G.S., 2007. Weights of evidence modeling for landslide hazard zonation mapping in part of Bhagirathi valley, Uttarakhanda. Current Science 92, 628-638.

Mathew, J., Jha, V.K., Rawat, G.S., 2009. Landslide susceptibility zonation mapping and its validation in part of Garhwal Lesser Himalaya, India, using binary logistic regression analysis and receiver operating characteristic curve method. Landslides 6, 17-26.

McClung, D.M., 2000. Extreme avalanche runout in space and time. Canadian Geotechnical Journal 37, 161-170.

Mcfall, R.M., 1999. Quantifying the information value of clinical assessments with signal detection theory.
http://www.findarticles.com/cf_0/m0961/1999_Annual/54442299/print.jhtml

Mitasova, H., Hofierka, J., 1993. Interpolation by regularized spline with tension .2. Application to terrain modeling and surface geometry analysis. Mathematical Geology 25, 657-669.

Mittal, S.K., Singh, M., Kapur, P., Sharma, B.K., Shamshi, M.A., 2008. Design and development of instrumentation network for landslide monitoring, and issue an early warning. Journal of Scientific & Industrial Research 67, 361-365.

Moglen, G.E. and Bras, R.L., 1995. The importance of spatially heterogeneous erosivity and the cumulative area distribution within a basin evolution model. Geomorphology 12, 173-185.

Montgomery, D.R., 2001. Slope distributions, threshold hillslopes, and steady-state topography. American Journal of Science 301, 432-454.

Montgomery, D.R., 2002. Valley formation by fluvial and glacial erosion. Geology 30, 1047-1050.

Montgomery, D.R. and Brandon, M.T., 2002. Topographic controls on erosion rates in tectonically active mountain ranges. Earth and Planetary Science Letters 201, 481-489.

Montgomery, D.R., Dietrich, W.E., Torres, R., Anderson, S.P., Heffner, J.T., Loague, K., 1997. Hydrologic response of a steep, unchanneled valley to natural and applied rainfall. Water Resources Research 33, 91-109.

Moore, I.D., Burch, G.J., Mackenzie, D.H., 1988. Topographic effects on the distribution of surface soil-water and the location of ephemeral gullies. Transactions of the ASAE 31, 1098-1107.

Moore, I.D., Grayson, R.B., Ladson, A.R., 1991. Digital terrain modeling - a review of hydrological, geomorphological, and biological applications. Hydrological Processes 5, 3-30.

Nefeslioglu, H.A., Gokceoglu, C., Sonmez, H., 2008. An assessment on the use of logistic regression and artificial neural networks with different sampling strategies for the preparation of landslide susceptibility maps. Engineering Geology 97, 171-191.

Neuhauser, B., Terhorst, B., 2007. Landslide susceptibility assessment using "weights-of-evidence" applied to a study area at the Jurassic escarpment (SW-Germany). Geomorphology 86, 12-24.

Noever, D.A., 1993. Himalayan sandpiles. Physical Review E 47, 724-725.

Ohlmacher, G.C., 2007. Plan curvature and landslide probability in regions dominated by earth flows and earth slides. Engineering Geology 91, 117-134.

Ohlmacher, G.C., Davis, J.C., 2003. Using multiple logistic regression and GIS technology to predict landslide hazard in northeast Kansas, USA. Engineering Geology 69, 331-343.

Pachauri, A.K., Gupta, P.V., Chander, R., 1998. Landslide zoning in a part of the Garhwal Himalayas. Environmental Geology 36, 325-334.

Pachauri, A.K., Pant, M., 1992. Landslide hazard mapping based on geological attributes. Engineering Geology 32, 81-100.

Page, M.J., Trustrum, N.A., Dymond, J.R., 1994. Sediment budget to assess the geomorphic effect of a cyclonic storm, New-Zealand Geomorphology 9, 169-188.

Pelletier, J.D., 1997. Kardar-Parisi-Zhang scaling of the height of the convective boundary layer and fractal structure of Cumulus cloud fields. Physical Review Letters 78, 2672-2675.

Rautela, P., Lakhera, R.C., 2000. Landslide risk analysis between Giri and Tons Rivers in Himachal Himalaya, India. International Journal of Applied Earth Observation and Geoinformation 2, 153-160.

Regmi, N.R., Giardino, J.R., Vitek, J.D., 2010b. Modeling susceptibility to landslides using the weight of evidence approach: Western Colorado, USA. Geomorphology 115, 172-187.

Regmi, N.R., Giardino, J.R., Vitek, J.D., Briaud, J.-L., 2007. Using immersive technology to map pre- and post- failure morphology of the Andy Gump Landslide: Grand Mesa, Colorado, USA. Geological Society of America, Abstracts with Programs 39, 509.

Regmi, N.R., Giardino, J.R., Vitek, J.D., Dangol, V., 2010a. Mapping landslide hazards in western Nepal: Comparing qualitative and quantitative approaches. Environmental and Engineering Geosciences 16, 127-142.

Reichenbach, P., Galli, M., Cardinali, M., Guzzetti, F., Ardizzone, F., 2005. Geomorphologic mapping to assess landslide risk: concepts, methods and applications in the Umbria Region of central Italy. In: T. Glade, M.G. Anderson and M.J. Crozier (Eds.), Landslide Hazard and Risk. John Wiley & Sons, England, pp. 429-468.

Remondo, J., Gonzalez-Diez, A., De Teran, J.R.D., Cendrero, A., 2003. Landslide susceptibility models utilising spatial data analysis techniques. A case study from the lower Deba Valley, Guipuzcoa (Spain). Natural Hazards 30, 267-279.

Roe, G.H., Montgomery, D.R. and Hallet, B., 2003. Orographic precipitation and the relief of mountain ranges. Journal of Geophysical Research-Solid Earth, 108, 2315, 12pp.

Roering, J.J., Kirchner, J.W., Sklar, L.S. and Dietrich, W.E., 2001. Hillslope evolution by nonlinear creep and landsliding: An experimental study. Geology 29, 143-146.

Rogers, W.P., 2003. Critical landslides of Colorado-a year 2002 review and priority list. Colorado Geological Survey, Open-File Report OF-02-16, 1map.

Rupke, J., Cammeraat, E., Seijmonsbergen, A.C., Van Westen, C.J., 1988. Engineering geomorphology of the Widentobel Catchment, Appenzell and Sankt-Gallen, Gallen, Switzerland - a geomorphological inventory system applied to geotechnical appraisal of slope stability. Engineering Geology 26, 33-68.

Sakellariou, M.G., Ferentinou, M.D., 2001. GIS-based estimation of slope stability. Natural Hazards Review 2, 12-21.

Santacana, N., Baeza, B., Corominas, J., De Paz, A., Marturia, J., 2003. A GIS-based multivariate statistical analysis for shallow landslide susceptibility mapping in La Pobla de Lillet area (Eastern Pyrenees, Spain). Natural Hazards 30, 281–295.

Santi, P.M., 1988. The kinematics of debris flow transport down a canyon. MS Thesis, Texas A&M University, College Station, Texas.

Schmidt, K.M., Montgomery, D.R., 1995. Limits to relief. Science 270, 617-620.

Sharp, W.D., Ludwig, K.R., Chadwick, O.A., Amundson, R., Glaser, L.L., 2003. Dating fluvial terraces by ^{230}TH/U on pedogenic carbonate, Wind River Basin, Wyoming. Quaternary Research 59, 139-150.

Silverman, B.W., 1984. Spline smoothing - the equivalent variable kernel-method Annals of Statistics 12, 898-916.

Simonett, D.S., 1967. Landslide distribution and earthquakes in the Bewani and Torricelli Mountains, New Guinea. In: J.N. Jennings and J.A. Mabutt (Eds.), Landform studies from Australia and New Guinea. Cambridge University Press, Cambridge, pp. 64-84.

Sinnock, S., 1981. Pleistocene drainage changes in Uncompaghre Plateau-Grand Valley region of western Colorado, including formation and abandonment of Unaweep Canyon: A hypothesis. New Mexico Geological Society Guidebook 32, 127-136.

Sklar, L. and Dietrich, W.E., 1998. River Longitudinal Profiles and Bedrock Incision Models: Stream Power and the Influence of Sediment Supply Geophysical Monograph 107, 237-260.

Small, E.E. and Anderson, R.S., 1998. Pleistocene relief production in Laramide mountain ranges, western United States: Reply. Geology 26, 1151-1152.

Snyder, N.P., Whipple, K.X., Tucker, G.E. and Merritts, D.J., 2000. Landscape response to tectonic forcing: Digital elevation model analysis of stream profiles in the Mendocino triple junction region, northern California. Geological Society of America Bulletin 112, 1250-1263.

Somfai, E., Czirok, A. and Vicsek, T., 1994. Power-law distribution of landslides in an experiment on the erosion of a granular pile. Journal of Physics A: Mathematical and General 27, L757-L763.

Søreide, K., 2009. Receiver-operating characteristic curve analysis in diagnostic, prognostic and predictive biomarker research. J. Clin. Pathol. 62, 1-5.

Spiegelhalter, D.J., 1986. A statistical view of uncertainty in expert systems. In: Gale, W. (Ed.), Artificial Intelligence and Statistics. Addison-Wesley, Reading, Massachusetts, pp. 17-55.

Speigelhalter, D.J., Knill-Jones, R.P., 1984. Statistical and knowledge-based approaches to clinical decision-support systems, with an application in gastroenterology. Journal of the Royal Statistical Society A 147, 35-77.

Spiker, E.C., Gori, P.L., 2003. National landslide hazards mitigation strategy-A framework for loss reduction. U.S. Geological Survey Circular 1244, pp. 56.

Stark, C.P., Guzzetti, F., 2009. Landslide rupture and the probability distribution of mobilized debris volumes. Journal of Geophysical Research-Earth Surface 114, F00A02, 16 pp.

Stark, C.P., Hovius, N., 2001. The characterization of landslide size distributions. Geophysical Research Letters 28, 1091-1094.

Stock, J. and Dietrich, W.E., 2003. Valley incision by debris flows: Evidence of a topographic signature. Water Resources Research, 39, 1089.

Strahler, A.N., 1957. Quantitative analysis of watershed geomorphology. Transactions of the American Geophysical Union 38, 913-920.

Styczen, M.E., Morgan, R.P.C., 1995. Engineering properties of vegetation. In: Morgan, R.P.C., Rickson, R.J. (Eds.), Slope Stabilization and Erosion Control: a Bioengineering Approach. E&FN Spon, London, pp. 5-58.

Suzen, M.L., Doyuran, V., 2004. Data driven bivariate landslide susceptibility assessment using geographical information systems: a method and application to Asarsuyu catchment, Turkey. Engineering Geology 71, 303-321.

Swets, J.A., 1988. Measuring the accuracy of diagnostic systems. Science in China Series E-Technological Sciences 240, 1285-1293.

Tangestani, M.H., 2004. Landslide susceptibility mapping using the fuzzy gamma approach in a GIS, Kakan catchment area, southwest Iran. Australian Journal of Earth Sciences 51, 439-450.

Tarboton, D.G., Bras, R.L. and Rodrigueziturbe, I., 1988. The fractal nature of river networks. Water Resources Research 24, 1317-1322.

United States Geological Survey (USGS), 2010. Landslide hazards program. http://landslides.usgs.gov/

Van Westen, C.J., 2000. The modeling of landslide hazards using GIS. Survey in Geophysics 21, 241-255.

Van Westen, C.J., Rengers, N., Soeters, R., 2003. Use of geomorphological information in indirect landslide susceptibility assessment. Natural Hazards 30, 399-419.

Van Westen, C.J., Rengers, N., Terlien, M.T.J., Soeters, R., 1997. Prediction of the occurrence of slope instability phenomena through GIS-based hazard zonation. Geologische Rundschau 86, 404-414.

Van Westen, C.J., Terlien, M.T.J., 1996. An approach towards deterministic landslide hazard analysis in GIS. A case study from Manizales (Colombia). Earth Surface Processes and Landforms 21, 853-868.

Varnes, D.J., 1978. Slope movement types and process. In: Schuster, R.L., Krizek, R.J. (Eds.), Landslides: Analysis and Control. Transportation Research Board, pp. 11 - 33.

Varnes, D.J., 1984. Landslide hazard zonation: a review of principles and practice. Commission on landslides of the IAEG, UNESCO, Natural Hazards, 3, 1-63.

Western Regional Climate Center, 2009. http://www.wrcc.dri.edu/cgi-bin/cliMAIN.pl?copaon.

Whipple, K.X., 2004. Bedrock rivers and the geomorphology of active orogens. Annual Review of Earth and Planetary Sciences 32, 151-185.

Whipple, K.X. and Tucker, G.E., 1999. Dynamics of the stream-power river incision model: Implications for height limits of mountain ranges, landscape response timescales, and research needs. Journal of Geophysical Research-Solid Earth 104, 17661-17674.

Whipple, K.X. and Tucker, G.E., 2002. Implications of sediment-flux-dependent river incision models for landscape evolution. Journal of Geophysical Research-Solid Earth, 107, 2039, 20pp.

Whitehouse, I.E., Griffiths, G.A., 1983. Frequency and hazard of large rock avalanches in the Central Southern Alps, New-Zealand. Geology 11, 331-334.

Williams, C.J., Lee, S.S., Fisher, R.A., Dickerman, L.H., 1999. A comparison of statistical methods for prenatal screening for Down syndrome. Applied Stochastic Models and Data Analysis 15, 89-101.

Wilson, C.J., Dietrich, W.E., 1987. The contribution of bedrock groundwater flow to storm runoff and high pore pressure development in hollows. In: Beschta, R.L., Blinn, T., Grant, G.E., Ice, G., Swanson, F.J. (Eds.), Erosion and Sedimentation in the Pacific Rim. International Association of Hydrological Sciences, Wallingford, pp. 49-60.

Wise, S., 2000. Assessing the quality for hydrological applications of digital elevation models derived from contours. Hydrological Processes 14, 1909-1929.

Wolman, M.G., Miller, J.P., 1960. Magnitude and frequency of forces in geomorphic processes. Journal of Geology 68, 54-74.

Wu, W.M., Sidle, R.C., 1995. A distributed slope stability model for steep forested basins. Water Resources Research 31, 2097-2110.

Xie, M.W., Esaki, T., Zhou, G.Y., 2004. GIS-based probabilistic mapping of landslide hazard using a three-dimensional deterministic model. Natural Hazards 33, 265-282.

Zadeh, L.A., 1965. Fuzzy sets. Information and Control 8, 338-353.

Zahiri, H., Palamara, D.R., Flentje, P., Brassington, G.M., Baafi, E., 2006. A GIS-based Weights-of-Evidence model for mapping cliff instabilities associated with mine subsidence. Environmental Geology 51, 377-386.

Zêzere, J.L., Rodrigues, M.L., Reis, E., Garcia, R., Oliveira, S., Vieira, G., Ferreira, A.B., 2004. Spatial and temporal data management for the probabilistic landslide hazard assessment considering landslide typology. In: Lacerda, W.A., Ehrlich, M., Fontura, S.A.B., Sayão, A.S.F. (Eds.), Landslides: Evaluation and Stabilization. Taylor & Fancis Group, London, pp. 117-123.

Zimmerman, H.J., 1996. Fuzzy Set Theory - and Its Applications. Kluwer-Nijhoff Publishing, Boston-Dordrecht-Lancaster, 435 pp.

APPENDIX A

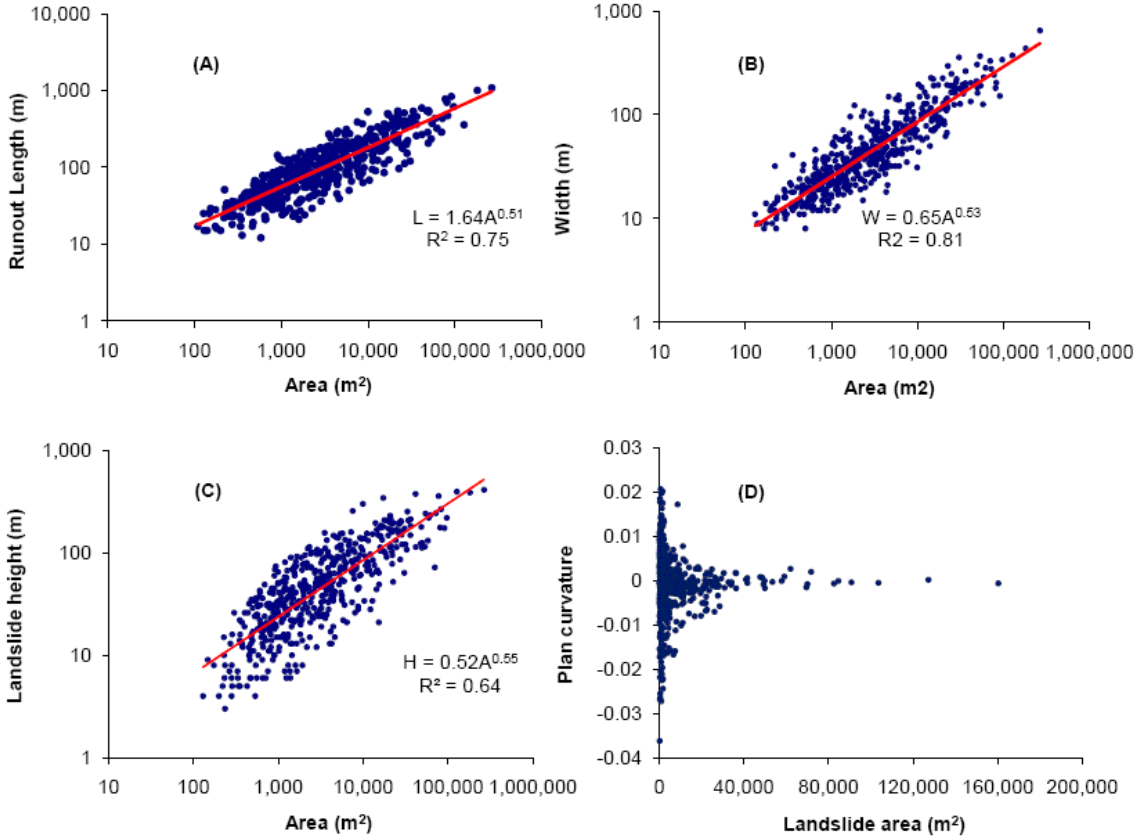

Relationships of shallow landslide areas and its morphologic parameters. A) Relationship of landslide areas and landslide runout lengths. The runout length of a landslide is defined as the planimetric length of a landslide from its crown to the toe. B) Relationship of landslide areas and the widths. C) Relationship of landslide areas and landslide heights. Landslide height is defined as a difference in elevation of the landslide toe and crown. D) Relationship of landslide areas and the plan curvatures of landslidse surfaces. The plot suggests that large landslides occur mostly in planar surface.

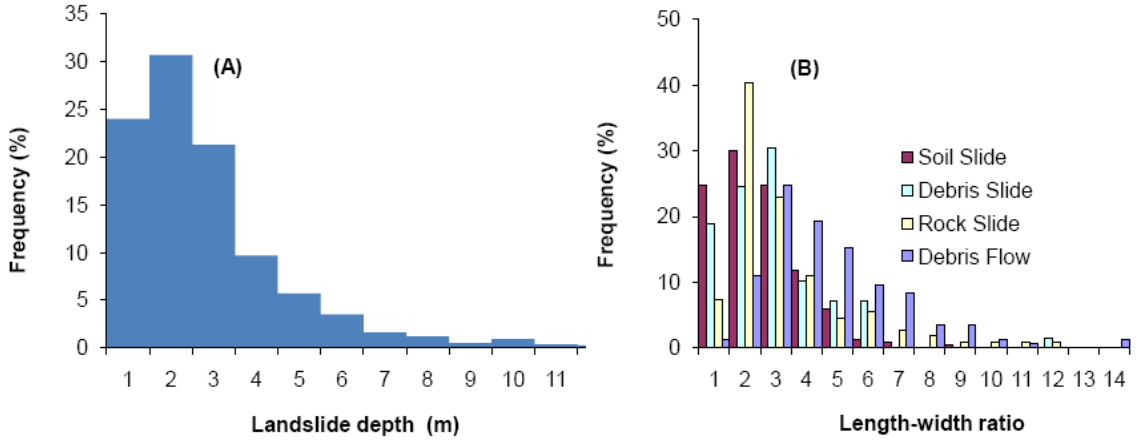

A) Distribution of average depths of shallow landslides. These depths are average depths of each landslide. The depth is calculated as the perpendicular distance from the surface of the landslide to the slip surface. B) Distribution of length-width ratios of each type of shallow landslides.

APPENDIX B

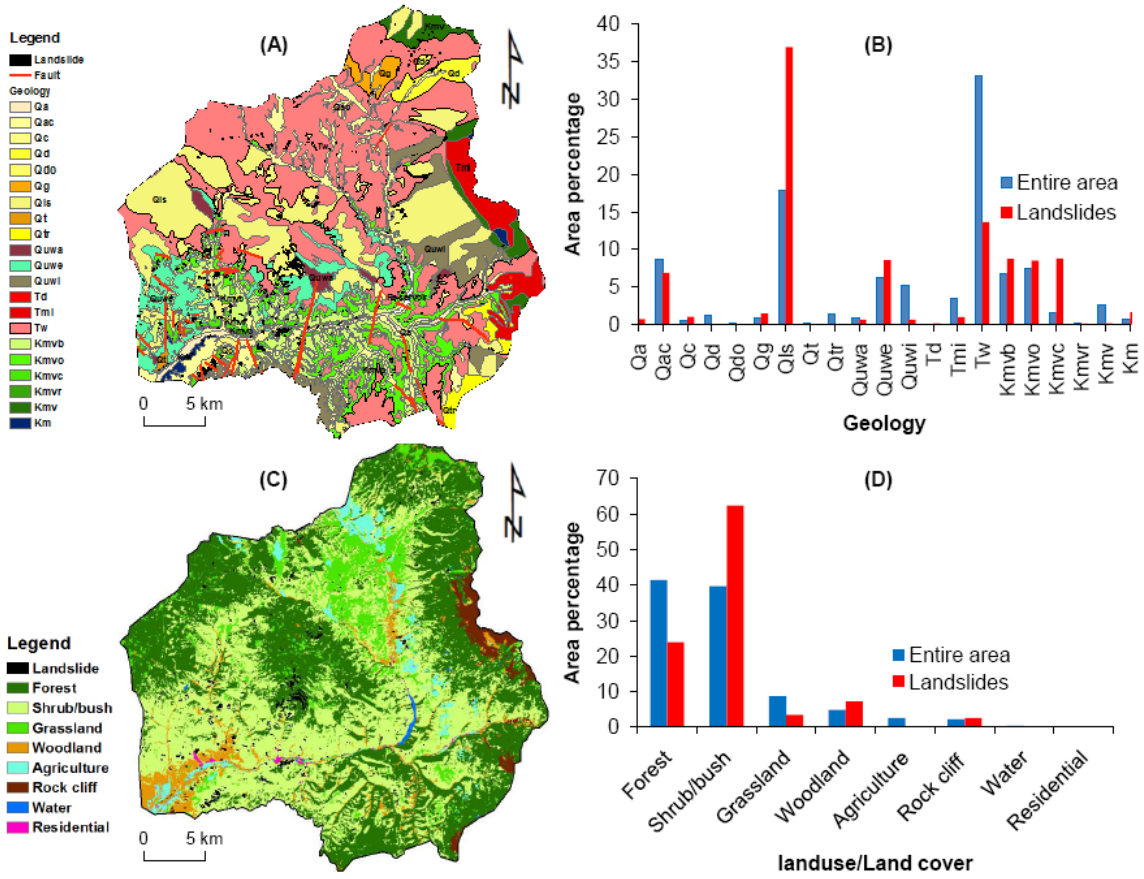

Distribution of geology and landcover in the entire area and landslides. A) Geological map, B) Distribution of lithology, C) Landcover map, and D) Distribution of landcover

Geology of the study area

Symbol	Formation	Age	Lithology
Qa	Alluvium	Holocene	Clay silt sand gravel and boulders; large components are subangular to rounded; well sorted to poorly sorted, commonly stratified; deposited in stream channels
Qac	Alluvium and colluvium undifferentiated	Holocene and pleistocene	May locally include alluvium, terrace deposits, and bedrock.
Qc	Colluvium	Holocene	Clay, silt, sand, gravel, and boulders; large components are subangular to subangular; commonly derieved from bedrock above or beneath deposit, deposited by sheet wash or slow downslope movement. May locally include landslides, alluvial deposits and bedro
Qd		Quaternary	Glacial drift
Qdo		Quaternary	Glacial drift
Qg		Quaternary	Gravel, alluvium
Qls	Landslide and mudflow deposits	Holocene and pleistocene	Clay, silt, sand, gravel, and boulders; heterogeneous to poorly sorted; cracks and scraps are locally common in upper part, hummocky topography and local closed depressions are common near base of deposits; formed by various combinations of slumping, slid
Qt	Alluvial terrace deposit	Holocene	Clay silt, sand and gravel and boulders which commonly are sorted and stratified. Occurs about 30-120 m above the present stream drainage; may locally include small deposits of alluvium and colluvium
Qtr	Talus and rock glacier deposits	holocene	Locally include areas of bedrock and colluvial, alluvial and landslide deposits
Quwa	Major alluvial deposit	Pleistocene	Surfaces of deposit are formed on Tertiary volcanic rocks and Wasatch Formation. Surfacew dips towards modern drainages, such as North Fork Gunnison River
Quwe	Unconsolidated deposits	Pleistocene	Derived from late Tertiary extrusive rocks and Wasatch Formation. Clay, silt and sand are primarily derived from the Wasatch Formation; gravel and boulders are primarily derived from the extrusive rocks (basalts) capping Grand Mesa. Heterogeneous to moder
Quwi	Unconsolidated deposits	Pleistocene	Similar to unconsolidated deposit (unit Quwe) except derieved from rocks of the Wasatch Formation and from intrusive rocks of the West Elk Mountains (Middle Tertiary granodiorites, quartz monzonites). May locally be composed primarily of material derieved
Td	Mafic dikes and dike like bodies	Tertiary	consists of basalt gabbros and associated rocks
Tmi		Tertiary	plutonic rock (phaneritic)
Tw	Wasatch formation	Eocene and Paleocene (Tertiary)	Varicolored (mostly various shades of brown, gray and red) claystone and mudstone with local lenses of sandstone, volcanic sandstone, and basal conglomerate. Large landslides and mudflows are common in claystone in steep slopes. Locally may contain small
Kmvb	Barren member	Upper Cretaceous	Interbedded sandstone, mudstone and shale; light brown to light gray. Sandstone is fine to veryfine grained; beds are lenticular and commonly range from a few feet to about 100 feet (30m) thick. Thin, non commercioal coal beds are locally present. About 7
Kmvo	Ohio creek member	Upper Cretaceous	Interbedded sandstone, mudstone and shale. Stratigraphic rank assignment is that of Johnson and May (1980). Sandstone is fine to coarse grained; locally conglomeratic, particularly in upper part; lenticular; and ranges from a few feet to about 200 ft (60
Kmvc	Coal bearing member	Upper Cretaceous	Interbedded sandstone mudstone, shale and siltstone. Contains coal beds and coal zones as much as 9m thick. Sandstone is fine to very fine grained, pale yellowish brown with calcareous cement, lenticular, beds commonly range from a few feet to
Kmvr	Rollins sandstone member	Upper Cretaceous	Sandstone, fine to veryfine grained, becomes coarser grained and more quartzose in upper part, silicious and some calcareous cement common and commonly uncemented, tan to very light gray; graditional contact with underlying Mancos Shale; elongate iron con
Kmv	Mesaverde Formation	Upper Cretaceous	Includes (from higher to lower). The Ohio Creek member (Kmvo), barren member (Kmvb), coal bearing member (Kmvc), and Rolling Sandstone Member (Kmvr). Consist of sandstone, shale, mudstone and coal. Commonly forms moderately steep slopes where underlain by
Km	Mancos shale	Upper Cretaceous	Shale and mudstone, light gray to medium gray and local thin impure limestone bed. Locally contain small deposits of unmapped alluvium and colluvium about 1200 - 1375 m thick

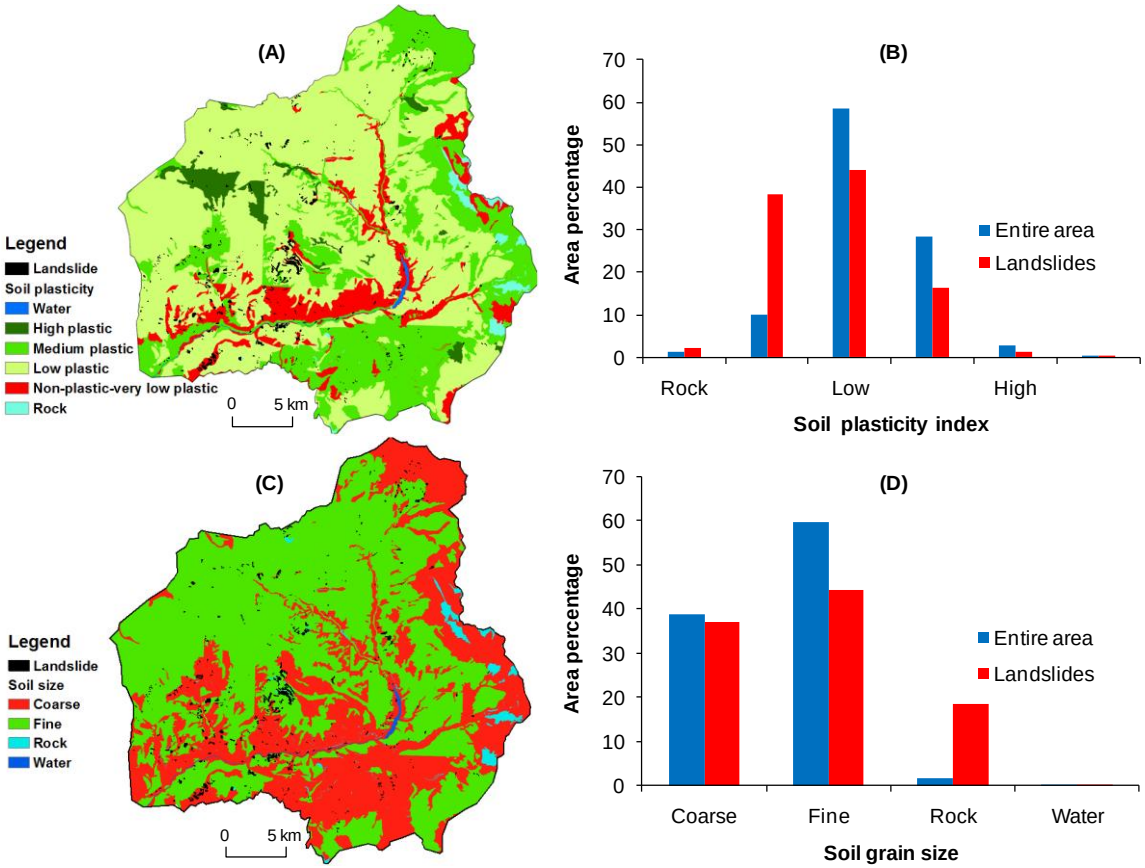

Distribution of soil plasticity index and soil grain size in the entire area and landslides. A) Soil plasticity map, B) distribution of soil plasticity index, C) soil grain size map, and D) distribution of soil grain size

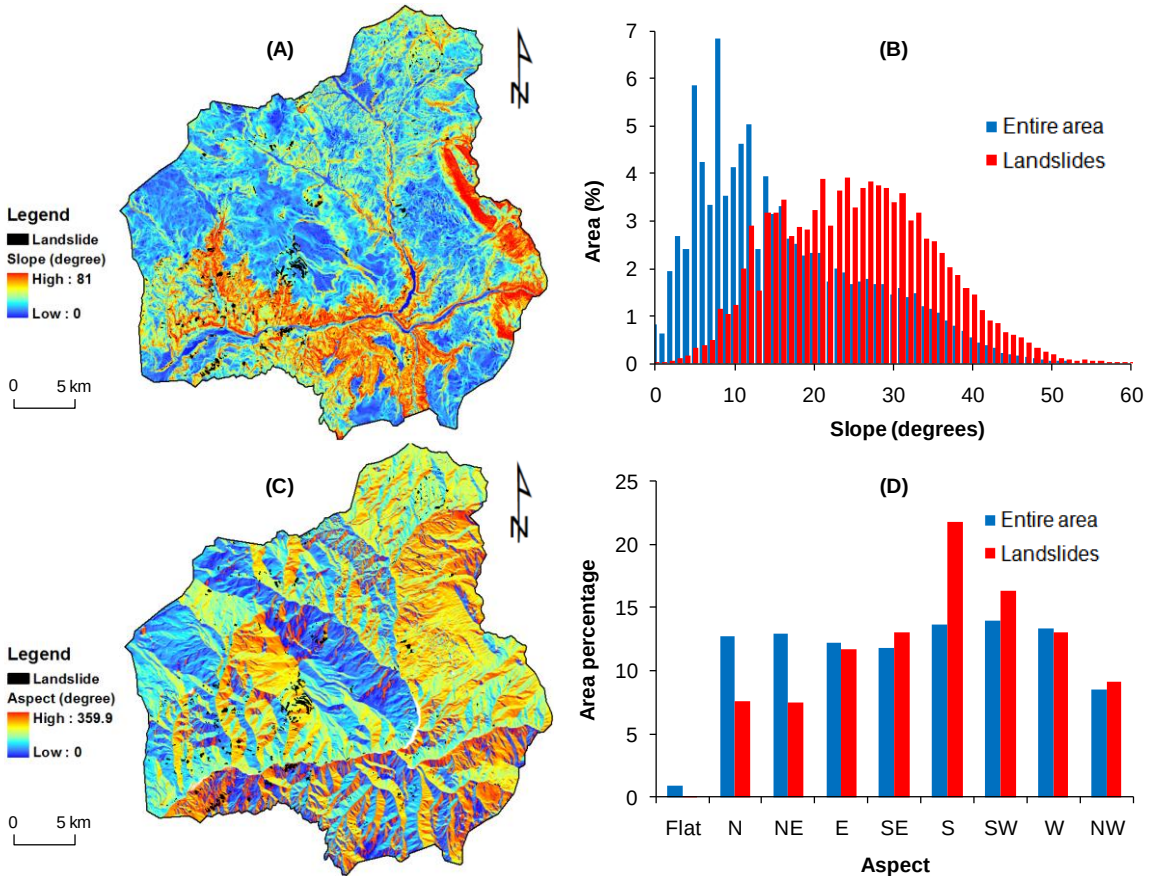

Distribution of slope and aspect in the entire area and landslides. A) Slope map, B) distribution of slope, C) aspect map, and D) distribution of aspect

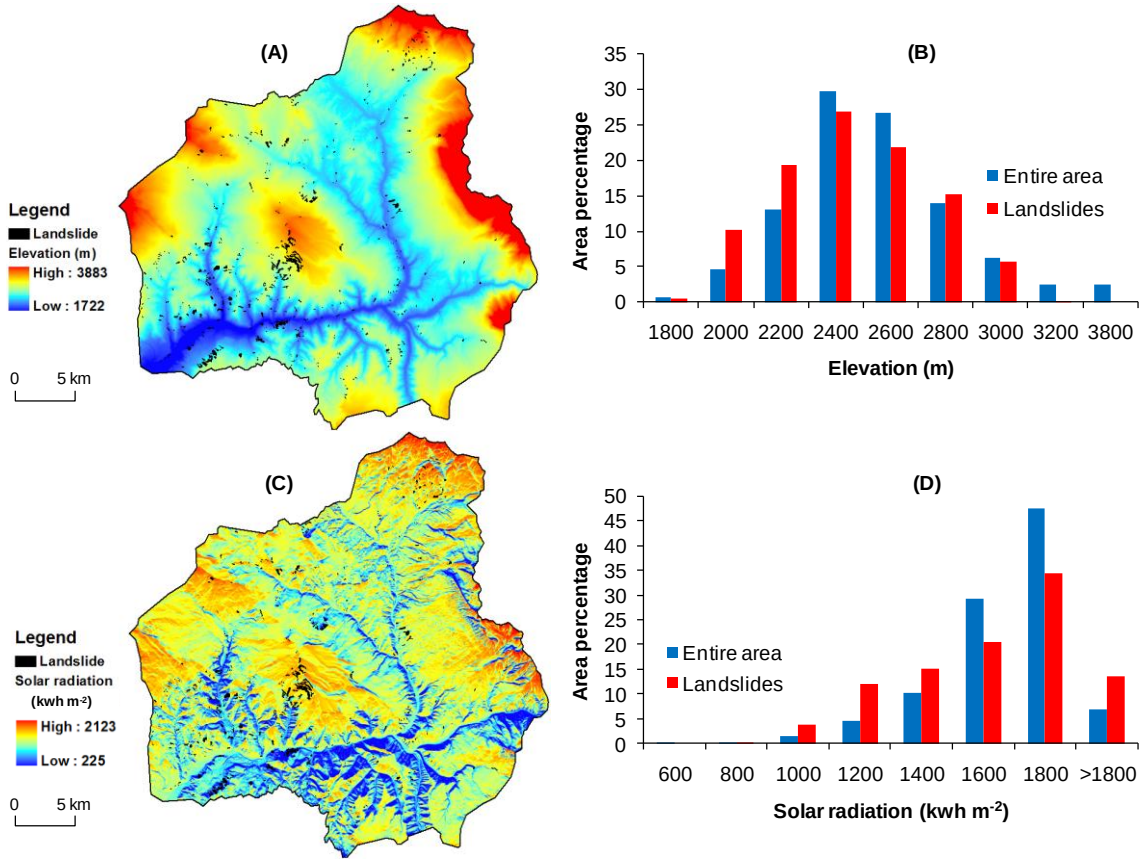

Distribution of elevation and solar radiation in the entire area and landslides. A) Elevation map, B) distribution of elevation, C) solar radiation map, and D) distribution of solar radiation

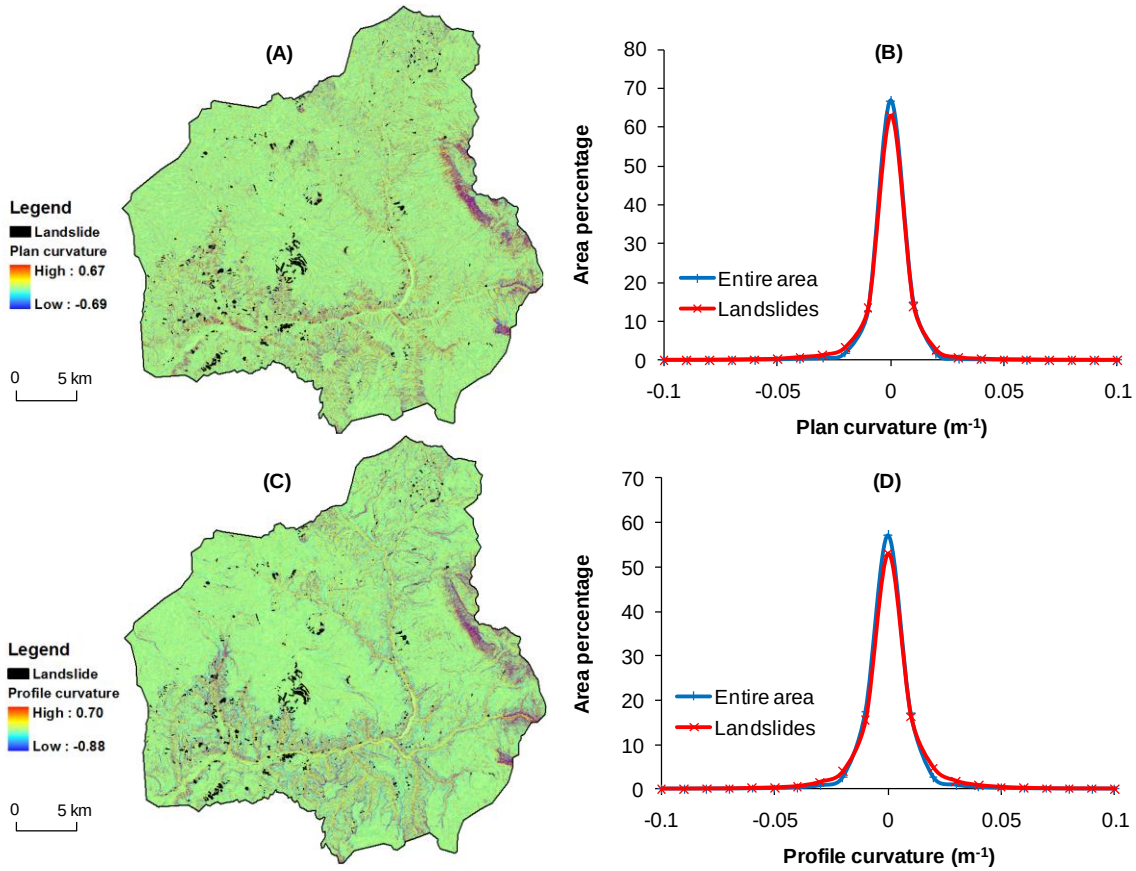

Distribution of plan curvature and profile curvature in the entire area and landslides. A) Plan curvature map, B) distribution of plan curvature, C) profile curvature map, and D) distribution of profile curvature

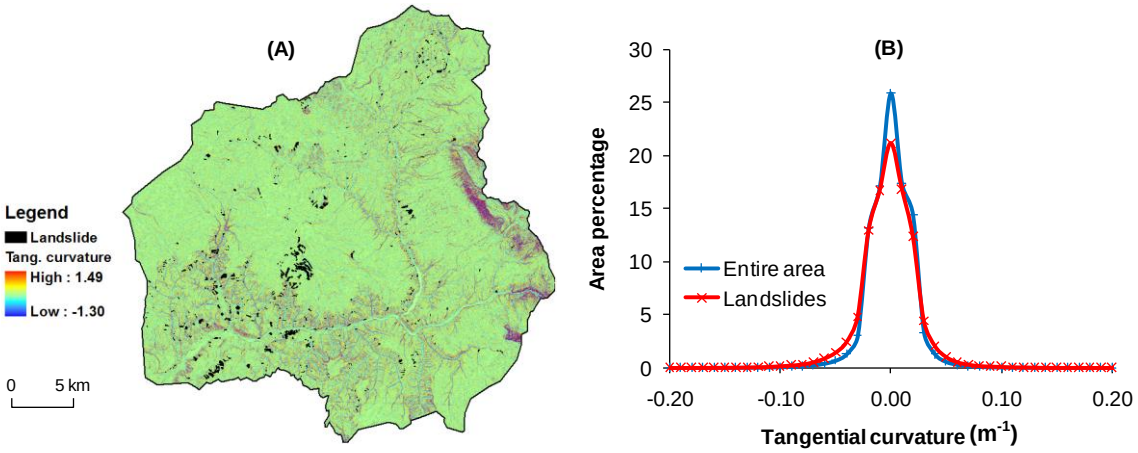

Distribution of tangential curvature in the entire area and landslides. A) Tangential curvature map, B) distribution of tangential curvature

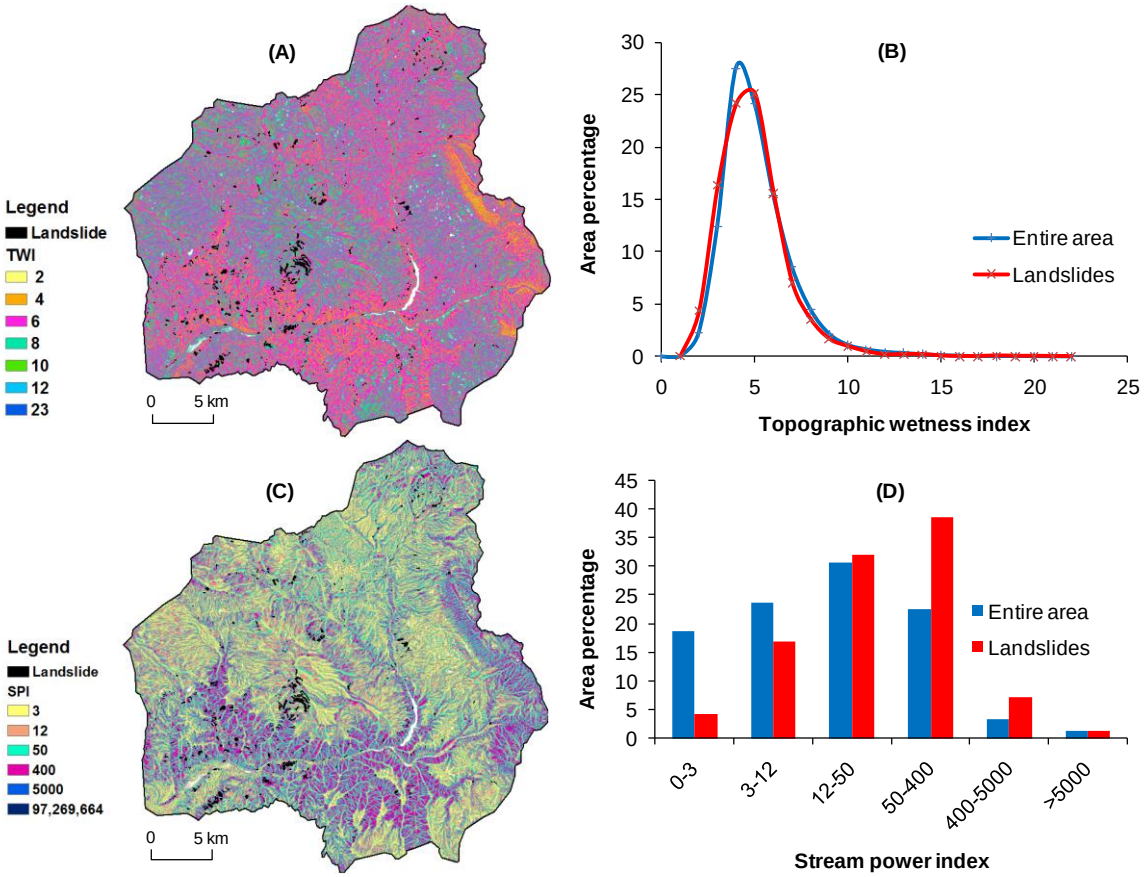

Distribution of topographic wetness index (TWI) and stream power index (SPI) in the entire area and landslides. A) TWI map, B) distribution of TWI, C) SPI map, and D) distribution of SPI

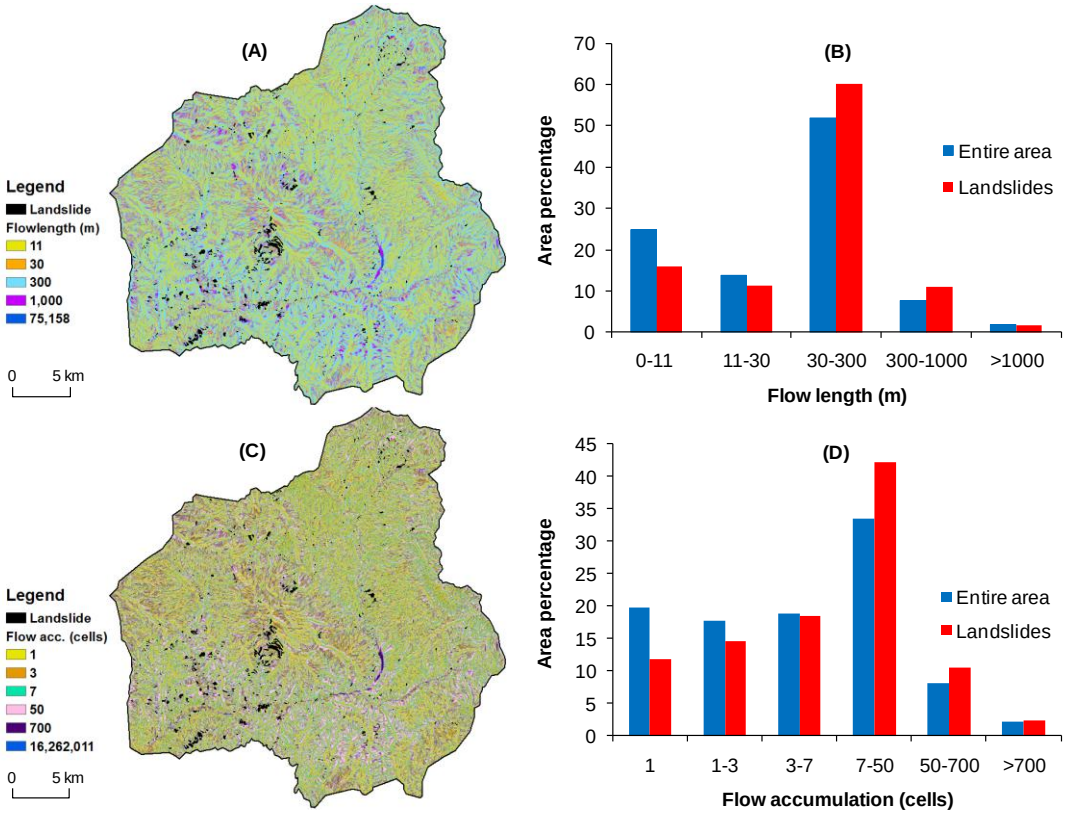

Distribution of flow length and flow accumulation in the entire area and landslides. A) Flow length map, B) distribution of flow length, C) flow accumulation map, and D) distribution of flow accumulation

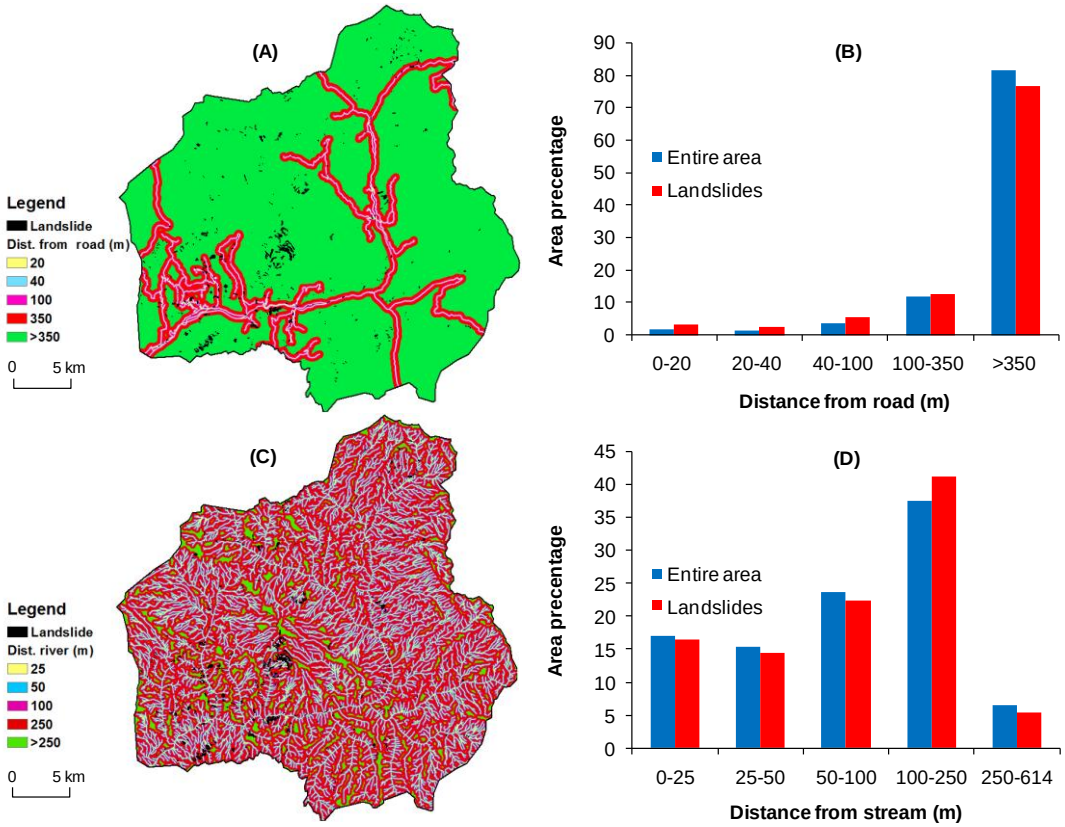

Distance from road and stream in the entire area and landslides. A) Distance from road map, B) distribution of distance from road classes, C) distance from stream map, and D) distribution of distance from stream

VITA

Name: Netra Raj Regmi

Address: Texas A&M University
Department of Geology & Geophysics
College Station, TX 77843-3115

Email Address: netraregmi@tamu.edu

Education: B.S., Geology, Tribhuvan University, Nepal, 1998
M.S., Geology, Tribhuvan University, Nepal, 2001
Ph.D., Geology, Texas A&M University, USA, 2010